Multiphysics Modeling of a Microchannel Methanol Steam Reformer for High Temperature Polymer Electrolyte Membrane Fuel Cell Systems

by

Munur Sacit Herdem

A thesis
presented to the University of Waterloo
in fulfillment of the
thesis requirement for the degree of
Doctor of Philosophy
in
Mechanical and Mechatronics Engineering

Waterloo, Ontario, Canada, 2019

Examining Committee Membership

The following served on the Examining Committee for this thesis. The decision of the Examining Committee is by majority vote.

External Examiner	Dr. Junjie Niu Assistant Professor
Co-Supervisor	Dr. Feridun Hamdullahpur Professor
Co-Supervisor	Dr. Siamak Farhad Assistant Professor
Internal Member	Dr. John Z. Wen Associate Professor
Internal Member	Dr. Xianguo Li Professor
Internal-external Member	Dr. Eric Croiset Professor

AUTHOR'S DECLARATION

This thesis consists of material all of which I authored or co-authored: see Statement of Contribution included in the thesis. This is a true copy of the thesis, including any required final revisions, as accepted by my examiners.

I understand that my thesis may be made electronically available to the public.

Statement of Contributions

Chapters 2 to 5 in this thesis are adapted from the following list of publications:

Chapter 2

Herdem MS, Younessi-Sinaki M, Farhad S, Hamdullahpur F. An overview of the methanol reforming process: comparison of fuels, catalysts, reformers and systems. *Int. J. Energy Res*. 2019, accepted. The preprint version of the article is used in this thesis.

I searched the literature, collected and analyzed data, and wrote the manuscript. Dr. Farhad and Dr. Hamdullahpur supervised the research and reviewed the manuscript. Dr. Younessi-Sinaki reviewed the article, prepared some figures for the accepted version of the manuscript, and contributed to the catalyst section of the paper.

Chapter 3

Herdem MS, Farhad S, Hamdullahpur F. Modeling and parametric study of a methanol reformate gas-fueled HT-PEMFC system for portable power generation applications. *Energy Convers. Manag.* 2015; 101:19–29.

I developed the simulation framework and prepared all results. I wrote the final manuscript under the direction of Dr. Farhad and Dr. Hamdullahpur. Dr. Farhad and Dr. Hamdullahpur also reviewed the paper.

Chapter 4

Herdem MS, Mundhwa M, Farhad S, Hamdullahpur F. Multiphysics Modeling and Heat Distribution Study in a Catalytic Microchannel Methanol Steam Reformer. *Energy Fuels* 2018; 32:7220-7234.

I developed the modeling framework, extracted, organized and prepared all results. Dr. Mundhwa gave me suggestions to improve the preliminary modeling framework, helped me clearly understand some concepts related to the topic, and reviewed the manuscript. I wrote the final version of the manuscript with direction from the journal reviewers, Dr. Farhad, and Dr. Hamdullahpur. Dr. Farhad and Dr. Hamdullahpur also reviewed the paper.

Chapter 5

Herdem MS, Mundhwa M, Farhad S, Hamdullahpur F. Catalyst layer design and arrangement to improve the performance of a microchannel methanol steam reformer. *Energy Convers. Manag.* 2019, 180: 149-161.

I developed the modeling framework, extracted, organized and prepared all results. Dr. Mundhwa reviewed the first version of the paper. I wrote the final version of the manuscript with direction from the journal reviewers, Dr. Farhad, and Dr. Hamdullahpur. Dr. Farhad and Dr. Hamdullahpur also reviewed the paper.

Abstract

One of the main challenges facing power generation by fuel cells is the difficulties of hydrogen fuel storage. Several methods have been suggested and studied by researchers to overcome this problem. Among these methods, using a fuel reformer as one of the components of the fuel cell system is considered a practical and promising alternative to hydrogen storage. Among many hydrogen carrier fuels that can be used in reformers, methanol is one of the most attractive due to its distinctive properties. Methanol reformate gas is ideal for feeding high temperature polymer electrolyte membrane fuel cells (HT-PEMFCs). Therefore, methanol reformate gas fueled HT-PEMFC systems are currently available in the market for portable, stationary and marine applications.

Although there are various reformer types to convert methanol to hydrogen rich syn-gas, microchannel plate heat exchanger reformers have some advantages that increase the system efficiency and decrease the system size. In particular, the microchannel plate heat exchanger methanol reformer can be a promising candidate to meet size demands and improve the system efficiency and start-up time to produce power in the range of 100 to 500 W for auxiliary unit power (APU) applications. Furthermore, recent improvements in new catalyst types for methanol reforming can enable the next generation of microchannel methanol reformers with less weight and higher efficiency to be designed.

Modeling of the microchannel reformers can be helpful to design next generation reformers. In this thesis, firstly, a methanol reformer system to produce power using HT-PEMFC for portable power generation applications is studied. This study is required for selecting inlet parameters for the multiphysics modeling of the microchannel methanol steam

reformer in the second and the third studies. In this study, a detailed parametric study using computer simulations is conducted to estimate the effects of steam-to-carbon (SC) ratio, reformer temperature, current density of the fuel cell, fuel cell temperature, cathode stoichiometric ratio, hydrogen utilization, and rate of power production on the reformate gas composition, fuel cell performance, input fuel flow rate, and heat duties of the system components. In particular, the effects of the reformate gas composition at various fuel cell temperatures on HT-PEMFC performance were examined. The results confirm that the CO molar ratio in the reformate gas increases by decreasing the SC ratio and increasing the reformer temperature. However, the adverse effect of CO molar ratio on fuel cell performance decreases at elevated fuel cell temperatures. The fuel cell voltage decreases by ~78% with the variation of the current density from 0.1 A/cm^2 to 1 A/cm^2 for 160ºC fuel cell temperature and 0.9% CO molar ratio in the reformate gas, while it decreases by ~61% for 180 ºC fuel cell temperature. In addition, an increase in the fuel cell temperature from 160ºC to 180ºC, the input fuel flow rate to produce a given power generation from the system decreases, while enough heat is still available in the system to provide the heat requirement of different system components.

In the second study, a steady state multiphysics model of a microchannel methanol reformer for hydrogen production is developed and validated for the purpose of studying the effects of catalyst layer structural parameters and heat supply strategies on the reformer performance. The aim of this study is to generate hydrogen from the reformer that can be used in HT-PEMFCs. The dimensions of the reformer and inlet flow rate of methanol are selected to produce enough hydrogen to feed fuel cells in the range of 100 to 500 W. This study

considers a 2-dimensional domain for the thin coating of the reforming catalyst to account for the internal diffusion limitations and the coating layer structural parameters. The multicomponent Maxwell-Stefan diffusion equation is implemented to account for diffusion fluxes inside the porous structure of the catalyst. The multiphysics model is validated using the reported experimental data by implementing four different reaction kinetics models of methanol steam reforming. This study considers the best fit kinetics model to evaluate the performance of the microchannel methanol reformer. The results show that the catalyst effectiveness factor is relatively low only at the entrance of the reformer for a catalyst layer thickness greater than 50 μm. In addition, this study reveals that for efficient use of the catalyst, the effective heat supply strategy should be improved. Additionally, the design feasibility of the segmented catalyst layer to achieve a certain amount of methanol conversion with less catalyst is demonstrated. It is revealed that for the same inlet conditions, the segmented catalyst layer design required 25% less reforming catalyst to achieve 90% conversion compared to the conventional continuous coating design.

In the last study, a numerical model is developed to predict the performance of a microchannel methanol steam reformer with different catalyst layer configurations to produce hydrogen-rich syngas for a HT-PEMFC. A solution schema is developed to compare continuous catalyst layer configurations and various segmented catalyst layer configurations without any convergence issue in the numerical analysis. In this work, heat is provided to the endothermic reforming-side via methanol combustion. The results show that higher heat transfer rates can be provided by applying segmented catalyst layer configurations, thus resulting in significant performance improvement of the microchannel methanol steam

reformer. The results reveal that methanol conversion can be increased by ~25% by using segmented catalyst layer configurations with less catalyst in the reforming and combustion sides. The results also indicate that even though there is no significant improvement in methanol conversion with increasing catalyst layer thickness, the greater catalyst layer thickness provides the advantage of reduced high temperature elevations across the reformer length. Overall, the segmented catalyst layer configurations can play an important role in designing the next generation of microchannel reformers for fuel cell power generation systems to maximize power, minimize reformer size, and decrease the required quantity of catalyst.

Acknowledgements

First of all, I wish to express my deep gratitude to my co-supervisors, Dr. Feridun Hamdullahpur and Dr. Siamak Farhad, for their advice and encouragement throughout this research thesis. I would like to thank Dr. Feridun Hamdullahpur for the interest he took in me whenever I needed his help, even though he had an extremely busy schedule. He has helped me to develop a great vision in many areas. In addition, he taught me how to keep calm in challenging situations in life. He will always remain the most inspiring person in my life.

I would like to thank my colleague and friend, Florin Saceleanu, for the time we spent in Waterloo.

I would like to express sincere thanks to Dr. Mayur Mundhwa for his suggestions related to the modeling and helping me to clearly understand some concepts related to chemistry.

I would like to thank my committee members, Dr. Eric Croiset, Dr. John Wen, Dr. Junjie Niu and Dr. Xianguo Li for their suggestions to help improve the quality of this thesis. I also greatly appreciate Dr. Michael Fowler`s questions and suggestions related to my study during my comprehensive exam.

I would like to thank Mr. Dennis Herman and the Chemical Engineering Department at the University of Waterloo for providing Aspen Plus software. I would also like to thank CMC Microsystems for providing access to COMSOL software that facilitated this research.

Last, but not least, I thank my family for their invaluable support during my entire life.

Table of Contents

List of Figures

List of Tables

List of Symbols

A_s	specific surface area ($m^2\ m^{-3}$)
b_{xx} and k_{xx}	pre-exponential factors for anode fuel cell model
C_p	specific heat ($J\ kg^{-1}\ K^{-1}$)
$C_{S_i}^T$	total surface concentration of site i ($mol\ m^{-2}$)
D	diffusion coefficient ($m^2\ s^{-1}$)
dp_a	mean particle size (nm)
d_{pore}	mean pore size (nm)
E_i	activation energy for rate constant of reaction i ($kJ\ mol^{-1}$)
E_{sp}	the specific energy of the system ($Wh\ kg^{-1}$)
F	Faraday`s constant ($C\ mol^{-1}$)
$\bar{f}_i$	fugacity of the species i in the gas mixture (atm)
f_i^o	fugacity of species i at its standard state (atm)
G	Gibbs free energy ($J\ mol^{-1}$)
H	height (m)
H_c	channel height (m)
H_r	reaction enthalpy ($J\ mol^{-1}$)
h_{in}/h_{out}	enthalpy ($J\ mol^{-1}$)
i	cell current density ($A\ cm^{-2}$)
i_o	exchange current density ($A\ cm^{-2}$)

I	electric current (A)
k	thermal conductivity (W m^{-1} K^{-1})
k_i	rate constant for reaction i (units depend on the form of the expression)
k_i^{∞}	pre-exponential term in Arrhenius expression
K_i	equilibrium constant of reaction i or adsorption coefficient for surface species i
L	reformer length (m)
LHV_{CH_3OH}	lower heating value of methanol (J kg^{-1})
M	molecular weight (g mol^{-1})
m_{CH_3OH}	the mass of the stored fuel (kg)
$\dot{m}_{CH_3OH}$	mass flow rate of methanol (kg s^{-1})
m_{FC}	mass of the fuel cell (kg)
m_{H2O}	mass of the stored water (kg)
m_{Ref}	mass of the complete reformer system (kg)
N	number of components
N_{cell}	number of cells
$\dot{n}_{C_xH_yO_z}$	molar ratio of fuel (mol s^{-1})
$\dot{n}_{H2O}$	molar ratio of steam (mol s^{-1})
$\dot{n}_{O_2}$	molar ratio of oxygen (mol s^{-1})
$\dot{n}_{xx}$	molar flow rate (mol h^{-1})
P	pressure (Pa)

P_{BOP}	balance of plant components power consumption (W)
P_{el}	power generation of the fuel cell stack (W)
p_i	partial pressure of component i (bar)
$\dot{Q}$	heat transfer flux (W m^{-2})
R	universal gas constant (J K^{-1} mol^{-1})
R_i	component reaction rate (kg m^{-3} s^{-1})
r_i	rate of reaction (mol kg^{-1} s^{-1})
R_{xx}	resistance (ohm.cm^2)
T	temperature (K)
t_{op}	the operation time (h)
u	velocity (m s^{-1})
u_f	hydrogen utilization ratio (-)
$V_{cell,op}$	cell operation voltage (V)
V_o	open circuit voltage (V)
x	number of carbon atoms
y	mol fraction

Greek Letters

δ_{cat}	catalyst layer thickness (m)
ε	characteristic Lennard-Jones energy (J)
η	catalyst effectiveness factor (-)
η_a	anode overpotential (V)

η_{sys}	system efficiency (-)
θ	surface coverage (-)
κ	porous media permeability (m^2)
λ	cathode stoichiometric ratio (-)
μ	viscosity (kg s^{-1} m^{-1})
ρ	density (kg m^{-3})
$\rho_{cat,c}$	density of the combustion catalyst layer (kg m^{-3})
$\rho_{cat,R}$	density of the reforming catalyst layer (kg m^{-3})
σ	characteristic length (Å)
τ	tortuosity (-)
ϕ	porosity (-)
ω	mass fraction (-)
Ω_D	diffusion collision integral

Subscript and superscripts

c	combustion
cat	catalyst
ch	channel
eff	effective
F	Fickian
g	gas phase
i, j	species indices

K	Knudsen
mix	mixture
MD	methanol decomposition
MS	Maxwell-Stefan
SR	steam reforming
R	reforming
rWGS	reverse water gas shift
WGS	water gas shift

List of Acronyms

APU	auxiliary power unit
ATR	auto-thermal reforming
BOP	balance of plant
DMFC	direct methanol fuel cell
EIA	Energy Information Administration
FC	fuel cell
FEM	finite element method
HT	high temperature
IEA	International Energy Agency
IRMFC	internal reformed methanol fuel cell
LT	low temperature
MCFC	molten carbonate fuel cell
O/C	oxygen to carbon ratio
O/Fuel	oxygen to fuel ratio
O/M	oxygen to methanol ratio
OSRM	oxidative steam reforming of methanol
PAFC	phosphoric acid fuel cell
PEMFC	polymer electrolyte membrane fuel cell
PROX	preferential oxidation
RMFC	reformed methanol fuel cell

S/C	steam to carbon ratio
S/Fuel	steam to fuel ratio
SMR	methanol steam reforming
SOFC	solid oxide fuel cell
STP	standard temperature and pressure
PEM	polymer electrolyte membrane
POX	partial oxidation
TEG	triethylene glycol
W_{th}	Watts thermal

Chapter 1
Introduction

1.1 Motivation and Objectives

Fuel cell (FC) technology is a promising technology for clean and efficient power generation. However, this technology is not widely used today. It is reported that the FC market size across the world was valued at only USD 3.21 billion in 2016 [1]. The most important reasons for this are: (1) the cost of this technology; (2) challenges related to hydrogen transportation, distribution and storage.

The cost of FCs must be reduced in order to stimulate more investment in research and development (R&D), which would result in much needed improvements in this field. At the same time, the demand for these fuel cells in the marketplace must increase, and this would spur needed investment. In other words, it is necessary to determine the most effective way to facilitate the widespread use of FC technology. Recent studies [2-4] have shown that FC systems have the potential to become more common in the market for some niche applications such as backup power generators, forklifts, aircraft auxiliary power unit (APU) applications, power generation applications in off-grid locations, etc. In addition, Shaw *et al.* [5] report that military personal power generators, consumer battery rechargers, and specialized laptop computers are also promising applications that require power in the range of 100 and 500 W.

Customers are willing to accept the higher price of fuel cell technology as compared to alternative technologies such as diesel generators and batteries for the niche markets mentioned above because of the unique combination of characteristics of the FC systems. These unique characteristics can be listed as: (1) quiet operation; (2) low emissions; (3) ability to operate in

extreme conditions; (4) relatively low maintenance costs; (5) quick refueling; (6) low vibration; (7) high fuel efficiency; (8) production of water and heat; (9) extended run time; (10) remote monitoring capability [2-5]. In particular, the extended run time is the most important motivation to prefer FC systems for these niche applications [2-4].

Other important barriers related to FC systems becoming more commonplace in the market are the difficulties of hydrogen transportation, distribution, and storage. Specifically, hydrogen storage is a serious issue for FC systems, which desire extended run times. Storage is difficult because hydrogen exists at a very low density at standard temperature and pressure conditions. Therefore, the occupied volume of the hydrogen gas under standard temperature and pressure conditions is much higher than other fuels [6]. Different storage methods such as compressed hydrogen at very high pressures and cryogenic storage can be used to decrease the occupied volume of the hydrogen. However, there are serious challenges related to the current hydrogen storage methods; for example, the high pressure requirement for compressed storage of hydrogen is an important issue. Additionally, the volume requirement is still very high even at elevated pressures for the compressed storage. It is reported [7] that the volume requirement is about 150 L to store 6 kg of hydrogen at 700 bar. The issue related to cryogenic storage of hydrogen is the evaporation of hydrogen in the tank, which is called the boil-off phenomenon [7]. This causes hydrogen losses between 0.3% and 5% per day depending on the current storage tank technology [8]. To overcome challenges related to hydrogen transportation, distribution, and storage, methanol can be used directly in direct methanol fuel cells (DMFCs), or it can be converted to hydrogen rich syngas by employing various reforming methods to feed the FC systems, serving as a practical and promising alternative to hydrogen storage.

Some of the important advantages of methanol are: (1) It can be easily stored under many environmental conditions because the boiling point of methanol is equal to 65 ^{o}C; (2) The existing fuel infrastructure with limited changes can be used for methanol distribution; (3) It does not include sulfur contents; (4) Its reforming processes are easier than other fuels such as methane, diesel or ethanol because methanol reforming can be achieved at low temperatures with low steam to carbon (S/C) ratios [9,10].

Due to the advantages of methanol mentioned above, it is currently used in the market as a fuel for some specific niche applications of FC power generation systems [11,12]. The direct usage of methanol without reforming is possible in DMFC systems; however, the DMFCs have cost limitations due to their high platinum content. Therefore, the DMFC systems in the market are generally used for small scale power generation applications of less than 100 W [2,11]. The methanol reformate gas fueled high temperature polymer electrolyte membrane fuel cells (HT-PEMFCs) are preferred in the market for power generation higher than 100 W [12]. The main advantage of the HT-PEMFCs is that they can tolerate CO up to 3% because of their high operation temperatures [13]. Thus, the methanol reformate gas can be directly feed to the HT-PEMFCs stack without any additional equipment to remove CO [12].

Steam reforming of methanol (SRM) is commonly used for commercial methanol reformate gas fueled HT-PEMFC systems [12] due to its higher efficiency than the other reforming processes. However, efficient and adequate heat transfer is very important for SRM because it is a highly endothermic process. Efficient heat transfer can be provided by using microchannel plate type heat exchanger reformers based on their high surface to volume ratio [14]. There are also other motivations to use microchannel plate heat exchanger reformers for the SRM process. The microchannel plate heat exchanger reformers improve the system dynamics, catalytic activity, and

mass transfer from the bulk flow to the catalyst surface [15-17]. Due to these advantages, higher performance can be obtained from the methanol reformate gas fueled HT-PEMFC systems with decreasing the system size.

Although many studies have been conducted related to microchannel plate heat exchanger methanol reformers, there are still some questions which must be answered to aid in the efficient design of a new generation of microchannel methanol reformers. Therefore, the focus of this study is to develop a model for microchannel plate heat exchanger methanol reformers in order to answer specific questions about the design of a new generation of microchannel methanol reformers for HT-PEMFC systems.

The main objectives of this thesis are as follows:

- Analyze a methanol reformate gas fueled HT-PEMFC system for power generation in the range of 100 to 500 W to investigate the effects of the main operation parameters on the system.
- Investigate the effects of temperature distribution on the performance of a microchannel methanol reformer.
- Develop a two dimensional (2D) steady state model to understand the effects of catalyst layer thickness on a microchannel plate heat exchanger methanol reformer, while considering different catalyst layer structural characteristics.
- Demonstrate the feasibility of various catalyst layer configurations to improve the performance of a microchannel plate heat exchanger methanol reformer and to decrease the amount of the catalyst needed.

1.2 Thesis Structure

There are six chapters including the introduction and conclusion in this thesis. Chapter 2 has been submitted to a peer reviewed journal and Chapter 3 to 5 have been published in peer reviewed journals. Each chapter is briefly summarized below.

Chapter 2 presents a critical review of the methanol reforming process. The main novelty of this chapter is its coverage of important aspects of methanol reforming processes for fuel cell power generation applications. In this chapter, the focus is on practical points related to methanol reforming. The chapter summarizes the recent studies related to this subject and explains promising applications of the methanol reformate gas fueled fuel cell systems. In the first section of this chapter, the studies covering the reforming of different fuels are presented and the characteristics of commercial reformate gas fueled systems are compared. Fuel reforming processes are also reviewed in this section. In the next section, advancements in methanol reforming technology are explained. The methanol reforming catalysts and reaction kinetics studies by various researchers are reviewed and the advantages and disadvantages of each catalyst are discussed; then the studies about different types of reformers are presented. In the last section of Chapter 2, methanol reformate gas fueled fuel cell systems are reviewed. Chapter 2 has been submitted to the *International Journal of Energy Research*.

Chapter 3 investigates the effects of different operational parameters on methanol reformate gas fueled HT-PEMFC systems for portable power generation applications. The system is simulated using Aspen Plus with Fortran calculator to conduct detailed parametric studies and estimate the system's efficiency. The contents of this chapter have been published in the journal of *Energy Conversion and Management* after peer review [18]. The results obtained in Chapter 3 are used to select inlet conditions for modeling the microchannel methanol reformer in Chapters 4 and 5.

Chapter 4 presents a steady state 2D multiphysics model of a microchannel methanol steam reformer to investigate the effects of catalyst layer thickness on the performance of a microchannel methanol steam reformer. The effects of temperature distribution on the reformer are also studied for isothermal and nonisothermal situations. In addition, the feasibility of the segmented catalyst layer to decrease the amount of the catalyst is demonstrated. The main novelty of this chapter is its consideration of a 2D domain for the thin coating of the reforming catalyst to account for the internal diffusion limitations and coating catalyst`s properties. This chapter has been published in the journal of *Energy and Fuels* [6].

Chapter 5 presents various catalyst layer configurations for the microchannel plate heat exchanger methanol steam reformer. The model that is developed in Chapter 4 is expanded in this chapter. The heat for the endothermic methanol steam reforming reactions is provided by coupling catalytic methanol combustion reactions on the opposite side. A methodology is also presented in the chapter to solve convergence issues in the numerical analysis. In addition, the effects of catalyst layer thickness on the performance and the temperature distribution of the reformer with variation of the catalyst layer configurations are investigated. Furthermore, the power generation of a HT-PEMFC stack is estimated for the optimal catalyst layer configurations. This chapter has been published by the journal of *Energy Conversion and Management* [19] after peer review.

Chapter 6 highlights the important results obtained in this thesis and gives recommendations for the future directions of this work.

Chapter 2

An Overview of the Methanol Reforming Process: Comparison of Fuels, Catalysts, Reformers, and Systems

The following chapter is a "pre-print" of an article accepted for publication in International Journal of Energy Research:

Herdem MS, Younessi-Sinaki M, Farhad S, Hamdullahpur F. An overview of the methanol reforming process: comparison of fuels, catalysts, reformers and systems. *Int. J. Energy Res*. 2019, accepted.

The final, official version of the article can be downloaded from the journal`s website via this DOI link when it becomes available:

DOI: 10.1002/er.4440

2.1 Introduction

Many organizations such as the World Energy Council [20], EIA [21], and IEA [22] predict that world energy requirements will dramatically increase in the near future. However, today, this increasing energy requirement issue is not sufficient to explain all of the studies in the energy field. To comprehend deeply, we should also consider the environment, energy security, affordable energy production, end use of energy including stationary power generation applications, portable power generation, applications, etc. In addition, one of these issues is sometimes more important than the others. For example, nowadays, energy security is a critical issue for the oil and gas importing countries because of the destabilization of these countries [23,24]. Of course, there is no magic to solve all of the issues related to energy. However, various unique solutions can be applied for each issue. Two possible solutions are diversification of energy supplies and choosing the appropriate technology for different applications.

Hydrogen is a very promising energy carrier to diversify our energy supply because it can be produced using a wide variety of sources, and it can be used for various purposes such as ammonia production [25], energy storage [26-29], methanol synthesis, diesel, and natural gas production [30].

Hydrogen as a fuel also has promising potential to produce power that is environmentally friendly and has high efficiency by employing fuel cells. One of the most important barriers to fuel cell systems becoming more commonplace for power generation applications - in particular for portable applications - involves the difficulties regarding hydrogen storage. Hydrogen has higher gravimetric energy density than hydrocarbon and alcohol fuels (see Fig. 1), but in terms of its volumetric energy density (Wh/l) it is significantly less dense than other fuels [31]. The reason is that the occupied volume of 1 kg of hydrogen as a gas under standard temperature and pressure conditions is much higher than that of hydrocarbon and alcohol fuels. For example, 1 kg of hydrogen has nearly six times as much energy (142 MJ) as compared to a kg of methanol (22.5 MJ). However, the occupied volume of 1 kg of methanol at 25^{o}C and 1 atm is about 1.26 L while this value is ~12300 L for 1 kg of hydrogen. To decrease the occupied volume of hydrogen, efficient methods of storage are required. These methods are: (1) Compressed gas at standard temperature and very high pressure; (2) Cryogenic liquid at standard pressure and 20 K; (3) Chemical storage by using Magnesium Hydride, Calcium Hydride, Sodium Hydride etc.; (4) Physical storage (metal organic framework) [8,32]. Despite the number of choices available, there are also many important issues related to these methods which need to be considered, such as the requirement of high pressure for compressed storage of hydrogen or expensive materials and very low temperatures for liquefaction of hydrogen [8]. To overcome these problems, alternative fuels

such as natural gas, ethanol, methanol, dimethyl ether (DME), gasoline and diesel can be converted to hydrogen rich gas using fuel reforming in order to provide the required fuel for fuel cells.

The other important motivation for the reforming of natural gas, ethanol, methanol, DME, gasoline and diesel is that these fuels can be produced from biomass in an environmentally friendly way. Although there are some ethical and social issues related to the first generation biofuels derived from food feedstocks, the second-generation biofuels will be derived from non-edible feedstocks such as wood, agricultural residues, forestry waste and municipal wastes [33-36]. There are currently demonstration, pilot and commercial second-generation biofuel plants in operation [35]. In addition, the third and fourth generation biofuels will be derived from algae. This process is currently in the research and development stage and presents a very attractive option for the production of biofuels [35].

Due to the aforementioned advantages of reforming alternative fuels, fuel reforming has received attention from a variety of research groups throughout the world. Many review studies have been undertaken to examine various aspects of fuel reforming. One of the early review papers was published by Haryanto *et al.* [37] in 2005 to examine and compare different catalysts (oxide catalysts, metal-mixture-based catalysts, and noble-metal-based catalysts) for steam reforming of ethanol (ESR). Contreras *et al.* [38] recently reviewed noble metals and non-noble metals as catalysts for ESR. They provided information about the major catalytic studies of ESR up to 2013. A review of solar thermal catalytic reforming of natural gas was conducted by Simakov *et al.* [39]. In this study, they presented equilibrium constraints of methane steam and dry reforming, and also critically evaluated recent studies related to various aspects of solar thermal reforming of methane catalysis. Sheu *et al.* [40] discussed recent developments and potential innovations such as chemical looping and membrane reactors in relation to solar methane reforming systems. Studies

of reforming processes for different types of fuels and the related hydrogen purification and CO reduction processes were reported by Qi *et al.* [41]. Hansen [42] focused on fuel processing systems with an emphasis on the industrial aspects of fuel cells and electrolyzers. LeValley *et al.* [43] introduced recent developments in steam reforming hydrogen production technologies and water gas shift catalysts. Recent and past research activities (such as catalyst development, reactor design and testing for reforming) and market applications for microreactors were explained in Ref. [15,44]. Iulionelli *et al.* [45] also provided an overview of studies on conventional and membrane reactors for methanol steam reforming. In addition to the mentioned studies, Sa *et al.* [46] illustrated the latest developments in copper-based and group 8-10 metal-based catalysts for methanol steam reforming, and Yong *et al.* [47] discussed methanol reforming Cu-based catalyst, surface reaction mechanisms, and reaction schemes. Palo *et al.* [48] in 2007 reviewed studies related to methanol steam reforming for hydrogen production to provide information about the methanol reforming systems, system challenges and catalysts. Sengodan *et al.* [49] recently (2018) discussed partial oxidation of methane, ethanol and methanol. They focused on recent improvements in catalysts for the partial oxidation of methane and alcohols. In addition, Zang *et al.* [10] recently reviewed the latest progress and achievements in integrated methanol steam reformer high temperature polymer electrolyte membrane fuel cell (HT-PEMFC) power generation systems.

As shown from the review papers mentioned above, there is no review paper in the literature that covers all of the aspects of methanol reforming. This review paper will mainly focus on current studies from 2010 to 2018 involving methanol reforming. Firstly, we will compare fuel reforming processes for different fuels by summarizing the works covering the reforming of different types of fuels using a thermodynamic framework. Secondly, we will discuss recent and

past research activities regarding methanol reforming. Then, different types of reformers and the effects of different parameters on methanol reforming will be explained. Information will then be provided on studies involving the integration of methanol reforming into reformate gas-fueled fuel cell systems. In this study, the main goal is to provide a clear definition of the key parameters and technologies used in methanol reforming for fuel cell applications.

2.1.1 An Overview of the Fuel Reforming Process

Fuel reforming is a conversion process whereby fuels are converted to hydrogen rich gas. Different types of fuels consisting of light hydrocarbons such as methane and ethane, liquid hydrocarbons such as diesel and jet fuels, and alcohols such as methanol and ethanol can be used for fuel reforming processes [50,51].

Steam reforming, partial oxidation, and oxidative steam reforming (or autothermal reforming) are three different processes to convert hydrocarbon and alcohol fuels to hydrogen rich gas. Advantages and disadvantages of these processes are shown in Table 2-1. Fuel and steam react in steam reforming via an endothermic reaction. The main advantages of steam reforming are the highest hydrogen yield can be obtained and reforming temperature is lower than partial oxidation and oxidative steam reforming [52, 53]. However, start-up time and dynamic response are two important issues related to this reforming process [53]. Conversion of fuels to hydrogen rich gas with oxygen is called partial oxidation and is an exothermic reaction. Partial oxidation can be employed for quick start-up and dynamic response [52,53]. Although partial oxidation has quick start-up and better dynamic response, the lower hydrogen yield and relatively high processing temperature are important challenges with regards to this reforming process. To achieve the advantages of both steam and partial oxidation reforming, steam and a certain amount of air can

be used together. This process is called oxidative steam reforming. Oxidative steam reforming can be endothermic, exothermic or thermally neutral, when the heat of reaction is equal to zero. For the thermally neutral situation, the oxidative steam reforming is called autothermal reforming.

Table 2-1 Advantages and disadvantages of reforming technologies (modified from [52,53]**).**

Type	Advantages	Disadvantages
Steam Reforming	• Highest H_2 yield • Oxygen not required • Most extensive industrial experience • Lowest process temperature • Best H_2/CO ratio for H_2 production	• Requires careful thermal management to provide heat for reaction, especially for (a) start-up and (b) dynamic response • Only works on certain fuels
Partial Oxidation	• Quick to start and respond because reaction is exothermic • Quick dynamic response • Less careful thermal management required • Works on many fuels • Low methane slip	• Lowest H_2 yield • Highest pollutant emissions (HCs, CO) • Low H_2/CO ratio • Very high processing temperatures
Autothermal reforming	• Simplification of thermal management by combining exothermic and endothermic reactions in same process • Compact due to reduction in heat exchangers • Quick to start • Lower process temperature than partial oxidation • Low methane slip	• Low H_2 yield • Limited commercial experience • Requires careful control system design to balance exothermic and endothermic processes during load changes and start-up

Global reactions for steam reforming, partial oxidation and oxidative steam reforming can be written as follows for hydrocarbons and alcohols (methanol and ethanol) [44, 51-53]:

Steam reforming of hydrocarbons:

$$C_xH_y + xH_2O \leftrightarrow xCO + \left(\frac{1}{2}y + x\right)H_2 \quad \text{(R.2.1)}$$

$\Delta H^o = hydrocarbon\ dependent, endothermic$

Steam reforming of methanol and ethanol:

$$CH_3OH + H_2O \leftrightarrow CO_2 + 3H_2 \ \ \Delta H^o = +49\ kJ/mol \quad \text{(R.2.2)}$$

$$CH_3CH_2OH + 3H_2O \leftrightarrow 6H_2 + 2CO_2 \ \ \Delta H^o = +173.3\ kJ/mol \quad \text{(R.2.3)}$$

Partial oxidation of hydrocarbons:

$$C_xH_y + \frac{x}{2}(O_2 + 3.76N_2) \leftrightarrow xCO + \frac{y}{2}H_2 + \left(\frac{x}{2}\right)3.76N_2 \quad \text{(R.2.4)}$$

$\Delta H^o = hydrocarbon\ dependent, exothermic$

Partial oxidation of methanol and ethanol:

$$CH_3OH + \frac{1}{2}(O_2 + 3.76N_2) \leftrightarrow CO_2 + 2H_2 + \left(\frac{1}{2}\right)3.76N_2 \ \ \Delta H^o = -193.2\ kJ/mol \quad \text{(R.2.5)}$$

$$CH_3CH_2OH + \frac{3}{2}(O_2 + 3.76N_2) \leftrightarrow 3H_2 + 2CO_2 + \left(\frac{3}{2}\right)3.76N_2 \ \ \Delta H^o = -552\ kJ/mol \quad \text{(R.2.6)}$$

Oxidative steam reforming of hydrocarbons:

$$C_xH_y + n(O_2 + 3.76N_2) + (x - 2n)H_2O \leftrightarrow xCO + \left(x - 2n + \frac{y}{2}\right)H_2 + (n)3.76N_2 \quad \text{(R.2.7)}$$

$\Delta H^o = hydrocarbon\ dependent, and oxygen/fuel ratio\ dependent.$ (It can be endothermic, exothermic, or thermally neutral).

Oxidative steam reforming of methanol and ethanol:

$$C_xH_yO_z + n(O_2 + 3.76N_2) + (x - 2n - z)H_2O \leftrightarrow xCO + \left(x - 2n - z + \frac{y}{2}\right)H_2 + n(3.76)N_2 \quad \text{(R.2.8)}$$

$\Delta H^o = changeable, depends\ on oxygen/fuel$ ratio

Coke formation reactions should also be considered for the reforming process because coke formation can rapidly deactivate the catalyst and block the reactor [54]. Dominant reactions that are responsible for coke formation are given as follows [54-58].

Coke formation by Boudouard reaction:

$$2CO(g) \leftrightarrow CO_2(g) + C(s) \;\; \Delta H^o = -172.4\ kJ/mol \quad \text{(R.2.9)}$$

Coke formation by CH_4 decomposition:

$$CH_4 \leftrightarrow 2H_2 + C(s) \;\; \Delta H^o = +74.9\ kJ/mol \quad \text{(R.2.10)}$$

Carbon monoxide reduction reaction:

$$CO(g) + H_2(g) \leftrightarrow H_2O(g) + C(s) \;\; \Delta H^o = -130.4\ kJ/mol \quad \text{(R.2.11)}$$

Carbon dioxide reduction reaction:

$$CO_2 + 2H_2 \leftrightarrow C + 2H_2O \;\; \Delta H^o = -90.1\ kJ/mol \quad \text{(R.2.12)}$$

2.2 Fuel Selection for Fuel Cell Applications and Reforming of Various Fuels

Different fuels can be used to feed fuel cells for power generation. However, the main question is how we can choose a suitable fuel for fuel cell power generation systems. To select a fuel, we should consider the application area of the system. As shown in Fig. 2-1, the fuel cell systems can be used for different applications. Possible applications of fuel cell power generation systems need different desired system properties that are listed in Fig. 2-1. For example, on-site availability of the fuel and high efficiency to produce power and heat are important for stationary power applications while start-up time, weight and volume of the system, long-run time are desired system properties for portable power generation applications.

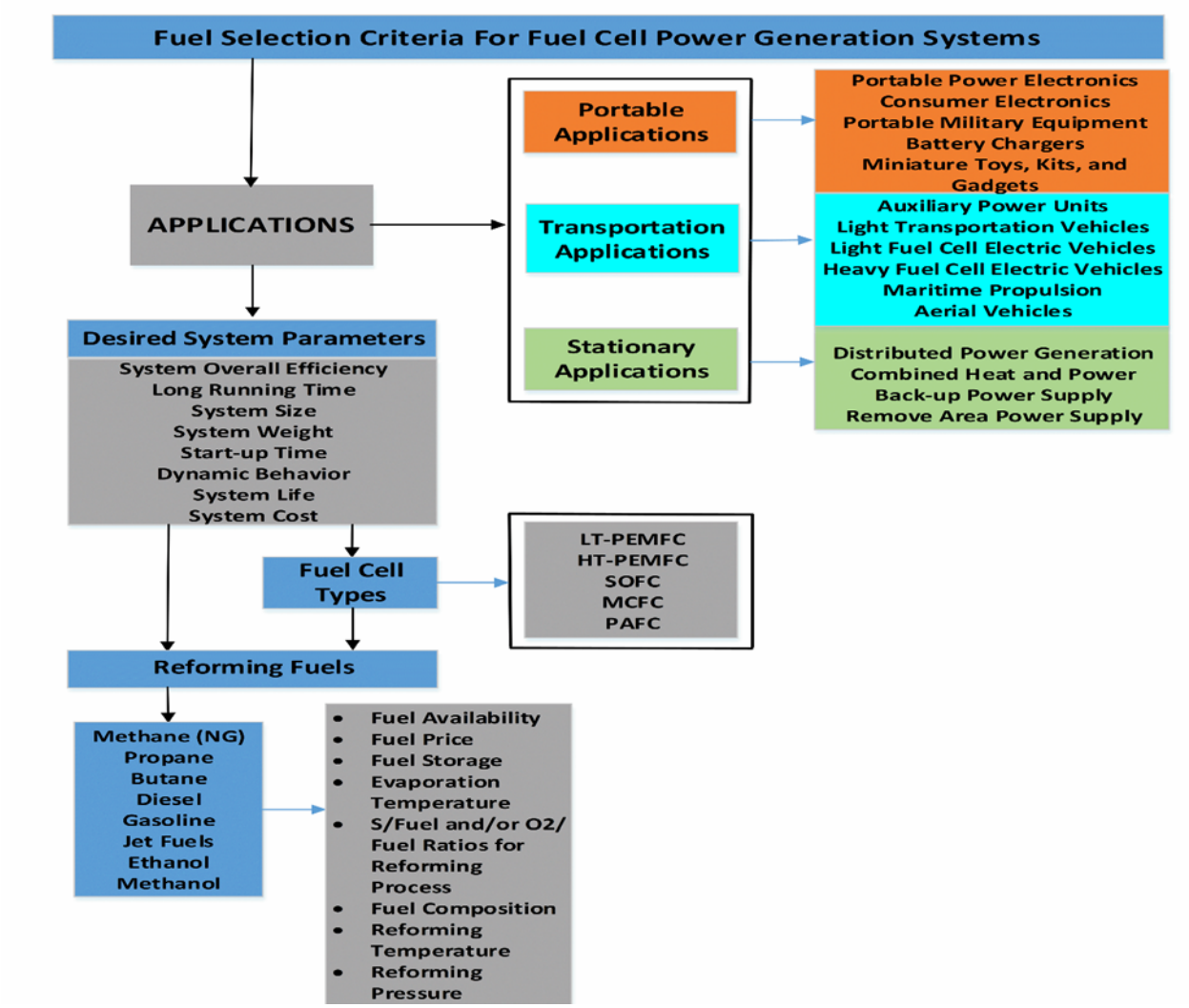

Figure 2-1 Reforming fuel selection criteria for fuel cell power generation systems (Refs. [2,48,59,60]**).**

To decide which fuel can be used for a particular application, different fuel properties such as density, boiling point, energy density, etc. should be considered. The properties and energy densities of various fuels are shown in Table 2-2 and Fig. 2-2, respectively. As seen in Table 2-2, the hydrogen density at gas phase is very low compared to the other fuels. The hydrogen density at 0 ^{o}C and 1 bar is only 0.09 kg m^{-3}. Therefore, its energy density is only equal to 0.0127 MJ/L at 0 ^{o}C and 1 bar. As illustrated in Fig. 2-2, the energy density of the hydrogen significantly increases at high pressures and 25 ^{o}C, and in the liquid phase at very low temperatures. However, its energy

density is still relatively lower than the other fuels. Due to the challenges related to hydrogen storage, hydrogen is not particularly suitable for the systems that need to run for long durations. Not only hydrogen storage but also hydrogen availability is a serious issue regarding usage of pure hydrogen for fuel cell power generation applications. To overcome these problems, reforming of alternative fuels can be used for the production of hydrogen rich syngas to feed a fuel cell.

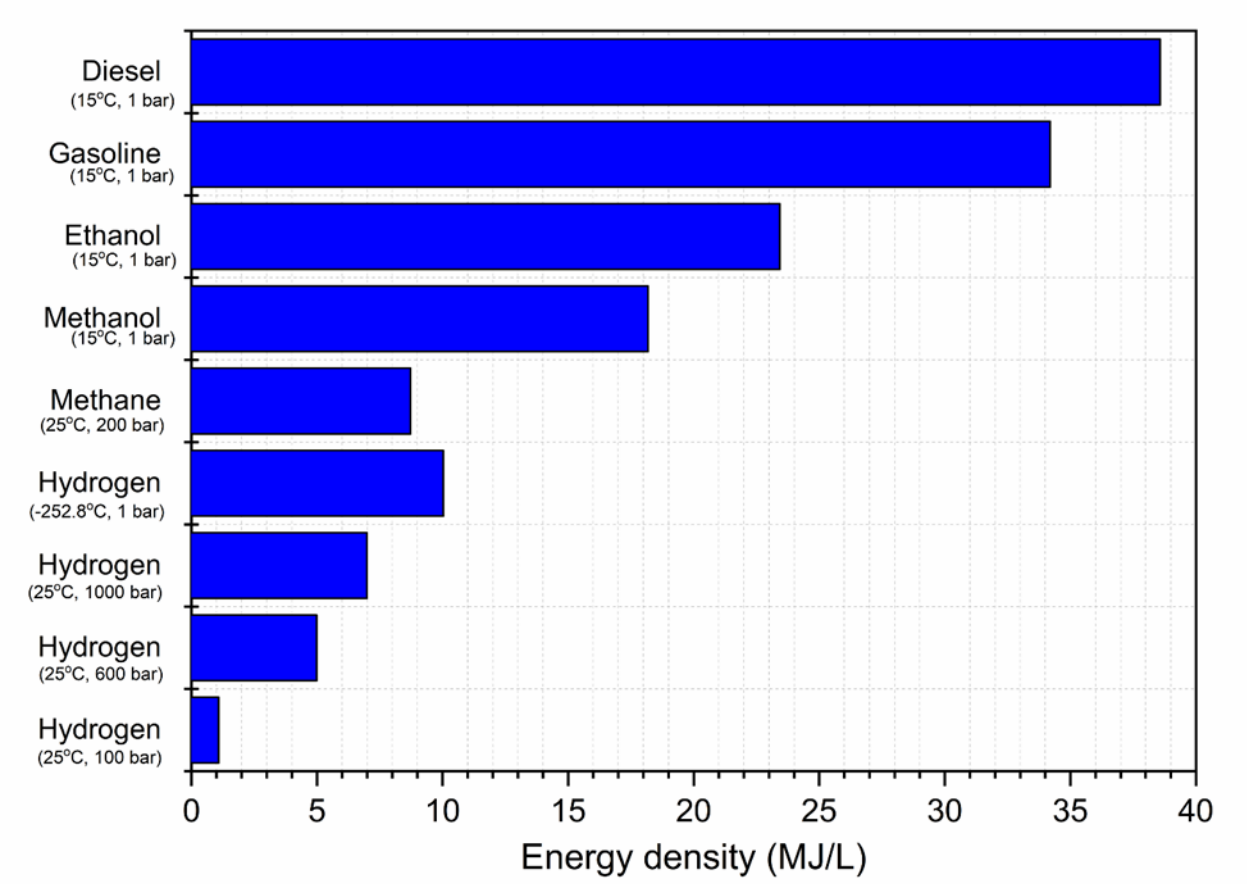

Figure 2-2 Energy density of different fuels. The values calculated by using the heating values and the density values in Table 1. The density values under given conditions on the figure for hydrogen were taken from Ref. [63], and the density under given condition on the figure for methane was taken from Ref. [64]. The energy densities at 0 °C and 1 bar for hydrogen and methane are 0.0127 MJ/L and 0.0397 MJ/L, respectively.

Table 2-2 Comparison of alternative fuels (Data from [6,61,62]**)**

	Hydrogen	**Methane**	**Dimethyl ether**	**Methanol**	**Ethanol**	**Gasoline[*1]**	**Diesel[*1]**
Formula	H_2	CH_4	CH_3OCH_3	CH_3OH	C_2H_5OH	C_7H_{16}	$C_{14}H_{30}$
Density [kg/m^3]	0.09[*2]	0.716[*2]	665	791[*3]	789[*3]	737[*3]	846[*3]
C content wt.%	0	75	52.2	37.5	52.1	86	86
H_2 content wt.%	100	25	13	12.5	13	14	14
LHV [MJ/kg]	120	50	28.62	19.9	26.7	43.4	42.6
HHV [MJ/kg]	141.7	55.5	43	23	29.7	46.4	45.6
Boiling point [°C]	-252.9	-161	-24.9	65	78	30-225	180-340
Sulfur Content (ppm[*4])	0	~7-25	0	0	0	~200	~250

[*1]The properties of these fuels depend on the composition. Average values are given on the table.
[*2] Density at P=1 bar and T=0 °C.
[*3] Density at P=1 bar and T=15 °C.
[*4] Mass basis.

Table 2-3 Impurity tolerances, operating temperatures, and main applications of commonly used fuel cells (Refs. [59, 65-68]).

Impurity Tolerance Levels	LT-PEMFC	HT-PEMFC	PAFC	MCFS	SOFC
CO	Poison (<10 ppm)	Poison (<3% at 180 °C)	Poison (<2% at 200°C)	Fuel	Fuel
CO_2	Diluent	Diluent	Diluent	Re-circulated	Diluent
Sulfur compounds	Poison (<1 ppm)	Poison (<20 ppm)	Poison (<100 ppm)	Poison (<1 ppm)	Poison (<1 ppm)
Other contaminants	Other contaminants should be considered such as halides, trace metals, and nitrogen compounds.				
Operating Temperatures (°C)	60-80	110-180[1]	160-220	600-700	800-1000
Main Application Area	Portable Applications (military and consumer electronics), APUs	APUs, Military portable power needs	Stationary applications, APUs	Stationary applications, APUs	Stationary applications, APUs

One of the most important points that should be considered in choosing a reforming fuel for fuel cell power generation systems is the properties of fuel cell types. To obtain the desired system properties, different fuel cell types are integrated into the system. For example, solid oxide fuel cells (SOFC) are suitable when high efficiency for power and heat generation is desired, while low temperature polymer electrolyte membrane fuel cells (LT-PEMFC) are used when the start-up time is critical for the power generation applications [59]. To select the best suitable reforming fuel for different fuel cell types, impurity tolerance levels of the fuel cells and the operation temperature of the fuel cells should be considered. In Table 2-3, impurity tolerance levels and operation temperatures for different types of fuel cells are shown. As shown in the table, all fuel cell types are sensitive to sulfur compounds. Therefore, sulfur levels must be decreased if the fuel includes sulfur compounds (see Table 2-2). As seen also in Table 2-3, the CO level in the reformate gas must be less than a certain level for some types of fuel cells to prevent poisoning of the fuel cell catalyst. In addition, close or identical reformation temperature and the operation temperature of the fuel cells are significant advantages used to decrease the system complexity.

Thermodynamic analysis is a practical tool to reveal optimum reformation temperature of various fuels and the effects of different operating parameters on the reformate gas composition. Therefore, thermodynamic analysis is commonly used in the literature in order to estimate the effects of reforming temperature, pressure, water-to-feed ratio, and oxygen-to-feed ratio on the equilibrium compositions of reforming processes, as well as to compare the feasibility of reforming various fuels and to obtain fundamental information such as coke formation boundaries and equilibrium conversion regarding different reforming processes. Garcia and Laborde [69] published in 1991 one of the early papers about thermodynamic analysis of the steam reforming of ethanol. Since then, there have been many papers related to thermodynamic analysis of

reforming different types of fuels. These papers are included in, but not limited to studies accomplished by Lutz *et al.* [70, 71] in 2003 and 2004, Ahmed and Krumpelt [72] in 2001, Fishtik *et al.* [73] in 2000, Lwin *et al.* [74] in 2000, Kang and Bae [75] in 2006, Liu *et al.* [76] in 2008, Shi and Bayless [77] in 2008, Authayanun *et al.* [78] in 2010, Li *et al.* [79] in 2011, Wang *et al.* [80] in 2012 and Cui and Kær in 2018 [81]. In these studies, Gibbs free energy minimization method has been commonly used to estimate equilibrium compositions of the reaction systems without requiring specific reactions, reaction kinetics, or catalyst information. For the Gibbs free energy minimization method, only possible components in the product must be defined. The Gibbs free energy minimization can be formulated as [31]:

$$\min_{n_i} \sum_{i=1}^{N} n_i \left(G_i^o(T) + RTln\left(\frac{P}{P_{ref}}\right) + RTln\left(\frac{n_i}{\sum_{j=1}^{N} n_j}\right)\right) \tag{2.1}$$

Specified chemical reactions with equilibrium constants [39, 82] can be used as a second method to estimate the equilibrium composition.

Effects of the reformation temperature and steam to fuel (S/Fuel) ratio (see Eq.2.2) conditions on steam reforming of methane, ethanol, gasoline and diesel (methanol reforming is mentioned in detail in the next section) were investigated in this review paper. The results were published in the literature, reproduced and organized to compare steam reforming of different process to give an overview to the readers.

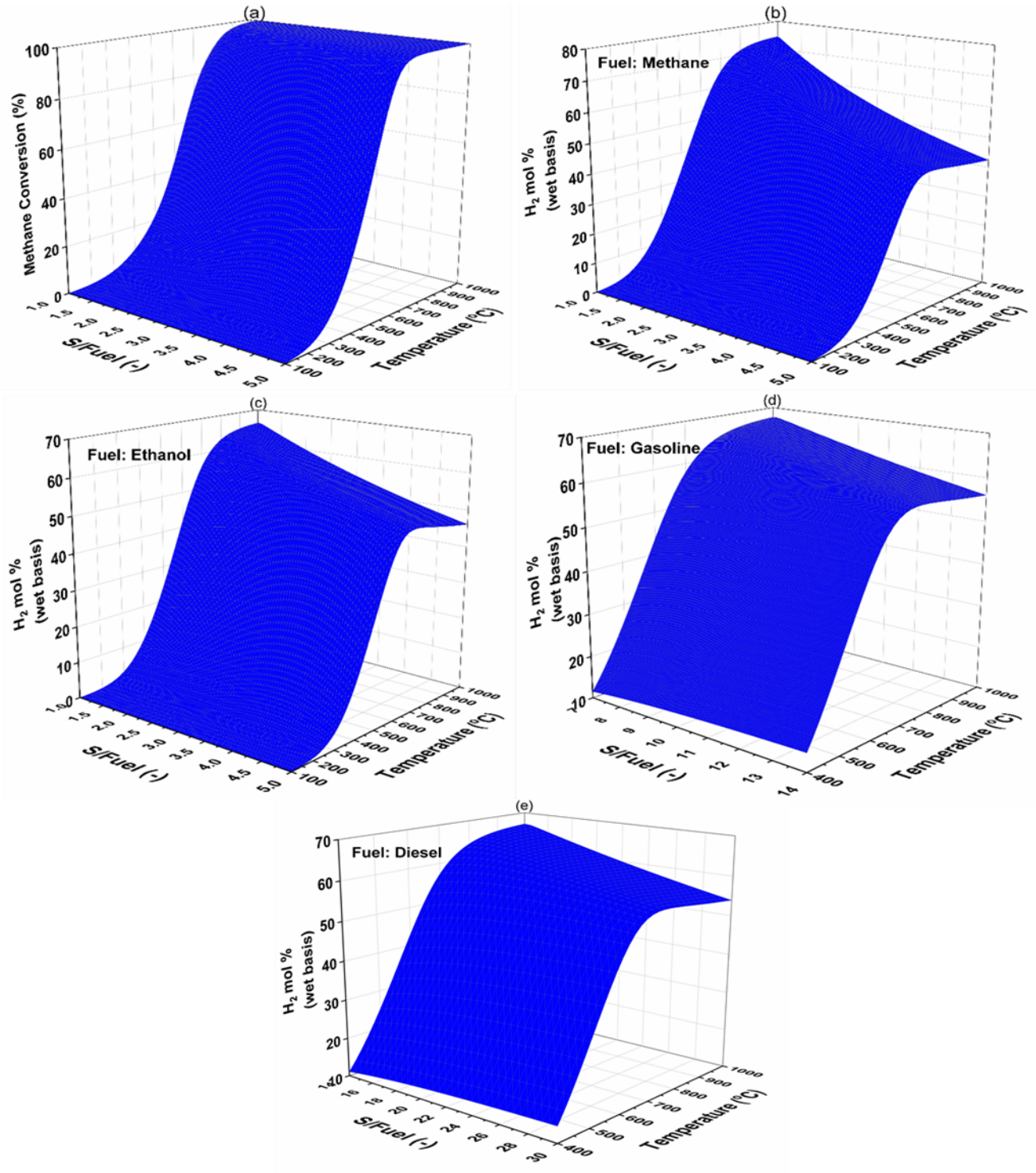

Figure 2-3 Change of the (a) methane conversion, and hydrogen mol % in the reformate gas for steam reforming of (b) methane, (c) ethanol, (d) gasoline, (e) diesel with variation of the S/Fuel ratio and the reformation temperature.

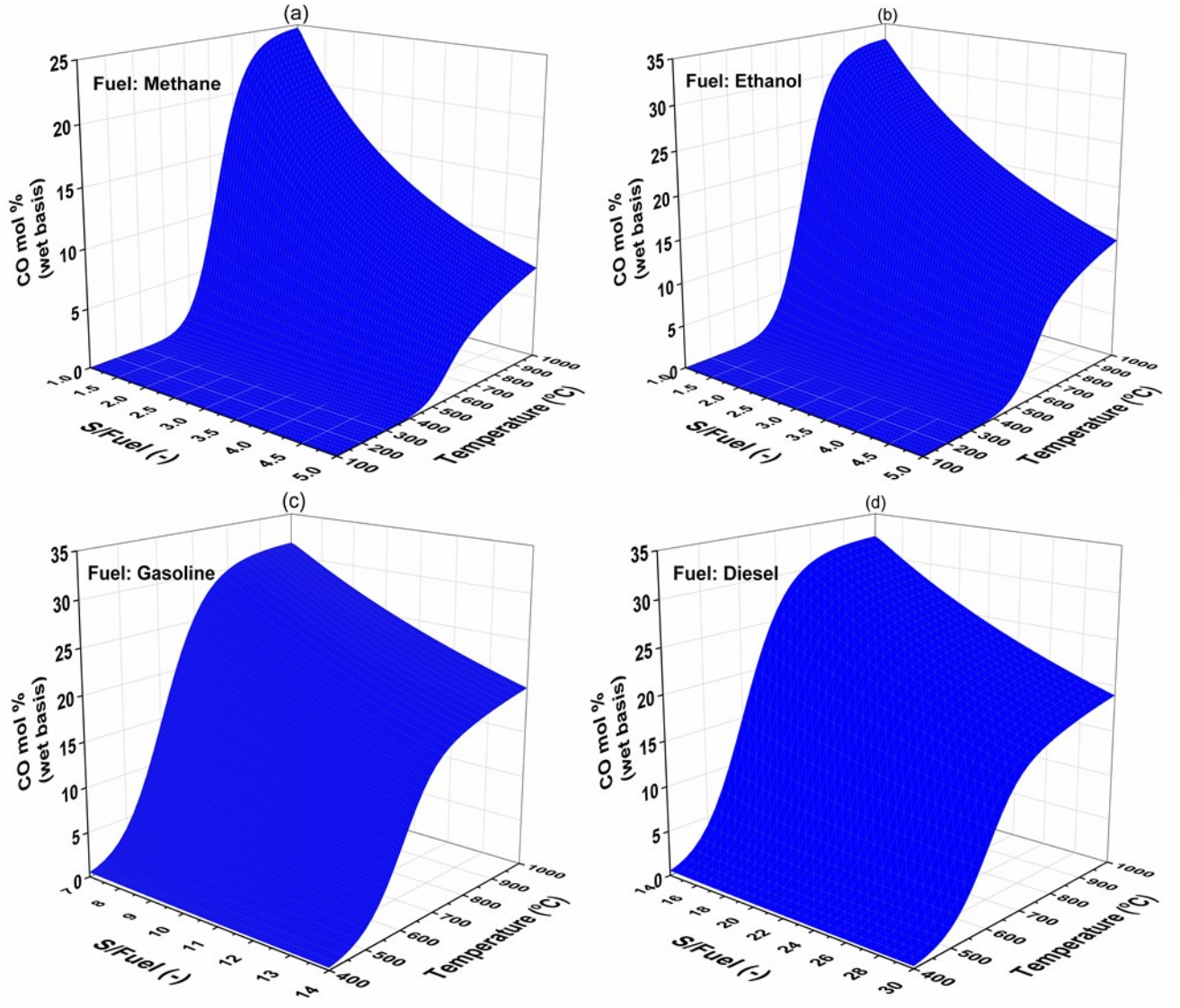

Figure 2-4 Change of the CO mol % in the reformate gas for steam reforming of (a) methane, (b) ethanol, (c) gasoline, and (d) diesel with variation of the S/Fuel ratio and the reformation temperature.

Gibbs free energy minimization method was used to estimate the equilibrium compositions. RGibbs reactor [82] in Aspen Plus [83] was employed for the minimization of Gibbs energy of the system. Fig. 2-3 shows the effects of the temperature and S/Fuel ratio on the methane conversion (Fig. 2-3(a)), and the hydrogen mol. % (wet basis) in the reformate gas for methane (Fig. 2-3(b)), ethanol (Fig. 2-3(c)), gasoline (Fig. 2-3(d)), and diesel (Fig, 2-3(e)). Effects of the

temperature and S/Fuel ratio on the CO mol. % (wet basis) are also illustrated in Fig. 2-4(a)-(d). S/Fuel ratio is defined as consumption of steam per mole of the reforming fuel:

$$\frac{S}{Fuel} = \frac{\dot{n}_{H_2O}}{\dot{n}_{C_xH_yO_z}} \tag{2.2}$$

As seen in the figures, relatively high temperature and S/Fuel ratio is necessary to achieve reforming of methane, ethanol, gasoline and diesel. In particular, the S/Fuel ratio needed to increase the amount of hydrogen in the reformate gas significantly increases for steam reforming of gasoline and diesel. High temperature and S/Fuel ratio are also required to achieve high conversion of methane because the reforming of methane is equilibrium limited. It can be also seen from the figures that the amount of CO in the reformate gas is very high for these fuels.

High reforming temperature and S/Fuel are generally not desired for power generation applications. In particular, they are serious issues for portable power generation applications because the size and complexity of the system increases with increasing reformer temperature and S/Fuel ratio. Therefore, these types of fuels such as natural gas, propane, LPG, and diesel, etc. are generally preferred in the market in the case that the system size and weight are not priority properties for the power generation applications. The information about reforming gas fueled commercial products can be seen in Table 2-4. The reforming of methanol can be achieved at low temperatures and the methanol reformate gas includes very low amounts of CO in the syngas compared to the reforming of various other fuels. In addition, methanol does not include sulfur compounds. Due to these properties of methanol, the methanol reformate gas can be chosen to decrease the size, the weight and the complexity of a fuel cell power generation system.

Table 2-4 Reformate gas-fueled commercial fuel cell systems.

Company	Product Name	Input Fuel	Fuel Cell Type	Net Power Output	Application	Ref.
Bloom Energy	ES-5710	Natural gas, Directed biogas	SOFC	250 kW_e	Commercial distributed power generation, EPS	[84]
EnerFuel	EnerFuel	Natural gas, Propane, LPG	HT-PEMFC	9 kW_e	Stationary applications such as web-based data collection, monitoring and remote control etc.	[85,86]
First Element	Methanol fueled FC power systems	Methanol	LT-PEMFC	From 2.5 to 15 kW_e (depends on the model)	Telecommunications, Railroads, Utilities and critical business IT operations, Distributed electric vehicle charging	[87,88]
UltraCell	XX55™	Methanol	HT-PEMFC	50 W_e (80 W_e peak with battery module)	Radio and satellite communication gear, Remote or mobile surveillance systems, Laptop computers and battery charging	[89,90]
SenerTec	Dachs InnoGen	Natural gas	LT-PEMFC	250-700 W_e, 210-950 W_{th}	Residential and commercial distributed CHP generation	[91]
Helbio	APS5000	Natural gas, Propane, LPG	LT-PEMFC	5 kW_e, 7 kW_{th} (hot water @65ºC)	Residential and commercial distributed CHP generation	[92]
Powercell	PowerCell PP (Prototype)	Diesel	LT-PEMFC	2.5 kW_e	Remote power stations	[93]

2.3 Methanol Reforming

Methanol is the simplest member of a group of organic chemicals and it consists of four parts hydrogen, one part oxygen and one part carbon. Currently, natural gas is used as a primary feedstock to produce methanol [94]. However, it can also be produced renewable sources such as municipal solid wastes (MSW), renewable electricity and waste CO_2 [95]. Various feedstocks, methanol production pathways, and the methanol market are shown in Fig. 2-5. As illustrated in Fig. 2-5, methanol has a large and diverse market potential. It can be used for the production of various chemical products, different fuels, and hydrogen.

Methanol is not preferred for central hydrogen production because of its relatively high cost compared to natural gas. The methanol price is approximately 4 times higher than natural gas [9]. Although methanol is not affordable for central hydrogen production, there are some advantages of hydrogen production from methanol by employing different reforming processes for some niche applications. One of the most important advantages of methanol reforming is that methanol reforming processes are easier than natural gas reforming processes. MSR can be achieved at less than 300 ^{o}C [102-105] while natural gas reforming can be achieved at around ~900 ^{o}C [9]. Oxidative steam reforming of methanol (OSRM) can also be achieved at relatively lower temperatures than natural gas and the other alternative fuels. Over 99% methanol conversion at around 350 ^{o}C has been reported for OSRM [106]. Other advantages of hydrogen production from methanol reforming are that methanol is sulfur free, and hydrogen rich methanol reformate gas includes only small amounts of CO. Furthermore, methanol can be easily stored because it is in a liquid phase under most environmental conditions.

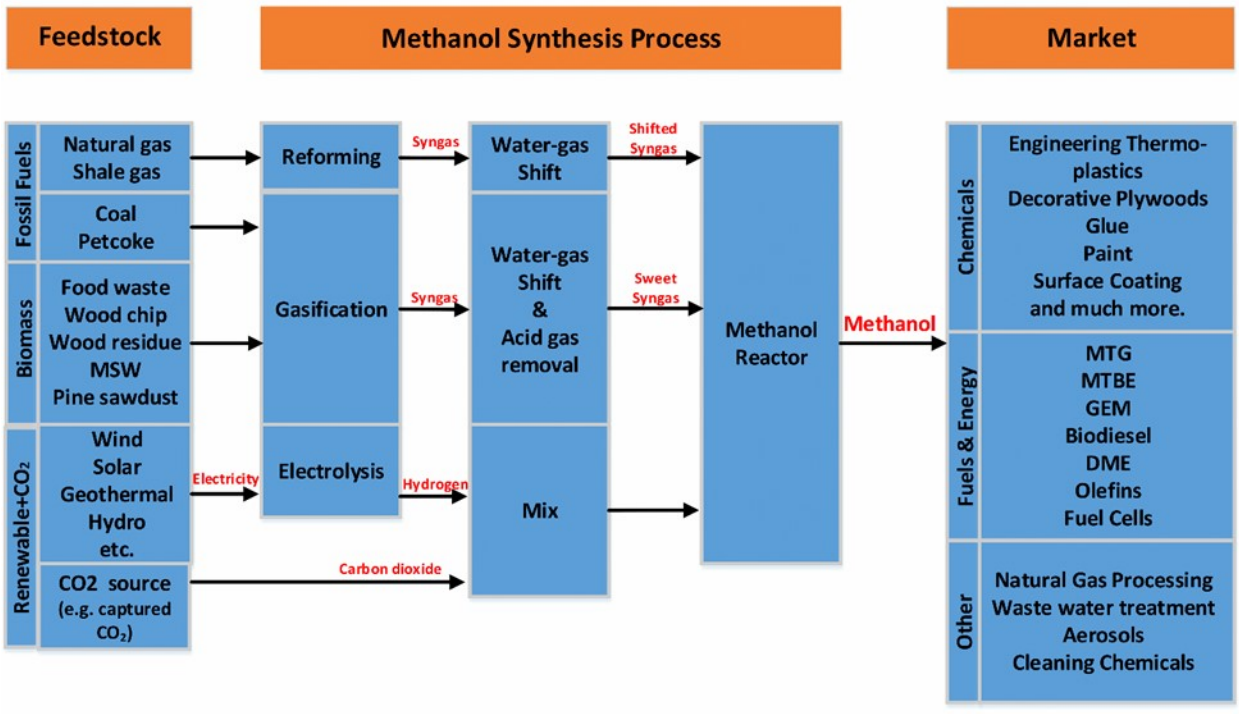

Figure 2-5 Methanol production and methanol usage in the market Refs. [95-101].

Due to the advantages of hydrogen production from methanol reforming, attention to studies related to methanol reforming has increased in recent years. Overall, the studies related to methanol reforming can be classified as reforming reactions kinetics and catalysis, reforming reactors, and studies relating to methanol reformate gas fuel cell systems. These studies are explained in detail in the following sections.

2.3.1 Effects of Important Operating Parameters on Methanol Reforming

The important parameters that affect the performance of methanol reformers can be listed as the reformer temperature (T_{ref}), steam to methanol (S/Methanol) ratio (some researchers use steam to carbon (S/C) ratio instead of S/Methanol ratio), and oxygen to methanol (O_2/Methanol) ratio (some researchers use oxygen to carbon O_2/C ratio (see Eq. 2.5) instead of O_2/Methanol). S/Methanol ratio and O_2/Methanol ratio can be defined as:

$$\frac{S}{Methanol} = \frac{S}{C} = \frac{\dot{n}_{H_2O}}{\dot{n}_{CH_3OH}} \quad (2.3)$$

$$\frac{O_2}{Methanol} = \frac{\dot{n}_{O_2}}{\dot{n}_{CH_3OH}} \quad (2.4)$$

$$\frac{O}{C} = \frac{2\dot{n}_{O_2}}{\dot{n}_{CH_3OH}} \quad (2.5)$$

Table 2-5 Different cases in the estimation of thermodynamically feasible products for methanol reforming [74, 80, 107, 108].

Case-1	H_2O, H_2, CO, CO_2, CH_3OH, C
Case-2	H_2O, H_2, CO, CO_2, CH_3OH, $HCOOH_3$, CH_3OCH_3, HCHO, HCOOH
Case-3	H_2O, H_2, CO, CO_2, CH_3OH, $HCOOH_3$, CH_3OCH_3, HCHO, HCOOH, CH_4
Case-4	H_2O, H_2, CO, CO_2, CH_3OH, $HCOOH_3$, CH_3OCH_3, HCHO, HCOOH, C
Case-5	H_2O, H_2, CO, CO_2, CH_3OH, $HCOOH_3$, CH_3OCH_3, HCHO, HCOOH, CH_4, C
Case-6	H_2O, H_2, CO, CO_2, CH_3OH, $HCOOH_3$, CH_3OCH_3, HCHO, HCOOH, CH_4, C, C_2H_6, C_3H_8, i-C_4H_{10}, n-C_4H_{10}, C_2H_5OH, C_3H_7OH, i-C_4H_9OH, n-C_4H_9OH, C_2H_6O
O_2 and N_2 are added into the products for OSRM.	

To understand the effects of the reformation temperature, S/Methanol and O_2/Methanol on the equilibrium compositions of the methanol reforming gas, some researchers such as Lwin *et al.* [74], Faungnawakij *et al.* [107], Wang and Wang [108], and Wang *et al.* [80], have performed thermodynamic analysis of methanol reforming. The main products in the syngas for methanol reforming are hydrogen, carbon dioxide, carbon monoxide and water. However, other products such as methane, formic acid, etc. can exist in the syngas. In addition, defining the optimal parameters to prevent coke formation is very important. Therefore, different product sets can be used to investigate the effects of the parameters on the production of the thermodynamically possible products. Different product sets that can be used in Refs. [74, 80, 107, 108] for thermodynamic analysis of MSR and OSRM are shown in Table 2-5.

We can summarize the general conclusions from these studies [74, 80, 107, 108] as: almost 100% methanol conversion can be obtained at different temperature ranges, so the methanol

reforming is not thermodynamically limited; the H_2 production rate can be increased with an increase in the reforming temperature because the methanol steam reforming (R.2.13) and decomposition reactions (R.2.15) are very endothermic; also, the CO content in the reformate gas increases with the elevated temperatures because of the water gas shift (WGS) reaction (R.2.14) which is exothermic exhibiting decreased CO conversion with increased reaction temperature; and the H_2 production dramatically decreases for oxidative methanol and partial oxidation reforming with increased O_2/Methanol because methanol partial oxidation is the dominant reaction for the high O_2/Methanol ratio. Although H_2 production decreases with oxidative methanol reforming, coke formation is reduced for OSRM. Furthermore, the energy demand for the methanol reforming is decreased by using oxygen with steam. The energy demand can also be equal to zero in the case of using a certain amount of O_2/Methanol ratio, and it is called autothermal methanol reforming. The OSRM is investigated in Refs. [80, 108]; however, the autothermal situation is not exactly explained by only considering the reactant temperature. Therefore, the hydrogen mol. % and the oxygen requirement for two different scenarios to achieve autothermal reforming of methanol are investigated using Aspen Plus v8.8 [83] in this work.

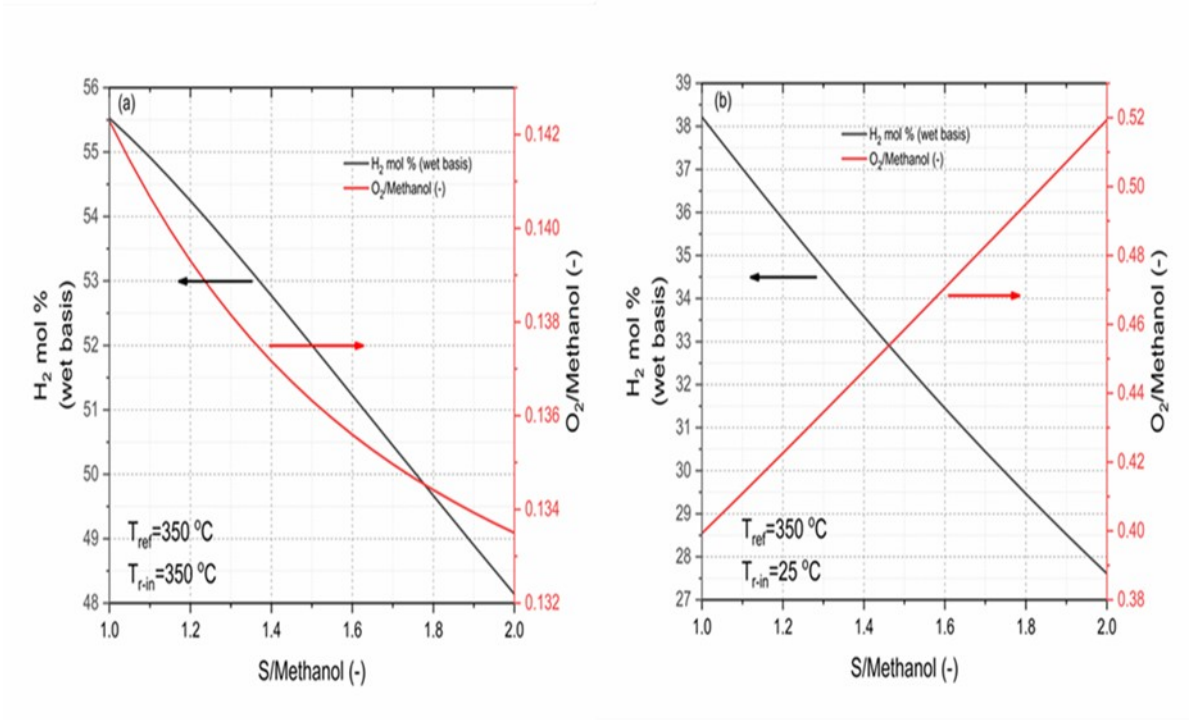

Figure 2-6 O_2/Methanol ratio and H2 mol % for autothermal reformation of methanol. (a) The reactants inlet temperature are equal to 350 ºC, (b) the reactants inlet temperature are equal to 25 ºC. The reformation temperature is 350 ºC for (a) and (b). The results are found for Case-2 (see Table 2-5).

Figs. 2.6(a) and (b) show the change of the hydrogen mol. % (wet basis) for autothermal methanol reforming. To obtain the results, the reformation of temperature is taken as 350 ºC while the S/Methanol ratio changes from 1 to 2. The amount of oxygen is calculated to achieve a thermal neutral situation with a certain amount of the S/Methanol ratio. Here, two scenarios are considered for the autothermal situation. For the first scenario (Fig. 2.6(a)), the O_2/Methanol ratio is found to achieve a thermal neutral situation for the reforming of methanol at 350 ºC. It is assumed that the reactant temperature is also equal to 350 ºC, and there is no energy demand to increase temperature of the reactants. For the other scenario (Fig. 2.6(b)), the energy requirement to increase the temperature of the reactants from 25 to 350 ºC are considered for the autothermal reforming of methanol. As shown from the figures, the hydrogen production dramatically decreases for the

second scenario (Fig. 2.6(b)) while the oxygen requirement is significantly increased compared to the first scenario (Fig. 2.6(a)). The complexity and the start-up of a system that uses methanol reformate gas can be decreased for the second scenario. On the other hand, the system efficiency must be considered to decide the final operation conditions.

From a thermodynamic point of view, we can reach these conclusions: (1) elevated temperatures and higher S/Methanol ratio are favorable for methanol reforming; and (2) the coke formation and energy demand of the reformation process can be decreased by using oxygen with steam. However, the type of catalysts and reformers that are used for the methanol reforming, and the desired system properties, should be considered for final selection of the operation parameters.

2.3.2 Methanol Reforming Catalysis and Reaction Kinetics

In this section, we focus on the effects of different methanol catalysts on methanol conversion as well as H_2 and CO yields in the reformate gas. In addition, we summarize the studies regarding methanol reforming reaction kinetics. The preparation methods of the catalysts, and the reaction mechanisms are beyond the scope of this review paper. The preparation methods can be found in Refs. [46, 107-110], and the reaction mechanisms are also available in Refs. [47, 51].

A methanol reforming catalyst should have high catalytic activity in order to achieve high methanol conversion and large amounts of H_2 production; also, it should be highly selective so that the CO generation can be decreased. In addition, the catalyst should have long term stability [46]. Many researchers have commonly studied Cu/ZnO based catalysts for methanol reforming because of their high activity at low temperatures and the fact that they favour the production of H_2 with low selectivity towards CO [47, 11]. In particular, H_2 and CO formation, methanol conversion, and deactivation of the commercially available Cu/ZnO-Al_2O_3 catalyst for methanol

reforming have been widely investigated in the literature [112-121]. Agrell *et al.* [117] studied MSR over a commercial $Cu/ZnO/Al_2O_3$ catalyst from Sud-Chemie (G-66 MR) in the temperature range between 175 and 350 ^oC. They observed 100% methanol conversion, and the H_2 mol ratio in the reformate gas was 70% (dry basis) at about 320 ^oC for $H_2O/CH_3OH=1.3$. Agarwal *et al.* [121] investigated the activity and deactivation of $Cu/ZnO/Al_2O_3$ catalysts for the MSR with the variation of the temperature from 220 to 300 ^oC at atmospheric pressure in a fixed bed reactor. They also used different $Cu/ZnO/Al_2O_3$ catalysts, whose properties are shown in Table 2-6. Their study revealed that the highest catalyst activity was obtained using CAT4 with a composition of $Cu/ZnO/Al_2O_3$ as 10/5/85 (wt.%). In addition, the lowest methanol conversion was found for CAT1 which includes 10% copper and no zinc oxide. Therefore, their results showed that the promoter zinc has a positive effect on the catalytic activity. Also, their results revealed that the CO yield in the reformate gas is less than the equilibrium values, based on the thermodynamics for water gas shift (WGS) reaction, at all reaction temperatures. The reason for less CO than the equilibrium values can be the formation of the CO_2 through a path other than (WGS) reaction. Also, they found that the deactivation of $Cu/ZnO/Al_2O_3$ catalysts to be a serious issue. Although the methanol conversion was 78% at 300 ^oC for the fresh catalyst, the conversion decreased to 67% for a run time of 20 h. The deactivation of the catalyst was later explained by the rate of coke formation, in particular at high reaction temperatures with low S/C.

Table 2-6 Specifications of different catalysts (adapted from Ref. [121].).

	CAT1	CAT2	CAT3	CAT4	CAT5	CAT6	CAT7
$Cu/ZnO/Al_2O_3$	10/0/90	3/12/85	5/10/85	10/5/85	10/7/83	12/6/82	15/7/78
Cu/Zn (Wt.%)	10/0	3/9.6	5/8	10/4	10/5.6	12/4.8	15/5.6
Final elemental catalyst composition Cu/Zn (Wt%)	9.1/0	2.7/8.9	4.1/6.8	9.2/3.6	8.9/4.3	10.6/3.4	13.4/4.3
Total pore volume (cc/g)	0.36	0.25	0.28	0.35	0.34	0.32	0.21
Average pore diameter (Å)[1)]	75	53	54	64	61	59	52
S_{BET} (m^2/g)	148	132	136	158	151	141	129

[1)] Angstrom 10^{-10} meter

As mentioned in the previous study (Ref. [121]), the deactivation of $Cu/ZnO/Al_2O_3$ catalysts is an important problem, which requires further analysis. Therefore, Patel & Pant [122] showed the advantages of Cerium (Ce) as a promoter in the catalyst to improve the activity and the stability of $Cu/ZnO/Al_2O_3$ catalysts. For the MSR, the cerium promoter increased the methanol conversion and H_2 selectivity as well as decreased the catalyst deactivation. Also, the CO formation in the products that were obtained was very low. The results showed that the CO ratio in the reformate gas was only 0.09 mol% at S/C=1.8 and 260°C for the Cu-Zn-Ce-Al oxide catalyst. Furthermore, the methanol conversion for the Cu-Zn-Ce-Al oxide catalyst decreased by 3% within a 20 h run-time while it decreased 14% for the $Cu/ZnO/Al_2O_3$ catalyst. Patel & Pant [123] also studied the OSRM using ceria promoted copper- alumina catalysts. Almost 100% methanol conversion was achieved for the Cu-Ce-Al catalyst with the weight percentage 30%-Cu, 20%-Ce, and 50%-Al at 280 °C; in addition, only 0.19% CO was observed. The researchers also found that the CO formation changed from 1000 ppm to 2300 ppm with the variation of the reaction temperature from 200 to 300 °C while the contact time, the oxygen-to-methanol (O/M) and the S/C ratio were equal to 15 $kg_{cat}\,smol^{-1}$, 0.15 and 1.5, respectively.

The CO level in the reformate gas is very important because PEMFCs which are commonly used in the market are very sensitive to CO as shown in Table 2-3. The change in the theoretical product composition based on thermodynamic equilibrium calculations (using Gibbs free energy minimization method) in the methanol reformate gas as a function of the reformation temperature is shown in Fig. 2-7. As seen, the CO dramatically decreases with the decrease of reformate temperature. Therefore, methanol reforming catalysis activity at low temperatures is significant to achieve a low level of CO in the reformate gas. Yu *et al.* [124] showed the high-quality H_2 production from methanol steam reforming using the $CuZnGaO_x$ catalyst at 150 ^oC with no detectable CO.

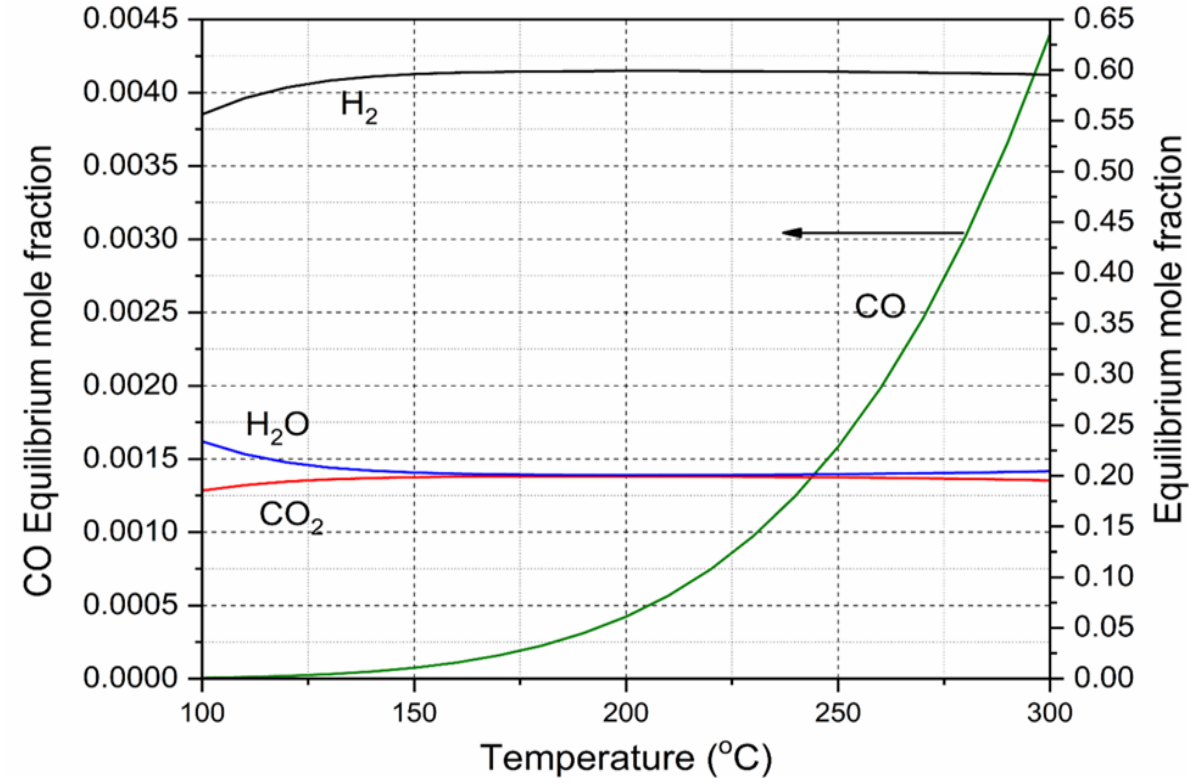

Figure 2-7 Variation of the methanol reformate gas composition as a function of temperature. CH_3OH: H2O=1:2 (1 mole methanol + 2 moles water). Calculations performed with the Aspen Plus v8.8 [83]**.**

Methanol reforming catalysis activity at low temperatures is also important because the methanol reformer, which operates at low temperatures, can be integrated into the anodic compartment of a high temperature PEM fuel cell (HT-PEMFC) [125-128]. Papavasiliou *et al.* [129] investigated CuMnOx catalysts for internal reforming methanol fuel cells. Their results showed that CuMnOx is a very efficient methanol steam reforming catalyst to use in the anodic compartment of a HT-PEMFC.

An increasing order of stability for the metals was reported by Hughes as: Ag<Cu<Au<Pd<Fe<Ni<Co<Pt<Rh<Ru<Ir<Os<Re [130]. Therefore, thermal sintering is also an important issue for the Cu based catalyst, and it is not stable at higher temperatures, e.g., >270 ºC [44]. Pd-Zn alloy catalysts have been investigated [131-135] as an alternative to Cu based catalysts because of the problems mentioned regarding Cu based catalysts. The results in Refs. [110,131] showed that Pd-Zn alloy based catalysts perform low selectivity to CO for MSR and have higher catalytic activity. Also, Dagle *et al.* [135] reported that the thermal sintering was not observed on the PdZnAl catalyst for 100 h time-on-stream at a temperature of 360 ºC.

Although Pd-Zn alloy catalysts have high activity, low selectivity, and exhibit more stability, the sensitivity of the Pd-Zn alloy catalysts to the preparation technique always involves the danger of metallic palladium formation, leading to the generation of large quantities of carbon monoxide [113]. To solve this problem, $Pd/In_2O_3/Al_2O_3$ [136] and $Pt/In_2O_3/Al_2O_3$ [137] catalysts were investigated as an alternative. Kolb *et al.* [137] compared novel $Pd/In_2O_3/Al_2O_3$ and $Pt/In_2O_3/Al_2O_3$ catalysts coated onto the micro-channels for methanol steam reforming. They found that the Pt catalyst was much more active than the Pd catalyst and its CO selectivity was still moderate compared to Pd. Two catalysts containing 15 wt. % Pt and Pd, respectively and 30

wt. % In_2O_3 were used for the MSR at S/C of 1.5 and it was found that the full methanol conversion temperature was observed than ~100 ºC lower reaction temperature for the Pt catalyst.

Studies regarding methanol reforming kinetics are summarized in Table 2-7. As shown in the table, researchers have generally worked on the kinetics of Cu based catalysts for MSR. One of the early papers from Peppley *et al.* [138], which is about the kinetic model of MSR on $Cu/ZnO/Al_2O_3$ catalysts, has been highly cited in the literature. Peppley *et al.* [138, 149] investigated reaction mechanisms and developed a comprehensive kinetic model based on analysis of the surface mechanism for MSR. They used three overall reactions, which are MSR (R.2.13), WGS (R.2.14), and methanol decomposition (MD) (R.2.15) in their kinetic analysis. The three reactions can be written as follows:

$$CH_3OH + H_2O \underset{-k_R}{\overset{k_R}{\rightleftharpoons}} CO_2 + 3H_2 \quad \text{(R.2.13)}$$

$$CO + H_2O \underset{-k_W}{\overset{k_W}{\rightleftharpoons}} CO_2 + H_2 \quad \text{(R.2.14)}$$

$$CH_3OH \underset{-k_D}{\overset{k_D}{\rightleftharpoons}} CO + 2H_2 \quad \text{(R.2.15)}$$

Power rate laws have also been used to explain the rate expressions. For example, Purnama *et al.* [120] used power laws by fitting the experimental data to develop rate expressions for steam reforming and water gas shift reactions. Wichert *et al.* [147] recently studied the kinetics of MSR over bimetallic $Pt/In_2O_3/Al_2O_3$ catalyst. They created two power laws and three Langmuir-Hinshelwood rate expressions for the modelling of the kinetic data. Their results revealed that the power rate laws were not suitable for the kinetic modelling of the $Pt/In_2O_3/Al_2O_3$ catalyst.

In general, the studies mentioned in this section regarding methanol reforming catalysis and reaction kinetics have focused on the investigation of catalyst activity and stability and finding accurate reaction rate expressions for different types of catalysts.

Table 2-7 Reaction rate expressions for methanol reforming for different catalysts and reforming processes.

Catalyst	Reforming Process	Rate Expression	Ref.
$Cu/ZnO/Al_2O_3$	MSR	$r_{SR} = \frac{k_R K^*_{CH_3O^{(1)}}\left(p_{CH_3OH}/p_{H_2}^{1/2}\right)\left(1-\left(p_{H_2}^3 p_{CO_2}/K_R p_{CH_3OH} p_{H_2O}\right)\right) C_{S_1}^T C_{S_{1a}}^T}{\left(1+K^*_{CH_3O^{(1)}}\left(p_{CH_3OH}/p_{H_2}^{1/2}\right)+K^*_{HCOO^{(1)}} p_{CO_2} p_{H_2}^{1/2}+K^*_{OH^{(1)}}\left(p_{H_2O}/p_{H_2}^{1/2}\right)\right)\left(1+K_{H^{(1a)}}^{1/2} p_{H_2}^{1/2}\right)}$ $r_{WGS} = \frac{k_W^* K^*_{OH^{(1)}}\left(p_{CO} p_{H_2O}/p_{H_2}^{1/2}\right)\left(1-\left(p_{H_2} p_{CO_2}/K_W p_{CO} p_{H_2O}\right)\right) C_{S_1}^{T^2}}{\left(1+K^*_{CH_3O^{(1)}}\left(p_{CH_3OH}/p_{H_2}^{1/2}\right)+K^*_{HCOO^{(1)}} p_{CO_2} p_{H_2}^{1/2}+K^*_{OH^{(1)}}\left(p_{H_2O}/p_{H_2}^{1/2}\right)\right)^2}$ $r_D = \frac{k_D K^*_{CH_3O^{(2)}}\left(p_{CH_3OH}/p_{H_2}^{1/2}\right)\left(1-\left(p_{H_2}^2 p_{CO}/K_D p_{CH_3OH}\right)\right) C_{S_2}^T C_{S_{2a}}^T}{\left(1+K^*_{CH_3O^{(2)}}\left(p_{CH_3OH}/p_{H_2}^{1/2}\right)+K^*_{OH^{(2)}}\left(p_{H_2O}/p_{H_2}^{1/2}\right)\right)\left(1+K_{H^{(2a)}}^{1/2} p_{H_2}^{1/2}\right)}$	[121,138]
CuO/ZnO	OSRM	$-R_{CH_3OH} = k_o \exp(-E_a/RT)\, p_{methanol}^{0.18} p_{O_2}^{0.18}/p_{H_2O}^{0.14}$	[115,139]
$CuO/ZnO/Al_2O_3$	MSR	$r_{SR} = k_1 p_{CH_3OH}^m p_{H_2O}^n$ $r_{RWGS} = k_2 p_{CO_2} p_{H_2} - k_{-2} p_{H_2O} p_{CO}$	[120]
$Cu/ZnO/Al_2O_3$	MSR	$-r_M = 2.19 \times 10^9 \exp\left(-103 \frac{kJ}{mol}/RT\right) p_M^{0.564} (11.6\ kPa + p_H)^{-0.647}$	[140]
$Cu/ZrO_2/CeO_2$	MSR	$r_{SR} = k_R p_{MeOH}^{m_1} p_{H_2O}^{m_2} - k_{-R} p_{CO_2}^{m_3} p_{H_2}^{3m_4}$ $r_D = k_D p_{MeOH}^{m_5}$ $r_{RWGS} = k_{-W} p_{CO_2}^{m_6} p_{H_2}^{m_7} - k_W p_{CO}^{m_8} p_{H_2O}^{m_9}$	[141]
Cu-Mn spinel oxide	MSR	$-r_{MeOH} = k_0 \exp(-E/RT)\, p_{MeOH}^a p_{H_2O}^b$	[142]

$CuO/ZnO/Al_2O_3$	MSR	$r_{SR} = \frac{k_{SR} K_{CH_3O^{(1)}} p_{CH_3OH} / p_{H_2}^{1/2} \left(1 - p_{H_2}^3 p_{CO} / K_{SR} p_{H_2O} p_{CH_3OH}\right)}{\left(1 + K_{CH_3O^{(1)}} p_{CH_3OH} / p_{H_2}^{1/2} + K_{OH^{(1)}} p_{H_2O} / p_{H_2}^{1/2} + K_{HCOO^{(1)}} p_{H_2}^{1/2} p_{CO_2}\right)\left(1 + \sqrt{K_{H^{(1a)}} p_{H_2}}\right)}$ $r_{RWGS} = \frac{k_{RWGS} K_{HCOO^{(1)}} P_{CO_2} P_{H_2}^{1/2} \left(1 - p_{H_2O} p_{CO} / K_{RWGS} p_{CO_2} p_{H_2}\right)}{\left(1 + K_{CH_3O^{(1)}} p_{CH_3OH} / p_{H_2}^{1/2} + K_{OH^{(1)}} p_{H_2O} / p_{H_2}^{1/2} + K_{HCOO^{(1)}} p_{H_2}^{1/2} p_{CO_2}\right)^2}$	[143]
Pd/ZnO	MSR	$-r_A = 2.9047 \times 10^{10} e^{-94800/RT} p_{MeOH}^{0.715} p_{H_2O}^{0.088}$	[144]
Pd/Zn	MSR	$-R_{methanol} = \frac{k_s K_{Me,Ads} c_{Me}}{(1 + K_{Me,Ads} c_{Me} + \sqrt{c_{H_2} / K_{H_2,Des}})^6}$	[145]
$Cu/ZnO/CeO_2/Al_2O_3$	OSRM	$r_{POM} = \frac{k_{POM} K_{CH_2O^{(1)}} K_{O^{(1)}} \left(p_{CH_3OH} p_{O_2}^{1/2} / p_{H_2}\right)\left[1 - \left(p_{H_2}^2 p_{CO_2} / K_{POM}^* p_{CH_3OH} p_{O_2}^{1/2}\right)\right]}{\left[1 + K_{CH_2O^{(1)}} p_{CH_3OH} / p_{H_2} + K_{OH^{(1)}} p_{H_2O} / p_{H_2}^{\frac{1}{2}} + K_{O^{(1)}} p_{H_2O} / p_{H_2} + K_{HCOOH^{(1)}} p_{CH_3OH} p_{H_2O} / p_{H_2}^2 + K_{HCOO^{(1)}} p_{H_2}^{\frac{1}{2}} p_{CO_2}\right]^2 \left[1 + K_{H^{(1a)}} p_{H_2}^{\frac{1}{2}}\right]}$ $r_{SR} = \frac{k_{SRM} K_{HCOOH^{(1)}} \left(p_{CH_3OH} p_{H_2O} / p_{H_2}^2\right)\left[1 - \left(p_{H_2}^3 p_{CO_2} / K_{SRM}^* p_{CH_3OH} p_{H_2O}\right)\right]}{\left[1 + K_{CH_2O^{(1)}} p_{CH_3OH} C_{S_1} / p_{H_2} + K_{OH^{(1)}} p_{H_2O} / p_{H_2}^{\frac{1}{2}} + K_{O^{(1)}} p_{H_2O} / p_{H_2} + K_{HCOOH^{(1)}} p_{CH_3OH} p_{H_2O} / p_{H_2}^2 + K_{HCOO^{(1)}} p_{H_2}^{\frac{1}{2}} p_{CO_2}\right]\left[1 + K_{H^{(1a)}} p_{H_2}^{\frac{1}{2}}\right]}$ $r_{RWGS} = \frac{k_{rWGS} K_{HCOO} \left(p_{H_2}^{\frac{1}{2}} p_{CO_2}\right)\left[1 - \left(p_{H_2O} p_{CO} / K_{RWGS}^* p_{H_2} p_{CO_2}\right)\right]}{\left[1 + K_{CH_2O^{(1)}} p_{CH_3OH} / p_{H_2} + K_{OH^{(1)}} p_{H_2O} / p_{H_2}^{\frac{1}{2}} + K_{O^{(1)}} p_{H_2O} / p_{H_2} + K_{HCOOH^{(1)}} p_{CH_3OH} p_{H_2O} / p_{H_2}^2 + K_{HCOO^{(1)}} p_{H_2}^{\frac{1}{2}} p_{CO_2}\right]^2}$	[146]
$Pt/In_2O_3/Al_2O_3$	MSR	$r = \frac{k_s n_z (n_z - 1) K_{CH_3OH} K_{H_2O} p_{CH_3OH} p_{H_2O}}{(1 + \sqrt{K_{CH_3OH} p_{CH_3OH}} + K_{H_2O} p_{H_2O})^3}$	[147]
$CuO/ZnO/Ga_2O_3$	MSR	$r_{MSR} = 8.51 \times 10^8 e^{-90800/RT} p_{MeOH}^{0.37} p_{H_2O}^{1.35} p_{H_2}^0 p_{CO_2}^0$	[148]

2.3.3 Methanol Reformers

According to the catalyst deployment in the reformers, methanol reformers can be classified as packed-bed and wash-coated reformers. These types of reformers have been commonly investigated in the literature. In addition, membrane reformers have been actively studied, although there are some serious issues related to their commercialization.

Karim *et al.* [150] studied nonisothermality in packed bed reactors for MSR to define the reactor dimensions to achieve isothermal conditions. The temperature profiles of the packed bed reactors were calculated with the variation of the internal diameters of the packed bed reactors by using an experimental study and 2D pseudo-homogeneous model in their study. The results of this study showed that the temperature gradients increased with increasing internal diameter (i.d) of the reactor. In addition, the results revealed that the reactor i.d should be close to 300 μm to achieve isothermal conditions in packed bed reactors.

Chein *et al.* [151] performed a numerical study to understand the effects of heat transfer on a circular reformer with a partially (which is the wall-coated reformer) or entirely filled (which is the packed bed reformer) catalyst layer. The main finding of their study was that a higher MSR temperature could be obtained using a partially filled catalyst layer compared to the packed bed reformer. Therefore, the methanol conversion could be increased for the partially filled catalyst layer.

A packed bed reformer to produce 100 W power by employing a PEMFC was modeled by Vadlamudi and Palanki [152]. They performed a parametric study to reveal the effects of S/M, inlet pressure and temperatures on the reformer.

An internally heated tubular packed bed methanol steam reformer was studied experimentally and numerically by Nehe *et al.* [153]. They used an internally heated tubular reactor to prevent heat loss, and so to supply effective heat transfer to the endothermic MSR reactions. Their results showed that for the same operating conditions, higher methanol conversion can be achieved using an internally heated configuration.

The performance of a miniaturized low temperature co-fired ceramic packed bed reactor in the temperature range of 300-400 ºC was defined by Pohar *et al.* [154]. They inserted 6.73 g of gallium-promoted copper ceria catalyst into an inner reaction chamber of dimensions 33.8 mm x 4 mm x 41.4 mm (width x depth x length). For optimal conditions, they achieved 95% methanol conversion at 400 ºC and a liquid flow rate of 0.15 mL/min.

Until now, the studies mentioned above regarding packed bed methanol reformers is for low power generation applications, namely, less than 100 W. In addition, the heat for endothermic MSR was supplied using external exothermic reaction (except Nehe *et al.* [153] study). Real *et al*. [155] showed the feasibility of hydrogen generation by a solar-based packed bed methanol steam reformer for stationary fuel cell systems. The heat requirement for the MSR was supplied by a non-concentrating solar thermal collector. In this work, two catalyst loadings of 100 and 140 mg of nanoparticles, inserted into the solar collector in the form of a packed bed, were studied. Their experimental work demonstrated that 100% methanol conversion was achieved for 100 mg catalyst and methanol-water mixture flow rate of 3 mL $min^{-1}m^{-2}$, while only 58.5% conversion was obtained for the flow rate of 6 $mLmin^{-1}m^{-2}$. Also, the complete conversion of the 140-mg reactor was obtained for the 4 $mLmin^{-1}m^{-2}$, while the conversion decreased 59.7% for the 9 $mLmin^{-1}m^{-2}$. Moreover, they found the maximum hydrogen production of 6.62 $L_{STP}min^{-1}m^{-2}$ for a reactor containing 140 mg catalyst and a liquid methanol-water mixture flow rate of 8 $mLmin^{-1}m^{-2}$.

Although the traditional packed bed reactors are widely employed in industry for methanol reforming, they suffer from axial temperature gradients [156]. In addition, sintering of the catalyst in the packed bed can cause an increasing pressure drop in the reformer [156]. To solve these issues, wash-coated microchannel reformers can be used for hydrogen production from methanol. They have large specific surface areas, so better heat and mass transfers than the packed bed can be obtained for wash-coated microchannel reactors [48, 157]. Due to enhanced heat transfer, higher methanol conversion at lower temperatures are obtained for wash-coated microchannel reformers [48]. Also, microchannel design can be maximized with deployment of the catalyst directly on the internal surface in the wash-coated reformers [156]. As well, the wash-coated reformers have a benefit from a pressure drop [156, 158]. Because of the aforementioned advantages of the wash-coated microstructured methanol reformers, the attention of researchers and companies has been dramatically increasing towards the wash-coated microstructured reformer technology. Kolb in 2013 [44] published a comprehensive review about the field of microstructured reactors for energy related topics. In addition, Holladay and Wang in 2015 [159] summarized the numerical models and reaction equations of microchannel reactors for both wash-coated and packed bed systems for microscale (power generation less than 5 W) hydrogen generation. Therefore, we only reviewed recent papers which discuss innovative approaches to increase wash-coated microchannel methanol reformers in our work.

Wang *et al.* [156] applied an innovative method. They used cold gas dynamic spray (CGDS) method to deposit catalyst coating in the plate type microchannel methanol reformer. This innovative method-CGDS, which consists of spray gun, powder feeding, heating, gas regulating, high-pressure gas source and powder recovering, is a technology based on gas dynamics. The catalyst particles are carried with high pressure gas such as nitrogen, helium, air etc. through the

spraying gun at the solid state at high speed. Gas is preheated to increase the speed of the particles in the cold spray. Wang *et al.* [156] used a reaction chamber with the dimensions of 6 mm x 6 mm x 125 mm in the plate-type stainless steel micro-reactor. In addition, the total catalyst in the reformer was 0.83 g. Their results indicated that the highest H_2 production rate was defined as 30.05 ml/min at the temperature range of 270 ºC.

Another innovative method to improve the performance of wash-coated microchannel methanol reformers was investigated by Mei *et al.* [157]. In the traditional wash-coated microchannel reactors, the catalyst support with a non-porous surface is used. They proposed an innovative micro-channel catalyst support with a micro-porous surface. The pores with a diameter of 60-150 μm and a depth of 50-100 μm were used in the micro-porous surface. The results showed that the H_2 production rate was 9.65 ml/min for the micro-channel catalyst support with the non-porous surface while it was 18.07 ml/min for the micro-porous surface at 300 ºC and a mixture of methanol and water with 1:1.2 molar ratio rate of 30 μl/min.

In another recent study, Pan *et al.* [160] experimentally compared the performance of micro-channel methanol reformers with the rectangular and tooth cross-sections. They illustrated that the performance of the reformer with mesh tooth microchannels was better than with mesh rectangular microchannels.

The catalyst coating methods for the wash-coated microchannel reformers are out of the scope of this review paper; however, interested readers can refer to Refs. [161-165].

The cost barrier of membrane reformers [48] is the main issue in commercializing them. If this issue is solved, they can also be another promising technology for methanol reforming. On the other hand, one of the most important advantages of the membrane reformers is that nearly 100%

pure hydrogen can be produced by employing membrane methanol reformers [48,166]. More detailed information regarding membrane reformers can be obtained from Iulianelli`s *et al.* review paper [45].

2.4 Reformed Methanol Fuel Cell Systems

A number of review papers [44, 48] reported studies conducted in methanol reforming fuel processors for fuel cell power generation systems. Kolb [44] dedicated one section to related microstructured fuel processors for the reforming of different kinds of fuels. Palo *et al.* [48] wrote a review paper in 2007 about methanol steam reforming for hydrogen production. In their study [48], they mentioned system challenges, military and consumer needs, and also summarized studies in the literature regarding properties and the performance of reformers in the given systems. In this section of our review paper, we specifically focus on recent studies from the perspective of methanol reformers and system performance. In other words, not only methanol performance is discussed, but also the system components, heat integration, the efficiency and control of the reformed methanol fuel cell systems are evaluated. Moreover, we emphasis on reformed methanol fuel cell systems for power generation in the range of 100 W to kW scales.

Methanol can be used as fuel for fuel cell power generation systems in two ways. In the first method, it can be used directly with direct methanol fuel cell (DMFC) systems. In the second method, reformate methanol gas which includes mainly H_2 can be used to feed fuel cells for power generation. For the first method, the system has a simpler structure because methanol is used directly for the DMFC without a fuel processor [158]. On the other hand, the important challenges for a large-scale commercialization of DMFCs are their lifetime and high production cost, as well typically having lower efficiency and power density [167,168]. Technical specifications of the

reformate-gas fueled PEMFC and DMFC systems for 300 W power generation are listed in Table 2-8 [169]. The results, shown in Table 2-8, were obtained for prototype systems; thus, the results are based on real operation conditions. As shown in this table, the DMFC system has lower fuel efficiency and energy density compared with the reformate-gas fueled PEMFC system.

Table 2-8 Technical specifications of portable fuel cell prototype systems (adapted from Ref. [169]**.).**

Requirement	RMFC	DMFC
Max output power W	300	300
System Weight (no fuel, kg)	16	20
Dimensions (cm)	38×30×25	29×51×29
Internal Li-ion Battery (Whr)	326	80
Voltage (VDC)	28	28
Fuel	Methanol/Water	Methanol
Runtime	Cartridge (1.2 L) =4 h	Cartridge (2 L) =8 h
Capability	APU+Battery Charging	APU+Battery Charging
Start-up time (min)	20	2
Fuel efficiency (%) (LHV)	34	16
Specific Power (W kg^{-1})	18	15
Power Density (W L^{-1})	10	6.9
Specific Energy (72 h mission, Wh kg^{-1})	618	591
Energy Density (72 h mission, Wh L^{-1})	423	349

Researchers have typically investigated low temperature PEMFCs (such as in Refs. [105, 158, 170- 174]) and HT-PEMFCs (such as in Refs. [106, 113, 175]) for the reformed methanol fuel cell systems. The main advantages of the PEMFCs are their low start-up time and high energy density; therefore, reformate methanol gas PEMFC systems may be a promising candidate to provide power for portable power electronics [105]. A system, which consists of a micro-structured evaporator, a micro-structured reformer and two stages of preferential oxidation of CO (PROX) reactor, micro-structured catalytic burner, and a PEMFC, was investigated to evaluate its performance for power generation from methanol by Men *et al.* [105]. The change of the activity and selectivity for each individual component was determined by them with the variation of the reaction temperature, S/C, contact time, and feed composition by employing performance tests. The width, depth and length of the elliptic microchannels were 600 μm, 250 μm, and 44 mm, respectively in their study. Also, the dimensions of the MSR and catalytic combustion were approximately 120 mm x 36 mm x 25 mm, respectively, while the PROX reactor dimensions were about 104 mm x 80 mm x 15 mm. They reported that this system is enough to produce 20 W of net electric power by fuel cell.

Another methanol steam reformer system to produce hydrogen for a PEMFC power generation system was investigated by Dolanc *et al.* [158]. Dolanc and co-workers designed and implemented a miniature reformer of methanol to feed a low temperature PEMFC with electric power up to 100 W. As shown in Fig. 2-8, this system consists of three subsystems which are the actuator unit, the reactor unit and the control unit. The actuator unit is used to generate and control the flow rates of the methanol and water to the reforming reactor, air to the PROX reactor, and the air/methanol mixture to the catalytic combustor. Methanol reformation takes place in the reactor unit. The reactor unit consists of a combustor, an electrical heater, methanol and water evaporators,

a reforming reactor, and PROX reactor. In the reactor unit, the electrical heater provides 10 W to ignite the combustor. The other subsystem, the control unit, is implemented in the system to meet the demands of the system. They found in their experimental results that the molar fraction of the reformate gas is CO_2=~21.56%, H_2O=~10.3%, CH_3OH=~2.2%, H_2=~65.3%, CH_4=0.2%, and CO=~0.4% for 50 mL h^{-1} of methanol flow rate, and 29 mL h^{-1} of water flow rate at 250 ºC of the reformer reactor temperature.

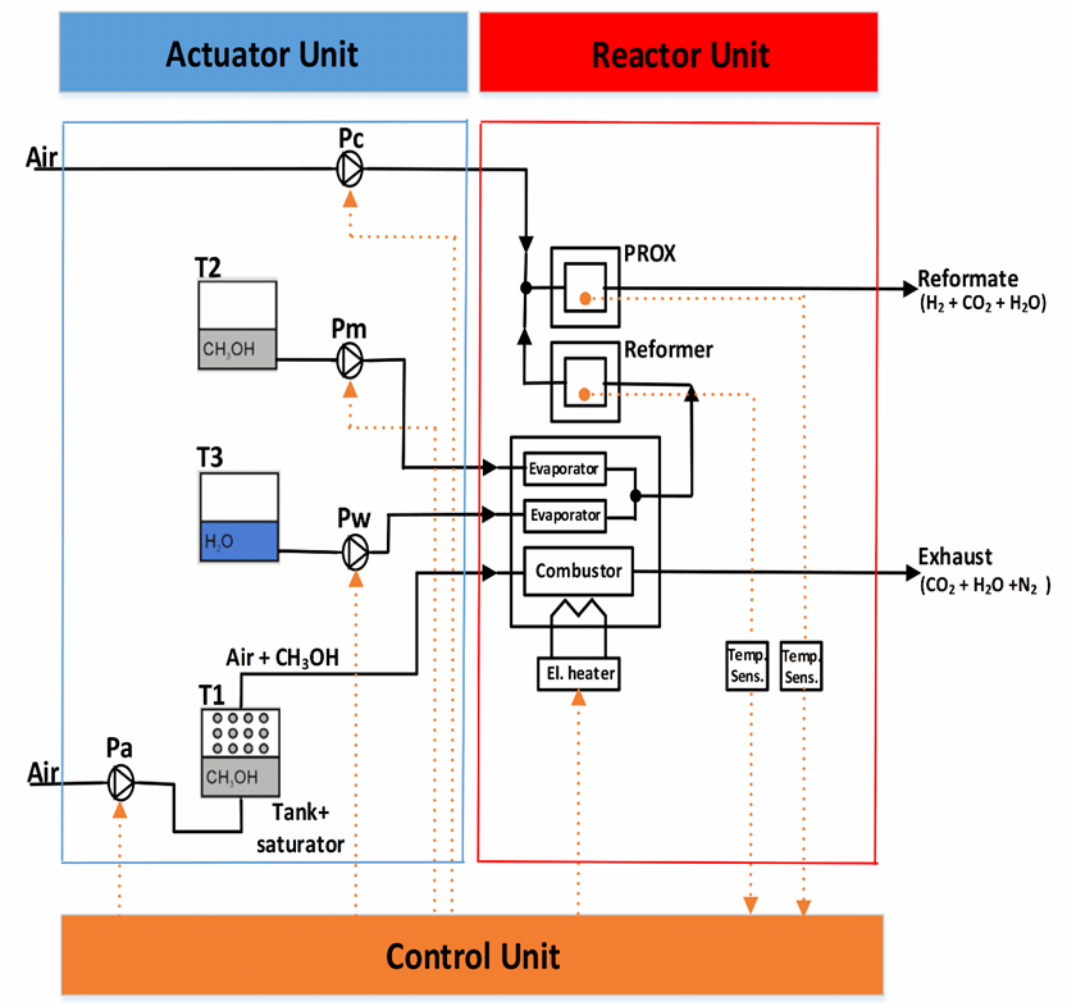

Figure 2-8 Technological scheme of the miniature fuel reformer system for portable power sources (modified from [158]**).**

They [158] also estimated the specific energy of the system by using the equation as follows:

$$E_{sp} = P_{el} t_{op} / (m_{CH_3OH} + m_{H_2O} + m_{Ref} + m_{FC}) \quad (2.6)$$

To find the specific energy, they calculated the stored fuel (m_{CH_3OH}) and water (m_{H_2O}) as 1.420 kg and 0.696 kg, respectively for the operation time of 24 hours; also, the mass of the complete reformer system for their fuel processor was 3 kg. Moreover, they assumed that the mass of low temperature PEMFC was around 1.3 kg for the 100 W power generations. Using these values, they found the specific energy of the system is 374 Wh kg^{-1}.

Low temperature PEMFCs have an advantage with respect to start-up time; however, high purity hydrogen is necessary to feed the PEMFC. In particular, low temperature PEMFCs are very sensitive to CO. Therefore, some additional equipment must be added to the system to decrease CO level in the reformate gas as mentioned in the previous paragraphs. This will increase the system complexity and balance-of-plant (BOP). This disadvantage can be overcome by using HT-PEMFCs. It has been reported that the HT-PEMFCs can tolerate CO up to 3% [176], while CO concentration as low as 10-20 ppm causes a significant loss in cell performance for the low temperature PEMFCs that operate at 80ºC [177]. Not only there is sensitivity to impurities in the reformate, but it should be noted that low temperature PEMFCs have several drawbacks, such as inefficient thermal and water management, and slow electrochemical kinetics. These issues can also be resolved by using the HT-PEMFCs at an elevated operation temperature. In addition, a comparison of a LT-PEMFC that works with hydrogen and methanol reformate gas fuelled HT-PEMFC systems can be seen in Table 2-9. As shown in this table, the methanol reformate gas fueled HT-PEMFC system is more economical than the PEMFC system in terms of electric energy price. The electricity energy price is 0,15 €/kWh_{DC} for the HT-PEMFC system while it is 0,68

€/kWh$_{DC}$ for the LT-PEMFC system [178]. Attention to reformed methanol fueled HT-PEMFCs systems has been increased in recent studies because of the reasons explained above.

Table 2-9 Comparison of a hydrogen fueled LT-PEMFC and methanol reformate gas fueled HT-PEMFC systems (modified from [178]**)**

	LT-PEMFC	**HT-PEMFC**
Fuel	H_2	CH_3OH
Fuel price[1] $/t	~10998	~382
Mass/Power kg/kW$_{el,DC}$	10	12-15
Volume/Power l/kW$_{el,DC}$	14	17
Fuel consumption g/kWh	72	440
Price[1] $/ kW$_{el,DC}$	~5788	~5788
Electric energy price[1] $/ kWh$_{DC}$	~0,79	~0,17
[1]In Ref. [178], Euro is used instead of (US) Dollar. For conversion, 1 Euro equals 1.16 US Dollar (Oct 1, 2018, 10.35 pm UTC).		

One of the leading companies, which manufactures reformed methanol HT-PEMFC systems, is Serenergy [12] in Denmark. H3-350 RMFC system produced by Serenergy is illustrated in Fig. 2-9. As shown in the figure, the main components of the system are an evaporator, a reformer and burner, and a HT-PEMFC stack. For this system, the additional components to remove the CO in the reformate gas are not necessary because of the high tolerance level to CO of the HT-PEMFC. The system is designed for the nominal output power of 350 [W], a rated output current of 16.5 [A] at 21 [V] [179]. The system weight and volume are 13.7 kg and 27 L, respectively, while fuel consumption is 0.44 L/h [181]. As presented in Figs. 2-9 (b) and (c), firstly the methanol/water

mixture (60/40 vol.% mixture of methanol and water [180]) enters the evaporator. After evaporation of the fuel mixture, it goes to the reformer, and the reformate gas feeds to the HT-PEMFC stack. It was recommended by the manufacturer that the H_2 over stoichiometry should be 1.35 to prevent anode starvation in the fuel cell [180]. Therefore, ~25% of the hydrogen in the reformate gas is not used for the power generation in the HT-PEMFC anode. The remaining hydrogen is used in a catalytic burner to provide the heat requirement of the reformer. Also, the process heat of the evaporator is supplied using the excess heat from the fuel cell.

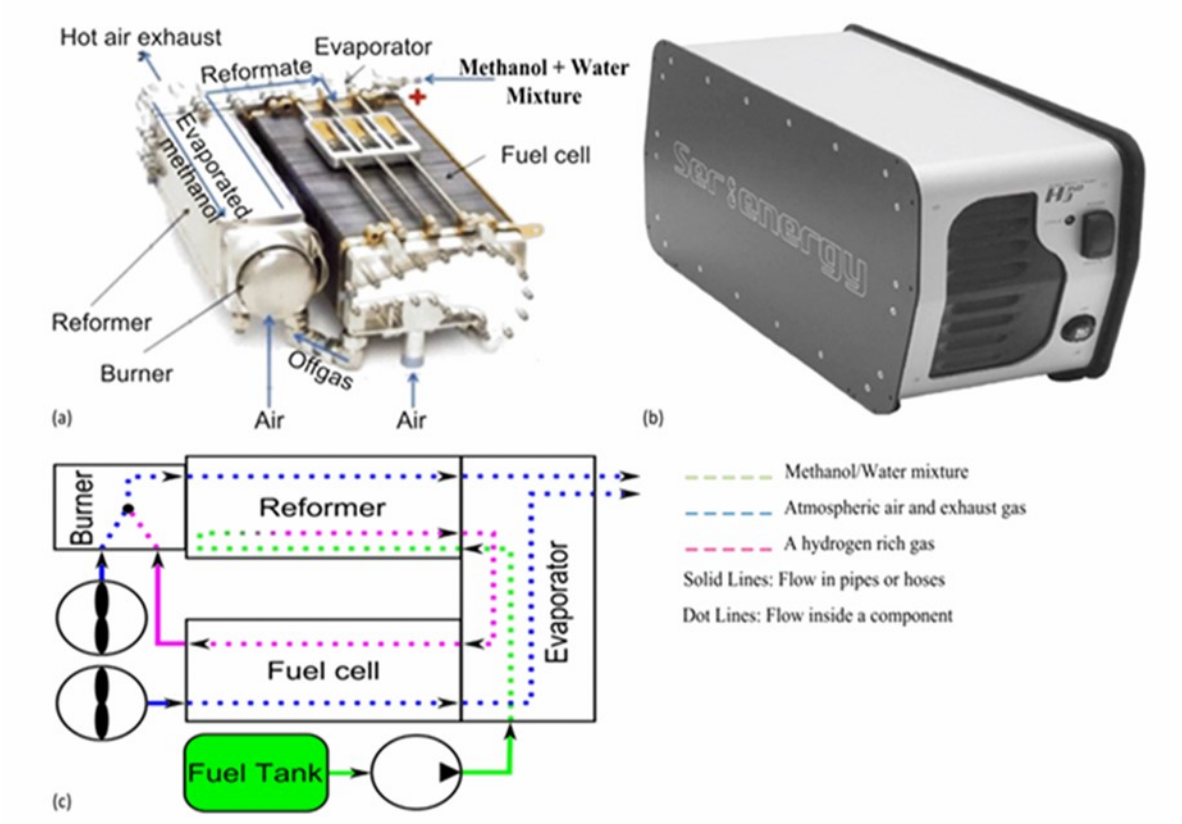

Figure 2-9 (a) Scheme , (b) picture , and (c) concept drawing of the commercial H3-350 RMFC system. Modified from Refs. [179, 188]**.**

H3-350 has been used as a reference system in some studies [18, 102, 179, 180, 182, 183]. Andreasen *et al.* [102] developed a cascade control strategy to test the methanol reformer used in the Serenergy H3-350 Mobile Battery Charger. They investigated the performance of the methanol reformer with the variations of the reformer operating temperature from 240 to 300 ^{o}C, and the methanol/water mixture fuel flow from 200 to 400 mL/h. In their work, the volume air flow to the burner was manipulated to control the burner temperature; therefore, the desired reference reformer temperature was obtained. Their results showed that H_2 and CO_2 contents in the reformate gas did not change significantly with the variations in the reformer temperature and fuel flow rate while there were significant changes in the CO and methanol contents in the reformate gas. For example, the CO increased from 0.142% (vol.% in dry reformate gas) to 1.11% with the change of the reformer temperature from 240 to 300^{o}C for 300 mL/h methanol/water mixture. For the same operation conditions, the methanol in the reformate gas decreased from 3.64% to 0.142%.

In the previous study, Andreasen *et al.* [102] did not consider the fuel cell performance with the variation of the reformer temperature. Therefore, Justesen and Andreasen [179] in another study defined the optimal reformer temperature by considering the fuel cell performance for a RMFC system based on a H3-350 module. They used Adaptive Neuro-Fuzzy Inference System (ANFIS) models to observe the effects of the reformer temperature on the system efficiency. The system efficiency was calculated by the following equation:

$$\eta_{sys} = \frac{P_{FC,out}}{P_{Fuel,in}} \tag{2.7}$$

In this equation, $P_{FC,out}$ is the fuel cell power output, which is equal to the multiplication of the fuel cell current and voltage, while $P_{Fuel,in}$ is the input power, which is calculated using the lower

heating value of the methanol in the fuel. They found the optimal constant reformer temperature to be 252ºC. For this reformer temperature, the efficiency was calculated as 32.08% at 170ºC of the fuel cell temperature.

Additional to the study mentioned above, a methanol reformed HT-PEMFC system for power generation under 100 W was investigated by Kolb *et al.* [106]. In this study, the authors studied a portable power generation device applying methanol reformate gas as fuel and high-temperature PEM fuel cell technology for a net power output of 100 W. They used a micro-channel methanol reformer with noble metal catalyst (Pd/ZnO catalyst). They employed the fuel cell stack, which consisted of 24 cells. 130 W (14.4 V and 9 A) power was produced from the fuel cell stack, and 30 W were reserved for the balance-of-plant components. For the reformer temperature 350ºC, the S/C=1.7, and the O/C=0.25, they reported that the methanol conversion is always 100%, while the CO yield and the H_2 yield are 1.8 and 50 vol. % (wet basis), respectively. For the same reformer temperature and the O/C ratio, with decreasing the S/C ratio from 1.7 to 1.5 the CO and H_2 contents increased to 2.09 and 53 vol. %, respectively.

Reformate-gas fueled HT-PEMFCs systems are also a promising technology for auxiliary power unit (APU) applications. For example, it can be used as an APU in heavy-duty trucks, service vehicles, light-duty vehicles, and luxury passenger vehicles [184]. Power demands for APU applications are typically in the kW scales. Methanol reformate-gas fuelled HT-PEMFCs systems have been recently investigated in Refs. [113, 175, 185]. Sahlin *et al.* [185] studied a reforming methanol system in an oil heated reformer system for 5 kW fuel cell system. Their work has two parts. In the first part, a dynamic model of the system was developed, while an experimental study was performed on different components of the system in the second part. The modeling work revealed an overall system efficiency of 27-30% on the basis of the fuel lower

heating value. In addition, the start-up of the reformer was found to be about 45 min in the experiments.

One of the first micro-structured methanol reformers with integrated anode off-gas combustion, which worked in the kW scale was designed, built, and tested by Kolb *et al.* [113]. They used oxidative steam reforming to convert methanol to hydrogen rich gas. Platinum/indium/alumina catalyst was used for the reformer side while platinum/alumina catalyst was employed on the after-burner side. They found the volume ratio of the gases in the reformate gas in dry basis: 68.4% H_2, 1.5% CO, 22.2% CO_2, 9.9% N_2 and 430 ppm CH_4 at S/C=1.3 and O/C=0.2. In addition, they estimated 11.4% H_2O, 0.4 ppm unconverted methanol and 8 ppm formic acid for the same reforming conditions. Their results revealed that the formic acid decreased to 6.1 ppm with the change of the S/C from 1.3 to 1.5. 6720 l/h H_2 was produced using 6.5 kg fuel processor including reformer and after burner with 3200 g/h methanol. Also, the methanol-water mixture evaporator, which has 54 plates with a total volume of 0.62 l and a weight of 2.2 kg, was used in this study.

As explained in Refs. [5, 169], the most promising applications of fuel cell systems involve power generation of up to 500 W. However, the system weight and balance-of-plant components are two critical parameters for the small-scale power generation applications. These parameters should be decreased for the large-scale commercialization of the fuel cell systems for power generation of up to 500 W. To achieve this, some researchers [125-127, 186,187] have recently investigated the feasibility of integrating the methanol reformer with the HT-PEMFC stack. Therefore, the heat requirement of the methanol steam reforming is provided using waste heat from the fuel cell, and additional heat exchangers can be eliminated in the system. This is an opportunity to decrease the system weight and volume and increase the efficiency. Recent

advancement in research related to integrated methanol steam reformer HT-PEMFC power generation systems were reviewed in Ref. [10].

In summary, the studies in regards to reformed methanol fuel cell systems can be classified into two main categories. In the first category, the researchers have focused on feasibility and defining operation parameters of the reformed methanol fuel cell systems for different type of applications. The second category is about integration of the new technologies to the systems to improve system performance for specific type of power generation applications.

2.5 Conclusion and Future Outlook

We presented the studies in literature regarding methanol reforming. The studies were evaluated and discussed with considering different aspects of fuel cell power generation systems. The important points in this review paper are summarized below:

- **Alternative fuels for fuel reforming.** Various fuels can be used for fuel reforming processes for fuel cell power generation applications. However, fuel selection is very important to achieve desired fuel cell system properties. The important factors about fuels which affect performance of fuel cell power generation systems are fuel availability, fuel price, fuel storage, fuel evaporation temperature, S/Fuel and/or O_2/Fuel ratios for the reforming processes, fuel composition, reforming temperature and pressure, and reformate gas composition. These factors should be evaluated with the desired system functions as shown in Figure 1. Among different hydrogen carrier fuels, methanol reforming is particularly very suitable for portable and small scale power generation applications because methanol is in liquid form at room temperature, it has a relatively low evaporation temperature, and low reforming temperature and pressure. In addition, methanol reformate

gas does not include sulfur, and it includes low amounts of CO. With these unique properties, the system size and weight, and balance of plant components can be decreased, also the life of the system can be increased.

- **Catalysts for methanol reforming.** Cu/ZnO-based catalysts for methanol reforming have been extensively studied by researchers. However, deactivation of the Cu/ZnO based catalysts are a serious issue. Therefore, research activities about methanol reforming catalysts changed after 2000s to improve activity and stability of the methanol reforming catalysts. The catalysts research activities after 2000s can be classified into two categories. In the first category, the studies have focused on more active and stable catalysts at high temperatures. Increasing of the catalysts activity and stability at high temperatures are particularly very important for oxidative steam reforming of methanol. The other category is for increasing the catalyst activity at low temperatures.
- **Methanol reformate gas fueled fuel cell systems.** Improvements in catalysts and reformers have occurred due to advancements in the development of the methanol reformate gas fueled fuel cell systems. In particular, the system size and weight have decreased with the more active catalyst and microstructured reformers. With these remarkable improvements, this should be noted that the fuel cell price is still the main barriers for methanol reforming fuel cell systems; therefore, the most suitable application areas for the market should be wisely defined.

Overall, the researchers have made many progress in the methanol reforming catalysts and reformers, and also integration of the new technologies into fuel cell systems. However, the existing works in the literature do not include enough information to explain viability of internal reformer methanol fuel cell systems for the market. Also, with these remarkable progresses, price

of the fuel cell technologies is still the main barrier for commercial applications of methanol reforming fuel cell systems.

Chapter 3
Modeling and Parametric Study of a Methanol Reformate Gas-fueled HT-PEMFC System for Portable Power Generation Applications

This chapter is reprinted in adopted form with permission from Journal of the Energy Conversion and Management:

MS Herdem, S Farhad, and F Hamdullahpur. Modeling and parametric study of a methanol reformate gas-fueled HT-PEMFC system for portable power generation applications, Energy Conversion and Management, 2015, 101, 19-29.

3.1 Introduction

Electric power requirements for outdoor applications and wireless industrial tools have been increasing every year. This requirement is currently approximated at 714 GWh in Europe [106]. In addition, the lack of access to electricity is a serious economic and social issue in the world, especially in underdeveloped and some developing countries [189]; drawing more attention to portable applications. Although batteries are a promising technology for small scale power storage for portable systems, their wide-scale application is limited because of weight restrictions [106]. Although a number of developmental challenges remain to be tackled, fuel cells can be considered as an alternative technology for portable power generation applications. Shaw *et al*. [5] report that military personal power generators, consumer battery rechargers, and specialized laptop computers are the most promising applications to use fuel cell technology in the market. They also explain that the hydrogen storage issue is one of the most important barriers for wider usage of hydrogen fuel cells; thus, energy storage densities must be improved using an inexpensive and convenient

hydrogen supply. To overcome the hydrogen transportation and storage barrier, hydrogen can be obtained using alternative fuels such as biogas [190, 191], ammonia [192], or from methanol [193], gasoline [194], ethanol, and other hydrocarbon fuels by employing fuel reformer technologies for fuel cell power supply systems. Methanol can be used as one of the most appropriate fuels for portable and stationary fuel cell applications because it can be produced using different sources such as natural gas, coal, and biomass. In addition, methanol can be stored easier than hydrogen; it has high hydrogen to carbon ratio and a low boiling temperature; it is liquid at atmospheric pressure and normal environment temperature; and it can be converted easily to hydrogen at lower temperatures than many other hydrocarbon fuels [48, 195]. Therefore, fuel cells coupled with methanol reformers have become progressively more attractive for portable applications.

There are many studies in the open literature which have been undertaken on various applications of reformer methanol fuel cell systems. Partial oxidation (POX) and auto-thermal reforming (ATR) technologies were experimentally investigated to produce hydrogen using a small methanol reformer for fuel cell application by Horng *et al.* [196]. Their results show that the optimum steady mode shifting temperature for their experiment is about 75 ^{o}C; in addition, they reported the most appropriate pre-set heating temperature for facilitating the most rapid response of the catalyst reformer. Furthermore, the hydrogen concentration produced in their experiment was as high as 49.1% with a volume flow rate up to 23.0 $Lmin^{-1}$, and 40.0% with a volume flow rate of 20.5 $Lmin^{-1}$ using auto-thermal and partial oxidation processes, respectively. Vadlamudi and Palanki [152] analyzed an autothermal reforming of methanol to supply enough hydrogen for generating 100 W power. They used fundamental principles of reaction engineering, fluid mechanics and heat transfer for modeling non-isothermal operation. They reported that pressure drop is negligible throughout reactor volume. They also found that the outlet flow rate of hydrogen

increases with higher inlet temperature; however, the reformer heat requirement increases for higher inlet temperature. Chein *et al.* [197] presented a methanol steam reforming for hydrogen production. The reforming with $CuO/ZnO/Al_2O_3$ catalysts and the methanol catalytic combustion with Pt catalyst were experimentally tested by them. They also studied the flow and heat transfer effects of three different reformer designs – including patterned microchannel with catalyst onto the channel wall, single plain channel with catalyst coated onto the bottom channel wall and inserted stainless mesh layer coated with catalyst − on the reactor performance. The best thermal efficiency among the three designs was obtained for the reactor with microchannel reformer and also higher methanol conversion in their experimental results. It is noted that many experimental reformers of the smaller scale and reformers for industrial applications use conventional Cu/ZnO catalysts [106]. Kolb *et al.* [106] have developed a system for portable power generation with an electrical net power output of 100 W. The system consists of oxidative (auto-thermal) steam reforming of methanol with a catalyst of higher activity than Cu/ZnO catalysts and a high temperature proton exchange membrane fuel cell (HT-PEMFC). The effects of the $CuO\text{-}ZrO_2\text{-}CeO_2\text{-}Al_2O_3$ catalysts on the methanol conversion were investigated by Baneshi *et al.* [193]. Their results show that the methanol conversion reaches 100% at 240 ^oC, and the catalyst has high lifetime. Lo and Wang [198-200] proposed a novel passively-fed methanol steam to remove the pump and for effective heat transfer to methanol steam reformer and evaporator from the catalytic combustor heater. The system was experimentally investigated, and the experimental results show the methanol conversion exceed 98% for reformer temperatures higher than 292 ^oC and the water/methanol feed ratio over 1.0 [198]. The main disadvantage of their system is the slow start-up time, which is about 30 minutes [199]. Kolb *et al.* [113] built and tested a methanol reformer for HT-PEMFC for mobile applications. For the reformer, they used micro-structured plate heat-

exchanger technology with a novel, highly active catalyst formulation for oxidative steam reforming of methanol. They could achieve a hydrogen production equivalent to the thermal power of 20 $kW_{thermal}$ from their reformer.

Many studies in the literature have focused on components design and/or power (or combined power and heat) production in kW range or less than 100 W using reformer systems and fuel cells. Our literature survey confirms that there is no any study to focusing on a few hundred watts power production using HT-PEMFCs and investigating the fuel cell performance with the variation of the methanol reformate gas composition. The main objective of this study is to estimate the fuel cell performance, the input fuel flow rate, and the heat duties of the system components with the variation of the methanol reformate gas composition for power generations as low as 500 W. A detailed parametric study to understand how the system can be improved is also conducted. The results in this study can be used for further development of the system for future studies.

3.2 System and Process Description

The simplified schematic of the power generation system investigated in this study is shown in Fig. 3-1. A commercially available methanol reformer system, H3-350 made by Serenergy [201], is chosen as a base system to define the system components and the input parameters. The main components of the H3-350 include an evaporator, a methanol steam reformer, a combustor, and a HT-PEMFC stack. The evaporator is used to convert liquid methanol-water mixture to a vapor mixture. Then the vapor fuel enters the methanol steam reformer and H_2 rich reformate gas is produced in the reformer. The main reactions that can take place in a methanol reformer are as follows [182]:

$$CH_3OH + H_2O \leftrightarrow 3H_2 + CO_2 \ (49.5 \frac{kJ}{mol}) \tag{3.1}$$

$$CH_3OH + \frac{1}{2}O_2 \leftrightarrow 2H_2 + CO_2 \ (-192.3 \frac{kJ}{mol}) \tag{3.2}$$

$$4CH_3OH + \frac{1}{2}O_2 + 3H_2O \leftrightarrow 4CO_2 + 11H_2 \ (0 \frac{kJ}{mol}) \tag{3.3}$$

$$CO + H_2O \leftrightarrow H_2 + CO_2 \ (-41 \frac{kJ}{mol}) \tag{3.4}$$

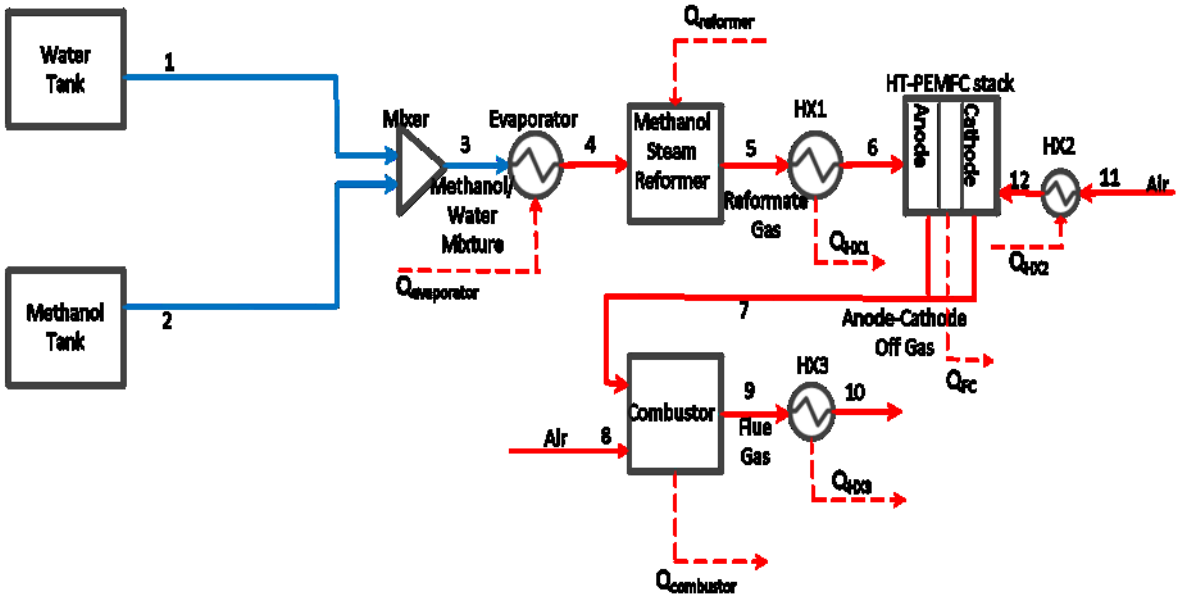

Figure 3-1 Schematic of the methanol reformer system.

The main compositions of the reformate gas are H_2, CO_2, H_2O, and CO. Partial oxidation and autothermal reforming of methanol can be used to convert the fuel to the reformate gas. However, the molar flow rate of H_2 in the reformate gas is higher for methanol steam reforming [196], as well as reactions in the reformer take place at lower temperatures [158]. Also, a low CO ratio can be obtained for the methanol steam reformer [51]. Therefore, the methanol steam reformer is preferred for this system. Methanol-water mixture can be converted to reformate gas

in the reformer using an appropriate catalyst type. Cu-based catalysts and noble metal-based catalysts are two types of catalyst that can be broadly used for the methanol steam reformer [51]. Copper-based catalysts have high activity with low temperatures and are selective, so they are commonly used for methanol steam reforming [46]. CuZn-based catalysts have also relatively low cost [182] so CuZn-based catalyst is considered as a reforming catalyst in this study. After obtaining reformate gas, firstly the gas temperature is decreased to the fuel cell temperature by employing the heat exchanger, and then enters the HT-PEMFC for electric power generation.

Although low and intermediate temperature polymer membrane fuel cells have higher efficiency for small scale power production, they need high purity hydrogen. In addition, because water management is a serious issue for these fuel cells, HT-PEMFC is employed for power generation in this study. There are several advantages of using HT-PEMFC for this system. These advantages include (a) water is in vapor phase so the water management is not an issue in these fuel cells; (b) HT-PEMFCs have faster electrochemical kinetics, and (c) the heat management is easier [202]. Other significant benefit of HT-PEMFCs for methanol reformer systems is that they have higher CO tolerance [203]. Up to 3% CO can be tolerated for HT-PEMFCs [176].

After the HT-PEMFC, anode and cathode off gases are burned as a fuel in the combustor to generate extra heat. The heat requirement for the reformer is supplied from the combustor. The recoverable heat from the fuel cell stack is used for evaporating the methanol-water mixture. In addition, the remaining heat to complete evaporation of the methanol-water mixture and increasing its temperature to 120 ^{o}C is provided from the combustor hot flue gases. To decrease the reformate gas temperature to the fuel cell temperature, the cathode inlet air is used. The remaining heat to increase the cathode inlet air temperature to the fuel cell temperature is supplied from the

combustor hot flue gases. The system which includes whole heat integration is shown in Figure S1 in the supplementary document.

3.3 Modeling of the System

Thermophysical properties for the modeling of the system are obtained by employing Aspen Plus version v7.3 [204]. Then, all the variables which are used for system modeling are transferred to an Excel spreadsheet for the parametric studies. The NRTL model is used to find thermophysical properties of the liquid methanol-water mixture and ideal gas model is used for the rest of the streams. Heat losses and pressure drops of the system components are assumed to be negligible. The components pressure is assumed at atmospheric pressure for the parametric studies. The main input parameters that are used for the system modeling is given in Table 3-1, and the input parameters in Table 3-2 is used to calculate the system efficiency.

Table 3-1 The input parameters of the system.

Input Parameters			**Ref.**
Fuel inlet temperature to the evaporator	25	^oC	
Fuel exit temperature from the evaporator	120	^oC	
Air -fuel ratio for the combustor	1.05	[-]	[218]
Air inlet temperature to the HX2	25	^oC	
Air molar composition	O_2=21%, N_2=79%		
Fuel cell parameters			[211,212]
Membrane thickness, t_{memb}	$0.1x10^{-3}$	m	
Open circuit voltage, V_o	0.95	V	
Symmetry factor, α	0.5	[-]	
Intermediate hydrogen step, n	2	[-]	
Universal gas constant, R	8.3143	$Jmol^{-1}K^{-1}$	
Faradays Constant, F	96485	$Cmol^{-1}$	
Number of cells, N	45	[-]	[177]
Cell area	45	cm^2	

Table 3-2 The input parameters to estimate the system efficiency of the system.

Input Parameters		Ref.
Heat loss from the fuel cell	20%	[221]
Pressure drop of the components	1.5 kPa	[221]
Air compressor isentropic efficiency	78%	[221]
Fuel pump isentropic efficiency	85%	[221]
Mechanical efficiency compressors/pumps	70%	[220]
Heat exchangers pinch temperature	≥20°C	
Hydrogen utilization ratio	0.8	
Cathode stoichiometric ratio	2	
Steam-to-carbon ratio	1.5	
Fuel cell power output	450 W	

3.3.1 Evaporator and Heat Exchangers

Steam-to-carbon ratio (SC) is calculated as [44]:

$$\frac{S}{C} = \frac{\dot{n}_{H_2O}}{\dot{n}_{CH_3OH}} \tag{3.5}$$

where, $\dot{n}_{H_2O}$ and $\dot{n}_{CH_3OH}$ are the molar ratio of the water (stream-1) and the methanol (stream-2) respectively.

The energy balance equation is used to estimate the heat duties of the evaporator and the heat exchangers in the system. The general energy balance equation is given in below [205]:

$$\dot{E}_{in} - \dot{E}_{out} = \frac{dE_{system}}{dt} \tag{3.6}$$

The evaporator and the heat exchangers are considered steady-state, and there is not any work interaction. Thus, Eq. (3.6) can be written as below:

$$\left(\dot{Q}_{in} - \dot{Q}_{out}\right) + \left(\dot{E}_{mass,in} - \dot{E}_{mass,out}\right) = 0 \tag{3.7}$$

3.3.2 Methanol Reformer and Combustor

Gibbs free energy minimization method is used to estimate composition of the reformate and the flue gas [206]:

$$\min_{n_i}(G^t)_{T,P} = \min_{n_i}(\sum_{i=1}^{c} n_i \bar{G}_i) = \min_{n_i}[\sum_{i=1}^{c} n_i \left(G_i^o + RT \frac{\bar{f}_i}{f_i^o} \right)] \quad (3.8)$$

This method is commonly used in the literature [82, 207] to calculate molar composition of a product in any chemical reactions. Because CuZn-based catalyst is used for the methanol steam reformer in this study, we decided to compare the results obtained from the equilibrium using Gibbs free energy minimization method with the experimental results that used CuZn-based catalyst (see the "Results and Discussion" for details). We concluded that the molar composition of CO calculated from the equilibrium assumption is much higher than that observed from the experiment. We also concluded that if the reformer approach temperature of -70 ^{o}C is adopted, the difference between the results calculated and obtained from experiments will be minimized. Of course, for the combustor, we assume that it is at equilibrium with the combustor temperature.

Heat transfers to the reformer and from the combustor are also calculated using energy balance. The combustor temperature is assumed 20 ^{o}C higher than the reformer temperature.

3.3.3 HT-PEMFC

Various numerical models for modeling HT-PEMFCs are available in the literature, such as the one-dimensional of HT-PEMFC in Ref. [208], and the three-dimensional model of it in Refs. [209, 210]. For this study, a semi-empirical model which has been developed by Korsgaard *et al.* [211, 212] is used for the modeling. This model has been also preferred by several researchers such as [213-217], because it is very useful for system simulation; in particular, for feasibility studies to estimate the effects of different parameters on the fuel cell. Detailed information about this model can be found in [211, 212]; thus, we only briefly explain this paper. This model is based on experimental studies. In experiments, the HT-PEMFC operating temperature changes from 160 °C to 200 ^{o}C for various gas compositions, which consist of H_2, CO, and CO_2. The CO level in the

gas composition changes from 0.1% to 10%. After the experimental studies, Korsgaard *et al.* [211, 212] developed equations for modeling HT-PEMFCs using regression analysis. The cell voltage without consideration of the anode over-potential is calculated from the following equation:

$$V_{cell} = V_0 - \frac{RT}{4\alpha F}\ln(\frac{i+i_0}{i_0}) - R_{ohmic}i - \frac{R_{conc}i}{\lambda - 1} \tag{3.9}$$

where, V_0 is the open circuit voltage. The Tafel equation and the charge transfer coefficient are shown in the second term. The ohmic loss is estimated using the third term and the losses due to cathode stoichiometry is calculated from the fourth term. Since the reformate gas includes CO, the voltage losses due to CO must be considered to estimate the cell operating voltage. The following equations are used to estimate the CO effect on the cell voltage [212]:

$$\rho\frac{d\theta_{H_2}}{dt} = 0 = k_{fh}y_{H_2}P\left(1 - \theta_{H_2} - \theta_{CO}\right)^n - b_{fh}k_{fh}\theta_{H_2}^n - i \tag{3.10}$$

$$\rho\frac{d\theta_{CO}}{dt} = 0 = k_{fc}y_{CO}P\left(1 - \theta_{H_2} - \theta_{CO}\right) - b_{fc}k_{fc}\theta_{CO} - \frac{ik_{ec}\theta_{CO}}{2k_{eh}\theta_{H_2}} \tag{3.11}$$

where, k_{fh} and k_{fc} are hydrogen and carbon monoxide adsorption rates, respectively while k_{ec} and k_{eh} are carbon monoxide and hydrogen electrooxidation rates, respectively. In addition, b_{fc} and b_{fh} show the carbon monoxide and hydrogen desorption rates, respectively. In equations 3.10 and 3.11, θ_{CO} and θ_{H_2} express the surface coverage of carbon monoxide and the surface coverage of hydrogen, respectively. Also, y_i in the above equations shows the molar fraction of the component i in the catalyst layer. Equations 3.10 and 3.11 are independent of time because the steady state conditions are considered in this study.

The anode over-potential is calculated as:

$$\eta_a = \frac{RT_{cell}}{\alpha F}\operatorname{arcsinh}\left(\frac{i}{2k_{eh}\theta_{H_2}}\right) \tag{3.12}$$

Using Eqs. 3.9-3.12, the cell operating voltage is estimated as:

$$V_{cell,op} = V_0 - \frac{RT}{4\alpha F}\ln(\frac{i+i_0}{i_0}) - R_{ohmic}i - \frac{R_{conc}i}{\lambda - 1} - \eta_a \quad (3.13)$$

The main input parameters for the fuel cell modeling are listed in Table 1. For the remaining parameters refer to [211, 212].

Additional equations are added in this study to find anode-cathode off-gases, power production of the HT-PEMFC stack, and heat transfer from the fuel cell. To calculate the anode-cathode off-gases it is assumed that only H_2 in the anode and O_2 in the cathode react and the other reformate gases (CO, CO_2, and H_2O) and N_2 are inert gases. The consumed H_2 and O_2, and produced H_2O are calculated as:

$$\dot{n}_{H_2,consumed} = \frac{I.N_{cell}}{2.F} \quad (3.14)$$

$$\dot{n}_{O_2,consumed} = \frac{I.N_{cell}}{4.F} \quad (3.15)$$

$$\dot{n}_{H_2O,produced} = \frac{I.N_{cell}}{2.F} \quad (3.16)$$

where, I is the stack current, N_{cell} is number of cells, and F is Faradays constant. The hydrogen utilization ratio and cathode stoichiometric ratio are also estimated from Eqs. 3.17, and 3.18, respectively [218]:

$$u_f = \frac{\dot{n}_{H_2,consumed}}{\dot{n}_{H_2,feed}} \quad (3.17)$$

$$\lambda = \frac{\dot{n}_{air,cath} * y_{O_2,air}}{\dot{n}_{H_2,feed} * u_f * 0.5} \quad (3.18)$$

where, u_f and λ are H_2 utilization ratio and cathode stoichiometric ratio, respectively.

The power production of the fuel cell stack can be found from:

$$P_{el} = V_{cell,op}.N_{cell}.I \tag{3.19}$$

The heat production in the fuel cell stack is also determined from [215]:

$$\dot{Q}_{heat,FC} = h_{in,c} * \dot{n}_{c,in} - h_{out,c} * \dot{n}_{c,out} + h_{in,a} * \dot{n}_{a,in} - h_{out,a} * \dot{n}_{a,out} - P_{el} \tag{3.20}$$

For the heat integration process, we assume that 80% of the fuel cell stack can be recovered.

The system efficiency is estimated using the net power production from the system and the lower heating value of the methanol. Ref [219] was used to estimate the missing components (such as temperature controllers, support electronics etc.) power consumption in the system. Overall system efficiency is calculated from:

$$\eta_{sys} = \frac{P_{el} - P_{BOP}}{\dot{m}_{CH_3OH} * LHV_{CH_3OH}} \tag{3.21}$$

3.4 Results and Discussion

Catalyst type, SC ratio, reformer temperature, catalyst contact times, and input fuel flow rate to the reformer are the key parameters that affect the molar composition of the reformate gas. As mentioned before, a CuZn-based catalyst has been chosen for the reformer in this study. In addition, a parametric study has been performed to estimate the effects of the SC ratio and the reformer temperature (the reaction temperature) on the molar composition of the reformate gas. The results have firstly been obtained using equilibrium at reformer temperature. As shown in Table 3-3, although the molar ratio of the H_2 and the CO_2 are very close to the experimental results, there is significant difference between the molar ratio of CO at equilibrium and its ratio in the experimental studies. To obtain more accurate results, an approach temperature was determined using the experimental studies in Refs. [102-105]. Gibbs free energy minimization method was also used for this method; however, the results were obtained after subtraction of the approach temperature (because its value is negative for this study) from the reformer temperature. Therefore,

the molar ratio of the CO is estimated to be very close to that obtained from experiments. The input fuel flow rate also plays an important role in determination of the CO molar ratio [175]. However, this ratio does not significantly change for small input fuel flow rate. The variation of the molar ratios of other gases with the change of the input fuel flow rate can be neglected [175]. For the system studied in this paper, the input fuel flow rate is not high enough to significantly affect the CO ratio. Thus, the results obtained from this study are satisfactory for the range of input fuel flow rates studied. The catalyst contact time also affects the composition of the reformate gas [105]. This can be considered for future studies.

The effect of the steam-carbon ratio and the reformer temperature on the H_2 molar ratio and the CO is shown in Figs. 3-2 and 3-3, respectively. As shown in these figures, the H_2 ratio decreases and the CO ratio increase with increasing the reformer temperature. The main reason for this is that CO conversion in the water gas shift reaction (Eq. 3.4) decreases at higher temperatures. As also shown in the figures, H_2 and CO ratio rise with a low steam-carbon ratio. The molar ratio of the H_2 in the reformate gas is about 60% at the reformer temperature of 240 ^oC and the SC=2. This ratio increases almost 21% for the same reformer temperature and the SC=1. The molar ratio of the H_2 is ~71% at the reformer temperature of 300 ^oC and the SC=1. The CO ratio decreases from ~1.8% to ~0.12% with increasing the SC from 1 to 2 at the reformer temperature of 240^oC. In addition, the CO ratio dramatically increases at elevated reformer temperatures and lower steam-carbon ratios. The highest molar ratio of the CO in the reformate gas is estimated to be ~3.45% at the reformer temperature of 300 ^oC and the SC=1.

Table 3-3 Validation of the model that is used for the methanol reformer simulation with Experimental Studies.

Mole Frac. Dry% (S/C=1.5)	**Equilibrium (T_{ref} =240 ºC)**	**Equilibrium [-70 ºC app. temp. (T_{ref}=240 ºC)]**	**Exp. (T_{ref}=240 ºC)**	**Equilibrium (T_{ref}=260 ºC)**	**Equilibrium [-70 ºC app. temp. (T_{ref}=260 ºC)]**	**Exp. (T_{ref}=260 ºC)**	**[102]**
H_2	74.69	74.91	70.1	74.61	74.87	71.6	
CO	1.21	0.3	0.172	1.63	0.48	0.365	
CO_2	24.1	24.77	24.4	23.78	24.64	24.8	
(S/C=1.5)	**Equilibrium (T_{ref} =280 ºC)**	**Equilibrium [-70 ºC app. temp. (T_{ref}=280 ºC)]**	**Exp. (T_{ref}=280 ºC)**	**Equilibrium (T_{ref} =300 ºC)**	**Equilibrium [-70 ºC app. temp. (T_{ref}=300 ºC)]**	**Exp. (T_{ref}=300 ºC)**	**[102]**
H_2	74.47	74.82	73.2	74.33	74.74	73.6	
CO	2.12	0.72	0.71	2.68	1.02	1.16	
CO_2	23.41	24.46	24.9	22.98	24.23	24.8	
(S/C=1.1)	**Equilibrium (T_{ref} =260 ºC)**	**Equilibrium [-70 ºC app. temp. (T_{ref}=260 ºC)]**	**Exp. (T_{ref}=260 ºC)**				**[103]**
H_2	70.91	72.57	73.4				
CO	5.01	2.3	1.6				
CO_2	20.3	22.66	25				
(S/C=1.1)	**Equilibrium (T_{ref} =240 - 260ºC)**	**Equilibrium [-70 ºC app. temp. (T_{ref}=240-260 ºC)]**	**Exp. (T_{ref}=240-260 ºC)**				**[104]**
H_2	~71.5-71	~72	73-74				
CO	~4-5	1.67-2.3	1.6-3				
CO_2	~21-20.3	23.18-22.65	24-25				
(S/C=2)	**Exp. (T_{ref}=235 ºC)**	**Equilibrium [-70 ºC app. temp. (T_{ref}=235 ºC)]**	**Exp. (T_{ref}=255 ºC)**	**Equilibrium [-70 ºC app. temp. (T_{ref}=255 ºC)]**	**Equilibrium [-70 ºC app. temp. (T_{ref}=275 ºC)]**	**Exp. (T_{ref}=275 ºC)**	**[105]**
CO	0.03-0.064	0.13	0.071-0.162	0.22	0.33	0.268-0.556	

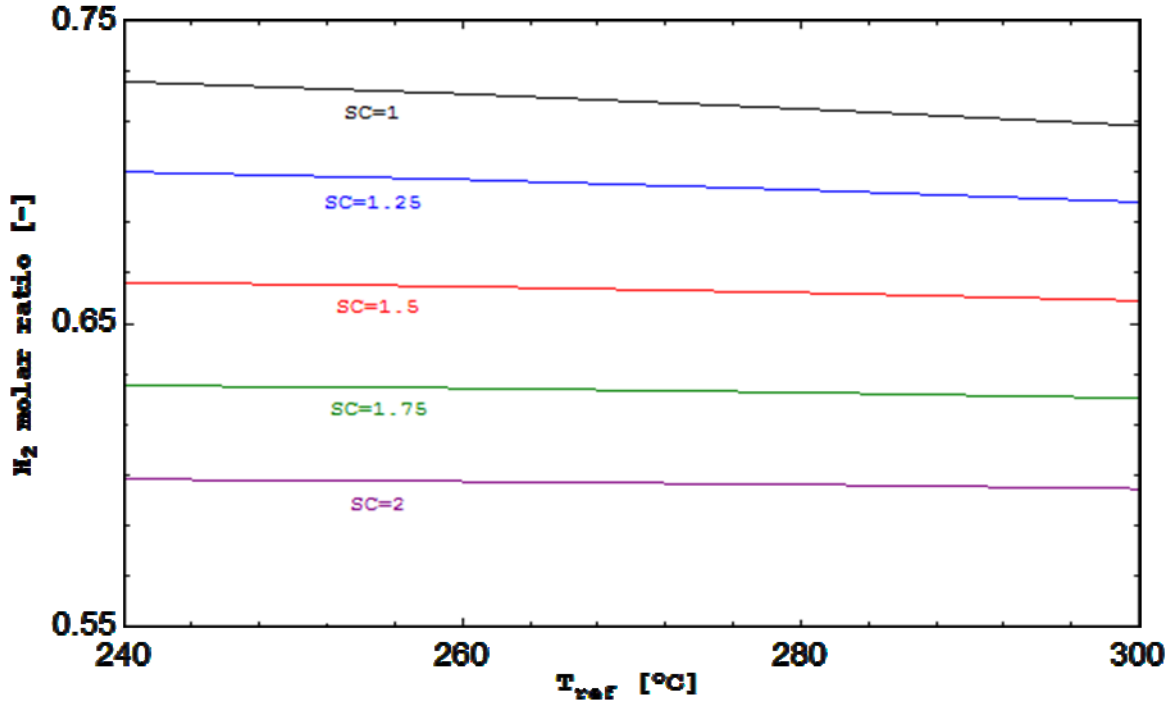

Figure 3-2 Effects of the steam carbon ratio and the reformer temperature on the H_2 molar ratio in the reformate gas.

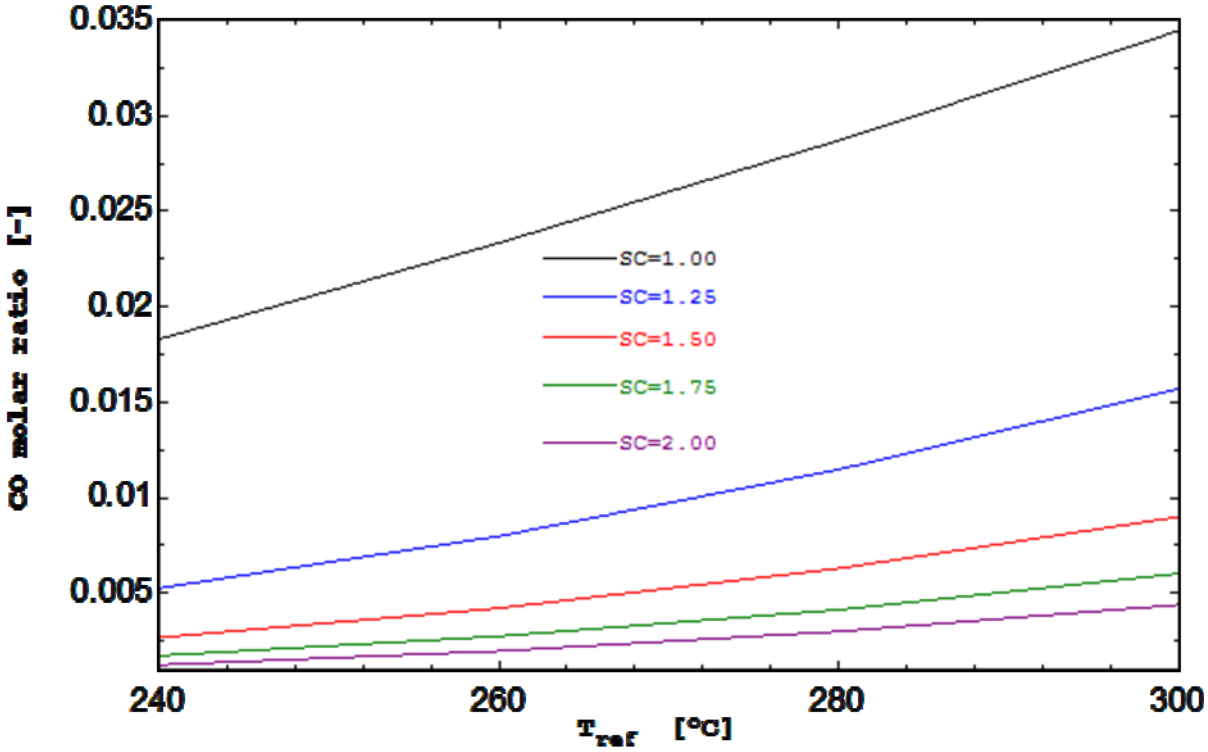

Figure 3-3 Effects of the steam carbon ratio and the reformer temperature on the CO molar ratio in the reformate gas.

Deactivation of the Cu-based catalyst occurs at high temperatures [44], thus temperatures above 300 ºC are not considered for parametric studies. In addition, high SC ratios are suggested to decrease the catalyst deactivation [220]. Therefore, in this study the values obtained for SC=1 are not used to estimate the fuel cell performance and the input fuel flow rate.

The effects of the current density, the fuel cell temperature, the SC ratio, the reformer temperature and the cathode stoichiometric ratio on the fuel cell voltage are shown in Figs. 3-4 - 3-6. As shown in the figures, the fuel cell voltage decreases with an increase in the current density. It can be seen in Fig. 3-4(a) that the fuel cell voltage decreases from ~0.68 V to ~0.3 V with an increasing in the current density from 0.1 A/cm^2 to 1 A/cm^2 for 240 ºC reformer temperature. For the same reformer temperature, the fuel cell voltage reduces from ~0.69 V to ~0.35 V and ~0.7 V to ~0.37 V for the fuel cell temperature 170 ºC (see Fig. 3-4(b)) and 180 ºC (see Fig. 3-4(c)), respectively. The highest decrease in the fuel cell voltage is found to be ~10.6% and ~3.7% for 1 A/cm^2 current density, and 160 ºC and 170 ºC fuel temperatures, respectively, with decreasing the SC of the reformer from 2 to 1.25 as shown in Figs. 3-5(a) and 3-5(b). The higher voltage losses are obtained with the lower fuel cell temperature; the main reason for this that the voltage losses due the CO in the reformate gas increase with the decreasing of the fuel cell temperature. The voltage losses due to the CO molar ratio in the reformate gas is shown in the supplementary document. The effects of the cathode stoichiometric ratio on the voltage loss of the fuel cell can be found from comparison of results in Fig. 3-4(a) and Fig. 3-6. As shown in these figures, less of a voltage loss is obtained for the cathode stoichiometric ratio=3. However, this voltage loss can be neglected at low current densities. For example, the voltage loss is estimated at ~0.62 V (in Fig. 3-4(a)) for 0.2 A/cm^2 at 240 ºC reformer temperature, and the cathode stoichiometric ratio=2, the voltage is found ~0.63 V (in Fig. 3-6) for the same parameters at the cathode stoichiometric

ratio=3. The same effect of the stoichiometric ratio on the voltage loss is also found in Ref. [213]. In addition, other results are verified with Ref. [213].

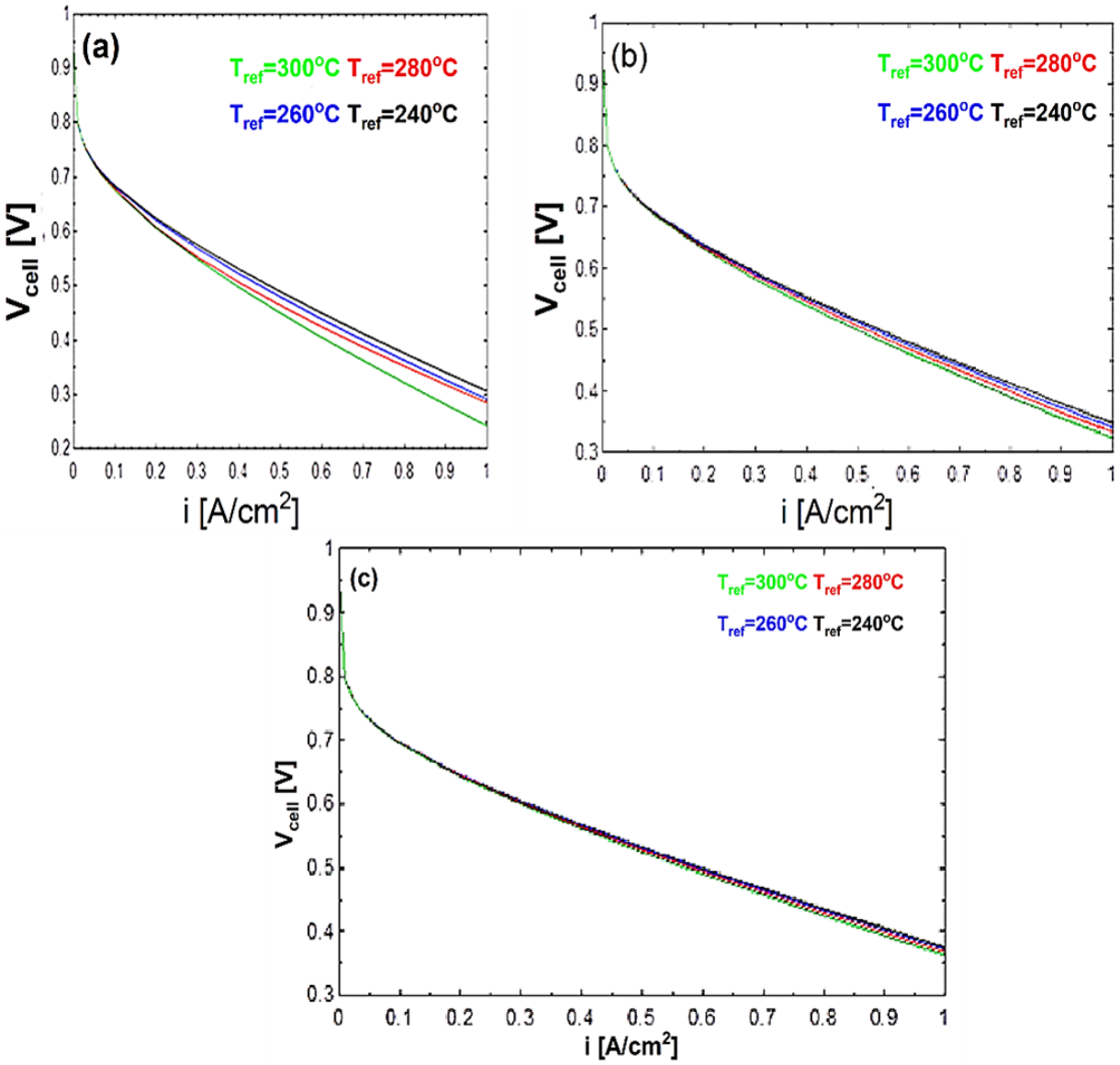

Figure 3-4 Effects of the reformer temperature and the current density on the fuel cell voltage. The results are obtained for: (a) T_{cell}=160 [°C], (b) T_{cell}=170 [°C], (c) T_{cell}=180 [°C], and SC=1.5, cathode stoichiometric ratio=2.

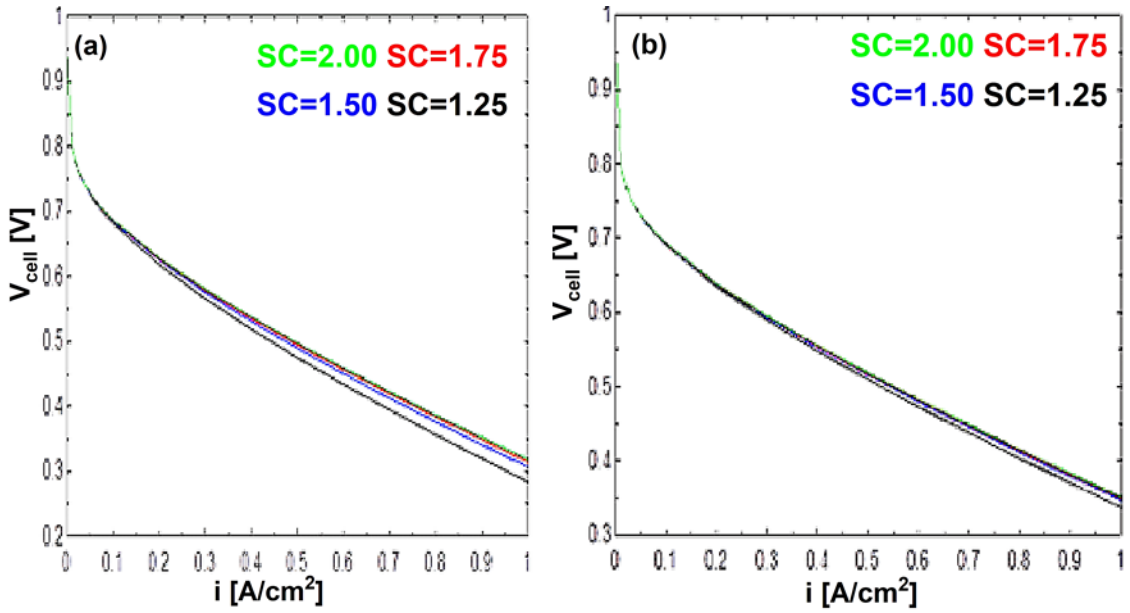

Figure 3-5 Effects of the steam carbon ratio and the current density on the fuel cell voltage. The results are obtained for: (a) T_{cell}=160 [ºC], (b) T_{cell}=170 [ºC], and T_{ref}=240 [ºC], cathode stoichiometric ratio=2.

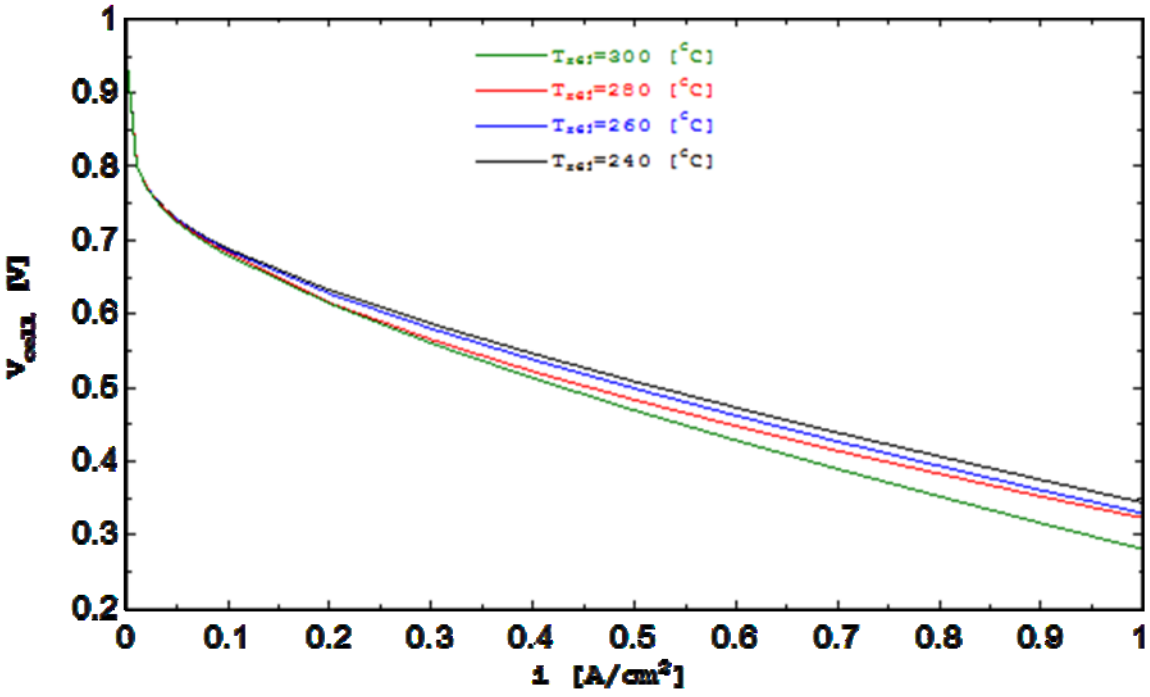

Figure 3-6 Effects of the reformer temperature and the current density on the fuel cell voltage. The results are obtained for T_{cell}=160 [ºC], SC=1.5, cathode stoichiometric ratio=3.

We can see from Figs. 4-6 that the fuel cell performance is better at elevated fuel cell temperatures. The main reasons for this are: (a) better electrochemical kinetics; (b) higher membrane proton conductivity; and (c) higher temperature of the fuel cell favors the CO-desorption [210-212]. However, PBI membrane in the HT-PEMFCs is doped with phosphoric acid to increase the proton conductivity, and it is not thermally stable at high temperatures. Therefore, the behavior of the acid for higher fuel cell temperatures must be considered [106, 202].

The fuel flow rate to produce a given electric power is also a key variable to decrease the system size and increase the system operational time. The change of the input fuel flow rate with fuel cell temperature, the producing power rate from the fuel cell stack, the reformer temperature and the hydrogen utilization ratio is found as demonstrated in Figs.3-7 – 3-9. The SC ratio is adjusted to 1.5 for all of the calculations. The input fuel flow rate refers to liquid methanol-water mixture (stream 3 in Fig.3-1). Variations of the input fuel flow rate to produce 350 W electric power employing the HT-PEMFC stack at 160 ºC, 170 ºC, and 180 ºC are shown in Figs. 3-7(a), 3-7(b), and 3-7(c), respectively. As shown in these figures, the fuel consumption is directly related to the fuel cell performance. The input fuel flow rate decreases with an increase in the fuel cell temperature and a decrease in the reformer temperature. The hydrogen utilization ratio is also an important parameter that affects the input fuel flow rate. The minimum fuel consumption is obtained ~11.2 mol/h for u_f=0.8, T_{ref}=240 ºC, and T_{cell}=160 ºC (Fig. 3-7(c)). In other words, ~0.305 l/h fuel (~0.26 kg/h fuel) is required to produce 350 W power. The maximum fuel consumption is estimated to be ~17.1 mol/h (~0.46 l/h) for u_f=0.6, T_{ref}=300 ºC, and T_{cell}=160 ºC (Fig. 3-7 (a)). The input fuel flow rate is reported as 0.44 l/h for the H3-350 methanol reformer system to produce net 350 W power [201]. It is expected that the effects of the variation of the reformer temperature on the fuel flow rate is more for the low fuel cell temperature. For example, the increase in the fuel

flow rate is ~8.5% for T_{cell}=160 ºC and the change of the reformer temperature from 240 ºC to 300 ºC, and u_f=0.6 (in Fig. 3-7(a)), while this increase is equal to ~3.2% and ~1.5% for T_{cell}=170 ºC and 180 ºC, respectively (in Figs. 3-7(b) and (c)).

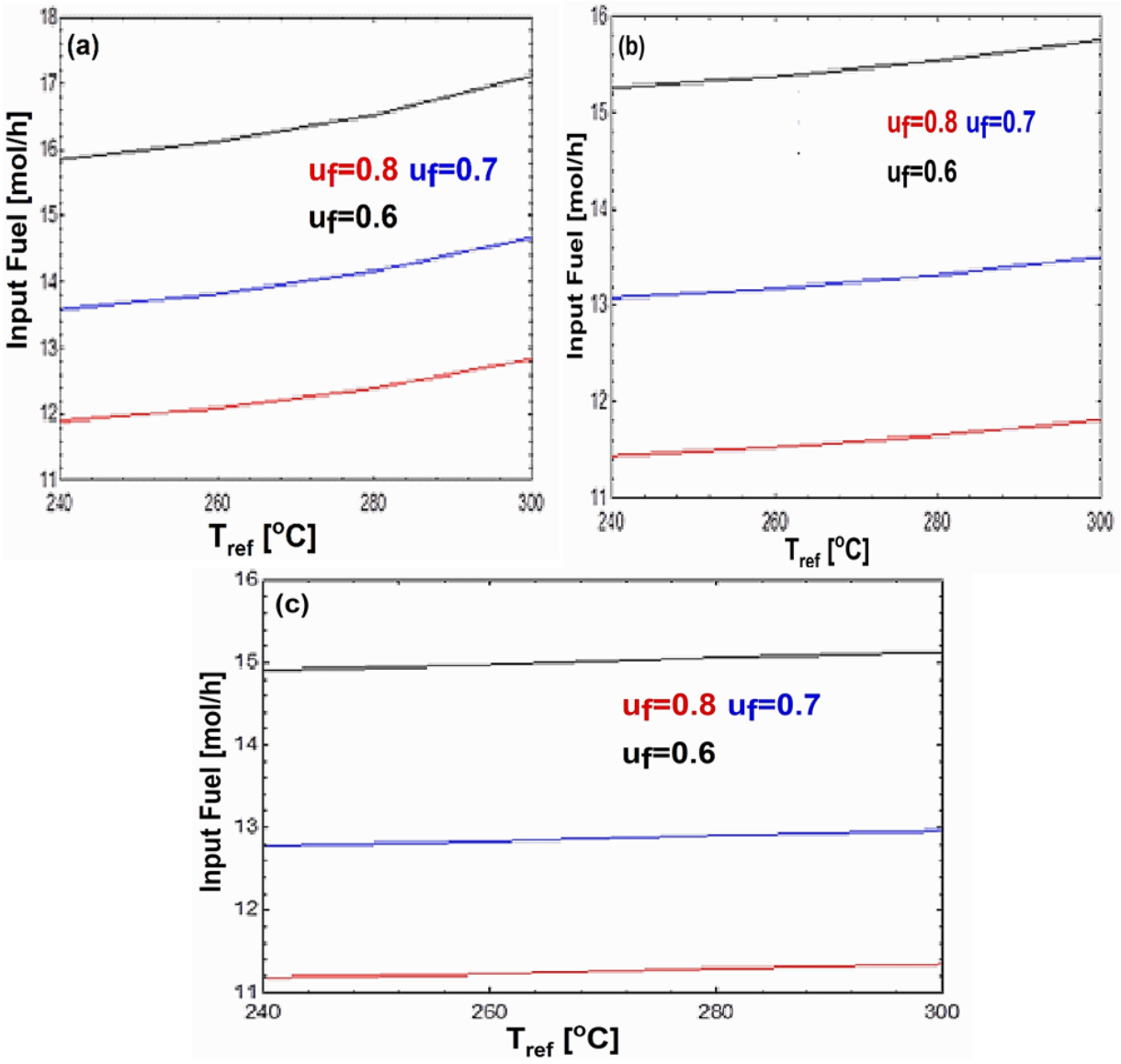

Figure 3-7 Effects of the reformer temperature and the hydrogen utilization factor on the input fuel to produce 350 W power from fuel cell. (a) T_{cell}= 160 [ºC], (b) T_{cell}= 170 [ºC], (c) T_{cell}= 180 [ºC], and SC=1.5, cathode stoichiometric ratio=2.

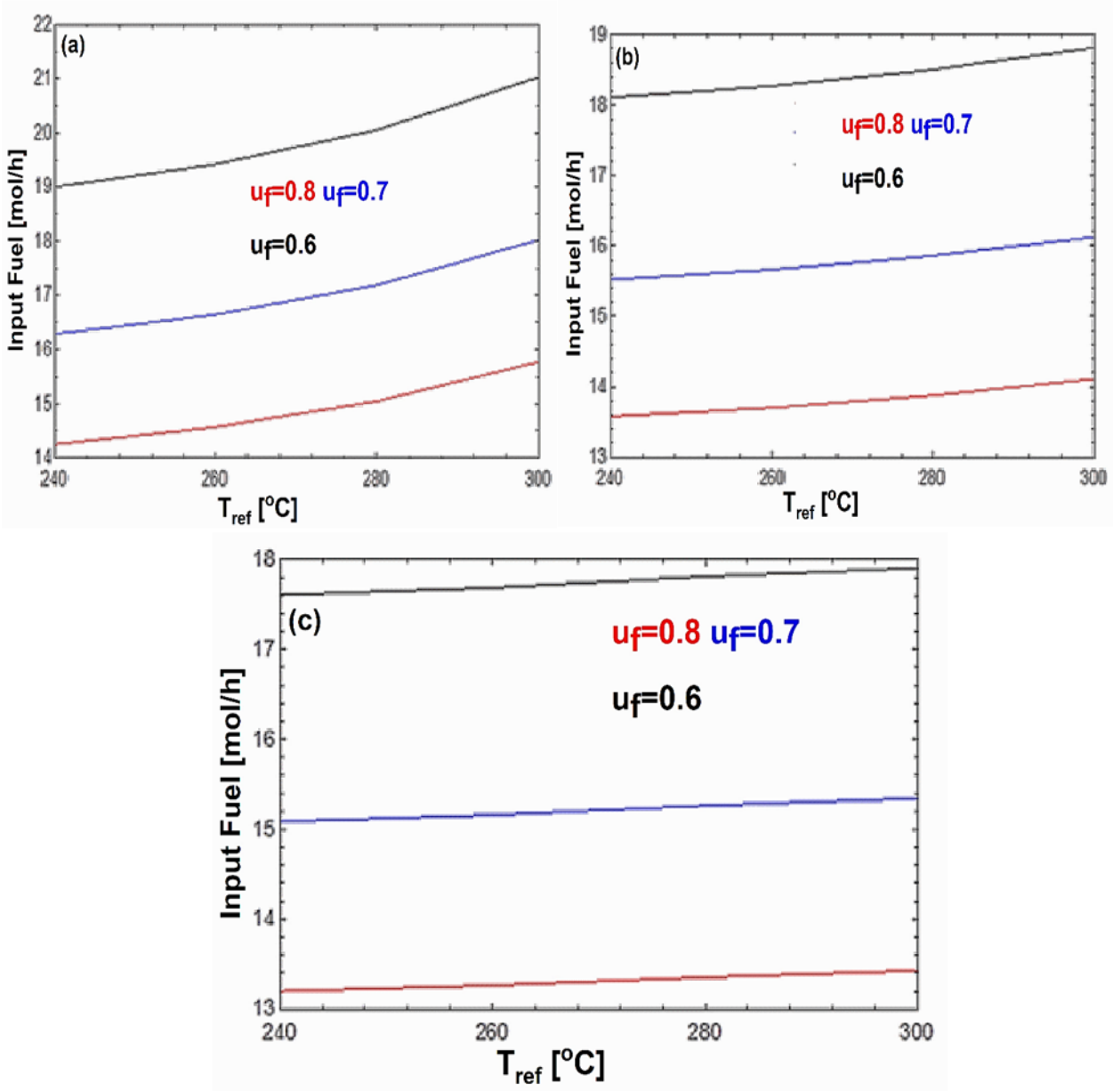

Figure 3-8 Effects of the reformer temperature and the hydrogen utilization factor on the input fuel to produce 400 W power from fuel cell. (a) T_{cell}= 160 [ºC], (b) T_{cell}= 170 [ºC], (c) Tcell= 180 [ºC], and SC=1.5, cathode stoichiometric ratio=2.

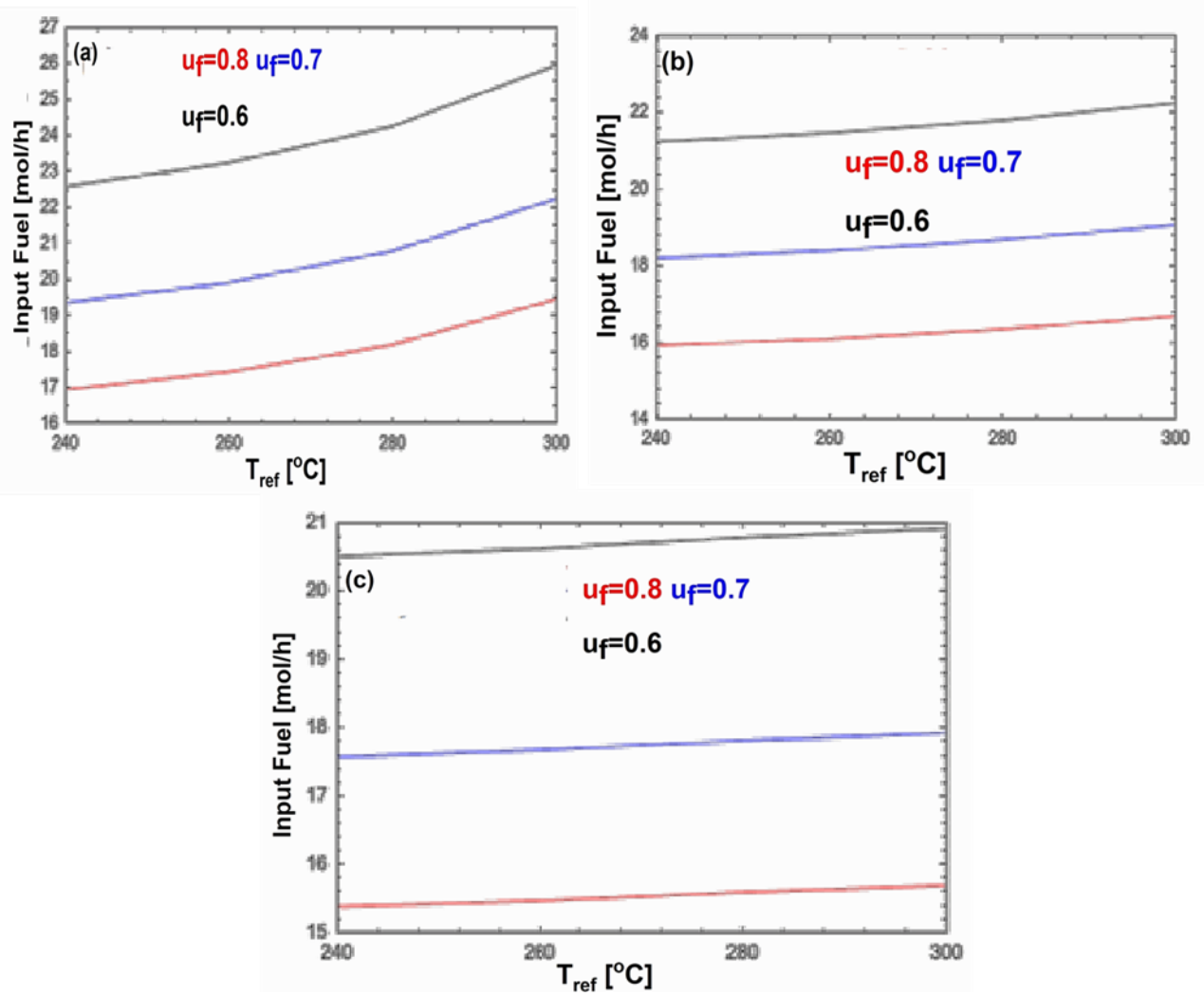

Figure 3-9 Effects of the reformer temperature and the hydrogen utilization factor on the input fuel to produce 450 W power from fuel cell. (a) T_{cell}= 160 [ºC], (b) T_{cell}= 170 [ºC], (c) T_{cell}= 180 [ºC], and SC=1.5, cathode stoichiometric ratio=2.

The requirement for the fuel to produce 400 W and 450 W is also shown in Figs. 3-8 and 3-9. The minimum values are ~13 mol/h and ~15.4 mol/h for 400 W and 450 W power production, respectively for u_f=0.8, T_{cell}=180 ºC, and T_{ref}=240 ºC. For the same hydrogen utilization and the reformer temperature, these values are ~14.3 mol/h and ~13.6 mol/h for T_{cell}=160 ºC and 170 ºC, respectively to produce 400 W power and ~16.9 mol/h and ~16 mol/h for 450 W of power production. Although a high hydrogen utilization ratio is favorable for the fuel consumption, heat production of the combustor should be considered with the variation of the hydrogen utilization

ratio. The hydrogen that is not consumed in the fuel cell is used in the combustor as a fuel, so the hydrogen utilization ratio is important for the heat production in the combustor.

The heat which must be transferred to the evaporator and the reformer, and the heat production in the fuel cell and the combustor are demonstrated in Figs. 3-10 – 3-13. The hydrogen utilization ratio is very important for the heat requirement and the production of the components. In addition, the cathode stoichiometric ratio is also very important for the heat production of the fuel cell and the combustor. Therefore, these parameter`s effects are considered in this study. The reformer temperature is also considered because it has an effect on the reformate gas composition.

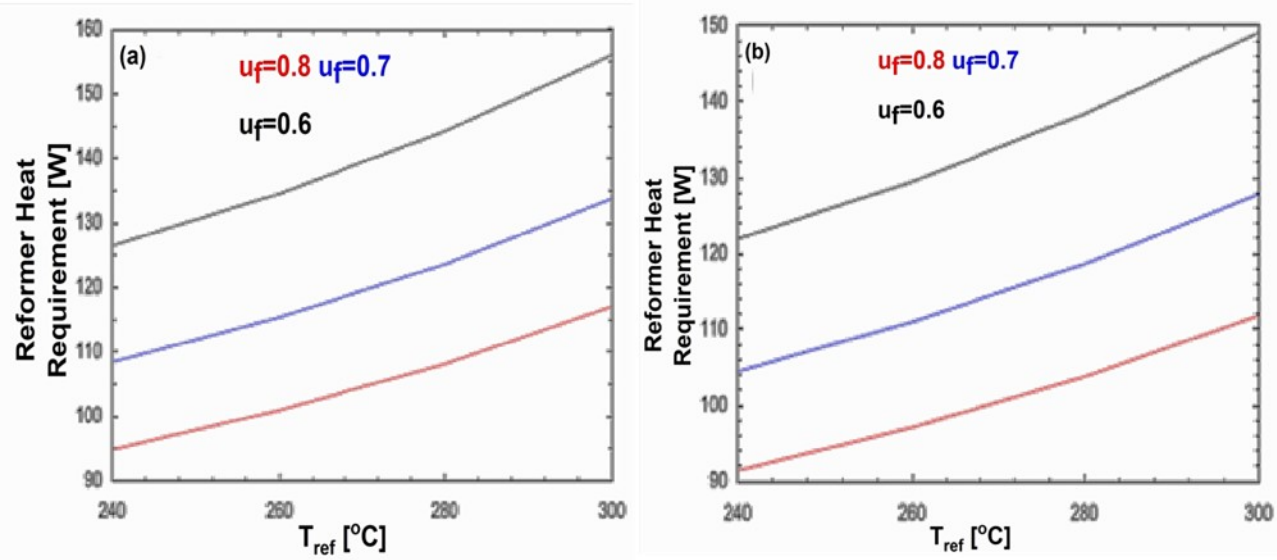

Figure 3-10 Effects of the reformer temperature and the hydrogen utilization factor on the heat requirement of the reformer to produce 350 W power from fuel cell. (a) T_{cell}= 160 [°C], cathode stoichiometric ratio=2, (b) T_{cell}= 160 [°C], cathode stoichiometric ratio=5, and SC=1.5.

The change of the heat requirement of the reformer is shown in Figs. 3-10(a) and 3-10(b). As shown in these figures, the heat requirement significantly changes with the hydrogen utilization and the reformer temperature; however, the cathode stoichiometric ratio is not significantly important for the change of the heat requirement. The increase of the heat requirement is almost 33% (from ~95 W to ~126 W) with the variation of the hydrogen utilization from 0.8 to 0.6 for

T_{ref}=240 ºC, and the cathode stoichiometric ratio=2. The reason of this change is to increase the input fuel flow rate to produce a given power with a low hydrogen utilization ratio. The heat requirement is also significantly changed from ~126 W to ~156 W with the variation of the reformer temperature from 240ºC to 300ºC for u_f=0.6, and the cathode stoichiometric ratio=2 (see Fig. 3-10 (a)). The molar ratio of the CO increases for high reformer temperatures, and so the voltage losses increase as well. Therefore, the input fuel rate increases to compensate these losses to produce power, and this causes a higher heat requirement. If we compare Figs. 3-10 (a) and 3-10 (b), we can see that the heat requirement of the reformer does not significantly change with the cathode stoichiometric ratio. The reason being that the fuel cell performance is slightly changed along with the change of the cathode stoichiometric ratio; as explained in the previous paragraphs.

The evaporator heat requirement is also illustrated in Figs. 3-11(a) and 3-11(b). The change of the heat requirement is directly related to the input fuel flow rate, like the reformer. Therefore, the same parameters have the same effects on the change of the heat requirement of both the evaporator and the reformer. The minimum heat requirement of the reformer is obtained as ~145 W for u_f=0.8, the cathode stoichiometric ratio=5, and T_{ref}=240 ºC (see Fig. 3-11 (b)), and the maximum ~217 W for u_f=0.6, the cathode stoichiometric ratio=2, and T_{ref}=300 ºC (see Fig. 3-11(a)).

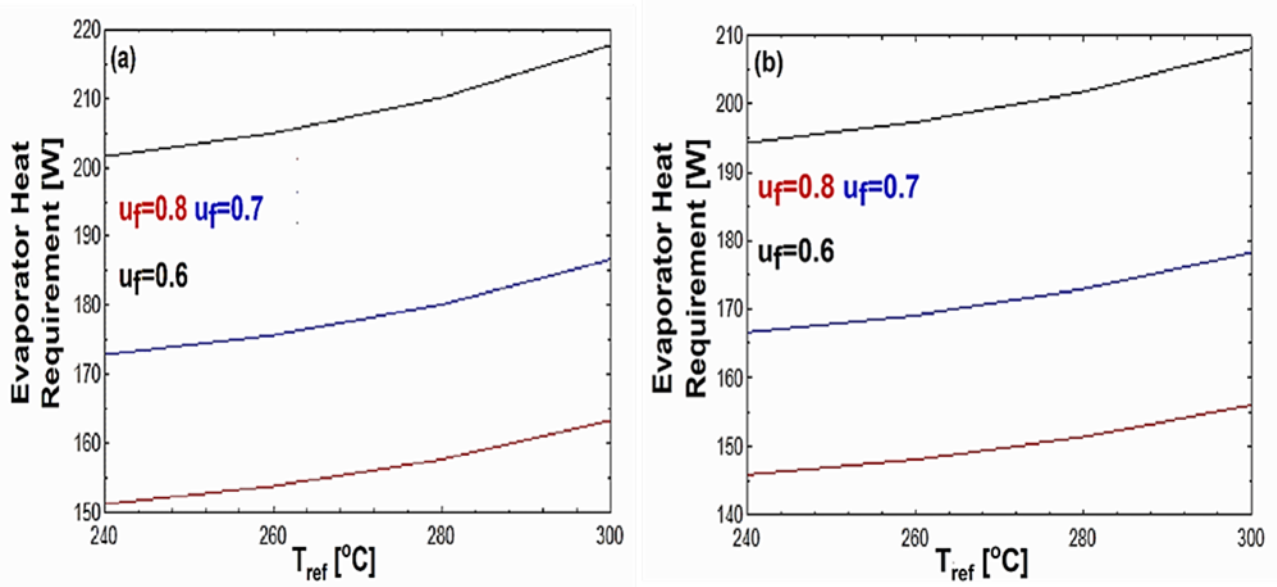

Figure 3-11 Effects of the reformer temperature and the hydrogen utilization factor on the heat requirement of the evaporator to produce 350 W power from fuel cell. (a) T_{cell}= 160 [ºC], cathode stoichiometric ratio=2, (b) T_{cell}= 160 [ºC], cathode stoichiometric ratio=5, and SC=1.5.

The heat production in the combustor is demonstrated in Figs. 3-12(a) and (b). In our calculations, the combustor temperature is set as 20 ºC higher than the reformer temperature for the parametric studies. If the oxygen ratio in the cathode off-gas to the fuel ratio in the anode off-gas less than 1.05, extra air is supplied to the combustor (stream-8 in Fig.1). As shown in Figs. 3-12(a) and 3-12(b), the hydrogen utilization ratio is a key variable for the heat production in the combustor. In addition, the cathode stoichiometric ratio has significant effect on the heat production of the combustor. When the cathode stoichiometric ratio is equal to 2, the production of enough heat for the reformer is possible with the change of the other parameters (see Fig. 3-10 (a) and Fig. 3-12 (a)). However, enough heat may not be produced at high cathode stoichiometric ratios. As seen in Fig. 3-12 (b), the heat production changes from ~72 W to ~8 W, with the variation of the reformer temperature from 240 ºC to 300 ºC for u_f=0.8, and the cathode stoichiometric ratio=5. As such, the amount of N_2 significantly increases along with the high cathode stoichiometric ratio, and this causes dilution of the fuel. Therefore, the heat production rapidly

reduces. In particular, this is very important for the high hydrogen utilization ratio, because the amount of hydrogen decreases considerably, and this causes a higher decrease in the heat production at high cathode stoichiometric ratios.

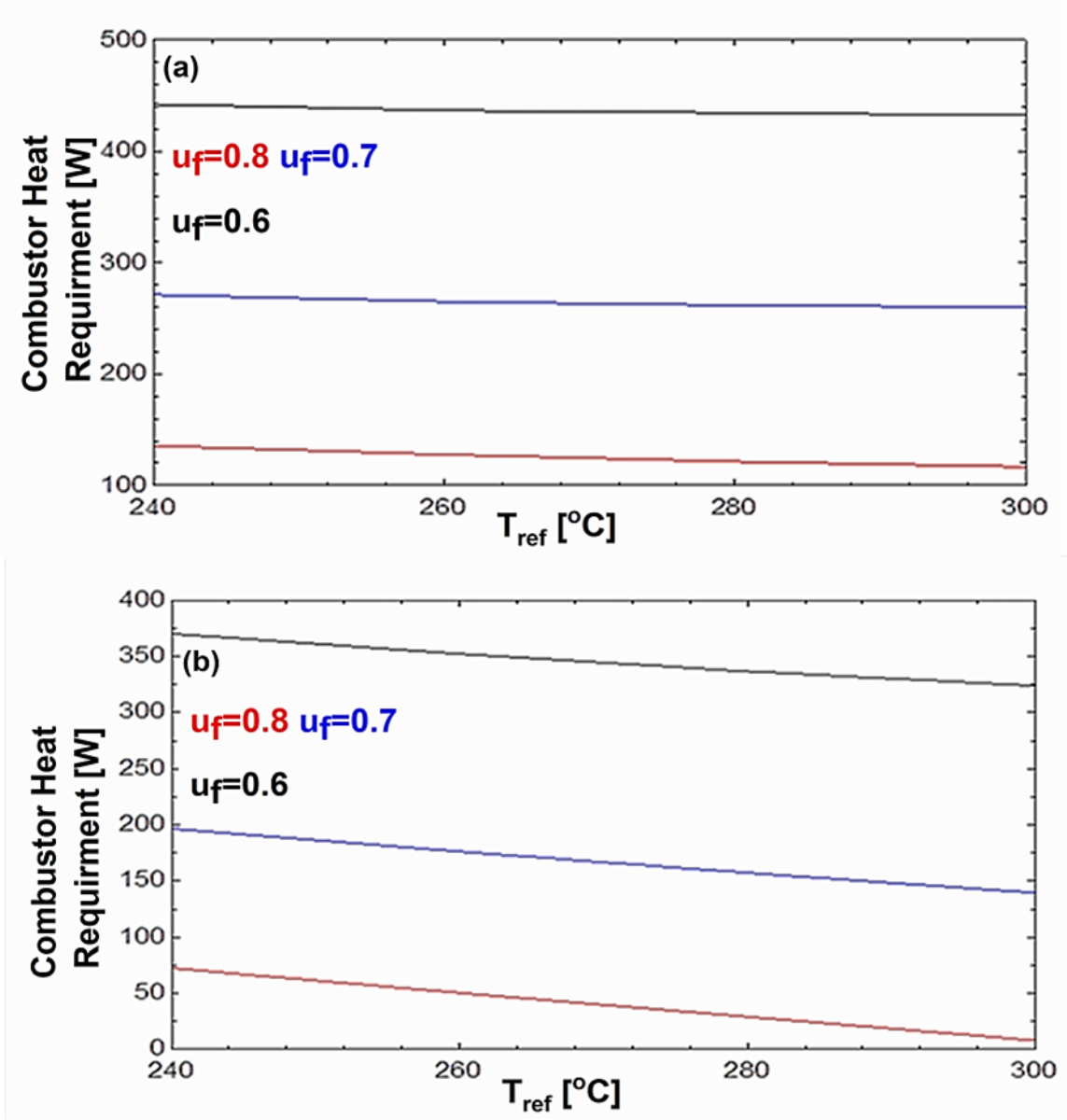

Figure 3-12 Effects of the reformer temperature and the hydrogen utilization factor on the heat production of the combustor to produce 350 W power from fuel cell. (a) T_{cell}= 160 [°C], cathode stoichiometric ratio=2, (b) T_{cell}= 160 [°C], cathode stoichiometric ratio=5, and SC=1.5.

The heat production from the fuel cell is shown in Fig. 3-13. Here, the effect of the hydrogen utilization ratio on the heat production is not considered, because there are only small variations with the hydrogen utilization ratio. Therefore, the results which are demonstrated in Fig. 3-13 are only obtained for u_f=0.6. The heat production from the fuel cell stack is around 335 W. Although the fuel cell stack cathode heat is used for the evaporator in the H3-350, the fuel cell heat cannot be used for the reformer, due to the fuel cell`s temperature. If high methanol conversion with low temperature (at the fuel cell temperature) can be achieved for future applications, the fuel cell stack heat can be used for both the evaporator and the reformer, in which case the combustor may be removed from the system. The heat duties of the other heat exchangers in Fig. 3-1 are shown in the supplementary document.

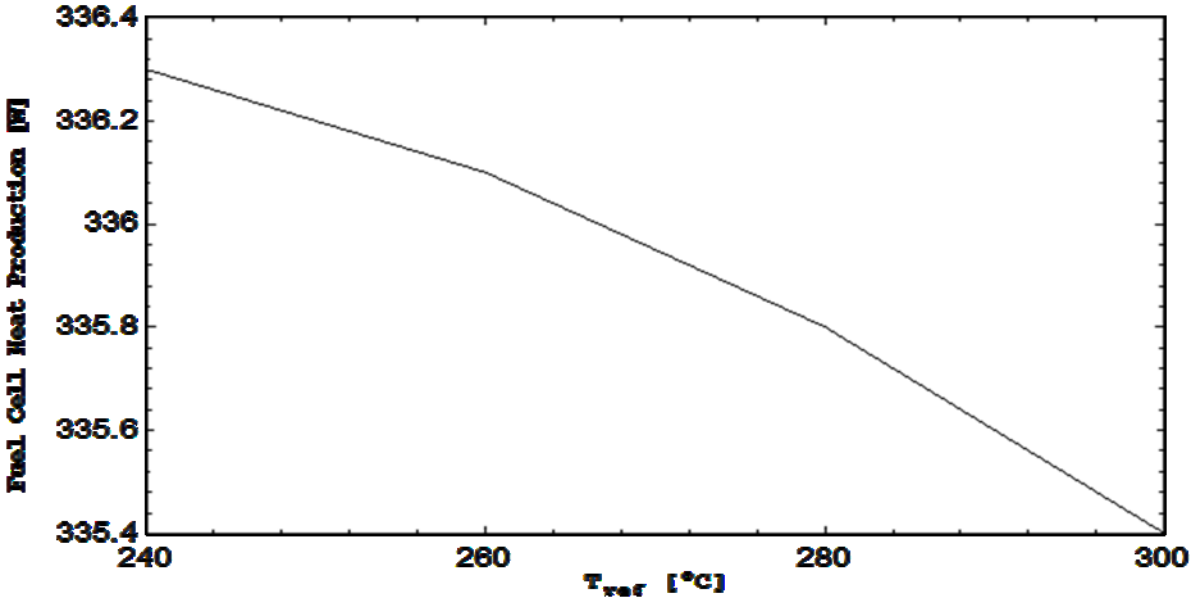

Figure 3-13 Fuel cell heat production for 350 W power generation. Tcell=160 [ºC], SC=1.5, cathode stoichiometric ratio=2.

The system efficiency is shown in Fig. 3-14. The efficiency is calculated for T_{ref}=240 ºC, and 300 ºC. As shown in the figure, the maximum efficiency is obtained as 35% for T_{cell}=180 ºC, and T_{ref}=240 ºC. For the same reformer temperature, the efficiency decreases to ~32% for T_{cell}=160 ºC. The efficiency change significantly with the fuel cell temperature for T_{ref}=300 ºC. The system

efficiency is ~34% for T_{cell}=180 ºC, while it is ~27% for T_{cell}=160 ºC. As mentioned previously, the main reason of this change is the CO molar ratio in the reformate gas that increases with increasing of the reformer temperature, and this causes decrease in the fuel cell performance.

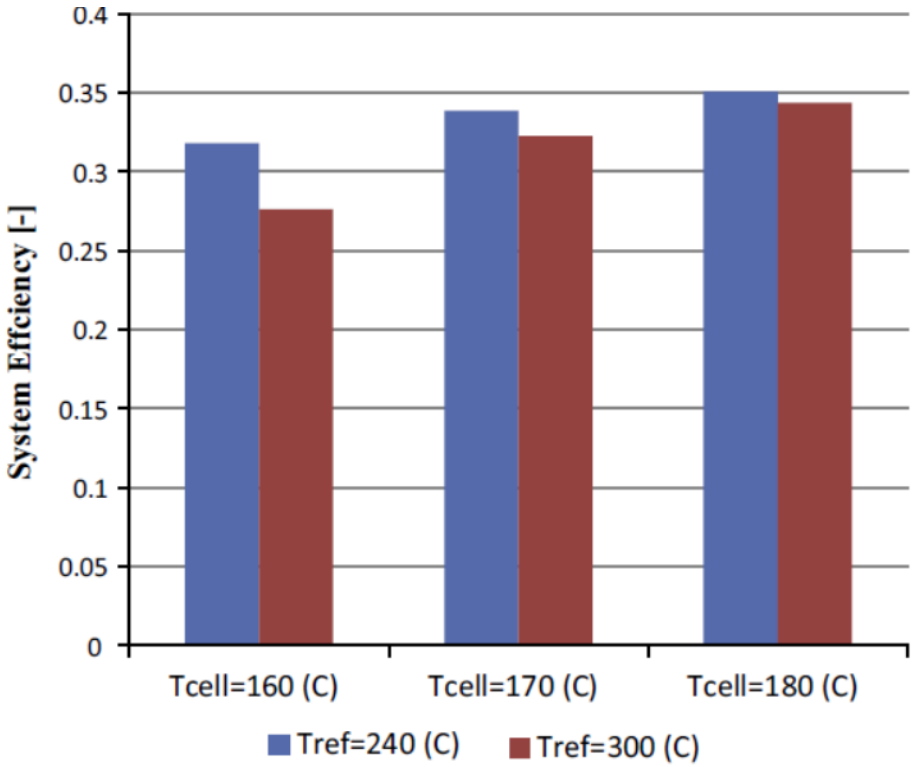

Figure 3-14 The system efficiency for 450 W power generation from the fuel cell stack.

3.5 Conclusions

The results found in this study show the different parameters effects on the reformate gas composition, the fuel cell performance, the input fuel flow rate, the heat requirement of the evaporator and the reformer, as well as the heat production of the combustor and the fuel cell stack. The highest fuel cell performance and the lowest input fuel flow rate to produce a given electric power have been obtained for the higher fuel cell temperature. The results indicated that the system can be operated 20 h with ~5.2 kg fuel to produce 350 W electric power from the fuel cell stack

for u_f=0.8, T_{ref}=240 ºC, and T_{cell}=180 ºC. The results also show that heat production from the combustor significantly reduces with a higher hydrogen utilization ratio.

Chapter 4
Multiphysics modeling and heat distribution study in a catalytic microchannel methanol steam reformer

This chapter is reprinted in adopted form with permission from American Chemical Society: MS Herdem, M Mundhwa, S Farhad, and F. Hamdullahpur. Multiphysics modeling and heat distribution study in a catalytic microchannel methanol steam reformer, Energy and Fuel, 2018, 32, 7220-7234.

4.1 Introduction

Hydrogen as a fuel has promising potential to produce power that is environmentally friendly and provides high efficiency by employing fuel cells. One of the most important barriers to fuel cell systems becoming more commonplace for power generation applications - in particular for portable applications - involves the difficulties regarding hydrogen transportation and storage infrastructure. Hydrogen has higher gravimetric energy density than hydrocarbon and alcohol fuels as shown in Table 1, but in terms of its volumetric energy density (Wh/l), it is significantly less dense than other fuels [31]. Therefore, to overcome hydrogen transportation and storage issues, alternative fuels can be converted to hydrogen rich gas using fuel reforming in order to provide the required fuel for fuel cells. There are several liquid oxygenated hydrocarbons [229], including methanol [18, 106, 230], ethanol [231], and glycerol [232] that possess the potential for renewable hydrogen production, and they are stored and transported more easily than gas fuels such as biogas [233] and methane [234]. Among the liquid oxygenated hydrocarbons, methanol stands out as an attractive fuel for the steam reforming process due to its low reforming temperature, low steam to carbon ratio, and proper miscibility with water. In particular, methanol is an ideal fuel to produce

hydrogen for high temperature proton exchange membrane (HT-PEM) fuel cells due to its unique properties mentioned above.

Table 4-1 **Comparison of specifications of Various Fuels** [223-228]**.**

Fuel	Major Chemical Compound	Specific Energy (MJ/kg)	Energy Density (MJ/l)	Density* (g/l)	Boiling Point (^{o}C)
Hydrogen	H_2	142.0	0.0128	0.0899[1]	-252.9
Methane	CH_4	55.5	0.0388	0.668[2]	-161
LPG	C_3-C_4	50.0	26.25-29	525-580	-42
Methanol	CH_3OH	22.5	17.82	792	65
Ethanol	C_2H_5OH	29.7	23.43	789	78
Gasoline	C_4-C_{12}	45.8	32.93	719	30-225
JP-4	C6-C11	45.8	34.4-36.73	751-802	45-280
JP-7	C10-C16	46.8	36.45-37.72	779-806	60-300
Diesel	C_9-C_{24}	45.3	38.5	~850	180-340

[1.)] Density at 0 ^{o}C and 1 atm.

[2)] Density at 20 ^{o}C and 1 atm.

*) For liquid fuels, density at 20^{o}C.

It is well known that steam reforming of methanol (SRM) is a highly endothermic process; hence it requires an efficient and adequate heat supply. This can be achieved in microchannel methanol reformers because they have high surface-to-volume ratio that can be as high as 10,000 to 50,000 m^2/m^3 [14]. In addition, thin layers of appropriate catalysts are coated on the surface of a plate/wall in a microchannel plate reformer, which improves the activity of the reforming catalyst [15]. Therefore, many researchers have investigated various aspects of the performance of microchannel methanol reformers.

Kaznetsov & Kozlov [235] used a two-dimensional (2D) model to understand temperature distribution and methanol conversion with variation of the external uniform and linearly falling heat flux. They did not consider the 2D catalyst layer domain and the effects of catalyst layer thickness on methanol conversion and temperature distribution. Chen *et al.* [236] performed a numerical simulation using Fluent software to evaluate the effects of the liquid feed rate, the reaction temperature, and the steam to carbon (S/C) ratio on the plate type microreformer for SRM. They employed the power rate law for the kinetic expressions and did not use any external heat supply to provide heat for the endothermic SRM reactions. Hsueh *et al.* [237] developed a numerical model of a microchannel plate methanol reformer to investigate the heat and mass transfer phenomena, along with flow configuration. They considered combustion of methanol in an adjacent parallel flow-channel to supply the required endothermic heat to the reforming sites. They reported that a higher Reynolds number in the combustion-channel than in the reforming-channel can improve the conversion of methanol on the reforming side. They also predicted 10% more methanol conversion in the reforming-channel in the case of counter-flow configuration compared to co-flow configuration. Hsueh and collaborators [238] also investigated the influence of the parallel flow field and the serpentine flow fields on a plate methanol steam micro-reformer and a methanol catalytic combustor. They found that the methanol conversion increased by 23% with the serpentine flow field. Fazeli and Behnam [239] modeled a wall-coated microchannel methanol reformer to examine the influence of reactor geometry on the reformer performance. They considered zigzag and straight plate designs and found that zigzag plate design provides better heat and mass transfer rates compared to the straight plate design. On the same path, Hao *et al.*[240] examined the influence of reformer geometry on the flow distribution. They also investigated the influence of the reforming-catalyst layer on the performance of a microchannel

methanol steam reformer. They found that with certain entrance design and channel inclination angle, uniform flow distribution can be achieved. Tadbir and Akbari developed two-dimensional (2D) [241] and three-dimensional (3D) [242] numerical models to investigate the influence of various parameters on a microchannel methanol reformer. They considered square channels with 700 μm sides for 2D and 3D models for the baseline case simulation runs. They estimated that enough hydrogen can be produced to feed a 30 W PEM fuel cell by employing a microchannel methanol reformer consisting of 1540 square channels with 20 mm length. Uriz *et al.*[243] investigated the effects of flow-distribution and heat losses via a computational fluid dynamics model of a microchannel methanol reformer consisting of 100 channels coated with Pd/ZnO catalyst. Recently, Sari and Sabziani [244] reported a 3D model of a microchannel methanol reformer and investigated the influence of inlet steam to methanol ratio, pre-heat temperature, channel geometry and size, and the level of external heat flux on the performance of a methanol reformer. Sari and Sabziani [244] found that maximum hydrogen molar flow rate can be obtained for inlet S/C = 1.4 and increasing inlet S/C ratio monotonically reduces the reaction temperature and carbon monoxide concentration. They also compared the accuracy of two diffusive flux models and found that the Maxwell-Stefan model showed better agreement with experimental results compared with the mixture-averaged model. A more detailed and comprehensive literature review regarding microchannel and microstructure reformers are presented by Kolb [44] and Holladay & Wang [159]. In addition to these works, some research groups have recently investigated feasibility of internal reforming of methanol fuel cell (IRMFC) system [127, 186, 187] and evaluated highly active and durable noble metal catalyst for external methanol steam reforming [113, 245].

The literature review has revealed that most research on numerical modeling of microchannel methanol reformers have considered the scale of the microchannel reformer to feed less than a 100 W fuel cell. However, fuel cells are more competitive with other alternative technologies such as batteries, diesel generators for military and auxiliary power unit applications [2,169] whose power requirements are more than 100 W. In addition, the numerical models developed for the microchannel methanol reformers have considered one-dimensional (1D) catalyst layer domain in the axial direction and ignored the internal diffusion limitation and the influence of the catalyst layer's thermal conductivity, porosity, pore diameter, tortuosity, effective diffusivity, permeability and internal diffusion limitation. To design and achieve the commercial product of new generation micro-channel methanol reformers, it is important to understand the effects of thermal management, and the microstructure of the catalyst layer.

In this study, our main goal is to investigate the effects on methanol conversion of catalyst layer thickness under various heat transfer scenarios to understand how the performance of microchannel methanol reformers can be increased and size can be decreased for power generation between 100 and 500 W. Firstly, various kinetic models based on power rate laws developed by Jiang *et al.*[246], Purnama *et al.*[120], and Sa *et al.*[143] and Langmuir-Hinshelwood macro-kinetic rate expressions developed by Peppley *et al.*[138] are compared with experimental data 247]. Then, the most appropriate rate expression for this study is selected to accurately estimate the methanol conversion and temperature of the reformer. Diffusion limitation through the catalyst layer is investigated by determining the catalyst effectiveness factor. In addition, parametric studies are performed to reveal the effects of the catalyst porosity on the microchannel methanol reformer. The porosity affects the pore size, tortuosity and effective physical properties of catalyst layers; thus, the porosity is considered for the parametric studies. Finally, the results obtained from

two different models are compared: a model with a 2D catalyst layer domain and another model with a 1D catalyst layer domain.

To achieve our goals, a 2D multiphysics model is employed which includes mass, momentum and heat transfer balance equations as well as the reaction kinetics equations and the properties of porous catalyst layer. The Maxwell-Stefan model is implemented into the model to estimate diffusive mass flux. Mean pore size of the catalyst is calculated by employing Kozeny's equation [248], and the tortuosity of the catalyst layer is estimated by using the Bruggeman equation [249].

4.2 Modeling framework

The 2D drawing of the microchannel reformer is illustrated in Fig. 4-1. The modeling work consists of a computational geometry with two domains: (1) porous catalyst layer and (2) reforming-channel for free flow. The model developed in this study considers the mass, momentum and energy conservation equations in both reforming channel and porous catalyst layer domains simultaneously and incorporates chemical reactions along the channel and catalyst layer thickness directions. The governing equations and boundary conditions that are presented in [250-252] were adopted in this study. In addition, numerical integration is implemented in the model to estimate the effectiveness and other parameters, and a step-wise solution method is developed to prevent possible convergence errors for this study. The step-wise solution method is also used to choose the values of the parameters for the parametric study. This section presents the physical properties, reaction kinetics, input conditions, boundary conditions, solution schema and assumptions used in this work in detail. Although the developed model is for a microchannel reformer for the reforming of methanol, it can be easily modified for the reforming of other fuels.

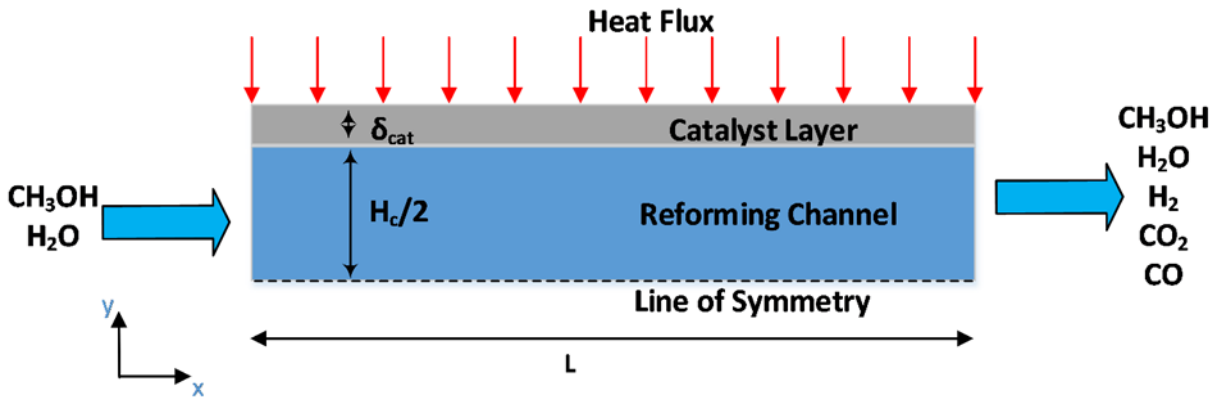

Figure 4-1 2D schematic of the simulated domains of the methanol steam reformer (not to scale).

4.2.1 Physical properties

The diffusivities, viscosities, thermal conductivities and heat capacities of pure components are calculated as a function of temperature. In addition, weight fractions of the components, which are CH_3OH, H_2O, H_2, CO_2 and CO are considered in order to estimate the physical properties of the gas mixture.

Binary diffusion coefficients are estimated by employing Eq. 4.1 [253]:

$$D_{ij} = \left(\frac{0.00266 T^{\frac{3}{2}}}{P_g M_{ij}^{\frac{1}{2}} \sigma_{ij}^2 \Omega_D} \right) \times 10^{-4} \tag{4.1}$$

where, T (K) and P_g (bar) are the temperature and pressure of the gas stream. Other variables (Ω_D, σ_{ij}, and M_{ij}) required for Eq. 4.1 are listed in Table B. 1 of the Supporting Information. The characteristic length and Lennard-Jones energy parameters are listed in Table B. 2 of the Supporting Information. The effective diffusivities (D_{ij}^{eff}) are applied to estimate the diffusive fluxes of various chemical species inside porous catalyst layer and are estimated by considering Knudsen (D_i^K) and binary (D_{ij}) diffusion coefficients [254] in Eq. 4.2:

$$D_{ij}^{eff} = D_{ji}^{eff} = \frac{\Phi}{\tau}\frac{1}{2}\left(\frac{1}{\frac{1}{D_i^k}+\frac{1}{D_{ij}}}+\frac{1}{\frac{1}{D_j^k}+\frac{1}{D_{ji}}}\right) \tag{4.2}$$

The Knudsen diffusion [255] and the tortuosity factor [187] required in Eq. 4.2 are computed as:

$$D_i^k = \frac{1}{3} d_{pore}\sqrt{\frac{8RT}{\pi M_i}} \tag{4.3}$$

$$\tau = \Phi^{-0.5} \tag{4.4}$$

In Eq. 4.3, d_{pore} is the mean pore size of the catalyst particles and it is estimated using Kozeny`s equation [248] as a function of the porosity (ϕ) and the mean particle size (dp_a) as:

$$d_{pore} = \frac{2}{3}\frac{\Phi}{1-\Phi} dp_a \tag{4.5}$$

The pure component viscosities (μ_i) are determined using Eq. 4.6 [256]:

$$\mu_i = \frac{aT^b}{1+\frac{c}{T}+\frac{d}{T^2}} \tag{4.6}$$

The constants (a, b, c, d) required in Eq. 4.6 are given in Table B. 3 of the Supporting Information. The gas mixture viscosity was calculated using the following semi-empirical formula [257]:

$$\mu_{mix} = \sum_{i=1}^{N}\frac{y_i\mu_i}{\sum_j y_j \Phi_{ij}} \tag{4.7}$$

Where N is the number of chemical species, y_i is the mole fraction of species *i*, and the dimensionless quantities Φ_{ij} is defined as:

$$\Phi_{ij} = \frac{1}{\sqrt{8}}\left(1+\frac{M_i}{M_j}\right)^{-\frac{1}{2}}\left[1+\left(\frac{\mu_i}{\mu_j}\right)^{\frac{1}{2}}\left(\frac{M_j}{M_i}\right)^{\frac{1}{4}}\right]^2 \tag{4.8}$$

The thermal conductivity of the gas mixture is estimated by employing the pure component thermal conductivities (k_i) instead of μ_i in Eq. 4.7 and the pure component thermal conductivities are estimated as [256]:

$$k_i = \frac{c_1 T^{c_2}}{1 + \frac{c_3}{T} + \frac{c_4}{T^2}} \tag{4.9}$$

The constants (c_1, c_2, c_3, c_4) in Eq. 4.9 are listed in Table B. 4 of the Supporting Information.

The heat capacity values for the pure components and for the gas mixture are computed using the following equations [205]:

$$\overline{c}_{p,i} = \propto + \propto_1 T + \propto_2 T^2 + \propto_3 T^3 \tag{4.10}$$

$$C_{p,mix} = \frac{\sum_{i=1}^{N} y_i \overline{c}_{p,i}}{M_{mix}} \tag{4.11}$$

where, M_{mix} is the molecular weight of the reformate gas mixture, and required constants are tabulated in Table B. 5 of the Supporting Information.

4.2.2 Reaction kinetics

The methanol steam reforming rate expressions reported in the literature can be divided into two main categories: (1) rate expressions based on power rate law [120, 140, 143, 246], and (2) rate expressions based on elementary surface-reaction mechanisms [138, 143, 258]. Three different rate expressions based on power rate laws [120, 143, 246] and the rate expressions derived from proposed elementary surface-reaction mechanisms [138] are chosen to determine which rate expression represents the experimental data of methanol steam reforming most accurately.

Jiang *et al.*[246] and Sa *et al.*[143] derived a rate expression based on the power rate law for the methanol steam reforming reaction given in Eq. 4.12:

$$CH_3OH + H_2O \rightarrow 3H_2 + CO_2 \qquad \Delta H^0_{298} = 49.5 \frac{kJ}{mol} \tag{4.12}$$

Purnama *et al.*[120] also used the power rate law to derive rate expressions; however, they also considered the reverse water gas shift reaction (Eq. 4.13) with the methanol steam reforming reaction (Eq. 4.12):

$$CO_2 + H_2 \leftrightarrow CO + H_2O \qquad \Delta H_{298}^0 = 41 \frac{kJ}{mol} \tag{4.13}$$

The kinetic model suggested by Peppley *et al.*[138] considered the methanol steam reforming reaction (Eq. 4.12), the methanol decomposition reaction (Eq. 4.14), and the water gas-shift reaction (Eq. 4.15):

$$CH_3OH \leftrightarrow 2H_2 + CO \qquad \Delta H_{298}^0 = 90.5 \frac{kJ}{mol} \tag{4.14}$$

$$CO + H_2O \leftrightarrow H_2 + CO_2 \qquad \Delta H_{298}^0 = -41 \frac{kJ}{mol} \tag{4.15}$$

Detailed information about the rate expressions are provided in the Supporting Information.

4.2.3 Inlet conditions and other parameters

The input parameters which are used for the modeling of the reformer are shown in Table 4-2. For the selection of parameters, we consider Refs. [259] and [18]. A methanol microchannel reformer with Pd/ZnO catalyst is experimentally examined in Ref. [259]. The results [259] show that the produced hydrogen from this reformer is enough to produce power in the range of 218-255 W using a commercial PEM fuel cell with 80% hydrogen utilization. Therefore, we use Ref. [259] to decide the dimensions of the reformer. In addition, a comprehensive parametric study was performed in Ref. [18] to investigate the effects of various parameters on a HT-PEM fuel cell system fed with hydrogen obtained by methanol steam reforming to produce power in the range of 100 to 500 W. Therefore, Ref. [18] is used to decide input temperature, flow rate and steam to carbon ratio to the reformer channel.

Table 4-2 The input parameters for the simulation of the microchannel reformer.

Parameter	Unit	Value
Inlet molar flow rate of methanol	[mol/h]	0.0247, 0.0371, 0.0494
Steam to carbon ratio	[-]	1.5
Inlet temperature of the input fuel flow rate	[K]	423.15
Pressure	[Pa]	101325
Height and width of the channel	[m]	700E-6
Length of the reformer	[m]	0.2
Catalyst layer thickness	[μm]	10, 20, 30, 40, 50, 60, 70, 80, 90, 100
Catalyst porosity	[-]	0.4, 0.8
Catalyst permeability	[m^2]	1e-16
Mean particle size of the catalyst	[nm]	36
Catalyst bulk density	[kg/m^3]	1300

A few assumptions are also considered for the development of the multiphysics model: (1) compressible ideal-gas law, (2) fully-developed inlet laminar flow, (3) the catalyst layer is isotropic, and (4) reactions take place in the catalyst layer.

Governing partial differential equations for the fluid flow, heat transfer and mass transfer are listed in Table 4-3.

The physical properties used for the equations in Table 4-3 are presented in the previous section. In addition, the gas mixture density (ρ_{mix}) is calculated by employing the ideal gas equation. Also, k_{eff} in Eq. 4.26 is the effective thermal conductivity [254]:

$$k_{eff} = \phi k_{mix} + (1 - \phi) k_{cat} \tag{4.26}$$

where, k_{cat} is the solid catalyst thermal conductivity, and it is estimated based on alumina, employing the following equation [260]:

$$k_{cat} = 5.85 + 15360 \frac{\exp(-0.002T)}{516 + T} \tag{4.27}$$

Table 4-3 The governing equations and the boundary conditions used for mathematical model.

The Reforming Channel

Momentum transport and mass conservation

$$\rho_{mix}\left(u_x\frac{\partial u_x}{\partial x}+u_y\frac{\partial u_y}{\partial y}\right)=-\frac{\partial P}{\partial x}+\frac{\partial}{\partial x}\left(2\mu_{mix}\frac{\partial u_x}{\partial x}-\frac{2}{3}\mu_{mix}\left(\frac{\partial u_x}{\partial x}+\frac{\partial u_y}{\partial y}\right)\right)+\frac{\partial}{\partial y}\left(\mu_{mix}\left(\frac{\partial u_x}{\partial y}+\frac{\partial u_y}{\partial x}\right)\right) \quad (4.16)$$

$$\rho_{mix}\left(u_x\frac{\partial u_y}{\partial x}+u_y\frac{\partial u_y}{\partial y}\right)=-\frac{\partial P}{\partial y}+\frac{\partial}{\partial y}\left(2\mu_{mix}\frac{\partial u_y}{\partial y}-\frac{2}{3}\mu_{mix}\left(\frac{\partial u_x}{\partial x}+\frac{\partial u_y}{\partial y}\right)\right)+\frac{\partial}{\partial x}\left(\mu_{mix}\left(\frac{\partial u_x}{\partial y}+\frac{\partial u_y}{\partial x}\right)\right) \quad (4.17)$$

Continuity equation

$$\rho_{mix}\left(\frac{\partial u_x}{\partial x}+\frac{\partial u_y}{\partial y}\right)+\left(u_x\frac{\partial \rho_{mix}}{\partial x}+u_y\frac{\partial \rho_{mix}}{\partial y}\right)=0 \quad (4.18)$$

Heat transport and energy conservation

$$\rho_{mix}C_{p,mix}\left(u_x\frac{\partial T}{\partial x}+u_y\frac{\partial T}{\partial y}\right)=k_{mix}\left(\frac{\partial^2 T}{\partial x^2}+\frac{\partial^2 T}{\partial y^2}\right) \quad (4.19)$$

Mass Transport

$$\rho_{mix}\left(\left(u_x\frac{\partial \omega_i}{\partial x}+u_y\frac{\partial \omega_i}{\partial y}\right)+\omega_i\left(\frac{\partial u_x}{\partial x}+\frac{\partial u_y}{\partial y}\right)\right)=\frac{\partial}{\partial x}\left(\rho_{mix}\omega_k\sum_{j=1\ j\neq i}^{N_g}D_{ij}^F\left(\frac{\partial x_j}{\partial x}+\frac{\partial x_j}{\partial y}+\left(\frac{x_j-\omega_j}{P}\right)\left(\frac{\partial P}{\partial x}+\frac{\partial P}{\partial x}\right)\right)\right)+\frac{\partial}{\partial y}\left(\rho_{mix}\omega_k\sum_{j=1\ j\neq i}^{N_g}D_{ij}^F\left(\frac{\partial x_j}{\partial x}+\frac{\partial x_j}{\partial y}+\left(\frac{x_j-\omega_j}{P}\right)\left(\frac{\partial P}{\partial x}+\frac{\partial P}{\partial x}\right)\right)\right) \quad (4.20)$$

Boundary Conditions

The inlet conditions: $x=0;\ \forall\ y$

$$u_x=u_{x,in},\ \omega_i=\omega_{i,in}, T=T_{in}$$

The outlet conditions: $x=L;\ \forall\ y$

$$P=P_{out}$$

$$\frac{\partial \omega_i}{\partial x}=0;\ \frac{\partial T}{\partial x}=0$$

Symmetry conditions at the channel center plane: $y=0;\ \forall\ x$

$$\frac{\partial u_x}{\partial y}=0;\ \frac{\partial \omega_i}{\partial y}=0;\ \frac{\partial T}{\partial y}=0$$

The Catalyst Layer (Porous Media)

Momentum transport and mass conservation

$$\frac{\mu_{mix}}{\kappa}u_x=-\frac{\partial P}{\partial x}+\frac{\partial}{\partial x}\left(2\frac{\mu_{mix}}{\phi}\frac{\partial u_x}{\partial x}-\frac{2}{3}\mu_{mix}\left(\frac{\partial u_x}{\partial x}+\frac{\partial u_y}{\partial y}\right)\right) \quad (4.21)$$

$$+\frac{\partial}{\partial y}\left(\frac{\mu_{mix}}{\phi}\left(\frac{\partial u_x}{\partial y}+\frac{\partial u_y}{\partial x}\right)\right)$$

$$\frac{\mu_{mix}}{\kappa}u_y=-\frac{\partial P}{\partial y}+\frac{\partial}{\partial y}\left(2\frac{\mu_{mix}}{\phi}\frac{\partial u_y}{\partial y}-\frac{2}{3}\mu_{mix}\left(\frac{\partial u_x}{\partial x}+\frac{\partial u_y}{\partial y}\right)\right)$$

$$+\frac{\partial}{\partial x}\left(\frac{\mu_{mix}}{\phi}\left(\frac{\partial u_x}{\partial y}+\frac{\partial u_y}{\partial x}\right)\right) \quad (4.22)$$

Continuity equation

$$\rho_{mix}\left(\frac{\partial u_x}{\partial x}+\frac{\partial u_y}{\partial y}\right)+\left(u_x\frac{\partial \rho_{mix}}{\partial x}+u_y\frac{\partial \rho_{mix}}{\partial y}\right)=0 \quad (4.23)$$

Heat transport and energy conservation

$$\rho_{cat}C_{p,cat}\left(u_x\frac{\partial T}{\partial x}+u_y\frac{\partial T}{\partial y}\right)=k_{eff}\left(\frac{\partial^2 T}{\partial x^2}+\frac{\partial^2 T}{\partial y^2}\right)+\rho_{cat}(-\Delta H_r)(-r_{SR})+A_s\dot{Q} \quad (4.24)$$

Mass Transport

$$\rho_{mix}\left(\left(u_x\frac{\partial \omega_i}{\partial x}+u_y\frac{\partial \omega_i}{\partial y}\right)+\omega_i\left(\frac{\partial u_x}{\partial x}+\frac{\partial u_y}{\partial y}\right)\right)$$

$$=\frac{\partial}{\partial x}\left(\rho_{mix}\omega_k\sum_{j=1\ j\neq i}^{N_g}D_{ij,eff}^{F}\left(\frac{\partial x_j}{\partial x}+\frac{\partial x_j}{\partial y}+\left(\frac{x_j-\omega_j}{P}\right)\left(\frac{\partial P}{\partial x}+\frac{\partial P}{\partial x}\right)\right)\right) \quad (4.25)$$

$$+\frac{\partial}{\partial y}\left(\rho_{mix}\omega_k\sum_{j=1\ j\neq i}^{N_g}D_{ij,eff}^{F}\left(\frac{\partial x_j}{\partial x}+\frac{\partial x_j}{\partial y}+\left(\frac{x_j-\omega_j}{P}\right)\left(\frac{\partial P}{\partial x}+\frac{\partial P}{\partial x}\right)\right)\right)+R_i$$

Boundary Conditions

The inlet conditions: $x=0;\ \frac{H_c}{2}<\forall y\leq\frac{H_c}{2}+\delta_{cat}$

$$u_x=0;\ \frac{\partial \omega_i}{\partial x}=0;\ \frac{\partial T}{\partial x}=0$$

The outlet conditions: $x=L;\ \frac{H_c}{2}<\forall y\leq\frac{H_c}{2}+\delta_{cat}$

$$u_x=0;\ \frac{\partial \omega_i}{\partial x}=0;\ \frac{\partial T}{\partial x}=0$$

Along the catalyst external wall interface: $y=\frac{H_c}{2}+\delta_{cat};\ \forall\ x$

$$u_x=0;\ \frac{\partial \omega_i}{\partial y}=0$$

Along the catalyst-reforming channel interface: $y=\frac{H_c}{2};\ \forall\ x$

Continuity: momentum, mass and heat flux components normal to the boundary are continuous across the boundary: $\vec{n}(N_{ch}-N_{cat})=0$

The effects of the parameters on the microchannel reformer in this study are investigated for isothermal and non-isothermal cases. For the non-isothermal study, the uniform heat-flux and non-uniform heat-flux are considered to supply the heat to the endothermic reforming sites. Eq. 4.28 is employed to change the heat flux for the uniform and non-uniform heat flux case studies:

$$\dot{Q} = \dot{Q}_{source} \exp(-ax)^n \tag{4.28}$$

where, $\dot{Q}$ denotes the heat flux (W/m^2), $\dot{Q}_{source}$ and a are adjustable parameters, and x the axial location. In addition, n is a constant and is equal to 0 and 1 for the uniform and non-uniform heat flux cases, respectively. Eq. 4.28 is previously used in Ref. [255] for non-uniform heat flux case studies for a microchannel methane reformer. This equation is particularly suitable to provide the highest heat flux at the entrance of the reformer, and almost zero heat flux at the exit of the reformer. Therefore, this equation is selected for our study. Further information and discussion in detail about the heat supply are provided in the results and discussion section.

Methanol conversion is calculated as a function of inlet and exit methanol flows:

$$\text{Conversion} = 1 - \frac{\int_0^{\frac{H_c}{2}} \rho_{CH_3OH} u dy \,|_{x=L}}{\int_0^{\frac{H_c}{2}} \rho_{CH_3OH} u dy \,|_{x=0}} \tag{4.29}$$

In addition, the effectiveness factor for the steam reforming reaction is calculated by:

$$\eta_{SR} = \frac{\frac{1}{\delta_{cat}} \int_{\frac{H_c}{2}}^{\delta_{cat}+\frac{H_c}{2}} r_{SR} dy}{r_{SR}\,|_{y=\frac{H_c}{2}}} \tag{4.30}$$

The governing equations in this section are solved by using the finite element method (FEM) with the simulation software package COMSOL Multiphysics 5.3. The most important issue is to obtain solutions for the governing equations on the thin catalyst layer; in particular, for high methanol conversion (up to 70%). Therefore, a stepwise solution approach is developed in order to prevent possible convergence errors. Firstly, it is assumed that there is no heat sink and heat source, then we obtain solutions for only flow, flow and chemical species. After that, the solutions are updated for all three: flow, chemical species, and heat transfer. Lastly, the heat sink

and source are added to obtain the final results. The solutions that are obtained in each step are used as initial values for the other step. After solving the equations, numerical integration is used to calculate Eq. 29 and Eq. 30. In addition, numerical integration is used to estimate the average value of the hydrogen production rate.

4.3 Model validation and selection of kinetic model

As mentioned earlier, three different rate expressions based on power rate laws [120, 143, 246] and the rate expressions based on the Langmuir Hinshelwood Hougen Watson approach and derived from elementary surface-reaction mechanisms [138] are compared against the experimental data of Kim and Kwon [247]. Kim and Kwon used a microchannel methanol reformer consisting of 13 channels, with the height, width and length of a single channel 1 mm x 0.5 mm x 20 mm. Reforming-catalyst (Cu/ZnO) with approximately 30 μm thickness was coated on the surface of the metal plate [247]. They carried out the experimental work at 150 °C, and the inlet flow rates between 0.01 and 0.5 ml/h with SC = 1.1. A uniform heat flux of 1,000 W/m^2 was supplied to the reformer. To validate the model, the exact dimensions of the experimental methanol steam reformer used by Kim and Kwon [247] are considered along with the same inlet conditions. The comparison of the methanol conversion between the experimental values and model predictions based on different kinetic models are illustrated in Fig. 4-2.

As shown in Fig. 4-2, there is excellent agreement between the experimental and the calculated methanol conversions of all four models with the highest R-squared value of 0.992 from Peppley`s *et al.*[138] kinetic model. Furthermore, the outlet temperature of the reformate gas is estimated within the ±5% error by using Peppley`s *et al.*[138] kinetic model as demonstrated in Fig. 4-3.

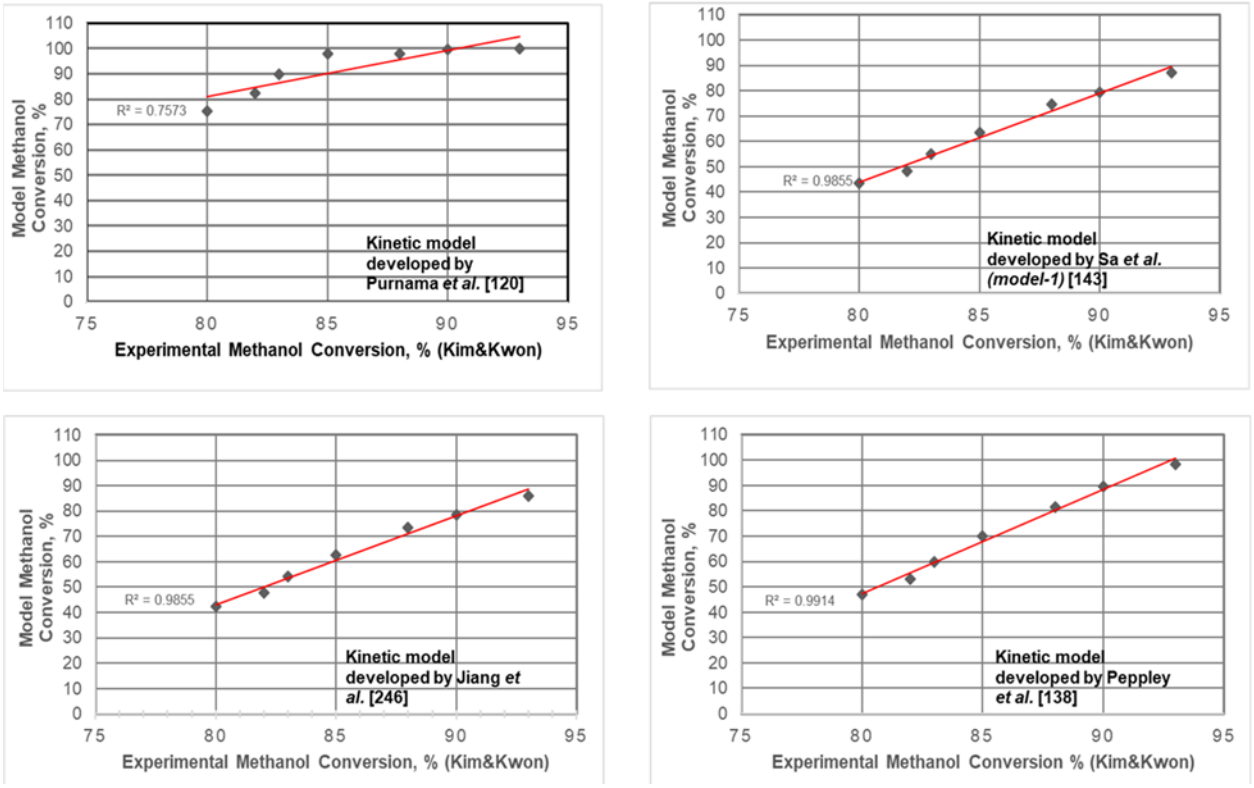

Figure 4-2 Comparison of the methanol conversion between experimental values and model predictions based on different kinetic models.

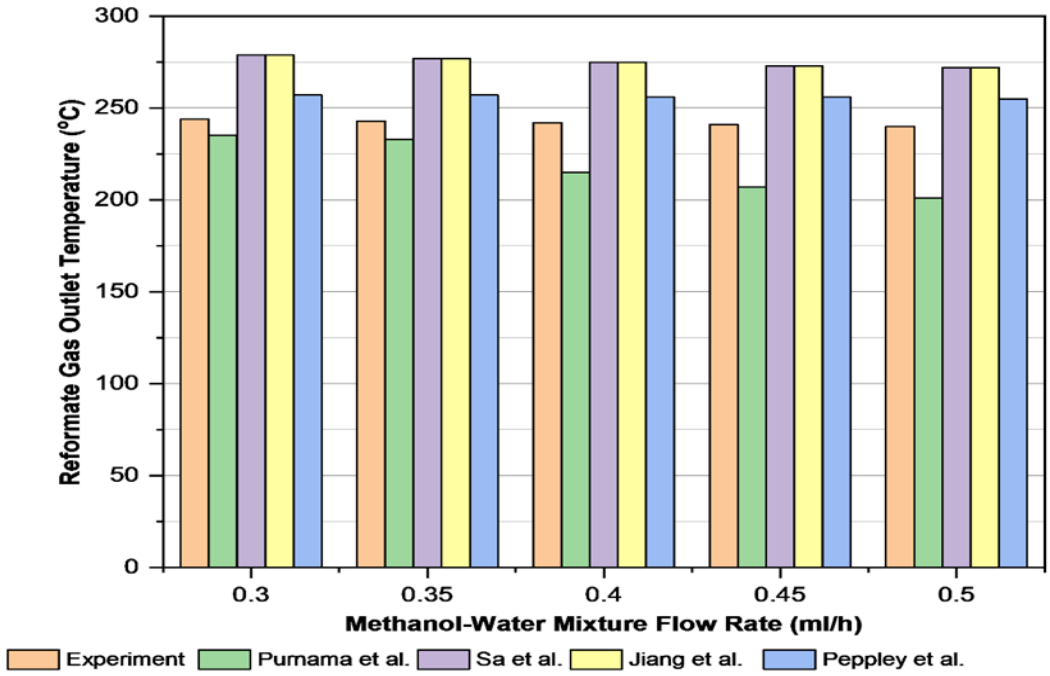

Figure 4-3 Comparison of the reformate gas outlet temperature between experimental values and model predictions based on different kinetic models.

Although much information is clearly given in Ref. [247], some information is not explained. For example, there are different types of commercial Cu-based catalysts for methanol steam reforming such as BASF K3-110, and BASF RP-60. BASF K3-110 was used in Peppley`s *et al*. study [138]; however, it was reported that BASF RP-60 was more active than BASF K3-110- particularly at low temperatures [261]. The information about the type of catalyst is not clearly mentioned in Ref. [247]. In addition, there is no information about the accuracy of the experimental data. These uncertainties may cause the deviation between the experimental data and the data that are obtained from the modeling. However, Peppley`s *et al.*[138] kinetics is the best option as considering the scope and objectives of this study. Therefore, the kinetic model developed by Peppley *et al.*[138] is selected in this study.

4.4 Results and Discussion

Commercial $CuO/ZnO/Al_2O_3$ catalysts are commonly used for methanol steam reforming in the market due to relatively low cost and high activity at low operating temperatures (between 250 ºC and 300 ºC) compared to other types of catalysts. However, an effective heat supply strategy should be devised to achieve high methanol conversion. In particular, the methanol conversion should be at least 90% in order to prevent serious degradation of HT-PEM fuel cells [262].

Various heat supply strategies have been used in the literature: combustion of methanol [241, 242], anode-off gas combustion [106], and uniform heat flux [235, 244, 259, 263]. In addition, some researchers recently investigated the feasibility of heat integration of a methanol steam reformer with a HT-PEM fuel cell [186, 264]. Additionaly, heat can be transferred to the reformer reactor by using various heat transfer fluids such as triethylene glycol (TEG) [265]. It should be noted that the uniform heat flux is generally used to provide heat to the reformer for experimental studies in research labs [247, 259]. In addition, the uniform heat flux supply can be suitable for small scale power generation (less than 30 W) by using a small battery in the system. However, the non-uniform heat flux is more realistic for commercial systems [18]. In this study, to reveal the effects of temperature distribution of the reformer, the performance of the micro-channel reformer is investigated for an iso-thermal case (as an ideal case), and a non-isothermal case with uniform and non-uniform heat fluxes.

Eq. 4.27 is used in this study to change the reformer temperature as explained in section 4.2.3. However, the references [106, 241, 242] and [244] are considered in selecting the parameters $\dot{Q}_{source}, a \; and \; n$ in Eq. 4.27. For example, the rate of heat transfer is high at the entrance of the reformer, and it approached zero at the exit of the reformer when combustion of methanol [241, 242] or anode-off gas combustion [106] are used to provide heat to the reformer. Therefore, the

temperature at the entrance increased significantly. To consider this situation, we chose high $\dot{Q}_{source}$, and a values for the non-uniform heat flux case study.

4.4.1 Isothermal study

The influence of catalyst layer thickness and porosity on the performance of a microchannel reformer is studied for an isothermal situation as an ideal case at 252 ºC. The methanol input fuel flow rate is equal to 0.0247 mol/h for the catalyst layer thicknesses from 10 to 50 μm while it is equal to 0.0494 mol/h for the variation of the catalyst layer thickness from 60 to 100 μm. The amount of the input methanol flow rate is increased 2 times for greater catalyst layer thickness to compare the effects of the catalyst layer thickness at the same reformer temperature. The catalyst porosity is 0.4 for Fig. 4, 5 and 6(a), and it is 0.8 for Fig. 6(b) and (c). The other parameters for modelling are listed in Table 4-2.

Figs. 4-4(a) and (b) show the variations of the methanol conversion with the change of the catalyst layer thickness. As seen in Fig. 4-4(a), the methanol conversion is very low for a thin catalyst layer. The conversion is equal to ~22% for $\delta_{cat} = 10$ μm at the exit of the reformer. The methanol conversion dramatically increases from ~22% to ~93% with the variation of the catalyst layer thickness from 10 to 50 μm as illustrated in Fig. 4-4(a). The conversions are also equal to ~42%, ~60%, and ~76% for the catalyst layer thicknesses of 20, 30 and 40 μm, respectively. The change of methanol conversion with the variation of the catalyst layer thickness from 60 to 100 μm can be seen in Fig. 4-4(b). The methanol conversion rises approximately 52% when the catalyst layer thickness is increased from 60 to 100 μm.

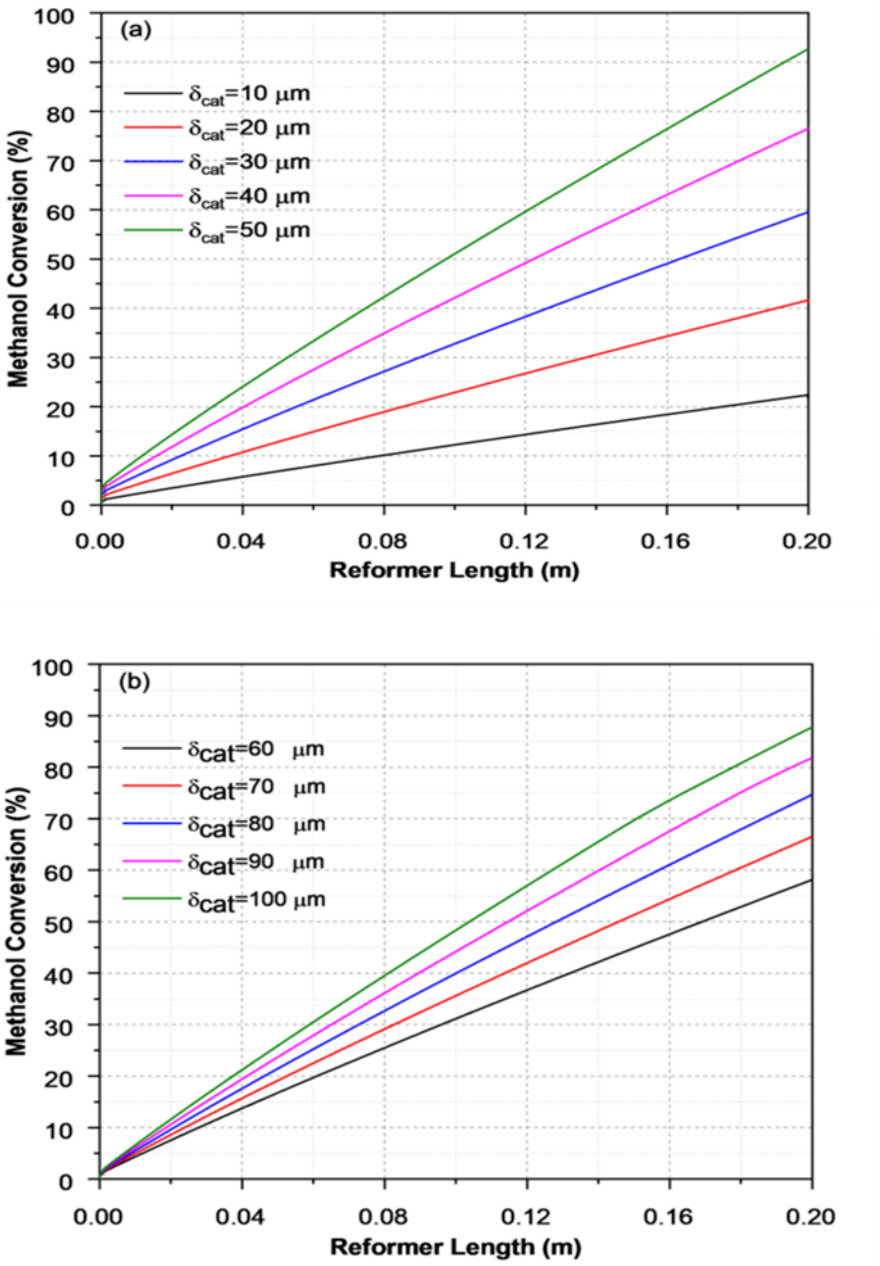

Figure 4-4 Change of the methanol conversion with variation of the catalyst layer thickness at 252 °C and ϕ=0.4, inlet methanol flow rate to the channel (a) 0.0247 (mol/h), (b) 0.0494 (mol/h).

Figs. 4-5(a) and (b) present the change of the rate of the steam reforming reaction as a function of the catalyst layer thickness and the axial direction of the reformer for the isothermal case study. As expected, the reaction rate rises significantly with an increase in the catalyst layer thickness for the isothermal case. The highest reaction rate is estimated for all the catalyst layer

thicknesses at the inlet of the reformer. As shown in Figs. 4-5(a) and (b), the reaction rate decreases along the axial direction of the reformer because the reactants are consumed along the reformer length. It can be understood from these results that the performance of the reformer can be improved with a thick catalyst layer; however, the mechanical stability of the catalyst layer, which is beyond the scope of this paper, and the catalyst effectiveness factor should be considered when making increases to the thickness of the catalyst layer.

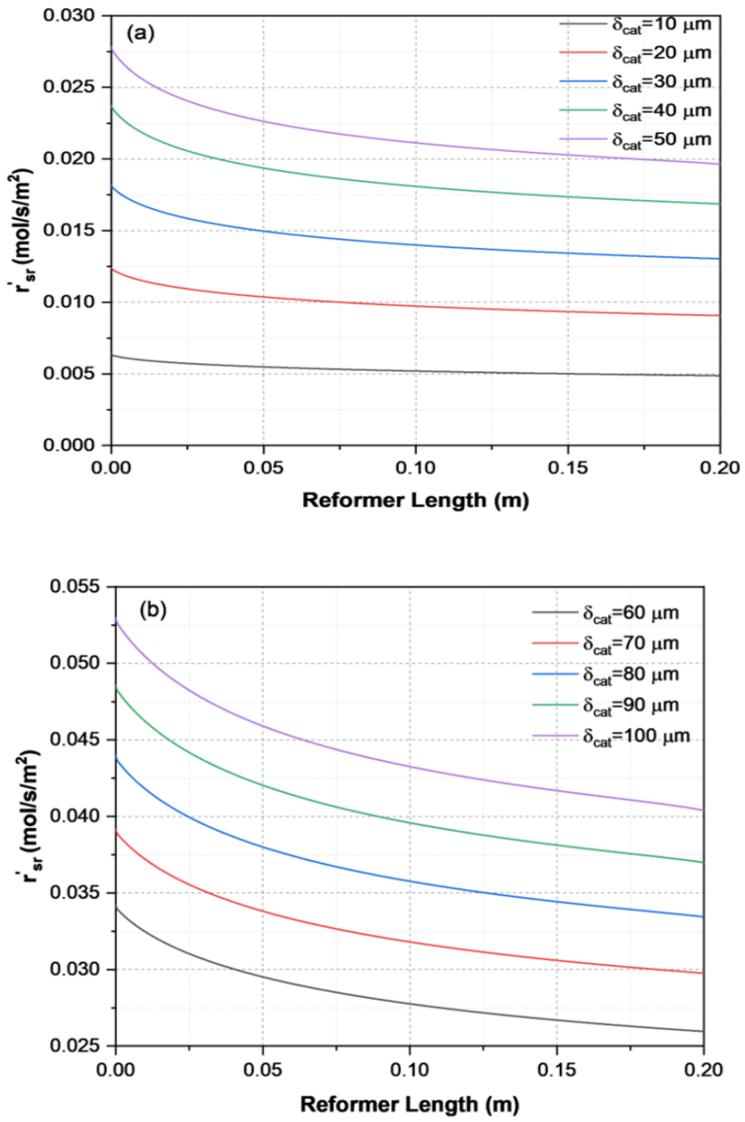

Figure 4-5 Change of the reaction rate of the steam reforming reaction with variation of the catalyst layer thickness at 252 ºC and ϕ=0.4, inlet methanol flow rate to the channel (a) 0.0247 (mol/h), (b) 0.0494 (mol/h).

The changes in the effectiveness factor for the steam reforming reaction with the variation of the catalyst layer thickness are shown in Figs. 4-6(a) and (b). In our study, the variation of the catalyst effectiveness factor across the axial direction of the reformer is defined as the ratio of the average reaction rate to the surface reaction rate at the top of the catalyst layer (see Eq. 4.29). The variation of the effectiveness factor with the catalyst layer thickness of 0.4 for the catalyst porosity at 252 ºC is shown in Fig. 4-6(a). As demonstrated in Fig. 4-6(a), although the effectiveness factor is very close to 1 for all of the catalyst layer thicknesses, it is relatively low at the entrance of the reformer for a thicker catalyst layer. Indeed, the effectiveness factor can also be calculated by using the Thiele modulus, which can be found as a function of the catalyst layer thickness, the reaction rate, the effective diffusivity, and the species concentration [255]:

$$\varphi_i^2 = \frac{\delta_{cat}^2 R_i(C_{i0})}{D_{i,eff}(C_{i0})C_{i0}} \tag{4.31}$$

For small Thiele modulus values, the effectiveness factor approaches 1, while the effectiveness factor decreases with large Thiele modulus values [266]. As shown in Eq. 4.31, the Thiele modulus increases with an increase in the catalyst layer thickness. The catalyst effectiveness factor changes from 0.83 to 0.9 for $\delta_{cat} = 100$ μm between the reformer inlet and 0.005 m, while it varied from ~0.98 to ~0.995 for $\delta_{cat} = 10$ μm. It can be also seen from Fig. 4-6(a) that the effectiveness factor is higher than 0.9 across the axial direction of the reformer for all the catalyst layer thicknesses up to 50 μm. It is less than 0.9 at the entrance of the reformer for the catalyst layer thickness greater than 50 μm. The effectiveness factor at the entrance of the reformer can be increased for higher effective diffusivity values. The effectiveness changes from ~0.83 to ~0.93 at the entrance of the reformer for $\delta_{cat} = 100$ μm with the variation of the porosity from 0.4 to 0.8 as shown in Fig. 4-6(b). However, it should be noted that there is no significant change in the methanol conversion with the variation of the porosity up to $\delta_{cat} = 50$ μm. Fig. 4-6(c) shows an increase in methanol

conversion (%) with the variation of the porosity from 0.4 to 0.8. The increase in methanol conversion is less than 1% up to 50 μm catalyst layer thickness with the change in porosity from 0.4 to 0.8. The meaningful change is only estimated for 100 μm catalyst layer thickness. The conversion at the exit of the reformer increases from ~88% to ~93% for $\delta_{cat} = 100$ μm with the variation of the porosity from 0.4 to 0.8.

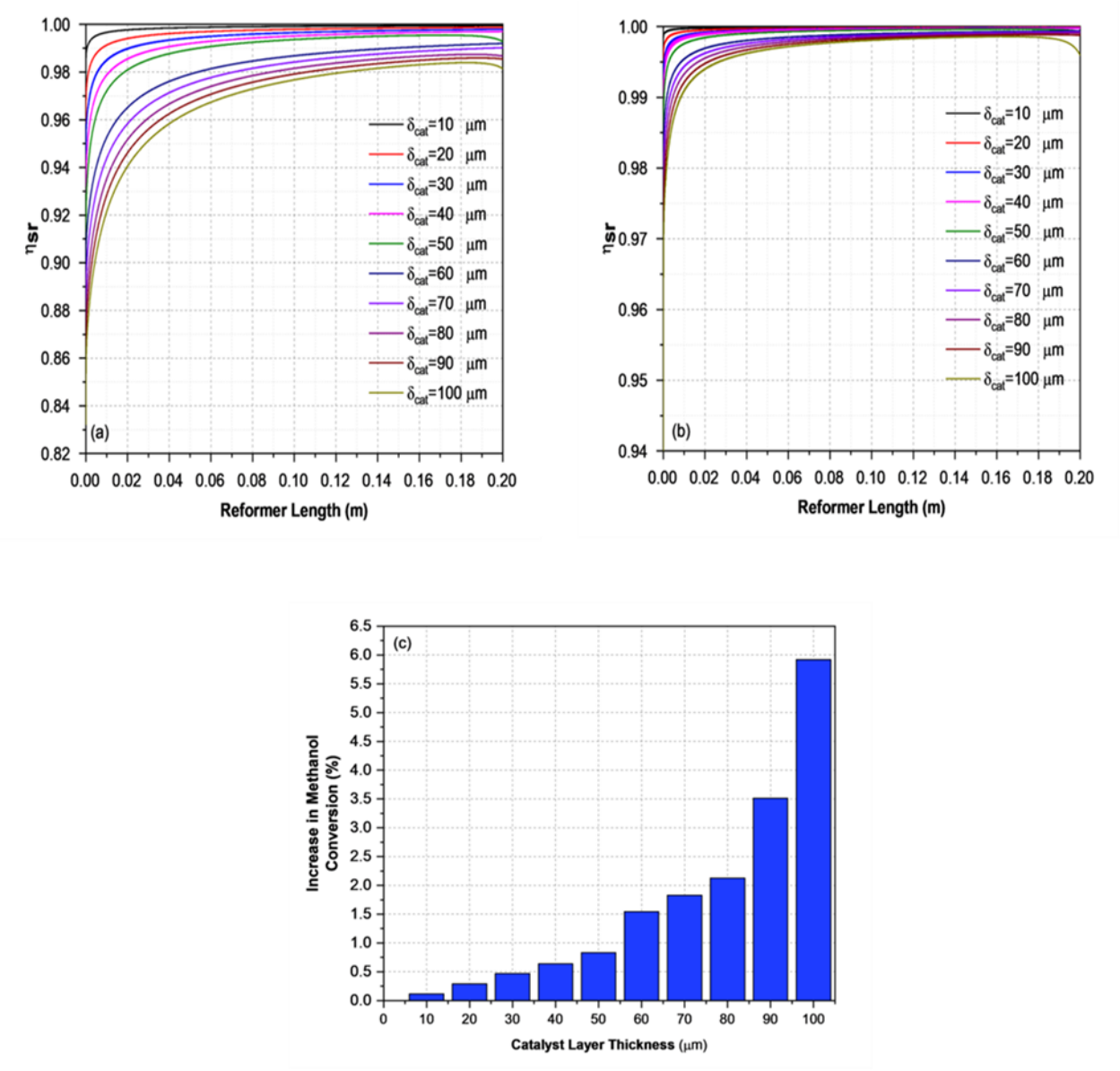

Figure 4-6 Change of the catalyst effectiveness for the steam reforming reaction and methanol conversion with the variation of the porosity and catalyst layer thickness at 252 ºC (a) ϕ=0.4, (b) ϕ=0.8, and (c) increase in methanol conversion (%) with the variation of the porosity from 0.4 to 0.8.

4.4.2 Uniform Heat Flux Case Study

Changes in temperature, reaction rate, methanol conversion and hydrogen production for uniform heat flux are presented in Figs. 4-7(a-d). The results are obtained as a function of the catalyst layer thickness and the axial direction of the reformer. The inlet methanol flow rate, the catalyst porosity, and the heat flux are equal to 0.0247 mol/h, 0.4, and 1500 W/m^2, respectively for all calculations. The other parameters for the modelling are implemented from Table 4-2.

Figs. 4-7(a-c) should be evaluated together to reach more concrete conclusions about the effects of temperature distribution on the reformer performance for the uniform heat flux case study. As seen in Fig. 4-7(a), the temperature change with the variation of the catalyst layer thickness is about the same from the reformer inlet and 0.025 m. The temperature increases from 150 ^{o}C to ~212 ^{o}C between the reformer inlet and 0.025 m. The methanol conversion is less than ~1% for the catalyst layer thicknesses of 30, 40 and 50 μm up to 0.025 m. This is due to low temperature in this region; therefore, the catalytic activity is very low. Higher temperatures are calculated for thinner catalyst layer thickness after 0.025 m as illustrated in Fig. 4-7(a). The reason for this is that the heat generation is higher for greater catalyst layer thickness because of the higher reaction rate (Fig. 4-7(b)). The temperature difference with the change of the catalyst layer thickness increases up to 0.075 m. At this point, the temperature is ~6 ^{o}C higher for the catalyst layer thickness of 30 μm than the temperature calculated for $\delta_{cat} = 40$ μm, while it is 10 ^{o}C higher than the temperature found for $\delta_{cat} = 50$ μm. The temperature difference does not change between 0.075 m and the exit of the reformer (0.2 m). The temperature is equal to ~267 ^{o}C, ~ 261 ^{o}C, and ~256 ^{o}C at the exit of the reformer for the catalyst layer thicknesses of 30, 40 and 50 μm, respectively.

The reaction rate is slightly higher at the exit of the reformer for greater catalyst layer thicknesses, although the temperature is lower. The methanol conversion is equal to ~81.7%, ~83.2%, and ~84.2% at the exit of the reformer for $\delta_{cat} = 30$, 40 and 50 μm, respectively as seen in Fig. 4-7(c), while the hydrogen production is ~0.061, ~0.062, and ~0.063 mol/h (Fig. 4-7(d)). It can be concluded from these results that there is no significant improvement on the performance of the reformer with an increase in catalyst layer thickness for the uniform heat flux supply.

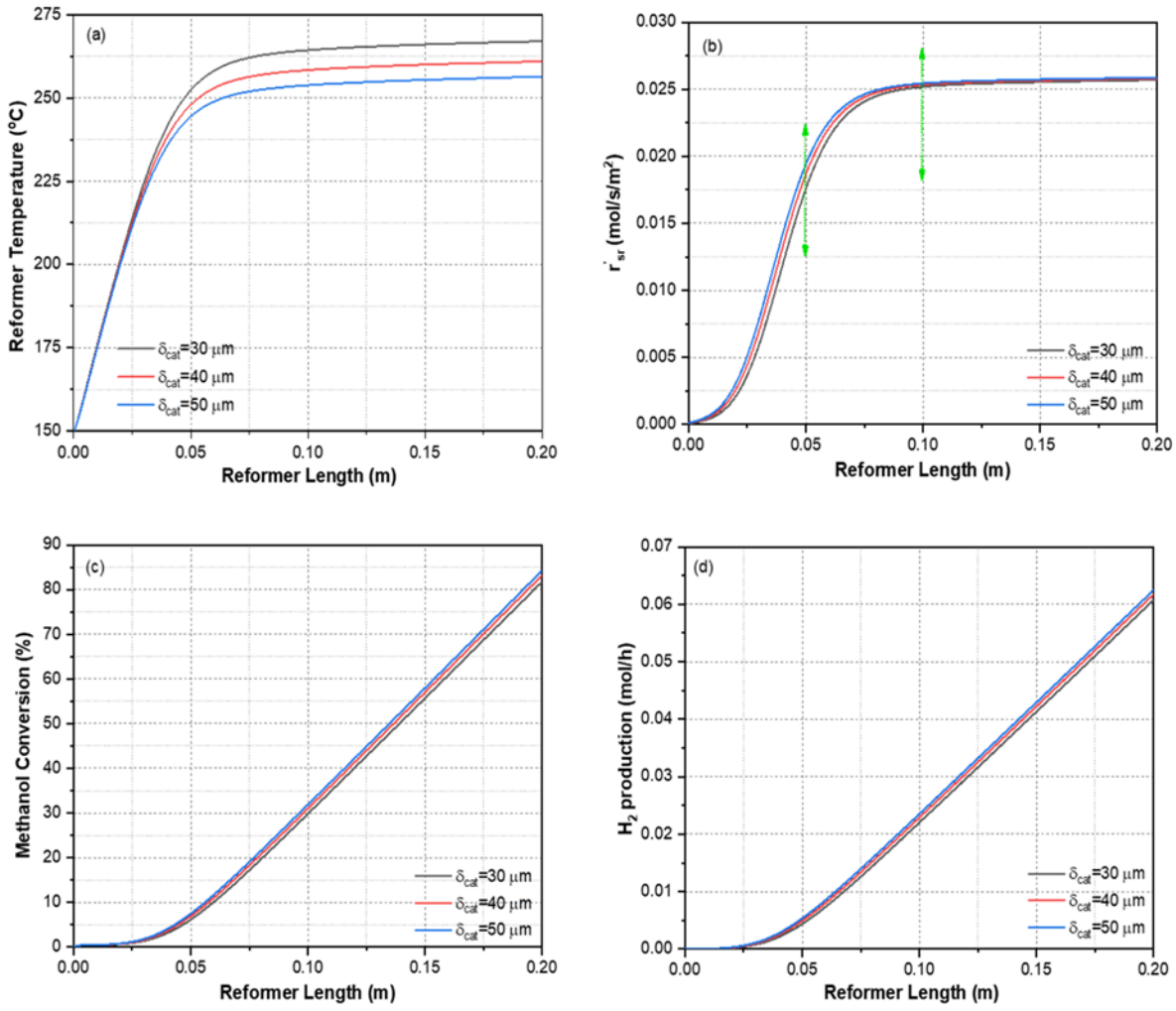

Figure 4-7 Change of (a) the reformer temperature, (b) the reaction rate of the steam reforming reaction, (c) the methanol conversion and (d) the hydrogen production with variation of the catalyst layer thickness. $\phi = 0.4$, inlet methanol flow rate to the channel is equal to 0.0247 (mol/h). $\dot{Q}_{source} = 1500\ W/m^2$, n = 0.

It should be noted that the results in Figs. 4-7(a-d) are presented with the variation of the catalyst layer thickness from 30 to 50 μm. The other results for catalyst layer thicknesses greater than 50 μm are not shown in this section because the methanol conversion is increased by a factor of only 0.032 with the variation of the catalyst layer thickness from 50 to 100 μm. In addition, our calculations show that the change in methanol conversion is almost negligible with the variation of the catalyst porosity for the uniform heat flux case study. As explained previously, the effectiveness factor is relatively low at the entrance of the reformer; specifically, for thicker catalyst layers. The effectiveness factor at the entrance increases with an increase in porosity; however, the temperature is very low at the entrance of the reformer, resulting in a lower utilization of catalyst at the entrance region for the uniform heat flux case. Therefore, there is no significant effect of the change of the porosity on the reformer performance for the uniform heat flux supply to the reformer.

4.4.3 Non-uniform Heat Flux Case Study

For the non-uniform heat flux case study, the heat flux is defined as a function of the axial location and it is equal to $\dot{Q} = 32500\exp(-100x)$ W/m^2. The same inlet conditions, which are used for the uniform heat flux case study, are also employed for the non-uniform heat flux case.

Figs. 4-8(a-d) demonstrate changes in the reformer temperature, reaction rate, methanol conversion and hydrogen production along the axial direction of the reformer with the variation of the catalyst layer thickness for the non-uniform heat flux case. As seen in Fig. 4-8(a), the temperature for all the catalyst layer thicknesses dramatically increases between the reformer inlet and 0.01 m. The temperature reaches its maximum value at 0.01 m, and it was ~313 ^{o}C, ~306 ^{o}C, ~301 ^{o}C for $\delta_{cat} = 30$, 40 and 50 μm, respectively. The reaction rate is very close along the axial direction of the reformer for the catalyst layer thicknesses of 30, 40, and 50 μm as shown in Fig.

4-8(b); however, the reaction rate is slightly higher for greater catalyst layer thicknesses up to 0.01 m. Therefore, the heat generation is higher for the greater catalyst layer thicknesses up to 0.01 m. This is the main reason that the temperature is higher for thinner catalyst layer thicknesses. After 0.01 m, the reformer temperature starts decreasing and is equal to ~212 ºC, ~207 ºC, and ~202 ºC at the reformer exit for $\delta_{cat} = 30$, 40 and 50 μm, respectively.

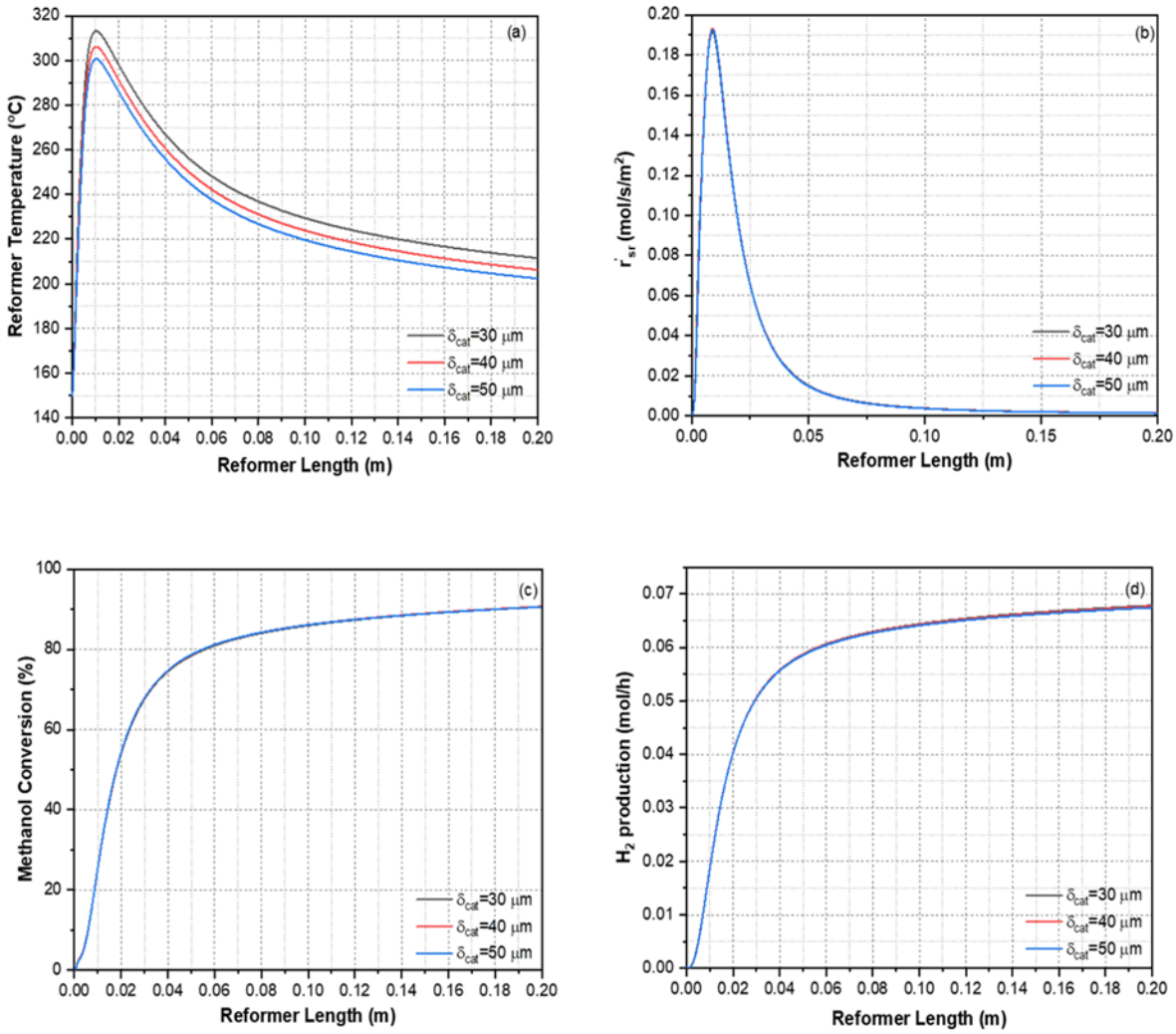

Figure 4-8 Change of (a) the reformer temperature, (b) the reaction rate of the steam reforming reaction, (c) the methanol conversion and (d) the hydrogen production with variation of the catalyst layer thickness. $\phi = 0.4$, inlet methanol flow rate to the channel is equal to 0.0247 (mol/h). $\dot{Q}_{source} = 32500\,W/m^2$, $a = 100$, $n = 1$.

The influence of variation of the catalyst thickness from 30 to 50 μm on the methanol conversion and the H_2 production is negligible for the non-uniform heat flux case as illustrated in Figs. 4-8(c) and (d). The methanol conversion and H_2 production are equal to ~90.5% and ~0.068 mol/h, respectively for $\delta_{cat} = 30$, 40 and 50 μm. Here, one of the most important results is that the increase in methanol conversion is ~5.3% between 0.1 m and the exit of the reformer. Moreover, the increase in methanol conversion is only ~1.4% between 0.16 m and the exit of the reformer. From these results, it can be understood that there is an opportunity to decrease the reformer size or amount of the catalyst with more effective heat supply to achieve a certain amount of methanol conversion for the non-uniform heat flux case.

The other important result is the hot spot formation for the non-uniform heat flux case. As demonstrates in Fig. 4-8(a), the temperature is higher than ~300 ºC between ~0.007 and ~0.02 m, and ~0.007 and ~0.015 m for $\delta_{cat} = 30$, and 40 μm, respectively, while it is higher than 300 ºC for $\delta_{cat} = 50$ μm between ~0.009 and ~0.012 m. The temperature should be less than 300 ºC for commercial Cu/ZnO catalysts because temperatures higher than 300 ºC can cause catalyst deactivation [44].

The influence of the variation of the porosity from 0.5 to 0.8 on the methanol conversion for the non-uniform heat flux supply to the reformer is illustrated in Fig. 4-9. The conversion increases 4.8%, 5.6% and 6.3% with the change in porosity from 0.5 to 0.8 for $\delta_{cat} = 30$, 40 and 50 μm, respectively. As explained previously, the effectiveness factor is relatively low at the entrance of the reformer; specifically, for thicker catalyst layers. Therefore, the highest increase in methanol conversion is obtained for $\delta_{cat} = 50$ μm.

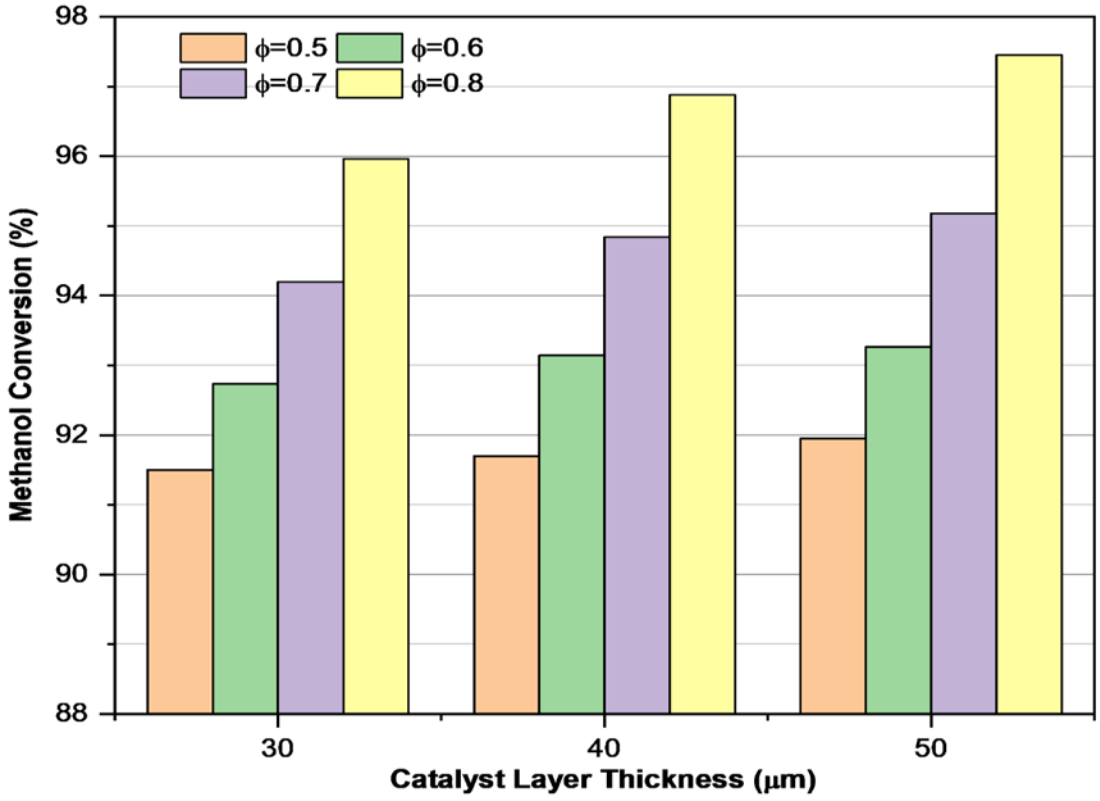

Figure 4-9 Change of the methanol conversion with variation of the catalyst layer thickness and porosity. Inlet methanol flow rate to the channel is equal to 0.0247 (mol/h). $\dot{Q}_{source} = 32500\,W/m^2, a = 100, n = 1.$

4.4.4 Segmented Catalyst Layer Configuration

As mentioned in section 4.4.3, the amount of catalyst can be decreased for case 3 by changing the design of the micro-channel reformer. Mundhwa *et al.*[251, 254] investigate the influence of segmented catalyst layer configurations on the performance of methane steam reforming in a catalytic plate reactor. Their results reveal that the high amount of methane conversion can be achieved with less catalyst. In this study, we also perform a calculation to understand the feasibility of segmented catalyst layer configuration to decrease the amount of catalyst. The segmented configuration can be seen in Fig. 4-10(a). The catalyst layer between 0.03 m and 0.08 m is removed, and the remaining area is coated with a 30 μm catalyst layer. It can be seen from Fig. 4-

8(c) and Fig. 4-10(b) that approximately identical methanol conversion is obtained with 25% less catalyst by using a segmented catalyst layer. The methanol conversion increased ~14% between 0.1 m and the exit of the reformer for the segmented catalyst layer, while the conversion changed by only ~5.3% (Fig. 4-8(c)) for the continuous catalyst layer configuration in the same region of the reformer. It should be also noted that an increase in local temperature is still an issue for the segmented catalyst layer configuration as shown in Fig. 4-10(a). The temperature in the catalyst layer exceeded 300 ºC between 0.0065 m and 0.019 m.

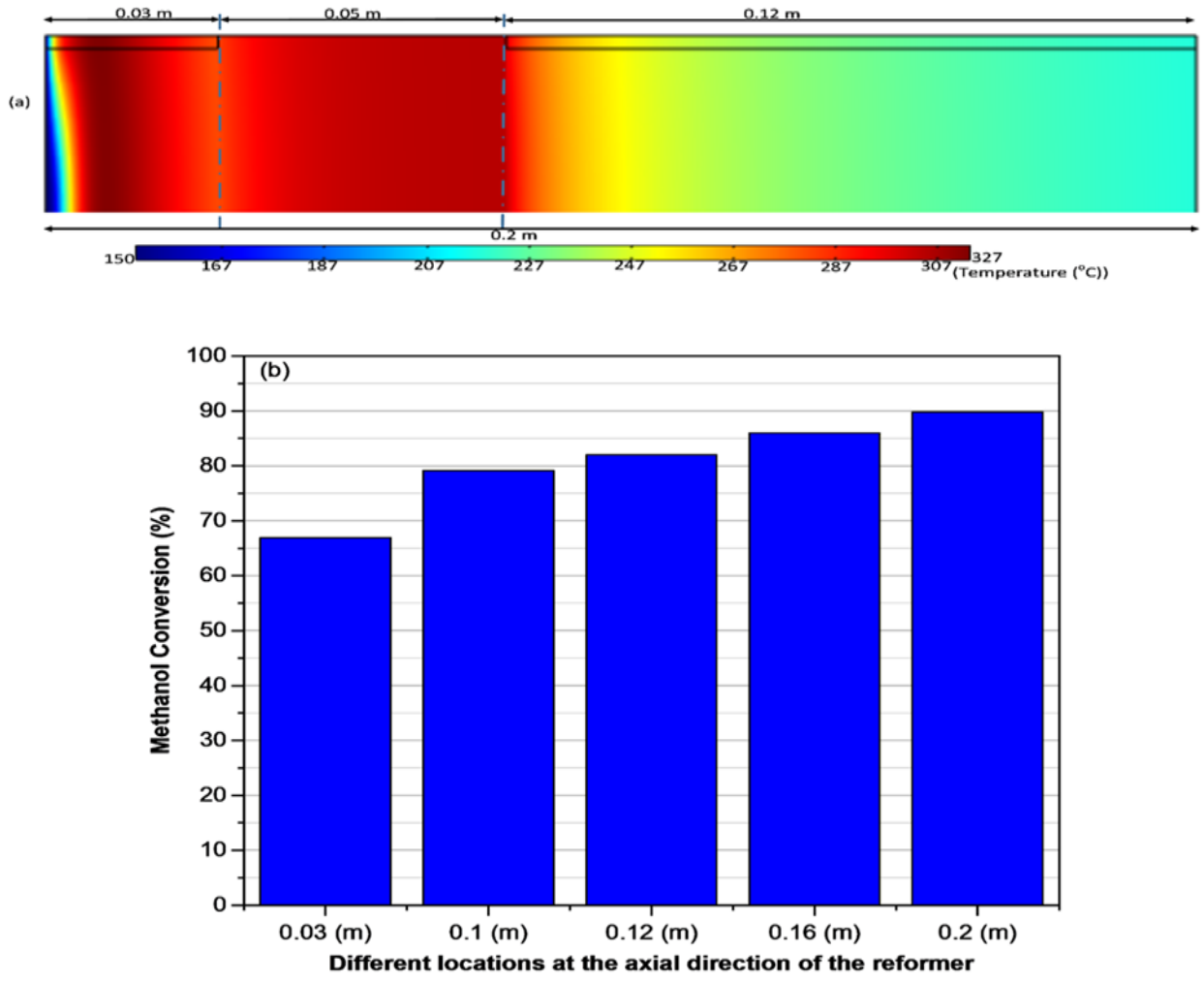

Figure 4-10 (a) Change of the reformer temperature, and (b) the methanol conversion at different location of the reformer, for segmented catalyst layer configuration. $\delta_{cat} = 30\ \mu m$, $\phi = 0.4$, inlet methanol flow rate to the channel is equal to 0.0247 (mol/h). $\dot{Q}_{source} = 32500\ W/m^2$, $a = 100$, and $n = 1$.

4.4.5 Comparison of the 2D and 1D Catalyst Layer Models

As mentioned in the introduction, the 1D catalyst layer domain has been already used by researchers for modelling the catalyst coated methanol reformer. In this section, our model which includes a 2D catalyst layer domain is compared with the model which includes 1D catalyst layer domain. The results are presented in Table 4-4. It should be noted that the constant in the non-uniform flux equation is updated in this section to compare both models together.

Table 4-4 Comparison of the model with 2D and 1D catalyst layer.

Comparison of the models for uniform heat flux supply, $\dot{Q} = 1500\ W/m^2$						
	The model with 2-D catalyst layer	The model with 1-D catalyst layer	Relative Error (%)	The model with 2-D catalyst layer	The model with 1-D catalyst layer	Relative Error (%)
Catalyst layer Thickness (μm)	Methanol Conversion (%)			H_2 Production (mol/h)		
30	81.76	82.63	**1.06**	0.0608	0.0615	**1.15**
40	83.18	84.23	**1.26**	0.0618	0.0626	**1.3**
50	84.21	85.43	**1.45**	0.0625	0.0635	**1.6**
Comparison of the models for non-uniform heat flux supply, $\dot{Q} = 30000 * \exp(-100x)\ W/m^2$						
	The model with 2-D catalyst layer	The model with 1-D catalyst layer	Relative Error (%)	The model with 2-D catalyst layer	The model with 1-D catalyst layer	Relative Error (%)
Catalyst layer Thickness (μm)	Methanol Conversion (%)			H_2 Production (mol/h)		
30	82.67	93.92	**13.6**	0.062	0.0706	**13.87**
40	82.68	98.92	**19.64**	0.062	0.0742	**19.67**
50	82.5	97	**17.5**	0.0615	0.0726	**18.05**

As shown in the Table, there is no significant difference between the results which are obtained from the models for uniform heat flux supply, whereas the differences between the two models for non-uniform heat flux case are ~13.6%, ~19.6%, and ~18% for δ_{cat} =30, 40 and 50 μm, respectively. Indeed, the internal mass transfer limitation and the effective properties such as effective thermal conductivity (see Eq. 4.25) are not considered for the model with 1D catalyst

layer domain. These two factors are specifically important at the entrance region of the reformer for non-uniform heat flux supply as explained in section 4.4.3. Therefore, there is a significant deviation between the results for non-uniform heat flux. It should be mentioned that the computational time is dramatically decreased by almost one fifth for the model with the 1D catalyst layer domain. Hence, this model may be only preferred for preliminary studies to examine the activity of different catalyst types and the effects of innovative methods on microchannel methanol reformers.

4.5 Conclusions

A 2D model is developed to study the effects of the catalyst layer thickness and porosity as well as the temperature distribution on the performance of a catalytic microchannel methanol steam reformer for the application of high-temperature PEM fuel cells. Consideration of the 2D catalyst layer domain and reaction kinetics make the model unique and comprehensive to conduct this study. The results reveal that the catalyst effectiveness factor is very close to unity for the catalyst layer thickness less than 50 μm. The catalyst effectiveness factor decreases for thicker catalyst layers. To improve the effectiveness factor, the catalyst porosity is increased; however, the methanol conversion changes slightly, even for the large changes in the porosity for the catalyst layer thickness less than 50 μm for the isothermal case study. On the other hand, the methanol conversion increases from ~90.5% to 97.5% for the catalyst layer thickness of 50 μm with the variation of the porosity from 0.4 to 0.8 for the non-uniform heat flux supply to the reformer. The results also show that temperature distribution in the microchannel reformer is one of the most influential factors in improving the performance of the reformer. In particular, effective heat supply strategies should be determined for the entrance region of the reformer because the reaction rate is very high at the entrance, and hot spot formation can occur at this region. In addition, it can

be seen from the results that the amount of catalyst can be decreased to achieve a certain amount of methanol conversion by using a segmented catalyst layer configuration.

The results obtain from the model that included the 2D catalyst layer domain and the model that included the 1D catalyst layer domain are also compared. This comparison indicates that the catalyst layer domain must be considered 2D for the non-uniform heat flux case study.

In future work, this model will be used to determine optimal designs for the microchannel methanol steam reformer. The model will be expanded to include combustion flow to supply heat for the endothermic methanol steam reforming process. In addition, segmented catalyst layer configuration will be used on both the combustion and reforming sides to increase the reformer performance and to prevent hot spot formation.

Chapter 5
Catalyst layer design and arrangement to improve the performance of a microchannel methanol steam reformer

This chapter is reprinted in adopted form with permission from Journal of the Energy Conversion and Management:

MS Herdem, M Mundhwa, S Farhad, and F. Hamdullahpur. Catalyst layer design and arrangement to improve the performance of a microchannel methanol steam reformer, Energy Conversion and Management, 2019, 180, 149-161.

5.1 Introduction

The most important issues related to widely used fuel cell power generation systems in the market are: (1) cost, (2) hydrogen distribution network and, (3) hydrogen storage [2, 267, 268]. Fuel cells have some unique features including: quiet operation, longer runtime to produce uninterruptible power and meet emergency power needs, reduction of CO_2 emissions, zero harmful emissions, operation under different climate conditions, and a minimal maintenance requirement [2, 269, 270]. Due to these features, customers are willing to accept the higher price of fuel cell technology as compared to the alternative technologies such as diesel generators and batteries for some niche markets. Some of the current and potential niche applications for fuel cell technology are: power generation for remote terminals in the oil and gas industry [2], telecommunications applications [269], forklifts [2], portable military power generators [5, 169], consumer battery rechargers [5], specialized laptop computers [5], aircraft applications [271], and marine applications [272]. Hydrogen distribution and storage are also important barriers for the niche applications mentioned

here. Alternative fuels can be converted to hydrogen rich gas by employing various technologies to overcome the challenges related to hydrogen distribution and storage [273].

The reforming of various fuels such as methane [274], bio-ethanol [275], glycerine [276], diesel [184], propane [277] and methanol [48, 278] to produce hydrogen rich syngas has been widely investigated in the literature. Although there are some drawbacks to the use of methanol such as its toxicity [35] and its availability and price [9] compared to other fuels and it is not suitable for central hydrogen production, a relatively lower process temperature and lower steam to carbon (S/C) ratio in steam reforming of methanol (SRM) are its great advantages [10, 18]. High reforming temperature and S/C ratio are generally not desired for power generation applications; in particular, they are serious issues for portable power generation applications as the size and complexity of the system increases with increasing reformer temperature and S/C ratio. The other benefits of reforming methanol can be summarized as: low sulfur content; good availability; easy storage and transport; production of methanol from biomass; and low CO content in the methanol reforming syngas [18, 48, 101, 270, 279]. Due to these advantages, methanol reformate gas fueled fuel cell systems are currently available in the market for a wide range of applications [280]. In addition, various aspects of methanol reforming; namely, the reforming reaction kinetics and catalysis [117, 137, 138, 148, 149], reforming reactors [153, 159, 281], and methanol reformate gas-fueled fuel cell systems [18, 113, 282] have received wide attention from various research groups.

Steam reforming has the highest efficiency compared to the other reforming methods, and is a common method of producing hydrogen rich syngas from methanol. However, it is a highly endothermic process; therefore, an efficient heat supply is necessary. An efficient heat supply can be provided via microchannel reactors because of their high surface to volume ratio [14]. In

addition, due to enhanced heat transfer, a higher methanol conversion at relatively low temperatures can be obtained for wash-coated microchannel reformers [48]. The performance of a microchannel reformer design can be maximized by deploying catalyst directly at the internal surface of the wash-coat [158]. Due to the aforementioned advantages of microchannel methanol reformers, the attention of researchers and companies has been dramatically increasing over recent decades.

The experimental studies, the numerical models and reaction equations of microchannel methanol reformers were reviewed in detail by Kolb in 2013 [44] and Holladay and Wang in 2015 [159]. The current studies related to microchannel methanol reformers were also summarized in our previous work in 2018 [6]. As shown in Refs. [6], [44], and [159], the early studies related to microchannel methanol reformers generally focused on low scale power generation. For example, the performance of microchannel methanol reformers was experimentally investigated for hydrogen production to feed a fuel cell for power generation in the range of 5-20 W in Refs. [103, 104, 283-287]. In addition, Wang et al. experimentally investigated the effect of catalyst activity distribution on packed bed [288] and coating bed [289] plate type microchannel methanol steam reformers. Although their studies [288, 289] are useful in understanding the effect of catalyst activity distribution on methanol steam reforming, there are some missing points in their studies. Firstly, they did not use an integrated catalytic combustor with the reformer to provide heat to the endothermic SRM. For practical applications, the sudden temperature increase at the entrance region is a serious issue for heat exchanger plate type microchannel reformers [44]. Thus, it is important to understand how the temperature changes with variations in different parameters. Additionally, the catalyst distribution was compared using the same amount of the continuous catalyst layer in their study [289]. The feasibility of decreasing the amount of catalyst is also very

important in designing the new generation of microchannel methanol steam reformers. Furthermore, the change in methanol conversion across the reformer length with variation of the catalyst layer thickness and the catalyst layer arrangement should be understood as a guide to optimize the reformer size.

The effects of various parameters such as the S/C ratio, reformer temperature, catalyst layer thickness, etc. were also numerically investigated for small-scale power generation applications by different research groups [235, 236, 239, 242, 244]. In all these earlier studies, many important catalyst parameters were ignored (e.g. catalyst layer's porosity, pore diameter, tortuosity, thermal conductivity, effective diffusivity, internal diffusion limitation) due to the developed models used a one-dimensional (1D) catalyst layer domain in the axial direction.

The recent research activities working on methanol steam reforming have been focused on improving the SRM catalysts that are active at low temperatures, and stable at elevated temperatures. The importance of catalytic activity at low temperatures (around 200 ºC) is that the methanol reformer can be integrated with HT-PEMFC (the integrated systems are called internal reforming methanol fuel cell (IRMFC) systems). Therefore, the overall system size and complexity can be decreased. Numerical and experimental studies have recently been published on the integration of microchannel methanol reformers and HT-PEMFC [127, 187, 264]. Although the activity of the catalyst and stability of the system were improved in some studies [127, 187, 264], there are still some serious issues related to IRMFC systems. One of the main problems is that the unconverted methanol in the syn-gas causes rapid performance degradation of the HT-PEMFC [10, 127]. To increase the methanol conversion, a low methanol flow rate is used for the current IRMFC system, and as a result, the power output from the HT-PEMFC is limited [10]. Another

important challenge regarding IRMFC is to develop a stable and cheap balance of plant component (BOP) materials such as gaskets and bipolar plates that can operate at elevated temperatures [10]. Researchers have also recently focused on finding a methanol reforming catalyst which is stable at elevated temperatures, as temperatures above 300 ^{o}C cause sintering and deactivation of the Cu based catalysts [113, 137]. Therefore, Kolb and his co-workers investigated a novel $Pt/In_2O_3/Al_2O_3$ catalyst for methanol steam reforming [137]. Their results revealed that the $Pt/In_2O_3/Al_2O_3$ catalyst was stable for 2000 h [113] above 300 ^{o}C, and had a 10 times higher activity than Cu-based catalysts [137]. The high activity of the $Pt/In_2O_3/Al_2O_3$ enables decreased system size and increased efficiency of the system [113]. However, the issue related to $Pt/In_2O_3/Al_2O_3$ is the high amount of Pt in the catalyst. The highest activity was obtained for a Pt content of 15 wt.% [137]. It is concluded from the reviewed literature that the methanol is a highly suitable fuel to produce hydrogen rich syngas for HT-PEMFC systems, and there is an opportunity to increase the system's efficiency and decrease the system size for specific applications with recent advances in methanol steam reforming catalysts. However, some key questions should be answered in order to design a next generation of microchannel methanol steam reformers. As mentioned earlier, studies in the literature have considered only the 1D catalyst layer domain in their models, and so the catalyst layer`s structural properties are ignored. Therefore, in our most recently published paper [6], we developed a numerical model that included a two-dimensional (2D) catalyst layer domain for a micro-channel methanol steam reformer to understand the effects of catalyst layer thickness and the catalyst layer properties including porosity, pore diameter, and tortuosity under various heat transfer scenarios. Our results [6] showed that the performance of a microchannel methanol reformer could be significantly increased in the case of decreasing large thermal gradients across the reformer length. The objective of this paper is to advance a mathematical model to study the

opportunities to improve the efficiency of a plate heat exchanger microchannel methanol steam reformer by using less catalyst to produce hydrogen for HT-PEMFC systems. The heat provided to the reformer section via methanol combustion and various segmented layer catalyst configurations is used to increase methanol conversion. The step-wise solution method is also implemented to prevent convergence issues in numerical calculations. In addition, the initial conditions and minimum size of the microchannel methanol reformer needed to achieve maximum power output from the HT-PEMFC are defined under specific restrictions involving the number of channels in the reforming and combustion sides, the minimum methanol conversion, and the power production range of the HT-PEMFC stack.

5.2 Modeling Framework

The proposed 2D steady-state model for a microchannel methanol steam reformer is described in this section. The computational domains that are used in this study can be seen in Figs. 5-1(a)-(d). The model includes five different domains: (1) the methanol combustion channel, (2) methanol combustion catalyst, (3) fecralloy plate, (4) methanol steam reforming catalyst and (5) methanol steam reforming channel. It should be noted that a 2D domain is used for the methanol steam reforming catalyst layer to incorporate the chemical reactions along the methanol reforming channel and the catalyst layer directions while a 1D domain is used for modeling the combustion catalyst layer. As shown in Figs. 5-1(a)-(d), four different catalyst configurations are investigated in this paper. These configurations are: (1) the continuous catalyst layer for both the reforming and the combustion side (Configuration-1), (2) the continuous catalyst layer for the reforming side, and the segmented catalyst layer for the combustion side (Configuration-2), (3) the segmented catalyst layer for both the reforming and the combustion side (Configuration-3), (4) the segmented catalyst layer for the combustion side, and the segmented catalyst layer with 1 inactive segment

for the reforming side (Configuration-4). Here, the inactive segment refers to the empty section and there is no catalyst in the inactive segment. The dimensions of these configurations are given in Table 5-1. The physical properties, equations, assumptions, chemical reactions and solution schema are explained below.

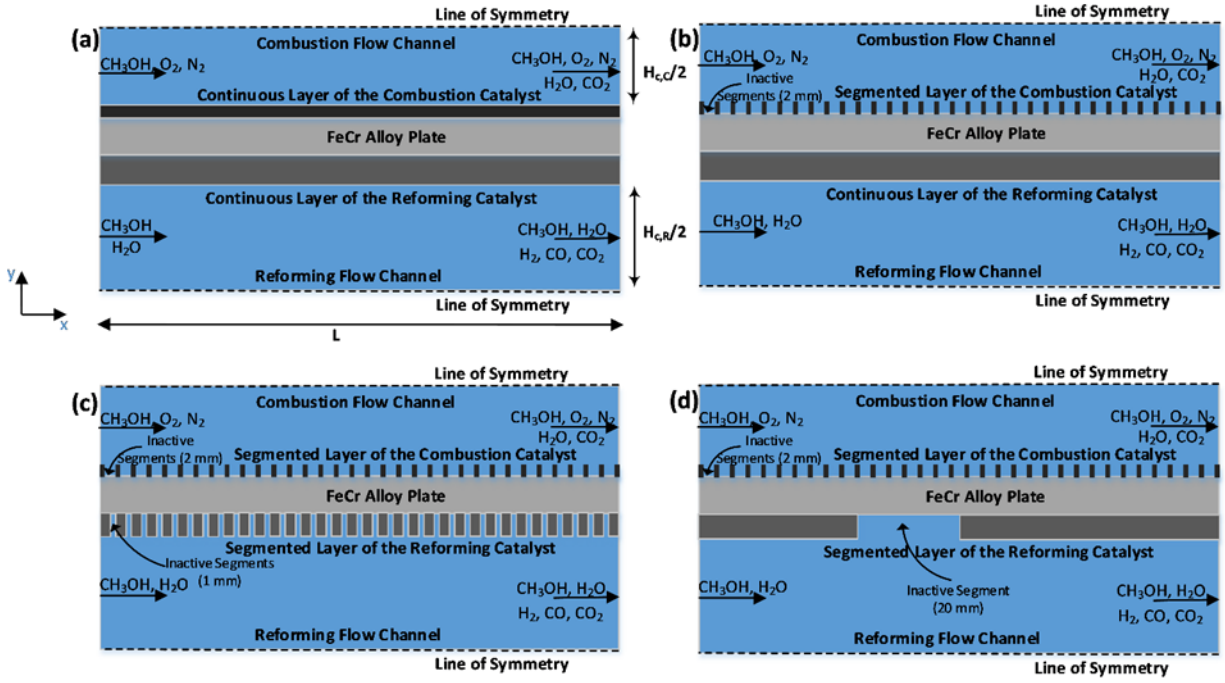

Figure 5-1 Two-dimensional view of the modeling domains of the microchannel methanol steam reformer. (a) Configuration 1: Continuous catalyst layer for both the reforming and the combustion side, (b) Configuration 2:Segmented layer for the combustion catalyst, and continuous layer for the reforming catalyst, (c) Configuration 3:Segmented layer for both the reforming and the combustion catalysts. (d) Configuration 4: Segmented layer for the combustion side, and the segmented layer with 1 inactive segment for the reforming catalyst.

5.2.1 Physical properties and input parameters

The viscosities, thermal conductivities, specific heats and diffusivities of the individual components and the gas mixtures are computed as a function of temperature. The individual components, CH_3OH, H_2O, H_2, CO_2, and CO, are considered in order to estimate the physical properties of the gas mixture on the reforming side while CH_3OH, O_2, N_2, CO_2, and H_2O are used for the combustion side. The density of the gas mixture is calculated using the ideal gas equation

for the reforming side and the combustion side. The diffusive mass flux is estimated by employing the Maxwell-Stefan model. The effective diffusivities of the chemical species inside the porous catalyst layer on the reforming side are found by considering the Knudsen and binary diffusion coefficients, and the porosity and the tortuosity of the catalyst layer [250, 251, 254]. The tortuosity is estimated using the Bruggeman equation [249], and the Knudsen diffusion is calculated as a function of the mean pore size of the catalyst. The mean pore size is found by employing Kozeny`s equation [248] as a function of the porosity and the mean particle size. The equations and the constants used to calculate the physical properties can be found in detail in our previous study [6]. It should be noted that the effective diffusivity is not implemented on the combustion side because a 1D catalyst layer [290] is used to model the combustion side. This approach is preferred considering our main objective in this work is to compare the effects of the catalyst layer thickness on the reforming side with various catalyst layer configurations for the same inlet conditions without any convergence issue. In addition, the viscosity and the thermal conductivity of the gas mixture on the combustion side are taken as constant values to prevent convergence problems. These values are estimated using Aspen Plus v8.8 [83] and can be seen in Table 5-1. As shown in Fig.5-1, a fecralloy plate is used between the combustion side and the reforming side. The physical properties of the fecralloy plate can also be seen in Table 5-1.

The input parameters and the dimensions of the domains that are shown in Figs.5-1 (a)-(d) for the modeling and the simulation of the microchannel methanol steam reformer are listed in detail in Table 5-1. The parameters used in this study are not based on arbitrary decisions. To choose these parameters, our previous studies [6, 18] are considered. For example, the S/C ratio was chosen as 1.5 to prevent coke formation [107]. The higher values are not chosen because the

heat integration of the methanol reformate gas fueled HT-PEMFC power generation system [18] is considered.

Table 5-1 The input and geometric parameters of the computational domains for the modeling.

Reforming Side				
Inlet molar flow rate of methanol, [mol/h]				0.0247
SC ratio, [-]				1.5
Inlet molar flow rate of steam, [mol/h]				$SC*F_{CH3OHr,in}$
Inlet temperature of the methanol & steam mixture, [°C]				150
Pressure, [Pa]				101325
Length, [m]				0.1
Height, [m]				$700*10^{-6}$
Width, [m]				$700*10^{-6}$
Catalyst layer thickness, [μm]				30, 35, 40, 45, 50
Catalyst porosity, [-]				0.4
Catalyst tortuosity, [-]				Porosity^(-0.5)
Catalyst permeability, [m^2]				1e-16
Mean particle size of the catalyst, [nm]				36
Catalyst density, [kg/m^3]				1300
	Conf.-1	Conf.-2	Conf.-3	Conf.-4
Length of inactive catalyst segment ,[mm]	n/a	n/a	1	20
Number of inactive catalyst segment, [-]	n/a	n/a	33	1
Combustion Side				
Inlet molar flow rate of methanol, [mol/h]				0.013
Inlet molar flow rate of oxygen, [mol/h]				$1.626*F_{CH3OHc,in}$
Inlet molar flow rate of nitrogen, [mol/h]				$(79/21)*F_{O2c,in}$
Inlet temperature of the input flow rate, [°C]				150
Pressure, [Pa]				101325
Length, [m]				0.1
Height, [m]				$500*10^{-6}$
Width, [m]				$700*10^{-6}$
Catalyst layer thickness, [μm]				16
Catalyst density, [kg/m^3]				2366.7
Thermal conductivity of the gas mixture, [W/(m.K)]				0.037
Viscosity of the gas mixture, [Pa.s]				2.43e-5
	Conf.-1	Conf.-2	Conf.-3	Conf.-4
Length of inactive catalyst segment ,[mm]	n/a	2	2	2
Number of inactive catalyst segment, [-]	n/a	34	34	34
Fecralloy Plate				
Length, [m]				0.1
Width, [m]				$700*10^{-6}$
Thickness, [m]				1.27e-4
Thermal conductivity, [W/(m.K)] (Ref. [52])				16.1
Density, [kg/m^3] (Ref. [52])				7250
Specific heat, [J/(kg.K)] (Ref. [52])				460

In addition, the dimensions of the reformer and the input methanol flow rate to the reforming side are selected while considering power generation in the range of 100 to 500 W from the HT-PEMFC system [18]. The optimum inlet temperature of the reactants is found based on our previous study [6]. Furthermore, it should be noted that the dimensions of the segmented catalyst layers are defined after parametric studies.

The physical properties and the input parameters presented in this section are used in the equations that can be found in our study [6]. The major differences in the models between this work and our previous work [6] are the combustion side and fecralloy plate. The same equations and the boundary conditions in Ref. [6] that are used for modeling the reforming channel are adapted to model the combustion side. However, the source term is added into the mass transfer equation to account for the rate of production or consumption for the combustion side. The source term is equal to zero for the internal domain of the combustion side, and it is calculated on the catalytic surface of the combustion side as:

$$S_{i,c} = \delta_{cat,c} \times R_{i,c} \tag{5.1}$$

where i refers to the components (CH_3OH, O_2, N_2, CO_2, and H_2O) inside the combustion side, $\delta_{cat,c}$ is the combustion catalyst layer thickness in m, and $R_{i,c}$ is the reaction rate of the component i in kg/(m^3.s). It should be explained that the source term is not used for the internal domain of the combustion side because the homogeneous reactions in the gas phase are negligible. It was shown that the homogenous reactions must be considered at high temperatures for catalytic combustion of hydrocarbons such as methane [291] and propane [292]. However, the homogeneous reactions can be neglected at low temperatures [293]. Therefore, the influence of the homogeneous reactions in the gas phase was not considered in this work. The reaction rate expressions for methanol combustion and steam reforming are explained in the next section.

The steady-state heat conduction equation (Eq. 2) is also added into our previous model [38] to obtain temperature distribution in a solid fecralloy plate:

$$\frac{\partial^2 T}{\partial x^2} + \frac{\partial^2 T}{\partial y^2} = 0 \tag{5.2}$$

In addition, the thermal insulation boundary condition is used at the boundaries x=0, $H_{R/2} + \delta_{cat,R} \leq y \leq H_{R/2} + \delta_{cat,R} + H_{Fecralloy}$, and x=0.1 m, $H_{R/2} + \delta_{cat,R} \leq y \leq H_{R/2} + \delta_{cat,R} + H_{Fecralloy}$ for the solution of Eq. 5.2.

5.2.2 Reaction Kinetics

The rate expressions based on the power rate law and the surface reaction mechanisms have been used in the open literature to model methanol reformers. Various power rate laws have been suggested by researchers [120, 140, 143, 246]. The main advantage of simple power rate law expressions is that they are easy to implement into the model to understand the effects of different parameters on methanol reforming. Therefore, the power rate law expressions have been commonly used in many studies [294-297] for the modeling of microchannel methanol reformers. However, there are some limitations related to power rate law expressions. Therefore, we selected Peppley et al.`s [138, 149] kinetic rate expressions based on elementary surface reaction mechanisms to model the reforming side of the microchannel reformer. The three overall reactions: methanol steam reforming (R.5.1), methanol decomposition (R.5.2), and the water-gas shift (R.5.3), are used to develop rate expressions for methanol steam reforming on $Cu/ZnO/Al_2O_3$ catalyst by Peppley et al. [138]. The reactions are listed as:

$$CH_3OH + H_2O \leftrightarrow CO_2 + 3H_2 \quad \text{(R.5.1)}$$

$$CH_3OH \leftrightarrow CO + 2H_2 \quad \text{(R.5.2)}$$

$$CO + H_2O \leftrightarrow CO_2 + H_2 \quad \text{(R.5.3)}$$

The reaction rate (mol kg_{cat}^{-1} s^{-1}) of the reactions given above are shown in Eqs. 5.3-5.5. We re-organize the reaction rate expressions in [138] using mathematical simplification for this work to prevent zero division errors in the model.

$$r_{SR} = \frac{k_R K^*_{CH_3O(1)} \left(P_{CH_3OH} - \left(\frac{P^3_{H_2} P_{CO_2}}{K_R P_{H_2O}} \right) \right) C^T_{S_1} C^T_{S_{1a}} S_C}{\left(P^{0.5}_{H_2} + K^*_{CH_3O(1)} P_{CH_3OH} + K^*_{HCOO(1)} P_{CO_2} P_{H_2} + K^*_{OH(1)} P_{H_2O} \right) \left(1 + K^{0.5}_{H(1a)} P^{0.5}_{H_2} \right)} \quad (5.3)$$

$$r_{MD} = \frac{k_D K^*_{CH_3O(2)} (P_{CH_3OH} - \left(\frac{P^2_{H_2} P_{CO}}{K_D} \right) C^T_{S_2} C^T_{S_{2a}} S_C}{\left(P^{0.5}_{H_2} + K^*_{CH_3O(2)} P_{CH_3OH} + K^*_{OH(2)} P_{H_2O} \right) \left(1 + K^{0.5}_{H(1a)} P^{0.5}_{H_2} \right)} \quad (5.4)$$

$$r_{WGS} = \frac{k_W K^*_{OH(1)} P^{0.5}_{H_2} (P_{CO} P_{H_2O} - \left(\frac{P_{H_2} P_{CO_2}}{K_W} \right) (C^T_{S_1})^2 S_C}{\left(P^{0.5}_{H_2} + K^*_{CH_3O(1)} P_{CH_3OH} + K^*_{HCOO(1)} P_{CO_2} P_{H_2} + K^*_{OH(1)} P_{H_2O} \right)^2} \quad (5.5)$$

The kinetic parameters that are used in Eqs. 5.3-5.5 can be found in detail in our previous study [6]. The rate of consumption or formation of the species for the reforming side in kg m^{-3} s^{-1} are listed as:

$$R_{CH3OH,R} = \rho_{cat,R}(-r_{SR} - r_{MD}) M_{CH3OH} \quad (5.6)$$

$$R_{H2O,R} = \rho_{cat,R}(-r_{SR} - r_{WGS}) M_{H2O} \quad (5.7)$$

$$R_{H2,R} = \rho_{cat,R}(3r_{SR} + 2r_{MD} + r_{WGS}) M_{H2} \quad (5.8)$$

$$R_{CO2,R} = \rho_{cat,R}(r_{SR} + r_{WGS}) M_{CO2} \quad (5.9)$$

$$R_{CO,R} = \rho_{cat,R}(r_{MD} - r_{WGS}) M_{CO} \quad (5.10)$$

The global reaction of the methanol combustion can be seen in R.5.4. The experimental studies related to methanol combustion on Pt/Al_2O_3 catalyst show that most of the catalytic

combustion takes place in the region near the entrance, and the activation energy and the reaction order depend on the degree of methanol conversion [298, 299]. While considering these realities, the power rate law (Eq. 5.11) suggested by Pasel et al. [298] is incorporated into the model to calculate the reaction rate of methanol combustion over the Pt/Al_2O_3 catalyst. The pre-exponential factor is taken from [300] and the reaction order and the activation energy are obtained from [301].

$$CH_3OH + 1.5O_2 \leftrightarrow 2H_2O + CO_2 \quad \text{(R.5.4)}$$

$$r_C = k_o \exp\left(\frac{-E_C}{RT}\right) C_{CH3OH}^n \qquad (5.11)$$

5.2.3 Computation schema

The partial differential equations for the modeling of the microchannel methanol steam reformer are solved using the finite element method (FEM) with the simulation software package COMSOL Multiphysics 5.3. The main assumptions used in the modeling are as follows:

- The microchannel reformer operates at steady state
- Ideal gas law behavior for flowing gases
- The flow in both half-channels is considered as fully developed laminar flow
- There is no reaction in the homogeneous phase; the reactions only take place in the catalyst layers
- No internal mass transfer limitation in the combustion catalyst layer
- Body forces are neglected
- No heat transfer by radiation

The main challenge to obtain solutions is the presence of convergence problems; in particular, for high methanol conversion (greater than 70%) and the entrance of the reformer. To solve these convergence problems, some physical properties for the combustion side are estimated using Aspen Plus v8.8, and the reforming rate expressions are simplified as mentioned in the previous sections. In addition, we update our solution method that was used in our other study [6]. Firstly, the solutions are obtained for only flow on both sides. Then, the solutions are obtained for flow and chemical reactions. In this step, the microchannel reformer is isothermal, and the solutions obtained in the first step are used as initial values in the second step. As a third step, the solutions are updated for flow, chemical reactions, and heat transfer. In the third step, the heat sink and the heat source were multiplied by 0.001, and the initial values are taken from the second step. Lastly, the values of the heat sink and the source are increased using a multiplication factor that changed from 0.001 to 1 to obtain the final solutions. The mapped mesh is used to discretize the continuous catalyst layer configurations for numerical solution. The main advantage of this mesh is to decrease computation time. However, the mapped mesh is not applicable for the segmented catalyst layer configurations because of the complex geometry. Therefore, the physically controlled mesh is used to discretize the segmented catalyst layer configurations. The mesh independency with a convergence criteria of 10^{-5} is obtained for a "Finer" element size in COMSOL software. The number of mesh elements varies from 56,100 to 345,460 depending on the geometry of the computational domain.

The results are firstly obtained for the continuous catalyst layer configuration. Then, the results of the continuous catalyst layer configuration are used as initial values to solve the model for the segmented catalyst layer configurations. After obtaining the results for all configurations,

the numerical integration is used to calculate the methanol conversion, hydrogen production rate, and heat flux for the reforming side and the combustion side.

5.3 Model Validation

The model was verified in the previous study [6] by comparing the results with the experimental data in Ref. [247] for methanol conversion and reformer temperature. Very good agreement was obtained for these values. For this work, the H_2 production rate in the syngas is also compared with the experimental data in [247]. As shown in Fig. 5-2(a), there is an excellent agreement between the results obtained by the model and the experiment in [247]. The maximum deviation between the results are found to be approximately +6%. Although the constant heat flux was used in Ref. [247] to provide heat to the reforming side, the comparison was intended to verify the results that were obtained in the reforming side under certain operating conditions. It should be also noted that there is no explanation regarding the experimental errors in Ref. [247]. Therefore, the H_2 production rate calculated by the model is also compared to the H_2 production rate at the equilibrium condition of the methanol steam reforming process. We show in another study [18] that a H_2 production rate for the methanol conversion greater than ~99% is very close to the H_2 production rate at the equilibrium condition. It can be seen from Fig. 5-2(b) that the maximum difference between the results is less than 0.6%.

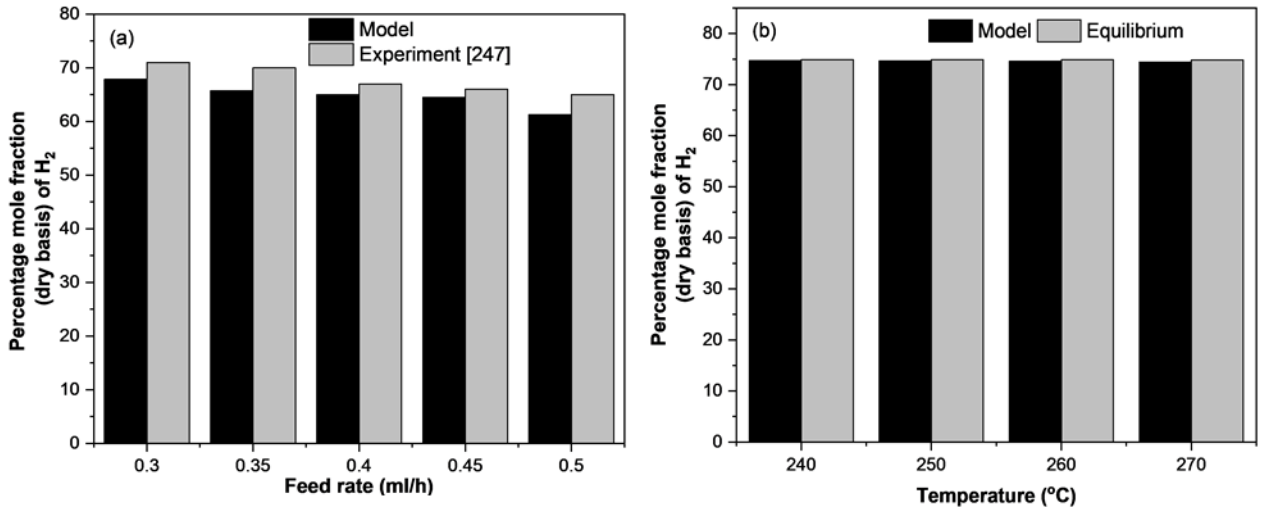

Figure 5-2 Comparison of the H2 production obtained by the model with (a) the results obtained from the experiment [247]. S/C=1.1, the inlet temperature of the methanol-water mixture is equal to 150 °C. The constant heat flux that is equal to 1000 W/m^2 is used to provide heat for the endothermic methanol steam reforming. (b) the results obtained for the equilibrium condition. S/C=1.5, and the reformer temperature is isothermal.

5.4 Results and Discussion

5.4.1 Base Case Modeling

The input parameters used for the base case simulation can be seen in Table 5-1. The catalyst layer thickness of the reforming side is equal to 30 μm for the base case. The results are obtained to understand temperature distribution change, the heat flux for combustion and reforming, the methanol conversion, and the hydrogen production rate with variation of the catalyst layer configuration. Different flow arrangements such as cross-flow, counter-flow and co-current flow can be used for coupling endothermic and exothermic reactions. These flow arrangements have been investigated in detail, and it was shown that the co-current arrangement is the best option for coupling endothermic and exothermic reactions [44]. Therefore, only the co-current flow arrangement is chosen in the present work.

In this study, four different catalyst layer configurations are used as explained in section 2. In the figures and text, these configurations refer to Configuration-1, Configuration-2,

Configuration-3, and Configuration-4. The dimensions of the segmented catalyst layer configurations are chosen to obtain the best possible performance by comparing various sizes of the segmented layers for both reforming and combustion catalysts. However, the size of segmented catalyst layers would be further optimized for future work to maximize the performance of the microchannel methanol reformer.

Temperature changes of the microchannel reformer with various catalyst layer configurations are illustrated in Figs. 5-3(a)-(e). It should be noted that the segmented catalyst layers on the combustion side are invisible in Figs. 5-3(b)-(d) because a 1D catalyst layer domain is used for the modelling of the combustion catalyst as explained in section 5.2. The segmented configurations of the combustion side can be seen in detail in Fig. 5-1. Figs. 5-3(a)-(d) show 2D temperature distribution of the microchannel reformer while Fig. 5-3(e) shows change of the average temperature of the reformer side as a function of the axial length. The focus of this study is to understand the effects of various catalyst layer configurations on methanol conversion and hydrogen production rate. Therefore, only the average temperature of the reforming side across the reformer length is illustrated in Fig. 5-3(e). As shown in Figs. 5-3(a) and (e), the temperature suddenly increases from 150 ºC to 200 ºC between the reformer`s inlet and x=0.0028 m for configuration-1. On the other hand, the temperature is found to be ~170 ºC at x=0.0028 m and the temperature reaches ~200 ºC at x=0.0049 m for the other configurations. The maximum temperature of ~306 ºC for configuration-1 is obtained at x=0.01 m. It is worth mentioning that the maximum temperature should be less than 300 ºC for Cu-based catalysts because temperatures greater than 300 ºC cause serious degradation of the catalyst [158]. The temperature starts decreasing at x=0.01 m for configuration-1. The temperature is equal to 256 ºC at x=0.04 m and dropped to 228 ºC at the reformer`s exit.

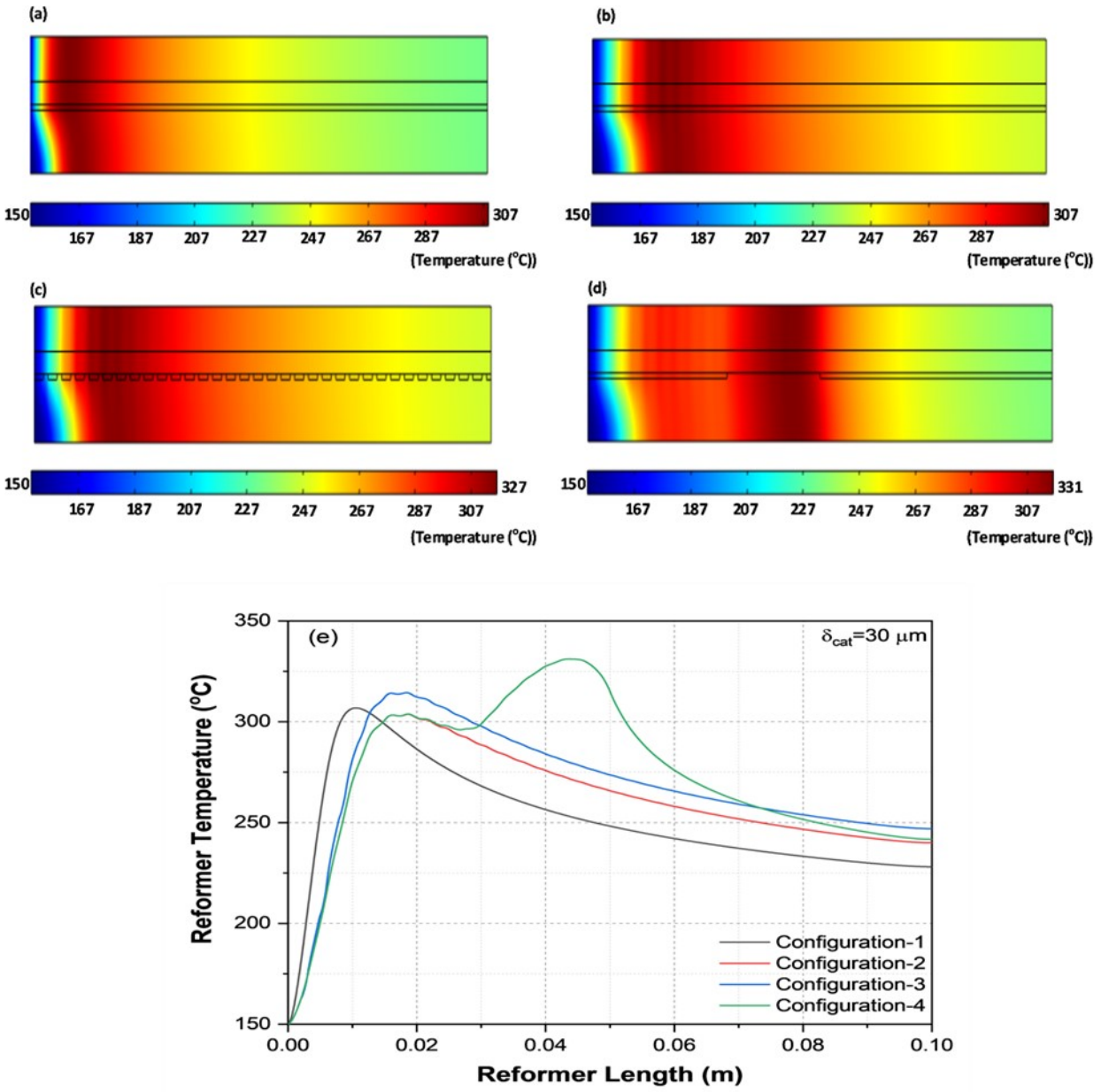

Figure 5-3 Change of the temperature of the microchannel reformer with different catalyst layer configurations : (a) Configuration-1, (b) Configuration-2, (c) Configuration-3, (d) Configuration-4. (e) Change of the average temperature of the microchannel reformer across the reformer length.

The maximum temperature of ~303 ºC is estimated at x=0.0186 m for configuration-2 while the maximum temperature is equal to ~314 ºC at x=0.016 m for configuration-3. As illustrated in Fig. 5-3(e), the temperature for configuration-1 is found to be higher than the temperature that was calculated for configurations-2 and 3 up to x=0.0148 m and x=0.0125 m,

respectively. After these points, the higher temperature is obtained for configurations-2 and 3. The temperature difference between configuration-2 and configuration-1 is approximately 12 ºC from x=0.018 m to the exit of the reformer while it is ~19 ºC for configuration-3 from 0.016 m to the exit of the reformer. The temperature at the exit of the reformer is equal to ~240 ºC and ~247 ºC for configurations-2 and 3, respectively.

It can be seen from Figs. 5-3(d) and (e), the temperature change trend for configuration-4 is different than the other configurations. The temperature firstly increases from 150 ºC to ~303 ºC between the reformer`s inlet and x=0.018 m. Then, it drops slightly up to a distance of x=~0.027 m and reaches its maximum value of ~331 ºC at x=~0.045 m. The temperature starts decreasing at x=0.045 m and it is equal to ~242 ºC at the reformer`s exit.

To understand the reasons for the variation of the temperature distribution of the reforming side with various catalyst layer configurations, the heat absorption of the reforming side and the heat production of the combustion side should be explained. Figs. 5-4(a) and (d) show the heat flux values for the reforming and the combustion sides. The absolute values of the heat flux for the reforming side is used in the figures. It can be shown from Fig. 5-4(a) that the heat flux value of the combustion side quickly increases at the inlet for configuration-1 due to a high combustion reaction rate in this region. The heat flux of the combustion side is equal to ~36.5 kW m^{-2} at x=0.028 m for configuration-1. The heat flux reaches its peak value of ~38 kW m^{-2} at x=0.0035 m, then it sharply decreases to 2 kW m^{-2} at x=0.018 m as seen in Fig. 5-4(a). The same situation is also valid for the heat flux of the reforming side. However, the heat flux values of the combustion side is estimated as ~50 kW m^{-2} at x=0.018 m for other configurations as illustrated in Figs. 5-4(b)-(d). In addition, it can also be seen from Figs. 5-4(a)-(d), the heat production in the combustion catalyst for configuration-1 is found to be lower than the other configurations across the reformer

length. As a result, the temperature for configuration-1 at the reformer`s exit is lower than the other configurations.

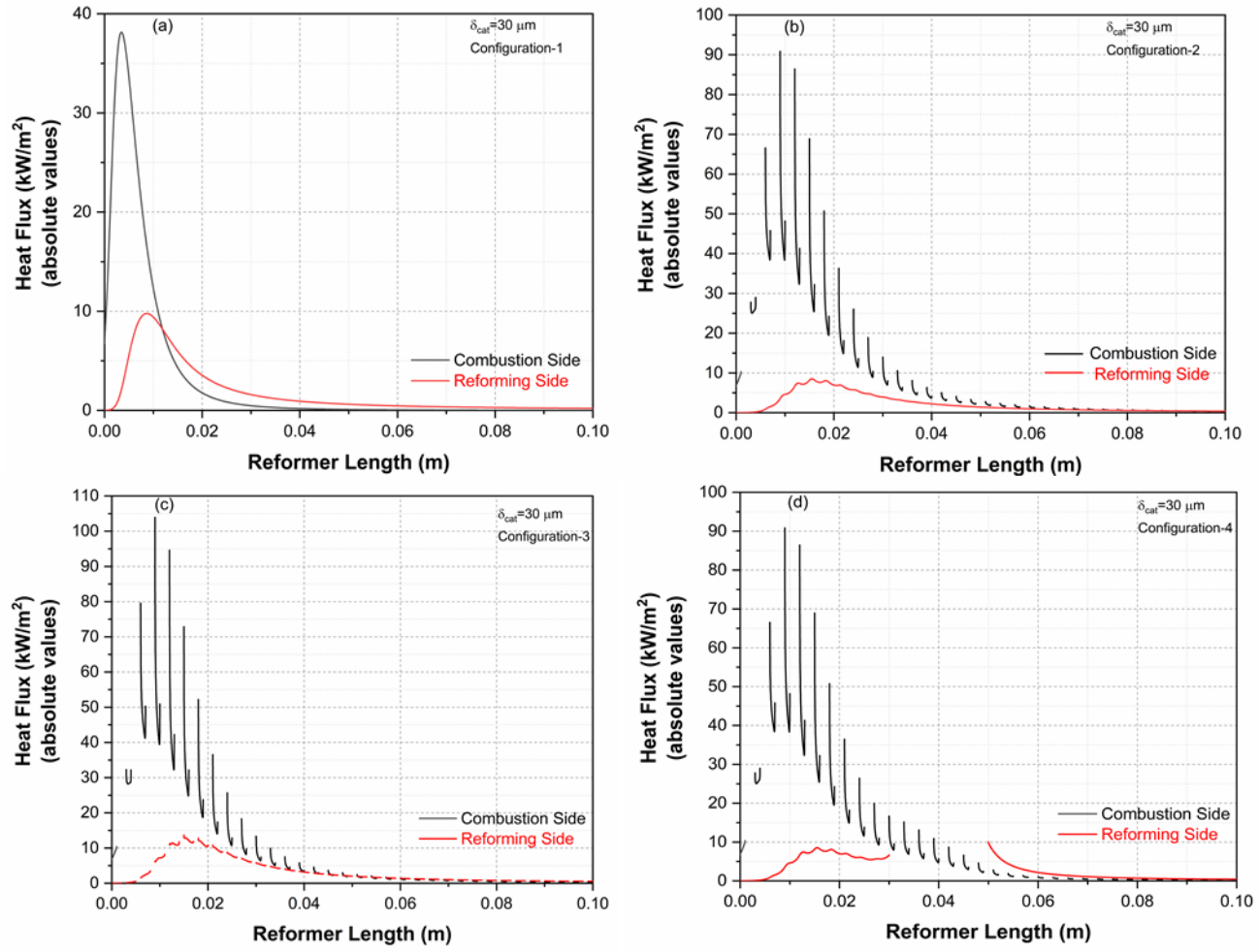

Figure 5-4 Change of the heat flux for the combustion and the reforming side with the variation of the catalyst layer configuration.

The maximum heat production in the combustion catalyst is ~90 kW m^{-2} at x=0.09 m for configurations-2 and 4 (Figs. 5-4(b) and (d)) while it is found to be ~104 kW m^{-2} at x=0.09 m for configuration-3 (Fig. 5-4(c)). The same maximum heat flux is obtained for configurations-2 and 4 because the continuous catalyst layer for the reforming side is used between the reformer`s inlet and x=0.03 m for both configurations. However, the maximum heat flux of the combustion side

for configuration-3 is estimated to be higher than configuration-2 and 4 because the segmented catalyst layer for the reforming side is used across the axial direction. In inactive segments of the reforming side, the heat absorption in the reforming catalyst is equal to zero; thus, higher maximum heat flux is obtained for configuration-3.

When the temperature (Figs. 5-3(a)-(e)) and the heat flux values (Figs. 5-4(a)-(d)) are evaluated and compared, it can be concluded that the temperature drops across the reformer length are lower for the segmented catalyst layer configurations. This significantly affects the performance of the microchannel reformer in terms of methanol conversion and hydrogen production rates. Figs. 5-5(a) and (b) show the change in the methanol conversion and the hydrogen production rate using different catalyst coating configurations. As shown, the methanol conversion at the reformer`s exit is found to be 60% for configuration-1 while it is ~75% for the other configurations. The highest methanol conversion is found to be 77.5% for configuration-4. In addition, the hydrogen production rate is estimated to be 0.045 mol/h for configuration-1 while it increases to 0.057 mol/h for configuration-4 as shown in Fig. 5-5(b). As shown in Fig. 5-5(b), almost the same hydrogen production rate is obtained for configuration-2 and configuration-4. At this point, it is worth mentioning that there is no significant effect of catalyst layer configuration changes on the value of local Reynolds number (Re). The maximum local Re number obtained is less than 100 on the reforming and the combustion side for all the configurations studied.

It can be understood from the overall result that the best performance is obtained for configuration-4. However, the temperature of the reformer is significantly increased between x=~0.03 m and x=~0.045 m for configuration-4. This can cause deactivation of the Cu based reforming catalyst.

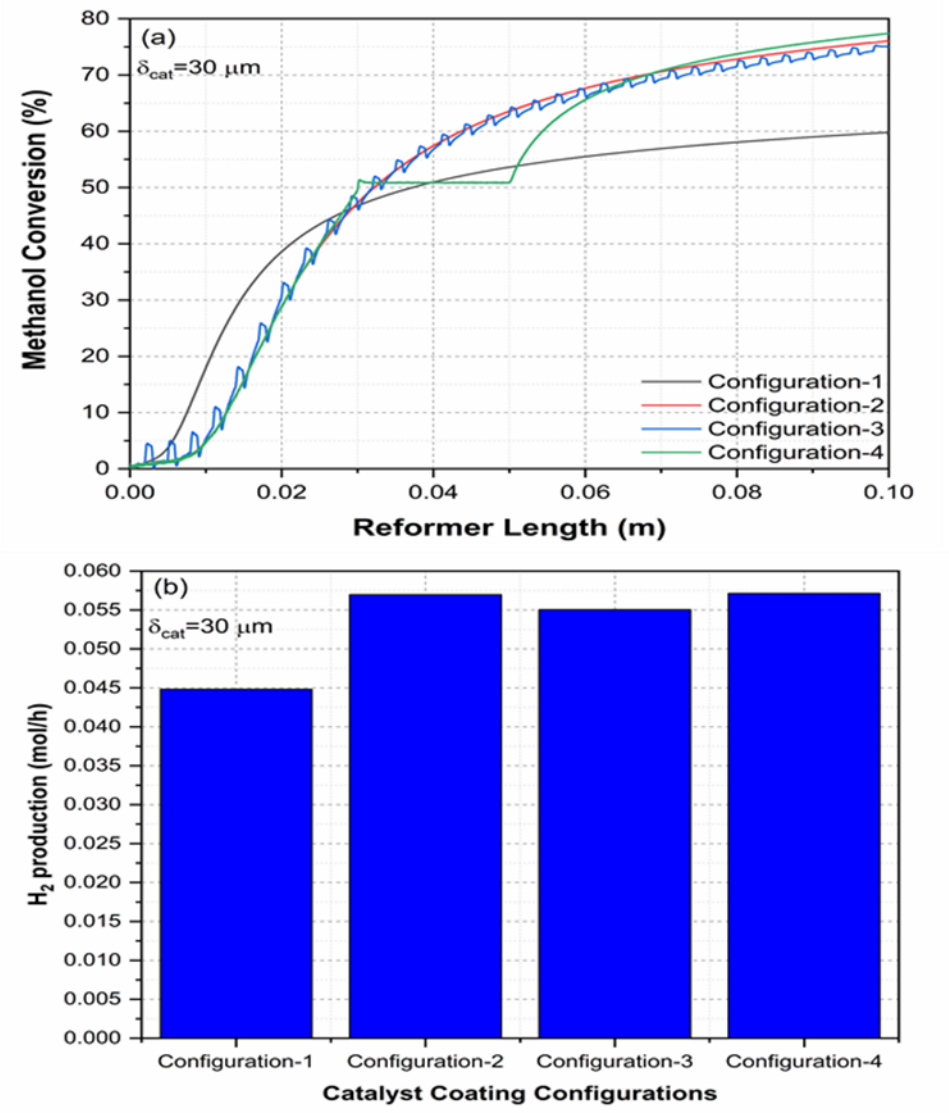

Figure 5-5 (a) Change of the methanol conversion across the reformer length with variation of the catalyst configurations. (b) Total hydrogen production rate (mol/h) with variation of the catalyst layer configuration.

5.4.2 Reforming Catalyst Thickness

Figs. 5-6(a)-(d) show temperature changes with variations in reforming catalyst layer thickness and configurations. As expected, similar trends are obtained for temperature changes with variation in the catalyst layer thickness. However, as demonstrated by Figs. 5-6(a)-(d), lower temperature is found when reforming catalyst thickness is increased. The temperature is calculated as ~225 ºC, ~237 ºC, ~244 ºC, and ~238 ºC at the reformer`s exit and for 35 µm reforming catalyst

thickness for configurations-1, 2, 3 and 4, respectively. On the other hand, the temperature at the reformer`s exit drops by ~2 ºC with a 5 µm increase in the thickness of the reforming catalyst.

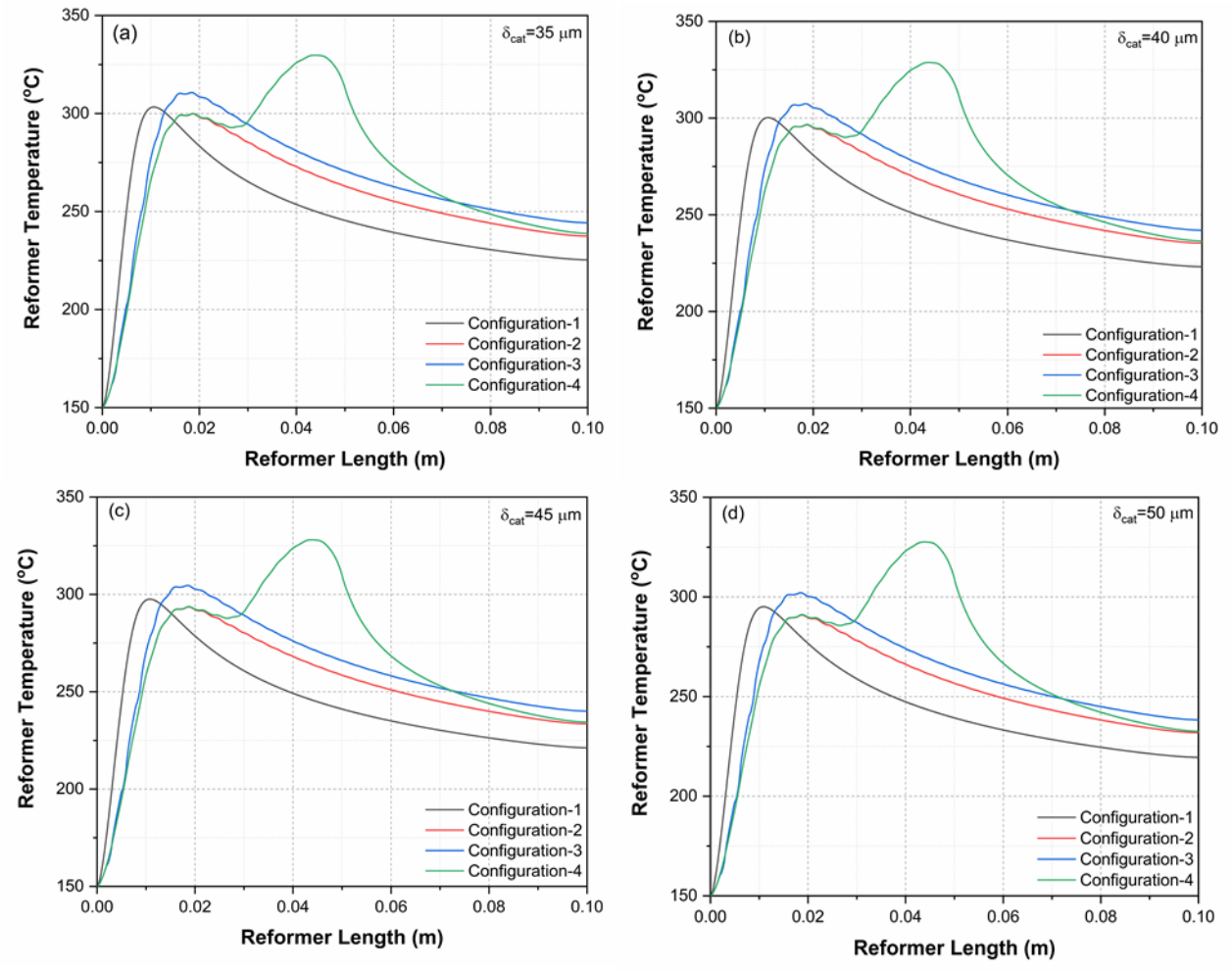

Figure 5-6 Change of the temperature across the reformer length with variation of the catalyst layer thickness and the configuration.

Change in the methanol conversion across the reformer length with variation in the catalyst thickness and configurations are also illustrated in Figs. 5-7(a)-(d). The maximum methanol conversion at the reformer exit is ~80.5% for 50 µm reforming catalyst thickness and configuration-4 (Figs. 5-7(d)). The methanol conversion rises slightly with an increase in the catalyst layer thickness. However, subsequent increases in the conversion are reduced with greater catalyst layer thickness. For example, the methanol conversion increased by ~1.05% for

configuration-4 with variation of the catalyst thickness from 35 µm to 40 µm; however, it increases by only ~0.7% with variation of the catalyst thickness from 45 µm to 50 µm.

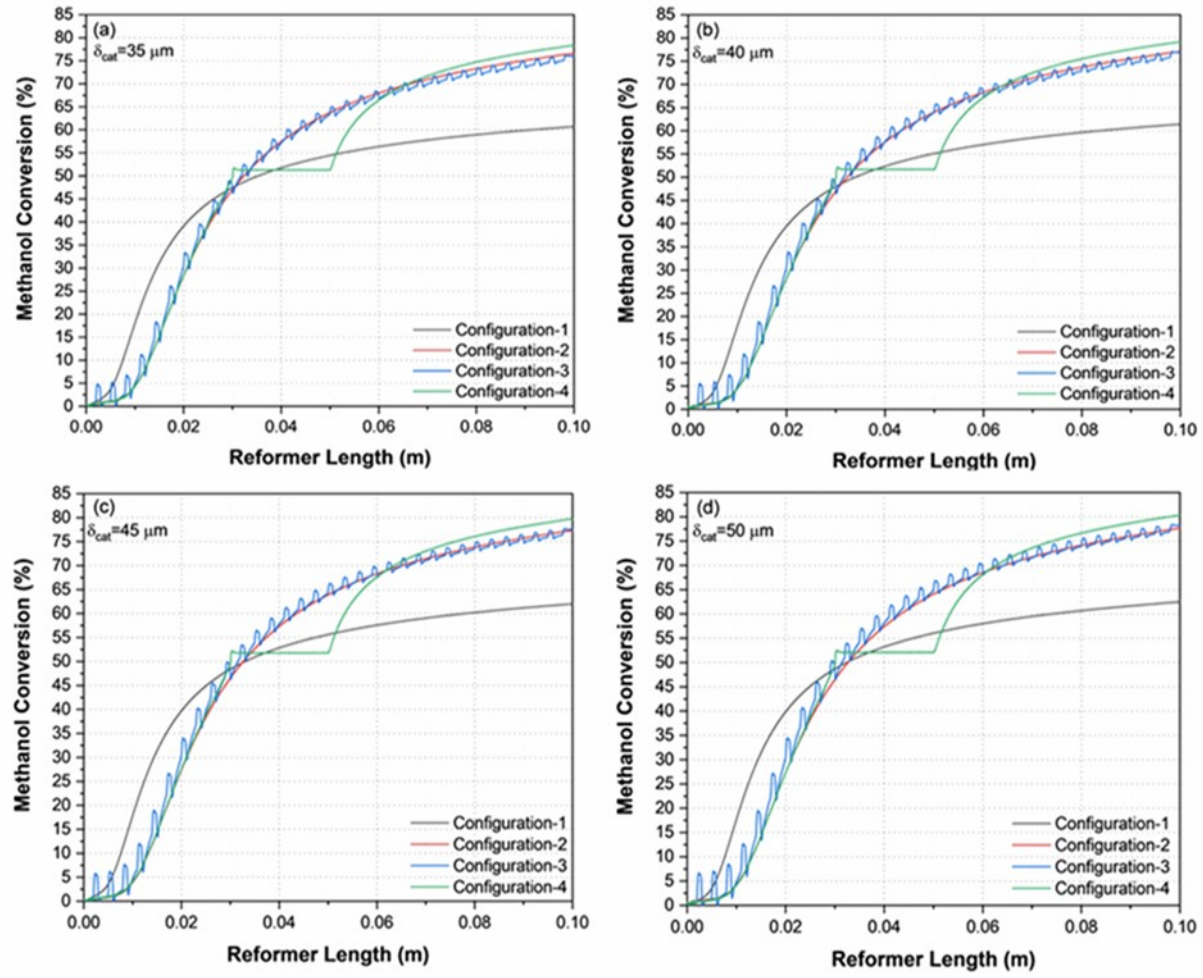

Figure 5-7 Change of the methanol conversion across the reformer length with variation of the catalyst layer thickness and the configuration.

In our previous study [6], we showed that methanol conversion significantly increased with greater catalyst layer thickness for the isothermal situation. For the non-isothermal situation, increases in methanol conversion drops with greater catalyst layer thickness because of the temperature drop across the reformer length. Therefore, more efficient heat may be provided to the reformer side by using different methods for greater catalyst layer thickness in order to utilize the catalyst more efficiently.

In addition, the cost of the microchannel reformer could also be considered for future studies to help determine optimal catalyst configurations. Indeed, it is possible to change the thickness of the catalyst across the reformer length [9] using various current catalyst coating methods [302, 303]. However, the cost may be a major drawback to using different catalyst layer configurations for microchannel reformers. Moreover, in this study, the effect of the internal mass transfer limitation in the combustion catalyst layer is not explored because this effect may not be significant once the thickness of the combustion catalyst layer is small [6] or the porosity of this layer is large [6, 255]. A decrease in the catalyst layer thickness is possible using various coating methods [302, 303]. The catalyst porous structure can also be changed with different coating methods [304, 305]. An increase of the thickness of this layer may mainly affect the increase of the methanol conversion with the segmented catalyst layer configurations. This study could be extended by considering the effects of the catalyst layers in the combustion side; however, this is beyond the scope of this paper.

5.4.3 HT-PEMFC power generation

Methanol reformate gas is very suitable to feed HT-PEMFCs because these fuel cells can tolerate CO up to 3% [306, 307], and they can operate at a temperature range of 120-200 ºC [308]. Therefore, additional components are not needed to decrease the amount of CO in the reformate gas for methanol reformate-gas fueled HT-PEMFC systems. In addition, the size and number of heat exchangers can be decreased because the reformation temperature of the methanol and the HT-PEMFC are very similar. However, the methanol conversion must be greater than 90% to prevent serious degradation of the HT-PEMFC [10]. Therefore, the inlet methanol flow rate and other inlet parameters must be chosen to achieve at least 90% methanol conversion.

In this section, the power output from the HT-PEMFC stack that used methanol reformate-gas is estimated. Configuration-2 and a 50 µm reforming catalyst thickness are chosen for microchannel methanol steam reforming because the best performance is obtained using these parameters. The other parameters and the dimensions for modeling the microchannel reformer are taken from Table 5-1. The input parameters for the fuel cell stack are listed in Table 5-2. The semi-empirical equations developed by Korsgaard et al. [211, 212] are used to estimate the power output of the HT-PEMFC stack.

Table 5-2 Methanol reformate-gas fueled HT-PEMFC power generation.

Input parameters and the restrictions for modeling	Unit	Value
Number of the cells in the fuel cell stack	[-]	25
Active area of the fuel cell	cm^2	45
Fuel cell operation temperature	°C	160
Hydrogen utilization ratio	[-]	0.8
Number of the channels in the reforming side	[-]	100
Number of the channels in the combustion side	[-]	100
Minimum methanol conversion requirement	[%]	90
Power output range	[W]	$100<P_{FC}<500$
The reforming catalyst thickness*[1]	[µm]	50
Output		
Inlet methanol flow rate to the reforming side per channel	[mol/h]	0.0198
Methanol conversion	[%]	99
Reforming gas composition (vol.%)		
H_2	[%]	66.4
H_2O	[%]	11.1
CO_2	[%]	21
CO	[%]	0.51
Power generation from the fuel cell stack	[W]	227.5
Explanation		
*1 The other parameters for modeling of the microchannel reformer are listed in Table 1. The configuration-2 was used for the catalyst configuration of the microchannel reformer.		

The composition of the reformate gas that is fed to the HT-PEMFC stack can be seen in Table 5-2. The inlet methanol flow rate to the reforming side per channel is equal to ~0.0198 mol/h. This value is found to produce maximum power in the range of 100 to 500 W by using 100 channels in the reforming side and 100 channels in the combustion side. The methanol conversion and the

H_2 production rate per channel are calculated as ~98.8% and ~0.059 mol/h, respectively, for ~0.0198 mol/h inlet methanol flow rate to the channel. For these conditions, it is possible to produce ~227 W power from the HT-PEMFC stack by using 100 channels in the reforming side.

5.5 Conclusions

The effects of continuous and segmented catalyst layer configurations in combustion and reforming channels of a methanol steam reformer on the temperature distribution, the methanol conversion, and the hydrogen production rate are studied. The effective heat is provided by the segmented catalyst layer configurations; thus, the performance of the microchannel methanol steam reformer is significantly improved. The results show that the methanol conversion is ~60% for the continuous catalyst layer configurations, while the conversion increases to ~75% with the segmented catalyst layer configurations. An increase in methanol conversion is not only an advantage of the segmented catalyst layer configuration, but it also provides the advantage of a decreased amount of catalyst in the combustion side and the reforming side of the reformer. For the segmented catalyst layer configuration (configurations-2, 3, 4), the amount of the combustion catalyst is decreased 68% while the amount of the reforming catalyst is decreased 33% and 20% for configurations-3 and 4, respectively.

The results also show that there is no significant increase in methanol conversion when increasing the catalyst layer thickness from 30 μm to 50 μm; however, the higher catalyst layer thickness can be used to prevent hot spot formation. The maximum methanol conversion per channel is found to be ~99% for configuration-2 with 50 μm reforming catalyst layer thickness and ~0.0198 mol/h inlet methanol flow rate per microchannel. For this case, enough hydrogen can be produced using 100 microchannels in the reforming side to produce ~227 W power using a HT-PEMFC stack.

Chapter 6
Conclusions and Future Work

6.1 Summary and Conclusions

In this thesis, two 2D steady state multiphysics CFD models have been developed for the modeling of a microchannel plate heat exchanger methanol steam reformer. To decide the inlet parameters for the modeling, first the power range for the promising market applications of the FC power generation systems was critically evaluated. Then, a methanol reformate gas fueled HT-PEMFC system was simulated using Aspen Plus with Fortran calculator. Some inlet parameters such as S/C ratio, and inlet flow rate of methanol etc. were defined in the system level study for the models presented in Chapters 4 and 5. The first model developed in this thesis (Chapter-4) was used to investigate the effects of catalyst layer structural characteristics, such as thickness, and porosity, on the performance and temperature distribution in a microchannel plate heat exchanger methanol steam reformer under isothermal and nonisothermal situations. The isothermal situation in this study was used as an ideal case to clearly show the effects of temperature distribution across the axial reformer length on the methanol conversion and hydrogen production rate. In the model, heat was provided for endothermic steam reforming reactions using variable and non-variable heat flux for the nonisothermal situation.

The results obtained in the first model showed that methanol conversion significantly increases with a rise in the methanol reforming catalyst layer thickness for the isothermal situation. However, the increase in methanol conversion changes slightly with a rise in catalyst layer thickness for the nonisothermal situation because of a temperature drop across the reformer length for higher catalyst layer thickness. The results also showed that the catalyst effectiveness factor at the entrance region of the microchannel methanol reformer should be specifically considered when

the catalyst layer thickness is higher than 50 μm and the catalyst porosity is equal to or less than 0.4.

For the second model of the microchannel methanol steam reformer that was developed in this work, the first model was expanded for the modeling of segmented catalyst layer configurations to balance the generated heat in the combustion side and the consumed heat in the reforming side in a microchannel plate heat exchanger methanol steam reformer. The main goals of balancing the heat generated and consumed within a microchannel methanol reformer are to: (1) decrease the amount of catalyst in the reforming and combustion sides; (2) increase the methanol conversion and hydrogen production rates; (3) prevent the sudden temperature increase at the entrance of the reformer side; and (4) decrease the temperature gradients across the axial reformer length.

A solution method was implemented in the second model for modeling of the segmented catalyst layer configurations. Solutions were firstly obtained for continuous catalyst layer configuration, then the obtained solutions were used as initial values for the isothermal solution of the segmented catalyst layer configurations. Then, a step-wise method was applied to obtain initial values for the nonisothermal solutions of the segmented catalyst layer configurations. In a step-wise solution method, a multiplication factor that changed from 0.01 to 1 was used for the generated heat in the combustion side and the consumed heat in the reforming side, and the initial values changed with variation of the multiplication factor. The final solutions were obtained when the multiplication factor was equal to 1. In addition, some mathematical simplifications were used for the rate expressions of the methanol reforming reactions. Furthermore, a few physical properties for the combustion side were estimated using Aspen Plus, and the constant values for these physical properties were used.

The second model showed that methanol conversion can be increased by using less catalyst for the segmented catalyst layer configurations. In addition, the results showed that the catalyst layer thickness in the reforming side should be optimized to prevent hot spot formation and decrease the axial temperature gradients. The optimal catalyst layer thickness for the reforming side was found to be 50 μm for $Cu/ZnO/Al_2O_3$ catalyst.

In summary, there is no significant effect of catalyst layer thickness on methanol conversion in the case of lower porosity and the nonisothermal situation. However, thicker catalyst layer can be useful to prevent hot spot formation. The segmented catalyst layer configurations can be used to increase methanol conversion and decrease axial temperature gradients. In particular, the segmented catalyst layer configurations can be useful for methanol reformate gas fueled HT-PEMFCs because high methanol conversion (higher than 90%) is very important to prevent degradation of the HT-PEMFCs. The higher conversion can be obtained using segmented catalyst layer configurations for the microchannel plate exchanger methanol reformer without increasing the size of the reformer. Overall, the model and the proposed solution method in this study can be used to improve the performance of commercial microchannel methanol reformers in this thesis.

6.2 Proposed Future Work

The findings in this thesis are useful in answering key questions for next generation microchannel methanol steam reformers. However, some points should be considered for future research.

The first point is that $Cu/ZnO/Al_2O_3$ catalyst was selected for the methanol steam reforming in this thesis because well-defined rate expressions of methanol steam reforming reactions over the $Cu/ZnO/Al_2O_3$ catalyst are available in the literature. On the other hand, novel catalysts for methanol reforming can be selected for modeling the microchannel plate heat

exchanger methanol reformers. Catalysts that are stable at high temperatures (over 300ºC) such as $Pt/In_2O_3/Al_2O_3$ can be used at the entrance of the reformer, while catalysts that are active at low temperatures (less than 220 ºC) such as $CuO/ZnO/Ga_2O_3$ can be used at the exit region of the reformer.

The second point is that the combustion rate expressions should be improved for future works. In this work, Pt/Al_2O_3 catalyst was used for the combustion reaction. Pt/Al_2O_3 is a promising catalyst for microchannel plate heat exchanger methanol reformers because methanol can be self-ignited over the Pt/Al_2O_3 catalyst. Therefore, methanol combustion can also be used for the start-up process of the reformer. However, the rate expressions should be improved to find the optimum inlet parameters for the combustion reaction. In addition, anode off-gas from the HT-PEMFC can be also used to provide heat to the reforming side after the start-up process; but accurate rate expressions should be defined to incorporate anode off-gas combustion into the model. Furthermore, a 1D catalyst layer was used for the combustion side in this study. To account for the internal mass transfer limitations of the combustion catalyst, the model could be expanded for future works.

The last point that should be considered is to obtain a solution on a thin catalyst layer coating. In particular, the computational time increases when the model is expanded to account for the internal mass transfer limitations of the combustion catalyst. There can also be serious convergence issues when obtaining solutions on thin catalyst layer coatings. To solve these issues, a reduced order model based on regression analysis could be used. Firstly, the catalyst effectiveness factor across the reformer length can be estimated, then some equations can be defined to estimate the catalyst effectiveness factor across the reformer length. These equations

can be implemented in the model. Therefore, the thin catalyst layer domain can be removed from the model.

References

[1]. Market Research Report. Fuel cell market size, share & trends analysis report by product (PEMFC, PAFC, SOFC, MCFC), by application (stationary, transportation, portable), by region, and segment forecasts 2018-2025. Published date: Jul, 2018.

[2]. Hardman S, Chandan A, Steinberger-Wilckens R. Fuel cell added value for early market applications. *J Power Sources* 2015;287:297–306.

[3]. Early markets: Fuel cells for backup power. U.S. Department of Energy, 2014. Website: https://www.energy.gov/sites/prod/files/2014/10/f19/ftco_early_mkts_fc_backup_power_fact_sheet.pdf. [accessed: 9-8-2018].

[4]. Kurt J, Saur G, Sprik S, Ainscough C. Backup power cost of ownership analysis and incumbent technology comparison. National Energy Laboratory, 2014. Website: https://www.energy.gov/eere/fuelcells/downloads/backup-power-cost-ownership-analysis-and-incumbent-technology-comparison. [accessed: 9-10-2018].

[5]. Shaw L, Pratt J, Klebanoff L, Johnson T, Arienti M, Moreno M. Analysis of H_2 storage needs for early market "man-portable" fuel cell applications. *Int. J. Hydrog Energy* 2013; 38:2810-2823.

[6]. Herdem MS, Mundhwa M, Farhad S, Hamdullahpur F. Multiphysics Modeling and Heat Distribution Study in a Catalytic Microchannel Methanol Steam Reformer. *Energy Fuels* 2018; 32:7220-7234.

[7]. Ren J, Musyoka NM, Langmi HW, Mathe M, Liao, S. Current research trends and perspectives on materials-based hydrogen storage solutions: a critical review. *Int. J. Hydrog Energy* 2017, 42(1):289-311.

[8]. Dincer I, Zamfirescu C. Sustainable energy systems and applications. Springer Science & Business Media, 2011.

[9]. Hydrogen Production Tech Team Roadmap 2017. Website: https://www.energy.gov/sites/prod/files/2017/11/f46/HPTT%20Roadmap%20FY17%20Final_Nov%202017.pdf [accessed: 08.10.2018].

[10]. Zhang J, Xiang Y, Lu S, Jiang SP. High Temperature Polymer Electrolyte Membrane Fuel Cells for Integrated Fuel Cell–Methanol Reformer Power Systems: A Critical Review. *Adv. Sustainable Syst.* 2018; 2; 1-19.

[11]. SFC Energy. Website: https://www.sfc.com/en/ [accessed: 27.10.2018].

[12]. Serenergy. Website: https://serenergy.com/ [accessed: 27.10.2018].

[13]. Haque MA, Sulong AB, Loh KS, Majlan EH, Husaini T, Rosli RE. Acid doped polybenzimidazoles based membrane electrode assembly for high temperature proton exchange membrane fuel cell: A review. *Int. J. Hydrog Energy* 2017, 42(14):9156-9179.

[14]. Lukyanov BN. Catalytic production of hydrogen from methanol for mobile, stationary and portable fuel-cell power plants. *Russ. Chem. Rev.* **2008**, *77* (11), 995-1016.

[15]. O'Connell M, Kolb G, Schelhaas KP, Wichert M, Tiemann D, Pennemann H, et al. Towards mass production of microstructured fuel processors for application in future distributed energy generation systems: A review of recent progress at IMM. *Chem Eng Res Des* 2012; 90:11–8.

[16]. Chen J, Liu B, Gao X, Xu D. Production of Hydrogen by Methane Steam Reforming Coupled with Catalytic Combustion in Integrated Microchannel Reactors. *Energies* 2018, 11(8): 2045.

[17]. Cao C, Dang D, Li Y, Xu J, Cheng Y. Managing temperature uniformity of thermally integrated micro reformers with different axial dimensions: A detailed numerical study. *Chem. Eng. Process.* 2018, 132:218-228.

[18]. Herdem MS, Farhad S, Hamdullahpur F. Modeling and parametric study of a methanol reformate gas-fueled HT-PEMFC system for portable power generation applications. *Energy Convers Manag* 2015; 101:19–29.

[19]. Herdem MS, Mundhwa M, Farhad S, Hamdullahpur F. Catalyst layer design and arrangement to improve the performance of a microchannel methanol steam reformer. *Energy Convers Manag* 2019, 180: 149-161.

[20] World Energy Resources, 2013 Survey. World Energy Council, 2013. Website: https://www.worldenergy.org/wp-content/uploads/2013/09/Complete_WER_2013_Survey.pdf [accessed: 15/01/2016].

[21] Annual Energy Outlook, 2015. U.S Energy Information Administration. Website: http://www.eia.gov/forecasts/aeo/ [accessed 15/01/2016].

[22] World Energy Outlook, 2015. International Energy Agency. Website: http://www.worldenergyoutlook.org/weo2015/ [accessed: 15/01/2016].

[23] Paklomov N. Oil and gas: energy becomes a political football. Telegraph, 2014. Website: http://www.telegraph.co.uk/sponsored/rbth/politics/10796400/oil-gas-political-football.html [accessed: 15/01/2016].

[24] Jonsson DK, Johansson B, Månsson A, Nilsson LJ, Nilsson M, Sonnsjö H. Energy security matters in the EU Energy Roadmap. *Energy Strateg Rev* 2015;6:48–56.

[25]. Hydrogen generation market by geography, by mode of generation&delivery, by applications and by technology-global trends&forecasts to 2019, September 2014. Website:

http://www.marketsandmarkets.com/Market-Reports/hydrogen-generation-market-494.html [accessed: 25/01/2016].

[26]. González EL, Llerena FI, Pérez MS, Iglesias FR, Macho JG. Energy evaluation of a solar hydrogen storage facility: comparison with other electrical energy storage technologies. *Int J Hydrog Energy* 2015;40:5518-5525.

[27]. Pellow MA, Emmott CJM, Barnhart CJ, Benson SM. Hydrogen or batteries for grid storage? A net energy analysis. *Energy Environ Sci* 2015;8:1938–52.

[28]. Ehret O, Bonhoff K. Hydrogen as a fuel and energy storage: Success factors for the German Energiewende. *Int J Hydrog Energy* 2015;40: 5526-5533.

[29]. Loisel R, Baranger L, Chemouri N, Spinu S, Pardo S. Economic evaluation of hybrid off-shore wind power and hydrogen storage system. *Int J Hydrog Energy* 2015;40:6727–39.

[30]. Tremel A, Wasserscheid P, Baldauf M, Hammer T. Techno-economic analysis for the synthesis of liquid and gaseous fuels based on hydrogen production via electrolysis. *Int. J Hydrog Energy* 2015;35:11457-11464.

[31]. Mitsos A. Man-portable power generation devices: product design and supporting algorithms. PhD diss., Massachusetts Institute of Technology, 2006.

[32]. Dutta S. A review on production, storage of hydrogen and its utilization as an energy resource. *J Ind Eng Chem.* 2014;20:1148-1156.

[33]. Vamvuka, D., 2011. Bio-oil, solid and gaseous biofuels from biomass pyrolysis processes—an overview. *Int. J. Energy Res.* 2011; 35(10): 835-862.

[34]. Rathour RK, Ahuja V,Bhatia RK, Bhatt AK. Biobutanol: New era of biofuels. *Int J Energy Res.* 2018;1–14.https://doi.org/10.1002/er.418014.

[35]. Sikarwar VS, Zhao M, Fennell PS, Shah N, Anthony EJ. Progress in biofuel production from gasification. *Prog. Energy Combust. Sci.* 2017;61:189-248.

[36]. Molino A, Larocca V, Chianese S, Musmarra D. Biofuels production by biomass gasification: A review. *Energies.* 2018;31;11(4):811.

[37]. Haryanto A, Fernando S, Murali N, Adhikari S. Current Status of Hydrogen Production Techniques by Steam Reforming of Ethanol: A Review. *Energy & Fuels* 2005;19:2098–106.

[38]. Contreras JL, Salmones J, Colín-Luna JA, Nuño L, Quintana B, Córdova I, et al. Catalysts for H2 production using the ethanol steam reforming (a review). *Int J Hydrog Energy* 2014; 39:18835–53.

[39]. Simakov DSA, Wright MM, Ahmed S, Mokheimer EMA, Roman-Leshkov Y. Solar thermal catalytic reforming of natural gas: A review on chemistry, catalysis and system design. *Catal Sci Technol* 2015;5:1991–2016.

[40]. Sheu EJ, Mokheimer EMA, Ghoniem AF. A review of solar methane reforming systems. *Int J Hydrog Energy* 2015;40:12929–55.

[41]. Qi A, Peppley B, Karan K. Integrated fuel processors for fuel cell application: A review. *Fuel Process Technol* 2007;88:3–22.

[42]. Hansen JB. Fuel processing for fuel cells and power to fuels as seen from an industrial perspective. *J Catal* 2015;328:280–96.

[43]. LeValley TL, Richard AR, Fan M. The progress in water gas shift and steam reforming hydrogen production technologies – A review. *Int J Hydrog Energy* 2014;39:16983–7000.

[44]. Kolb G. Review: Microstructured reactors for distributed and renewable production of fuels and electrical energy. *Chem Eng and Process: Process Intensif* 2013;65:1–44.

[45]. Iulianelli A, Ribeirinha P, Mendes A, Basile A. Methanol steam reforming for hydrogen generation via conventional and membrane reactors: A review. *Renew Sustain Energy Rev* 2014; 29:355–68.

[46]. Sá S, Silva H, Brandão L, Sousa JM, Mendes A. Catalysts for methanol steam reforming-A review. *Appl Catal B Environ* 2010;99:43–57.

[47]. Yong ST, Ooi CW, Chai SP, Wu XS. Review of methanol reforming-Cu-based catalysts, surface reaction mechanisms, and reaction schemes. *Int J Hydrog Energy* 2013;38:9541–52.

[48]. Palo DR, Dagle RA, Holladay JD. Methanol steam reforming for hydrogen production. *Chem Rev* 2007;107:3992–4021.

[49]. Sengodan S, Lan R, Humphreys J, Du D, Xu W, Wang H, Tao S. Advances in reforming and partial oxidation of hydrocarbons for hydrogen production and fuel cell applications. *Renew Sustain Energy Rev.* 2018;28;82:761-80.

[50]. Cheekatamarla PK, Finnerty CM. Reforming catalysts for hydrogen generation in fuel cell applications. *J Power Sources* 2006;160:490–9.

[51]. Liu K., Song C., Subramani V., eds. Hydrogen and syngas production and purification technologies. Hoboken, NJ: Wiley, 2010.

[52]. Holladay JD, Hu J, King DL, Wang Y. An overview of hydrogen production technologies. *Catal Today* 2009;139:244–60.

[53]. O`Hayre RP, Cha SW, Colella W, Prinz FB. Fuel cell fundamentals. Vol. 2. New York: John Wiley & Sons, 2006.

[54]. Rabenstein G, Hacker V. Hydrogen for fuel cells from ethanol by steam-reforming, partial-oxidation and combined auto-thermal reforming: a thermodynamic analysis. *J Power Sources* 2008; 185:1293-1304.

[55]. Nahar GA, Madhani SS. Thermodynamics of hydrogen production by the steam reforming of butanol: analysis of inorganic gases and light hydrocarbons. *Int. J. Hydrog Energy* 2010; 35:98-109.

[56]. Wang N, Perret N, Foster A. Sustainable hydrogen production for fuel cells by steam reforming of ethylene glycol: A consideration of reaction thermodynamics. *Int. J. Hydrog Energy* 2011;36:5932-5940.

[57]. Parmar RD, Kundu A, Karan K. Thermodynamic analysis of diesel reforming process: mapping of carbon formation boundary and representative independent reactions. *J Power Sources* 2009;194:1007-1020.

[58]. Miguel CV, Soria MA, Mendes A, Madeira LM. Direct CO2 hydrogenation to methane or methanol from post-combustion exhaust streams - A thermodynamic study. *J Nat Gas Sci Eng* 2015; 22:1–8.

[59]. Sharaf OZ, Orhan MF. An overview of fuel cell technology: Fundamentals and applications. *Renew Sustain Energy Rev* 2014;32:810–53.

[60]. Garche J, Jürissen L. Applications of Fuel Cell Technology: Status and Perspectives. The Electrochem. Soc. Interface 2015;24:39-43.

[61]. Engineering ToolBox, (2003). Fuels - Higher and Lower Calorific Values. Website: https://www.engineeringtoolbox.com/fuels-higher-calorific-values-d_169.html [accessed:06/09/2018].

[62]. Semelsberger TA, Borup RL, Greene HL. Dimethyl ether (DME) as an alternative fuel. *J Power Sources* 2006;156;2:497-511.

[63]. Lai Q, Paskevicius M, Sheppard DA, Buckley CE, Thornton AW, Hill MR, Gu Q *et al*. Hydrogen storage materials for mobile and stationary applications: current state of the art. *Chem. Sus. Chem.* 2015;8;17:2789-2825.

[64]. Peace Software. Website: http://www.peacesoftware.de/einigewerte/methan_e.html [accessed: 23.09.2018].

[65]. Kalmula B, Kondapuram VR. Fuel processor - Fuel cell integration: Systemic issues and challenges. *Renew Sustain Energy Rev* 2015;45:409–18.

[66]. Wilberforce T, Alaswad A, Palumbo A, Dassisti M, Olabi AG. Advances in stationary and portable fuel cell applications. *Int J Hydrog Energy* 2016;41:16509-16522.

[67]. Li X. Principles of fuel cells. Taylor & Francis Group, New York 2006.

[68]. Serenergy. HT-PEM basics. Website: http://serenergy.com/forside-test/technology/ht-pem-basics/ [accessed: 10.10.2016].

[69]. Garcia EY, Laborde MA. Hydrogen production by the steam reforming of ethanol: thermodynamic analysis. *Int. J. Hydrog Energy* 1991;16:307-312.

[70]. Lutz AE, Bradshaw RW, Keller JO, Witmer DE. Thermodynamic analysis of hydrogen production by steam reforming. *Int. J. Hydrog Energy* 2003;28:159-167.

[71]. Lutz AE, Bradshaw RW, Bromberg L, Rabinovich A. Thermodynamic analysis of hydrogen production by partial oxidation reforming. *Int. J. Hydrog Energy* 2004;29:809-816.

[72]. Ahmed S, Krumpelt M. Hydrogen from hydrocarbon fuels for fuel cells. *Int. J. Hydrog Energy* 2001;26:291-301.

[73]. Fishtik I, Alexander A, Datta R, Geana D. A thermodynamic analysis of hydrogen production by steam reforming of ethanol via response reactions. *Int. J. Hydrog Energy* 2000; 25:31-45.

[74]. Lwin Y, Daud WRW, Mohamad AB, Yaakob Z. Hydrogen production from steam–methanol reforming: thermodynamic analysis. *Int. J. Hydrog Energy* 2000; 25: 47-53.

[75]. Kang I, Bae J. Autothermal reforming study of diesel for fuel cell application. *J Power Sources* 2006;159:1283-1290.

[76]. Liu S, Zhang K, Fang L, Li Y. Thermodynamic analysis of hydrogen production from oxidative steam reforming of ethanol. *Energy & Fuels* 2008;22:1365-1370.

[77]. Shi L, Bayless DJ. Analysis of jet fuel reforming for solid oxide fuel cell applications in auxiliary power units. *Int. J. Hydrog Energy* 2008;33:1067-1075.

[78]. Authayanun S, Arpornwichanop A, Paengjuntuek W, Assabumrungrat S. Thermodynamic study of hydrogen production from crude glycerol autothermal reforming for fuel cell applications. *Int. J. Hydrog Energy* 2010;35:6617-6623.

[79]. Li J, Yu H, Yang G, Peng F, Xie D, Wang H, et al. Steam reforming of oxygenate fuels for hydrogen production: A thermodynamic study. *Energy & Fuels* 2011;25:2643–50.

[80]. Wang J, Chen H, Tian Y, Yao M, Li Y. Thermodynamic analysis of hydrogen production for fuel cells from oxidative steam reforming of methanol. *Fuel* 2012;97: 805-811.

[81]. Cui, X. and Kær, S.K. Thermodynamic analysis of steam reforming and oxidative steam reforming of propane and butane for hydrogen production. *Int. J. Hydrog Energy* 2018; 43; 29:13009-13021.

[82]. Herdem MS, Farhad S, Dincer I, Hamdullahpur F. Thermodynamic modeling and assessment of a combined coal gasification and alkaline water electrolysis system for hydrogen production. *Int. J. Hydrog Energy* 2014;39:3061-3071.

[83]. AspenTech. Aspen Plus v8.8; 2015.

[84]. Bloomenergy. ES-5710. Website: http://c0688662.cdn.cloudfiles.rackspacecloud.com/downloads_pdf_Bloomenergy_DataSheet_ES-5710.pdf [accessed: 05.02.2017].

[85]. ENERFUEL. Stationary power solutions. Website: http://enerfuel.com/solutions/stationary-power-solutions/ [accessed: 05.02.2017].

[86]. ENERFUEL. Technology. Website: http://enerfuel.com/technology/ [accessed:05.02.2017].

[87]. First Element Energy. Liquid methanol fueled fuel cell power system. Website: http://firstelementenergy.com/wp-content/uploads/2014/02/FEE-MeOH-1-pg-Product-Data-Sheet-Metric-20151.pdf [accessed: 05.02.2017].

[88]. First Element Energy. FAQ. Website: http://firstelementenergy.com/faq/ [accessed: 05.02.2017].

[89]. UltraCell. Extreme mobile power for demanding applications. Website: http://www.ultracell-llc.com/assets/XX55_Data_Sheet_SY011011_Rev_01.pdf [accessed: 05.02.2017].

[90]. A brief introduction to fuel cells, 2008. Website: http://auvac.org/uploads/publication_pdf/Fuel%20Cells.pdf [accessed: 05.02.2017].

[91]. Dachs InnoGen. The innovative CHP solution for low heating demand. Website: https://senertec.com/wp-content/uploads/2016/09/Dachs-InnoGen-EN.pdf [accessed: 05.02.2017].

[92]. Helbio. APS5000 fuel cell CHP system. Website: http://www.helbio.com/assets/Uploads/Units.pdf [accessed: 05.02.2017].

[93]. POWERCELL. PowerCell PP fuel cell system (3 kW) prototype. Website: http://www.powercell.se/wp-content/uploads/2016/04/PowerCell-Datasheet-PowerPac.pdf [accessed: 05.02.2017].

[94]. Marc Alvarado. Methanol Industry Overview 2017. Website: https://ngi.stanford.edu/sites/default/files/Alvarado_Stanford_Methanol_Meeting_2017.pdf [accessed: 22.09.2108].

[95]. Feedstock/Supply. Methanol Institute. Website: https://www.methanol.org/feedstocksupply/ [accessed: 21/09/2018].

[96]. Al-Douri A, Sengupta D, El-Halwagi MM. Shale gas monetization–A review of downstream processing to chemicals and fuels. *J. Nat. Gas. Sci. Eng*. 2017;45:436-455.

[97]. Li MMJ, Tsang SCE. Bimetallic catalysts for green methanol production via CO_2 and renewable hydrogen: a mini-review and prospects. *Catal. Sci. Technol.* 2018;8;14:3450-3464.

[98]. Matzen M, Alhajji M, Demirel Y. Chemical storage of wind energy by renewable methanol production: Feasibility analysis using a multi-criteria decision matrix. *Energy* 2015;93:343-353.

[99]. Carvalho L, Lundgren J, Wetterlund E, Wolf J, Furusjö E. Methanol production via black liquor co-gasification with expanded raw material base–Techno-economic assessment. *Appl. Energy* 2018; 225:570-584.

[100]. Collodi G, Azzaro G, Ferrari N, Santos S. Demonstrating Large Scale Industrial CCS through CCU–A Case Study for Methanol Production. *Energy Procedia* 2017;114:122-138.

[101]. Rivarolo M, Bellotti D, Magistri L, Massardo AF. Feasibility study of methanol production from different renewable sources and thermo-economic analysis. *Int. J. Hydrog. Energy.* 2016; 41;4:2105-2116.

[102]. Andreasen SJ, Kær SK, Sahlin S. Control and experimental characterization of a methanol reformer for a 350 W high temperature polymer electrolyte membrane fuel cell system. *Int. J. Hydrog. Energy.* 2013;38:1676-1684.

[103]. Park GG, Seo DJ, Park SH, Yoon YG, Kim CS, Yoon WL. Development of microchannel methanol steam reformer. *Chem Eng J* 2004;101:87–92.

[104]. Park GG, Yim SD, Yoon YG, Lee WY, Kim CS, Seo DJ *et al*. Hydrogen production with integrated microchannel fuel processor for portable fuel cell systems. *J Power Sources* 2005; 145:702-706.

[105]. Men Y, Kolb G, Zapf R, Tiemann D, Wichert M, Hessel V *et al*. A complete miniaturized microstructured methanol fuel processor/fuel cell system for low power applications. *Int. J. Hydrog. Energy.* 2008;33:1374-1382.

[106]. Kolb G, Schelhaas KP, Wichert M, Burfeind J, Heßke C, Bandlamudi G. Development of a Micro-Structured Methanol Fuel Processor Coupled to a High-Temperature Proton Exchange Membrane Fuel Cell. *Chem. Eng. Technol* 2009;32:1739-1747.

[107]. Faungnawakij K, Kikuchi R, Eguchi K. Thermodynamic evaluation of methanol steam reforming for hydrogen production. *J. Power Sources* 2006;161;1:87-94.

[108]. Wang S, Wang S. Thermodynamic equilibrium composition analysis of methanol autothermal reforming for proton exchanger membrane fuel cell based on FLUENT Software. *J. Power Sources* 2008;185;1:451-458.

[109]. Ross JRH. Heterogeneous catalysis: fundamentals and applications. Elsevier, 2011.

[110]. Chin YH, Wang Y, Dagle RA, Li XS. Methanol steam reforming over Pd/ZnO: Catalyst preparation and pretreatment studies. *Fuel Process. Technol*. 2003;83:193-201.

[111]. Pojanavaraphan C, Luengnaruemitchai A, Gulari E. Effect of catalyst preparation on Au/Ce1-xZrxO2 and Au–Cu/Ce1− xZrxO2 for steam reforming of methanol. *Int. J. Hydrog Energy* 2013;38:1348-1362.

[112]. Udani PP, Gunawardana PVDS, Lee HC, Kim DH. Steam reforming and oxidative steam reforming of methanol over CuO–CeO2 catalysts. *Int. J. Hydrog Energy* 2009;34:7648-7655.

[113]. Kolb G, Keller S, Tiemann D, Schelhaas KP, Schürer J, Wiborg O. Design and operation of a compact microchannel 5kW el, net methanol steam reformer with novel Pt/In2O3 catalyst for fuel cell applications. *Chem. Eng. J.* 2012;207:388-402.

[114]. Amphlett JC, Mann RF, Weir RD. Hydrogen production by the catalytic steam reforming of methanol: Part 3: Kinetics of methanol decomposition using C18HC catalyst. *Can. J. Chem. Eng.* 1988; 66:950-956.

[115]. Reitz TL, Ahmed S, Krumpelt M, Kumar R, Kung HH. Characterization of CuO/ZnO under oxidizing conditions for the oxidative methanol reforming reaction. *J. Mol. Catal. A: Chem* 2000; 162:275-285.

[116]. Choi Y, Stenger HG. Fuel cell grade hydrogen from methanol on a commercial Cu/ZnO/Al2O3 catalyst. *Appl Catal B Environ* 2002;38:259–69.

[117]. Agrell J, Birgersson H, Boutonnet M. Steam reforming of methanol over a Cu/ZnO/Al2O3 catalyst: a kinetic analysis and strategies for suppression of CO formation. *J. Power Sources* 2002;106:249-257.

[118]. Thurgood CP, Amphlett JC, Mann RF, Peppley BA. Deactivation of Cu/ZnO/Al_2O_3 catalyst: Evolution of site concentrations with time. *Top Catal* 2003;22:253–9.

[119]. Twigg MV, Spencer MS. Deactivation of copper metal catalysts for methanol decomposition, methanol steam reforming and methanol synthesis. *Top Catal* 2003; 22:191-203.

[120]. Purnama H, Ressler T, Jentoft RE, Soerijanto H, Schlögl R, Schomäcker R. CO formation/selectivity for steam reforming of methanol with a commercial CuO/ZnO/Al_2O_3 catalyst. *Appl. Catal. A Gen* 2004;259:83-94.

[121]. Agarwal V, Patel S, Pant KK. H_2 production by steam reforming of methanol over Cu/ZnO/Al_2O_3 catalysts: transient deactivation kinetics modeling. *Appl. Catal. A Gen* 2005; 279:155-164.

[122]. Patel S, Pant KK. Activity and stability enhancement of copper–alumina catalysts using cerium and zinc promoters for the selective production of hydrogen via steam reforming of methanol. *J. Power Sources* 2006;159:139-143.

[123]. Patel S, Pant KK. Hydrogen production by oxidative steam reforming of methanol using ceria promoted copper-alumina catalysts. *Fuel Process. Technol.* 2007;88:825–32.

[124]. Yu KMK, Tong W, West A, Cheung K, Li T, Smith G, et al. Non-syngas direct steam reforming of methanol to hydrogen and carbon dioxide at low temperature. *Nat Commun* 2012; 3:1230.

[125]. Avgouropoulos G, Paxinou A, Neophytides S. In situ hydrogen utilization in an internal reforming methanol fuel cell. *Int. J. Hydrog Energy* 2014;39:18103-18108.

[126]. Avgouropoulos G, Papavasiliou J, Ioannides T, Neophytides S. Insights on the effective incorporation of a foam-based methanol reformer in a high temperature polymer electrolyte membrane fuel cell. *J. Power Sources* 2015;296:335-343.

[127]. Avgouropoulos G, Schlicker S, Schelhaas KP, Papavasiliou J, Papadimitriou KD, Theodorakopoulou et al. Performance evaluation of a proof-of-concept 70 W internal reforming methanol fuel cell system. *J. Power Sources* 2016;307:875-882.

[128]. Avgouropoulos G, Neophytides SG. Performance of internal reforming methanol fuel cell under various methanol/water concentrations. *J. Appl. Electrochem.* 2012;42:719-726.

[129]. Papavasiliou J, Avgouropoulos G, Ioannides T. CuMnOx catalysts for internal reforming methanol fuel cells: application aspects. *Int. J Hydrog Energy* 2012;37:16739-16747.

[130]. Hughes R. Deactivation of catalysts. Academic Pr, 1984.

[131]. Chin YH, Dagle R, Hu J, Dohnalkov AC, Wang Y. Steam reforming of methanol over highly active Pd/ZnO catalyst. *Catal. Today* 2002;77:79-88.

[132]. Liu S, Takahashi K, Ayabe M. Hydrogen production by oxidative methanol reforming on Pd/ZnO catalyst: effects of Pd loading. *Catal. Today* 2003;87:247-253.

[133]. Iwasa N, Mayanagi T, Nomura W, Arai M, Takezawa N. Effect of Zn addition to supported Pd catalysts in the steam reforming of methanol. *Appl. Catal. A Gen.* 2003; 248:153-160.

[134]. Liu S, Takahashi K, Fuchigami K, Uematsu K. Hydrogen production by oxidative methanol reforming on Pd/ZnO: catalyst deactivation. *Appl. Catal. A Gen.* 2006;299:58-65.

[135]. Dagle RA, Platon A, Palo DR, Datye AK, Vohs JM, Wang Y. PdZnAl catalysts for the reactions of water-gas-shift, methanol steam reforming, and reverse-water-gas-shift. *Appl. Catal. A Gen.* 2008;342:63-68.

[136]. Men Y, Kolb G, Zapf R, O'Connell M, Ziogas A. Methanol steam reforming over bimetallic Pd–In/Al_2O_3 catalysts in a microstructured reactor. *Appl. Catal. A Gen.* 2010; 380:15-20.

[137]. Kolb G, Keller S, Pecov S, Pennemann H, Zapf R. Development of microstructured catalytic wall reactors for hydrogen production by methanol steam reforming over novel Pt/In2O3/Al2O3 catalysts. *Chem. Eng. Trans* 2011;24:133-138.

[138]. Peppley BA, Amphlett JC, Kearns LM, Mann RF. Methanol–steam reforming on Cu/ZnO/Al2O3 catalysts. Part 2. A comprehensive kinetic model. *Appl. Catal. A Gen.* 1999; 179:31-49.

[139]. Chan SH, Wang HM. Thermodynamic and kinetic modelling of an autothermal methanol reformer. *J. Power Sources* 2004;126:8-15.

[140]. Lee JK, Ko JB, Kim DH. Methanol steam reforming over Cu/ZnO/Al2O3 catalyst: kinetics and effectiveness factor. *Appl. Catal. A Gen.* 2004;278:25-35.

[141]. Mastalir A, Frank B, Szizybalski A, Soerijanto H, Deshpande A, Niederberger M et al. Steam reforming of methanol over $Cu/ZrO_2/CeO_2$ catalysts: a kinetic study. *J. Catal.* 2005; 230:464-475.

[142]. Papavasiliou J, Avgouropoulos G, Ioannides T. Combined steam reforming of methanol over Cu–Mn spinel oxide catalysts. *J. Catal.* 2007;251:7-20.

[143]. Sá S, Sousa JM, Mendes A. Steam reforming of methanol over a CuO/ZnO/Al2O3 catalyst, part I: Kinetic modelling. *Chem. Eng. Sci.* 2011; 66:4913-4921.

[144]. Cao C, Xia G, Holladay J, Jones E, Wang Y et al. Kinetic studies of methanol steam reforming over Pd/ZnO catalyst using a microchannel reactor. *Appl. Catal. A Gen.* 2004; 262:19-29.

[145]. Pfeifer P, Kölbl A, Schubert K. Kinetic investigations on methanol steam reforming on PdZn catalysts in microchannel reactors and model transfer into the pressure gap region. *Catal. Today* 2005;110:76-85.

[146]. Patel S, Pant KK. Kinetic modeling of oxidative steam reforming of methanol over Cu/ZnO/CeO2/Al2O3 catalyst. *Appl. Catal. A Gen.* 2009;356:189-200.

[147]. Wichert M, Zapf R, Ziogas A, Kolb G, Klemm E. Kinetic investigations of the steam reforming of methanol over a Pt/In2O3/Al2/O3 catalyst in microchannels. *Chem. Eng. Sci.* 2016; 155:201-209.

[148]. Ribeirinha, P., Mateos-Pedrero, C., Boaventura, M., Sousa, J., Mendes, A. CuO/ZnO/Ga2O3 catalyst for low temperature MSR reaction: Synthesis, characterization and kinetic model. *Appl. Catal. B.* 2018; 221:371-379.

[149]. Peppley BA, Amphlett JC, Kearns LM, Mann RF. Methanol–steam reforming on Cu/ZnO/Al2O3. Part 1: the reaction network. *Appl. Catal. A Gen.* 1999; 179:21-29.

[150]. Karim A, Bravo J, Datye A. Nonisothermality in packed bed reactors for steam reforming of methanol. *Appl. Catal. A Gen.* 2005; 282:101-109.

[151]. Chein RY, Chen LC, Chen YC, Chung JN. Heat transfer effects on the methanol-steam reforming with partially filled catalyst layers. *Int. J. Hydrog Energy* 2009;34:5398-5408.

[152]. Vadlamudi VK, Palanki S. Modeling and analysis of miniaturized methanol reformer for fuel cell powered mobile applications. *Int. J. Hydrog Energy* 2011;36:3364-3370.

[153]. Nehe P, Reddy VM, Kumar S. Investigations on a new internally-heated tubular packed-bed methanol–steam reformer. *Int. J. Hydrog Energy* 2015;40:5715-5725.

[154]. Pohar A, Hočevar S, Likozar B, Levec J. Synthesis and characterization of gallium-promoted copper–ceria catalyst and its application for methanol steam reforming in a packed bed reactor. *Catal. Today* 2015; 256:358-364.

[155]. Real D, Dumanyan I, Hotz N. Renewable hydrogen production by solar-powered methanol reforming. *Int. J. Hydrog Energy* 2016;41:11914-11924.

[156]. Wang G, Wang F, Li L, Zhao M. Methanol steam reforming on catalyst coating by cold gas dynamic spray. *Int. J. Hydrog Energy* 2016;41:2391-2398.

[157]. Mei D, Feng Y, Qian M, Chen Z. An innovative micro-channel catalyst support with a micro-porous surface for hydrogen production via methanol steam reforming. *Int. J. Hydrog Energy* 2016;41:2268-2277.

[158]. Dolanc G, Belavič D, Hrovat M, Hočevar S, Pohar A, Petrovčič J et al. A miniature fuel reformer system for portable power sources. *J. Power Sources* 2014;271:392-400.

[159]. Holladay JD, Wang Y. A review of recent advances in numerical simulations of microscale fuel processor for hydrogen production. *J. Power Sources* 2015;282: 602-621.

[160]. Pan M, Feng Z, Jiang L. Reaction characteristics of methanol steam reforming inside mesh microchannel reactor. *Int. J. Hydrog Energy* 2016;41:1441-1452.

[161]. Laguna OH, Domínguez MI, Centeno MA, Odriozola JA. Forced deactivation and postmortem characterization of a metallic microchannel reactor employed for the preferential oxidation of CO (PROX). *Chem. Eng. J.* 2016; 302:650-662.

[162]. Cruz S, Sanz O, Poyato R, Laguna OH, Echave FJ, Almeida LC et al. Design and testing of a microchannel reactor for the PROX reaction. *Chem. Eng. J.* 2011; 167:634-642.

[163]. Laguna OH, Ngassa EM, Oraá S, Álvarez A, Domínguez MI, Sarria FR et al. Preferential oxidation of CO (CO-PROX) over CuOx/CeO2 coated microchannel reactor. *Catal. Today* 2012; 180:105-110.

[164]. Laguna OH, Domínguez MI, Oraá S, Navajas A, Arzamendi G, Gandía LM et al. Influence of the O2/CO ratio and the presence of H2O and CO2 in the feed-stream during the preferential oxidation of CO (PROX) over a CuOx/CeO2-coated microchannel reactor. *Catal. Today* 2013; 203:182-187.

[165]. Laguna OH, Castaño MG, Centeno MA, Odriozola JA. Microreactors technology for hydrogen purification: Effect of the catalytic layer thickness on CuOx/CeO2-coated microchannel reactors for the PROX reaction. *Chem. Eng. J.* 2015; 275:45-52.

[166]. Ghasemzadeh K, Andalib E, Basile A. Evaluation of dense Pd–Ag membrane reactor performance during methanol steam reforming in comparison with autothermal reforming using CFD analysis. *Int. J. Hydrog Energy* 2016; 41:8745-8754.

[167]. Joghee P, Malik JN, Pylypenko S, O'Hayre R. A review on direct methanol fuel cells–in the perspective of energy and sustainability. *MRS Energy Sustain* 2015; 2: E3.

[168]. Mehmood A, Scibioh MA, Prabhuram J, An MG, Ha HY. A review on durability issues and restoration techniques in long-term operations of direct methanol fuel cells. *J. Power Sources* 2015; 297:224-241.

[169]. Thampan T, Shah D, Cook C, Novoa J, Shah S. Development and evaluation of portable and wearable fuel cells for soldier use. *J. Power Sources* 2014;259:276-281.

[170]. Lindström B, Pettersson LJ. Development of a methanol fuelled reformer for fuel cell applications. *J. Power Sources* 2003;118:71-78.

[171]. Boettner DD, Moran MJ. Proton exchange membrane (PEM) fuel cell-powered vehicle performance using direct-hydrogen fueling and on-board methanol reforming. *Energy* 2004; 29:2317-2330.

[172]. Pan C, He R, Li Q, Jensen JO, Bjerrum NJ, Hjuldman HA *et al*. Integration of high temperature PEM fuel cells with a methanol reformer. *J. Power Sources* 2005;145:392-398.

[173]. Wei W, Pai CC. Control of a heat-integrated proton exchange membrane fuel cell system with methanol reforming. *J. Power Sources* 2009;194:920-930.

[174]. Hotz N, Zimmerman R, Weinmueller C, Lee MT, Grigoropoulos CP, Rosengarten G *et al*. Exergetic analysis and optimization of a solar-powered reformed methanol fuel cell micro-powerplant. *J. Power Sources* 2010; 195:1676-1687.

[175]. Andreasen SJ, Ashworth L, Sahlin S, Jensen HCB, Kær SK. Test of hybrid power system for electrical vehicles using a lithium-ion battery pack and a reformed methanol fuel cell range extender. *Int. J. Hydrog Energy* 2014; 39:1856-1863.

[176]. Oh K, Jeong G, Cho E, Kim W, Ju H. A CO poisoning model for high-temperature proton exchange membrane fuel cells comprising phosphoric acid-doped polybenzimidazole membranes. *Int. J. Hydrog Energy* 2014;39:21915-21926.

[177]. Rangel CM, Sousa T. Technology Watch Report: High Temperature Polymer Electrolyte Fuel Cells. Fuel Cells and Hydrogen Unit of LNEG, Portugal (2011).

[178]. Gentner C. A HT-PEM fuel cell system model for the electric power supply on ships. MOSES Workshop Sion 2017. Website: https://ipese.epfl.ch/wp-content/uploads/2018/07/Gentner-TU-Hamburg-A-HT-PEM-fuel-cell-system-model-for-the-electric-power-supply-on-ships.pdf [accessed: 30.09.2018].

[179]. Justesen KK, Andreasen SJ. Determination of optimal reformer temperature in a reformed methanol fuel cell system using ANFIS models and numerical optimization methods. *Int. J. Hydrog Energy* 2015;40:9505-9514.

[180]. Justesen KK, Andreasen SJ, Pasupathi S, Pollet BG. Modeling and control of the output current of a Reformed Methanol Fuel Cell system. *Int. J. Hydrog Energy* 2015;40:16521-16531.

[181]. Methanol Power System H3-350, Serenergy. Website: http://serenergy.com/wp-content/uploads/2015/10/H3-350_datasheet_v2.0-0313.pdf [accessed:03/03/2016].

[182]. Andreasen SJ, Kær SK, Sahlin LS, Justesen KK. Design and Control of High Temperature PEM Fuel Cell Systems using Methanol Reformers with Air or Liquid Heat Integration. In 5th International Conference FDFC2013. 2013.

[183]. Justesen KK, Andreasen SJ, Shaker HR. Dynamic modeling of a reformed methanol fuel cell system using empirical data and adaptive neuro-fuzzy inference system models. *J Fuel Cell Sci Technol* 2014;11:021004.

[184]. Liu Y, Lehnert W, Janßen H, Samsun RC, Stolten D. A review of high-temperature polymer electrolyte membrane fuel-cell (HT-PEMFC)-based auxiliary power units for diesel-powered road vehicles. *J. Power Sources* 2016;311:91-102.

[185]. Sahlin SL, Andreasen SJ, Kær SK. System model development for a methanol reformed 5 kW high temperature PEM fuel cell system. *Int. J. Hydrog Energy* 2015;40:13080-13089.

[186]. Ribeirinha P., Abdollahzadeh M., Sousa, J.M., Boaventura M., Mendes A. Modelling of a high-temperature polymer electrolyte membrane fuel cell integrated with a methanol steam reformer cell. *Appl. Energy* 2017;202:6-19.

[187]. Ribeirinha P, Schuller G, Boaventura M, Mendes A. Synergetic integration of a methanol steam reforming cell with a high temperature polymer electrolyte fuel cell. *Int. J. Hydrog Energy* 2017; 42;19:13902-13912.

[188]. Specchia S. Fuel processing activities at European level: A panoramic overview. *Int. J. Hydrog Energy* 2014;39:17953–68.

[189]. Detchan R&Leeuwen RV. Policy: Bring Sustainable Energy To The Developing World. April 2014, Website: http://www.nature.com/news/policy-bring-sustainable-energy-to-the-developing-world-1.15034 [accessed 14.01.15].

[190]. Farhad S, Hamdullahpur F, Yoo Y. Performance Evaluation of Different Configurations of Biogas-Fuelled SOFC Micro-CHP Systems for Residential Applications. *Int. J. Hydrog Energy,* 2010; 35;8:3758-3768.

[191]. Authayanun S, Aunsup P, Patcharavorachot Y, Arpornwichanop A. Theoretical Analysis of a Biogas-Fed PEMFC System with Different Hydrogen Purifications: Conventional and Membrane-Based Water Gas Shift Processes. *Energy Convers. Manag.* 2014;86; 60-69.

[192]. Farhad S, Hamdullahpur F. Conceptual Design of a Novel Ammonia-Fuelled Portable Solid Oxide Fuel Cell System. *J. Power Sources* 2010;195;10:3084-3090.

[193]. Baneshi J, Haghighi M, Jodeiri N, Abdollahifar M, et al. Homogeneous Precipitation Synthesis of CuO-ZrO_2-CeO_2-Al_2O_3 Nanocatalyst Used in Hydrogen Production via Methanol Steam Reforming for Fuel Cell Applications. *Energy Convers. Manag.* 2014; 87;928-937.

[194]. Bisaria V, Smith RJ. Hydrogen Production by Onboard Gasoline Processing–Process Simulation and Optimization. *Energy Convers. Manag.* 2013; 76;746-752.

[195]. Alarif A, Elkamel A, Croiset E. Steady-State Simulation of a Novel Annular Multitubular Reactor for Enhanced Methanol Production. Ind. Eng. Chem. Res. 2013; 52;44:15387-15393.

[196]. Horng RF, Chou HM, Lee CH, Tsai HT. Characteristics of Hydrogen Produced by Partial Oxidation and Auto-Thermal Reforming in a Small Methanol Reformer. *J. Power Sources* 2006;161;2:1225-1233.

[197]. Chein RY, Chen YC, Lin YS, Chung JN. Experimental Study on the Hydrogen Production of Integrated Methanol-Steam Reforming Reactors for PEM Fuel Cells. Int. J. Therm. Sci. 2011; 50;7:1253-1262.

[198]. Lo KF & Wong SC. A Passively-Fed Methanol Steam Reformer with Catalytic Combustor Heater. *Int. J. Hydrog. Energy* 2011;36;17:10719-10726.

[199]. Lo KF, Wong SC. A Novel Passive Feeding Method for Methanol Steam Reformers. *Int. J. Hydrog. Energy* 2011;36;13:7500-7504.

[200]. Lo KF, Wong SC. A Passively-Fed Methanol Steam Reformer Heated with Two-Stage Bi-Fueled Catalytic Combustor. *J. Power Sources* 2012;213:112-118.

[201]. H3-350 – Off-Grid Battery Charger, Serenergy. Website: http://serenergy.com/products/systems/h3-350/ [accessed 14.01.15].

[202]. Jiao K, Li X. Water Transport in Polymer Electrolyte Membrane Fuel Cells. *Prog. Energy Combust. Sci*. 2011;37;3:221-291.

[203]. Zhang J, Xie Z, Zhang J, Tang Y, et al. High Temperature PEM Fuel Cells. *J. Power Sources* 2006;160;2:872-891.

[204]. AspenTech. Aspen Plus v7.3:2011.

[205]. Cengel YA, Boles MA. *Thermodynamics: An Engineering Approach*. Vol. 5. New York: McGraw-Hill, 2011.

[206]. Authayanun S, Mamlouk M, Arpornwichanop A. Maximizing the Efficiency of a HT-PEMFC System Integrated with Glycerol Reformer. *Int. J. Hydrog. Energy* 2012;37;8: 6808-6817.

[207]. Hajjaji N. Thermodynamic Investigation and Environment Impact Assessment of Hydrogen Production from Steam Reforming of Poultry Tallow. *Energy Convers. Manag.* 2014;79;171-179.

[208]. Cheddie D, Munroe N. Mathematical Model of a PEMFC Using a PBI Membrane. *Energy Convers. Manag*. 2006;47;11:1490-1504.

[209]. Cheddie D, Munroe N. Three Dimensional Modeling of High Temperature PEM Fuel Cells. *J. Power Sources* 2006;160;215-223.

[210]. Jiao K, Li X. A Three-Dimensional Non-isothermal Model of High Temperature Proton Exchange Membrane Fuel Cells with Phosphoric Acid Doped Polybenzimidazole Membranes. *Fuel Cells* 2010;10;3:351-362.

[211]. Korsgaard AR, Refshauge R, Nielsen MP, Bang M, et al. *Experimental Characterization and Modeling of Commercial Polybenzimidazole-Based MEA Performance. J. Power Sources* 2006;162;239-245.

[212]. Korsgaard AR, Nielsen MP, Bang M, Kær SK. Modeling of CO Influence in PBI Electrolyte PEM Fuel Cells. ASME 2006 4th International Conference on Fuel Cell Science, Engineering and Technology. ASME, 2006.

[213]. Zuliani N, Taccani R. Microcogeneration System Based on HTPEM Fuel Cell Fueled with Natural Gas: Performance Analysis. *Appl. Energ*. 2012;97;802-808.

[214]. Harikishan RE, Jayanti S. Thermal Management Strategies for a 1 kW_e Stack of a High Temperature Proton Exchange Membrane Fuel Cell. *Appl. Therm. Eng.* 2012;48;465-475.

[215]. Korsgaard AR, Nielsen MP, Kær SK. Part one: A Novel Model of HTPEM-Based Micro-Combined Heat and Power Fuel Cell System. *Int. J. Hydrog. Energy* 2008;33;7:1909-1920.

[216]. Arsalis A, Nielsen MP, Kær SK. Modeling and Optimization of a 1 kW_e HT-PEMFC-Based Micro-CHP Residential System. *Int. J. Hydrog. Energy* 2012;37;3:2470-2481.

[217]. Arsalis A, Nielsen MP, Kær SK. Application of an Improved Operational Strategy on a PBI Fuel Cell-Based Residential System for Danish Single-Family Households. *Appl. Therm. Eng.* 2013;50;704-713.

[218]. Samsun RC, Pasel J, Janßen H, Lehnert W, et al. Design and Test of a 5 kW_e High-Temperature Polymer Electrolyte Fuel Cell System Operated with Diesel and Kerosene. *Appl. Energ* 2014;114;238-249.

[219]. Jensen MF. High Temperature PEM; part of the solution. Danish Korean PEM Fuel Cell Workshop, 2013. Website: http://www.kdfuelcell.net/KDFuelCell/Programme [accessed 10.04.15].

[220]. Valdes-Solis T, Marban G, Fuertes AB. Nanosized Catalysts for the Production of Hydrogen by Methanol Steam Reforming. *Catal. Today* 2006;116;3:354-360.

[221]. Lin Y, Kui J, Qing D, Yan Y. *Exergy Analysis of High-Temperature Proton Exchange Membrane Fuel Cell Systems. Int. J. Green Energy* 2015;12;9: 917-929.

[222]. Authayanun S, Mamlouk M, Scott K, Arpornwichanop A. Comparison of high-temperature and low-temperature polymer electrolyte membrane fuel cell systems with glycerol reforming process for stationary applications. *Appl. Energy* 2013;109;192-201.

[223]. Subramani V, Sharma P, Zhang L, Liu K. In *Hydrogen and syngas production and purification technologies*; Liu, K., Song, C., Subramani, V., Eds.; Wiley: Hoboken, New Jersey, 2010; Chapter 2, pp.14-126.

[224]. Speight JG. In *Fuel Cells: Technologies for Fuel Processing*; Shekhawat, II D., Spivey, J.J., Berry, D.A., Eds.; Elsevier: 2011.; Chapter 3, pp. 29-46.

[225]. Fuel Densities and Specific Values. <http://www.engineeringtoolbox.com/fuels-densities-specific-volumes-d_166.html> [accessed: 14.05.2018].

[226]. The Science and Properties of LPG. < http://www.elgas.com.au/blog/453-the-science-a-properties-of-lpg> [accessed:14.05.2018].

[227]. Liquefied Petroleum Gas (LPG). <https://www.iocl.com/products/lpgspecifications.pdf> [accessed: 14.05.2018].

[228]. California Energy Commission. <http://www.energy.ca.gov/lng/faq.html> [accessed:14.05.2018].

[229]. Hedayat N, Du Y, Ilkhani H. Pyrolyzable pore-formers for the porous-electrode formation in solid oxide fuel cells: A review. *Ceram. Int.* 2016, 44, 4561-4576.

[230]. Romero-Pascual E, Soler J. Modelling of an HTPEM-based micro-combined heat and power fuel cell system with methanol. *Int. J. Hydrogen Energy* 2014, *39* (8), 4053-4059.

[231]. Gaudillere C, Gonzalez JJ, Chica A, Serra, JM. YSZ monoliths promoted with Co as catalysts for the production of H_2 by steam reforming of ethanol. *Applied Catalysis, A: General* 2017, 538, 165-173.

[232]. Carrero A, Vizcaino AJ, Calles JA, Garcia-Moreno L. Hydrogen production through glycerol steam reforming using Co catalysts supported on SBA-15 doped with Zr, Ce and La. *J. Energy Chem.* 2017, 26, 42-48.

[233]. Tjaden B, Gandiglio M, Lanzini A, Santarelli M, Jarvinen M. Small-scale biogas-SOFC plant: technical analysis and assessment of different fuel reforming options. *Energy Fuels* 2014, *28* (6), 4216-4232.

[234]. Mamaghani AH, Najafi B, Casalegno A, Rinaldi F. Predictive modelling and adaptive long-term performance optimization of an HT-PEM fuel cell based micro combined heat and power (CHP) plant. *Appl. Energy* 2017, 192, 519–529.

[235]. Kuznetsov VV, Kozlov SP. Modelling of methanol-to-hydrogen steam reforming with a heat flux distributed along a microchannel. *Thermophys. Aeromech.* 2008, *15* (3), 509-517.

[236]. Chen FC, Chang MH, Kuo CY, Hsueh CY, Yan WM. Analysis of a plate-type microreformer for methanol steam reforming reaction. *Energy Fuels* 2009, *23* (10), 5092-5098.

[237]. Hsueh CY, Chu HS, Yan WM, Chen CH. Numerical study of heat and mass transfer in a plate methanol steam micro reformer with methanol catalytic combustor. *Int. J. Hydrogen Energy* 2010, 35, 6227–38.

[238]. Hsueh CY, Chu HS, Yan WM, Leu GC, Tsai JI. Three-dimensional analysis of a plate methanol steam micro-reformer and a methanol catalytic combustor with different flow channel designs. *Int. J. Hydrogen Energy* 2011, *36* (21), 13575-13586.

[239]. Fazeli A, Behnam M. Hydrogen production in a zigzag and straight catalytic wall coated micro channel reactor by CFD modeling. *Int. J. Hydrogen Energy* 2010, 35, 9496–9503.

[240]. Hao Y, Du X, Yang L, Shen Y, Yang Y. Numerical simulation of configuration and catalyst-layer effects on microchannel steam reforming of methanol. *Int. J. Hydrogen Energy* 2011, 36, 15611–21.

[241]. Tadbir MA, Akbari MH. Methanol steam reforming in a planar wash coated microreactor integrated with a micro-combustor. *Int. J. Hydrogen Energy* 2011, 36, 12822–32.

[242]. Tadbir MA, Akbari MH. Integrated methanol reforming and oxidation in wash-coated microreactors: A three-dimensional simulation. *Int. J. Hydrogen Energy* 2012, 37, 2287–2297.

[243]. Uriz I, Arzamendi G, Diéguez PM, Echave FJ, Sanz O, Montes M, Gandia LM. CFD analysis of the effects of the flow distribution and heat losses on the steam reforming of methanol in catalytic (Pd/ZnO) microreactors. *Chem. Eng. J.* 2014, 238, 37–44.

[244]. Sari A, Sabziani J. Modeling and 3D-simulation of hydrogen production via methanol steam reforming in copper-coated channels of a mini reformer. *J. Power Sources* 2017, 352, 64–76.

[245]. Liu D, Men Y, Wang J, Kolb G, Liu X, Wang Y, Sun, Q. Highly active and durable Pt/In2O3/Al2O3 catalysts in methanol steam reforming. *Int. J. Hydrogen Energy* 2016, *41* (47), 21990-21999.

[246]. Jiang CJ, Trimm DL, Wainwright MS, Cant NW. Kinetic study of steam reforming of methanol over copper-based catalysts. *Applied Catalysis, A: General* 1993, *93* (2), 245-255.

[247]. Kim T, Kwon S. Design, fabrication and testing of a catalytic microreactor for hydrogen production. *J. Micromech. Microeng.* 2006, 16, 1752–1760.

[248]. Skorokhod VV, Get'man OI, Zuev AE, Rakitin SP. Correlation between the particle size, pore size, and porous structure of sintered tungsten. *Powder Metall. Met. Ceram.* 1988, *27* (12), 941-47.

[249]. Tjaden B, Cooper SJ, Brett DJ, Kramer D, Shearing PR. On the origin and application of the Bruggeman correlation for analysing transport phenomena in electrochemical systems. *Curr. Opin. Chem. Eng.* 2016, 12, 44-51.

[250]. Mundhwa M, Parmar RD, Thurgood CP. A comparative parametric study of a catalytic plate methane reformer coated with segmented and continuous layers of combustion catalyst for hydrogen production. *J. Power Sources* 2017, 344, 85–102.

[251]. Mundhwa M, Thurgood CP. Numerical study of methane steam reforming and methane combustion over the segmented and continuously coated layers of catalysts in a plate reactor. *Fuel Process. Technol.* 2017, 158, 57–72.

[252]. Caglar OY, Demirhan CD, Avci AK. Modeling and design of a microchannel reformer for efficient conversion of glycerol to hydrogen. *Int. J. Hydrogen Energy* 2015, 40, 7579–85.

[253]. Poling BE, Prausnitz JM, O`Connell JP. *The properties of liquids and gases*; Mcgraw-Hill: New York, 2000; 5th edition.

[254]. Mundhwa M, Thurgood CP. Improved performance of a catalytic plate reactor coated with distributed layers of reforming and combustion catalysis for hydrogen production. *React. Chem. Eng.* **2018**, 3, 487-514.

[255]. Cao C, Zhang N, Dang D, Cheng Y. Hybrid modeling of integrated microchannel methane reformer for miniaturized GTL application using an effectiveness factor submodel based on complex surface chemistry. *Chem. Eng. J.* 2017, 316, 715-26.

[256]. Perry RH, Green DW. *Perry's Chemical Engineers' Handbook*; Mcgraw-Hill: New York, 2008; 8th edition.

[257]. Bird RB, Stewart WE, Lightfoot EN. *Transport Phenomena*; John Wiley & Sons: New York, 2007; revised 2nd edition.

[258]. Patel S, Pant KK. Experimental study and mechanistic kinetic modeling for selective production of hydrogen via catalytic steam reforming of methanol. *Chem. Eng. Sci.* 2007, *62* (18-20), 5425-5435.

[259]. Sanz O, Velasco I, Pérez-Miqueo I, Poyato R, Odriozola JA, Montes M. Intensification of hydrogen production by methanol steam reforming. *Int. J. Hydrogen Energy* 2016, 41, 5250–5259.

[260]. Munro RG. Evaluated material properties for a sintered alpha-alumina. *J. Am. Ceram. Soc.* 1997, 80, 1919–1928.

[261]. Ribeirinha P, Abdollahzadeh M, Boaventura M, Mendes A. H_2 production with low carbon content via MSR in packed bed membrane reactors for high-temperature polymeric electrolyte membrane fuel cell. *Appl. Energy* 2017, 188, 409-419.

[262]. Thomas S, Vang JR, Araya SS, Kær SK. Experimental study to distinguish the effects of methanol slip and water vapour on a high temperature PEM fuel cell at different operating conditions. *Appl. Energy* 2017, 192, 422–36.

[263]. Ni M. 2D heat and mass transfer modeling of methane steam reforming for hydrogen production in a compact reformer. *Energy Convers. Manage* 2013, 65, 155-163.

[264]. Ribeirinha P, Alves I, Vázquez FV, Schuller G, Boaventura M, Mendes A. Heat integration of methanol steam reformer with a high-temperature polymeric electrolyte membrane fuel cell. *Energy* 2017, 120, 468–477.

[265]. Schuller G, Vázquez FV, Waiblinger W, Auvinen S, Ribeirinha P. Heat and fuel coupled operation of a high temperature polymer electrolyte fuel cell with a heat exchanger methanol steam reformer. *J. Power Sources* 2017, 347, 47–56.

[266]. Fogler HS. *Elements of chemical reaction engineering*; Prentice Hall: Upper Saddle River, New Jersey, 2005; 4th edition.

[267]. Amirante R, Cassone E, Distaso E, Tamburrano P. Overview on Recent Developments in Energy Storage: Mechanical, Electrochemical and Hydrogen Technologies. *Energy Convers. Manage* 2017, 132, 372-87.

[268]. da Silva Veras T, Mozer TS, da Costa Rubim Messeder dos Santos D, da Silva César A. Hydrogen: Trends, Production and Characterization of the Main Process Worldwide. *Int. J. Hydrogen Energy* 2017, 26, 2018-33.

[269]. Ma Z, Eichman JD, Kurtz JM. Fuel Cell Backup Power System for Grid Service and Micro-Grid in Telecommunication Applications: Preprint. No. NREL/CP-5500-70990. *National Renewable Energy Lab.(NREL)*, Golden, CO (United States), 2018.

[270]. Development project has resulted in great commercial success, August 2017. <https://serenergy.com/development-project-has-resulted-in-great-commercial-success/ > [accessed: 27.08.2018].

[271]. Waiblinger W, Kallo J, Schirmer J, Friedrich KA. High temperature polymer electrolyte fuel cell systems for aircraft applications, Ch. 23. In *high temperature polymer electrolyte fuel cells*. Editors: Li, Q.; Aili, D.; Hjuler, H.A.; Jensen, J.O. Springer, Switzerland, 2016. pp. 511-524.

[272]. Tronstad T, Åstrand HH, Haugom GP, Langfeldt L. Study on the use of fuel cells in shipping. *European Maritime Safety Agency*, 2017.

[273]. Abdalla AM, Hossain S, Nisfindy OB, Azad AT, Dawood M, Azad AK. Hydrogen Production, Storage, Transportation and Key Challenges with Applications: A Review. *Energy Convers. Manage* 2018, 165, 602-27.

[274]. Xu JG, Froment GF. Methane Steam Reforming, Methanation and Water-Gas Shift .1. Intrinsic Kinetics. *Aiche J.* 1989, 35, 88-96.

[275]. Ni M, Leung DYC, Leung MKH. A Review on Reforming Bio-Ethanol for Hydrogen Production. *Int. J. Hydrogen Energy* 2007, 32, 3238-47.

[276]. Sabio E, Álvarez-Murillo A, González JF, Ledesma B, Román S. Modelling the Composition of the Gas Obtained by Steam Reforming of Glycerine. *Energy Convers. Manag.* 2017, 146, 147-57.

[277]. Schädel BT, Duisberg M, Deutschmann O. Steam Reforming of Methane, Ethane, Propane, Butane, and Natural Gas over a Rhodium-Based Catalyst. *Catal. Today* 2009, 142, 42-51.

[278]. Wang J, Wu J, Xu Z, Li M. Thermodynamic Performance Analysis of a Fuel Cell Trigeneration System Integrated with Solar-Assisted Methanol Reforming. *Energy Convers. Manag.* 2017, 150, 81-89.

[279]. Zhou C, Shah K, Doroodchi E, Moghtaderi B. Equilibrium Thermodynamic Analyses of Methanol Production via a Novel Chemical Looping Carbon Arrestor Process. *Energy Convers. Manag.* 2015, 96, 392-402.

[280]. The methanol fuel cell system-an alternative power generation system. Website: <https://serenergy.com/> [accessed: 27.08.2018].

[281]. Ribeirinha P, Abdollahzadeh M, Pereira A, Relvas F, Boaventura M, Mendes A. High Temperature PEM Fuel Cell Integrated with a Cellular Membrane Methanol Steam Reformer: Experimental and Modelling. *Appl. Energy* 2018, 215, 659-69.

[282]. Lotrič A, Sekavčnik M, Pohar A, Likozar B, Hočevar S. Conceptual design of an integrated thermally self-sustained methanol steam reformer high temperature PEM fuel cell stack man portable power generator. *Int. J. Hydrogen Energy* 2017, 42, 16700-13.

[283]. Reuse P, Renken A, Haas-Santo K, Gorke O, Schubert K. Hydrogen Production for Fuel Cell Application in an Autothermal Micro-Channel Reactor. *Chem. Eng. J.* 2004, 101, 133-41.

[284]. Kundu A, Jang JH, Lee HR, Kim SH, Gil JH, Jung CR, Oh YS. MEMS-Based Micro-Fuel Processor for Application in a Cell Phone. *J. Power Sources* 2006, 162, 572-8.

[285]. Shah K, Ouyang X, Besser RS. Microreaction for Microfuel Processing: Challenges and Prospects. *Chem. Eng. Technol.* 2005, 28, 303-13.

[286]. Chang KS, Tanaka S, Esashi M. A Micro-Fuel Processor with Trench-Refilled Thick Silicon Dioxide for Thermal Isolation Fabricated by Water-Immersion Contact Photolithography. *J. Micromechanics Microengineering* 2005, 15, 171-8.

[287]. Kim T. Micro Methanol Reformer Combined with a Catalytic Combustor for a PEM Fuel Cell. *Int. J. Hydrogen Energy* 2009, 34, 6790-8.

[288]. Wang G, Wang F, Li L, Zhang G. Experiment of catalyst activity distribution effect on methanol steam reforming performance in the packed bed plate-type reactor. *Energy* 2013, 51, 267-272.

[289]. Wang G, Wang F, Li L, Zhang G. Experimental investigation of axially non-uniform catalysis for methanol steam reforming. *J. Power Sources* 2014, *250*, 306-312.

[290]. Zanfir M, Baldea M, Daoutidis P. Optimizing the catalyst distribution for countercurrent methane steam reforming in plate reactors. *AIChE Journal* 2011, *57*(9), 2518-2528.

[291]. Karagiannidis S, Mantzaras J, Jackson G, Boulouchos K. Hetero-/homogeneous combustion and stability maps in methane-fueled catalytic microreactors. *Proc. Combust. Inst.* 2007, 31(2), 3309-3317.

[292]. Stefanidis GD, Vlachos DG. Controlling homogeneous chemistry in homogeneous− heterogeneous reactors: application to propane combustion. *Ind. Eng. Chem. Res.* 2009, 48(13), 5962-5968.

[293]. Karakaya C, Deutschmann O. Kinetics of hydrogen oxidation on Rh/Al2O3 catalysts studied in a stagnation-flow reactor. *Chem. Eng. Sci.* 2013, *89*, 171-184.

[294]. Hsueh CY, Chu H Sen, Yan WM. Numerical Study on Micro-Reformer Performance and Local Transport Phenomena of the Plate Methanol Steam Micro-Reformer. *J. Power Sources* 2009, 187, 535-43.

[295]. Hsueh CY, Chu H Sen, Yan WM, Chen CH. Transport Phenomena and Performance of a Plate Methanol Steam Micro-Reformer with Serpentine Flow Field Design. *Appl. Energy* 2010, 87, 3137-47.

[296]. Chein R, Chen YC, Chung JN. Axial Heat Conduction and Heat Supply Effects on Methanol-Steam Reforming Performance in Micro-Scale Reformers. *Int. J. Heat Mass Transf.* 2012, 55, 3029-42.

[297]. Chen J, Yan L, Song W, Xu D. Comparisons between Methane and Methanol Steam Reforming in Thermally Integrated Microchannel Reactors for Hydrogen Production: A Computational Fluid Dynamics Study. *Int. J. Hydrogen Energy* 2018, 31, 14710-28.

[298]. Pasel J, Emonts B, Peters R, Stolten D. A Structured Test Reactor for the Evaporation of Methanol on the Basis of a Catalytic Combustion. *Catal. Today* 2001, 69, 193-200.

[299]. Chein R, Chen YC, Chen JY, Chung JN. Premixed Methanol–Air Combustion Characteristics in a Mini-scale Catalytic Combustor. *Int. J. Chem. React. Eng.* 2016, 14(1), 383-393.

[300]. Gribovskiy AG, Makarshin LL, Andreev DV, Klenov OP, Parmon VN. Thermally autonomous microchannel reactor to produce hydrogen in steam reforming of methanol. *Chem. Eng. J.* 2015, *273*, 130-137.

[301]. Klenov OP, Makarshin LL, Gribovskiy AG, Andreev DV, Parmon VN. CFD Modeling of Compact Methanol Reformer. *Chem. Eng. J.* 2015, 282, 91-100.

[302]. Casanovas A, Saint-Gerons M, Griffon F, Llorca, J. Autothermal generation of hydrogen from ethanol in a microreactor. *Int. J. Hydrogen Energy* 2008, *33*(7), 1827-1833.

[303]. Schwarz O. Development of a Microstructured Reactor for Heterogeneously Catalyzed Gas Phase Reactions and its Application in the Oxidative Dehydrogenation of Propane. Ph.D. Dissertation, Technischen Universitat Berlin, 2008.

[304]. Germani G, Stefanescu A, Schuurman Y, Van Veen AC. Preparation and characterization of porous alumina-based catalyst coatings in microchannels. *Chem. Eng. Sci.* 2007, *62*(18-20), 5084-5091.

[305]. Guan G, Kusakabe K, Taneda M, Uehara M, Maeda H. Catalytic combustion of methane over Pd-based catalyst supported on a macroporous alumina layer in a microchannel reactor. *Chem. Eng. J.* 2008, 144(2), 270-276.

[306]. Abdul Rasheed RK, Chan SH. Transient Carbon Monoxide Poisoning Kinetics during Warm-up Period of a High-Temperature PEMFC - Physical Model and Parametric Study. *Appl. Energy* 2015, 140, 44-51.

[307]. Arsalis A, Kær SK, Nielsen MP. Modeling and Optimization of a Heat-Pump-Assisted High Temperature Proton Exchange Membrane Fuel Cell Micro-Combined-Heat-and-Power System for Residential Applications. *Appl. Energy* 2015, 147, 569-81.

[308]. Sun H, Xie C, Chen H, Almheiri S. A Numerical Study on the Effects of Temperature and Mass Transfer in High Temperature PEM Fuel Cells with Ab-PBI Membrane. *Appl. Energy* 2015, 160, 937-44.

[309]. Wan Y, Zhou Z, Cheng Z. Hydrogen production from steam reforming of methanol over $CuO/ZnO/Al_2O_3$ catalysts: Catalytic performance and kinetic modeling. *Chin. J. Chem. Eng.* 2016, 24, (9), 1186-94.

Appendix A

Supporting Information of Chapter-3

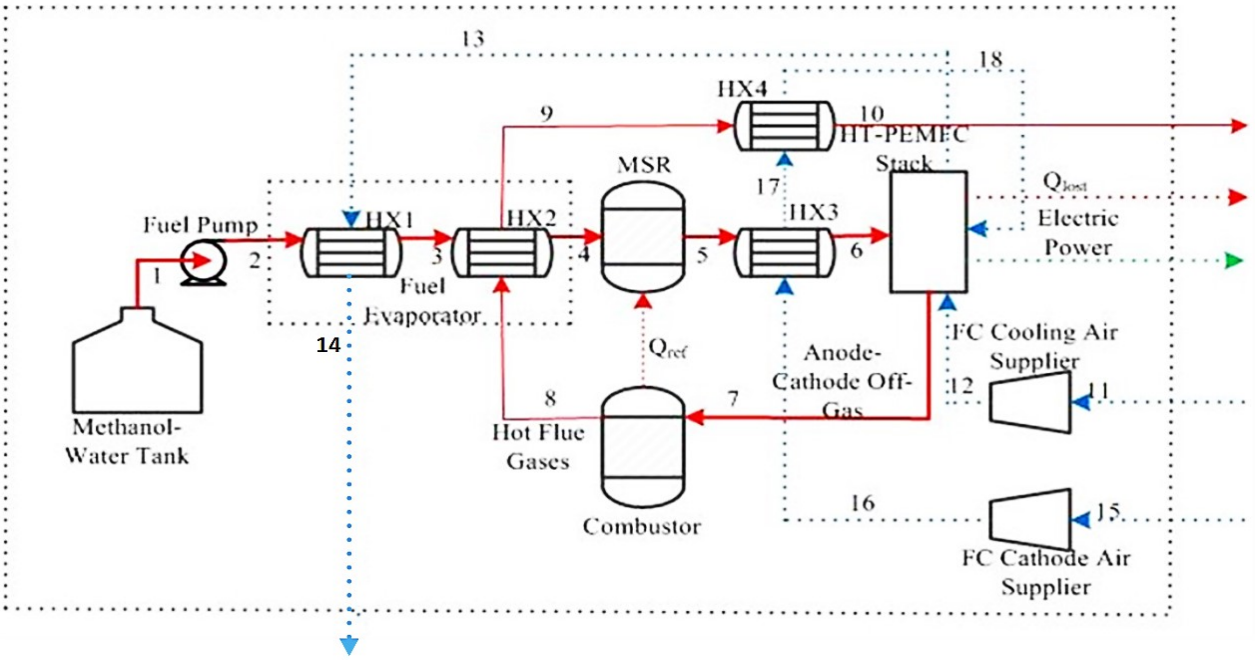

Figure S1 Schematic of methanol reformer system.

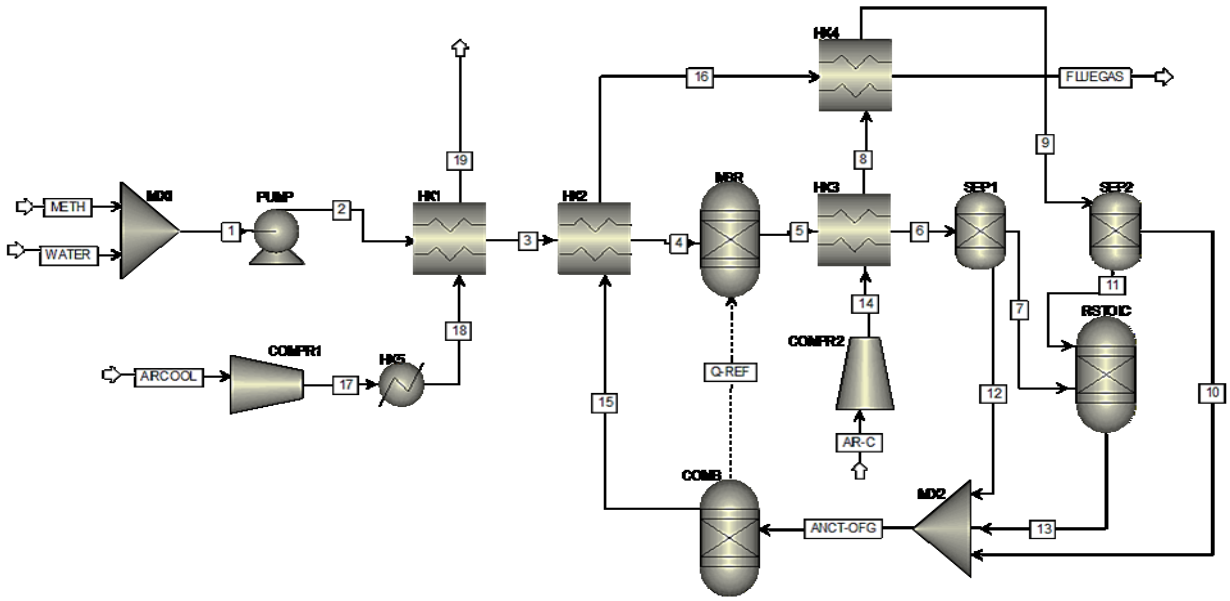

Figure S2 Aspen Plus Flowsheet of the methanol reformate gas high temperature PEM fuel cell system.

Table S1 Detailed description of the blocks used for the simulation.

Block name	Aspen Block Type	Explanation
MIX1	Mixer	Mixes the methanol and water. Fortran calculator is used to define the S/C ratio.
PUMP	Pump	Increases the pressure of the methanol-water mixture.
HX1	MHeatX	Provides enough heat to vaporize the methanol-water mixture.
HX2	MHeatX	Provides heat to reach the desired inlet temperature of the reactants to the reformer.
MSR	RGibbs	Used to estimate the methanol reformate syn-gas composition.
HX3	MHeatX	Decreases the syn-gas temperature to the fuel cell operation temperature. In addition, this block is used to increase the cathode air temperature.
SEP1	Sep	Separates unused hydrogen and the inert gases in the anode. The unused hydrogen is calculated with Fortran Calculator.
HX4	MHeatX	Increases the cathode air temperature to the operation temperature of the fuel cell. Heat is provided using the hot flue gases.
SEP2	Sep	Separates unused air in the cathode.
RSTOIC	Rstoic	Used to calculate the water production in the fuel cell.
MIX2	Mixer	Mixes anode-cathode off gas.
COMB	RGibbs	Estimates the heat production of the anode-cathode off gas combustion. Heat that is produced in the combustion is used for the methanol steam reforming process.
COMPR1	Compr	Increases the pressure of the air that is used to cool the fuel cell stack.
HX5	Heater	Provides heat to the cooling air. The amount of heat that is removed from the fuel cell stack is calculated with Fortran Calculator.
COMPR2	Compr	Increases the pressure of the cathode air. The amount of the cathode air is calculated with Fortran Calculator.
Further Explanations: The power generation of the fuel cell stack and the balance of the plant components are estimated using the equations in Chapter-3. The equations are used in Fortran Calculator in Aspen Plus to estimate the fuel cell voltage, power generation of the fuel cell, net power generation of the system, and the system efficiency.		

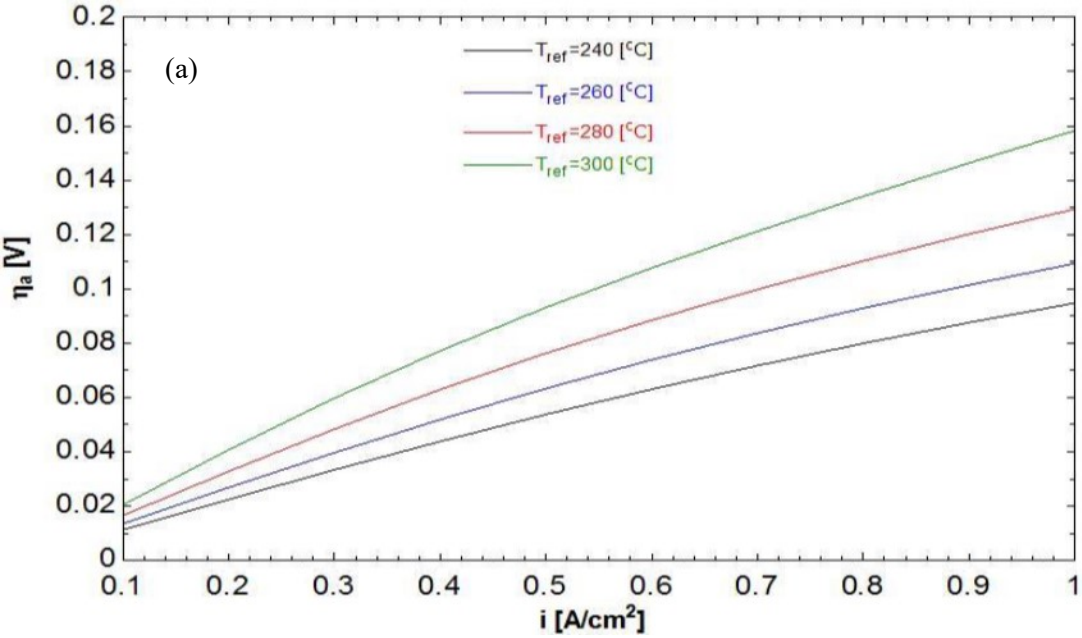
(a)
T_{ref}=240 [°C]
T_{ref}=260 [°C]
T_{ref}=280 [°C]
T_{ref}=300 [°C]
η_a [V]
i [A/cm^2]
0.2
0.18
0.16
0.14
0.12
0.1
0.08
0.06
0.04
0.02
0
0.1
0.2
0.3
0.4
0.5
0.6
0.7
0.8
0.9
1

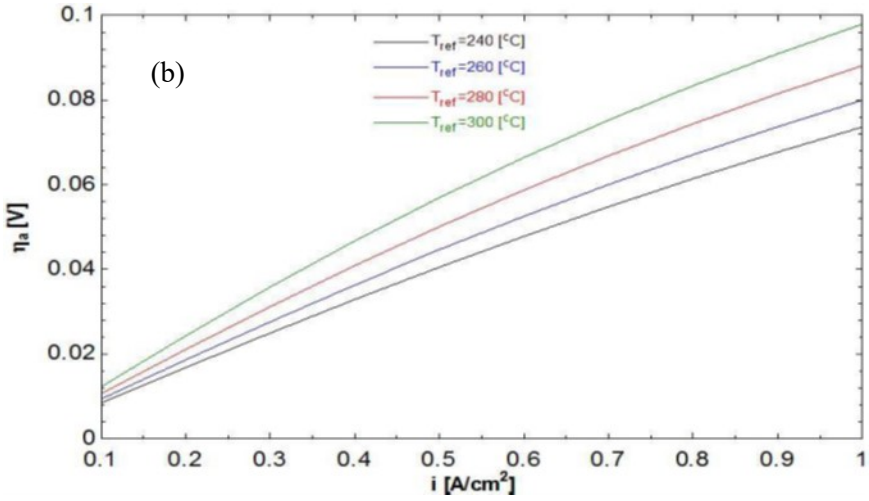
(b)
T_{ref}=240 [°C]
T_{ref}=260 [°C]
T_{ref}=280 [°C]
T_{ref}=300 [°C]
η_a [V]
i [A/cm^2]
0.1
0.08
0.06
0.04
0.02
0
0.1
0.2
0.3
0.4
0.5
0.6
0.7
0.8
0.9
1

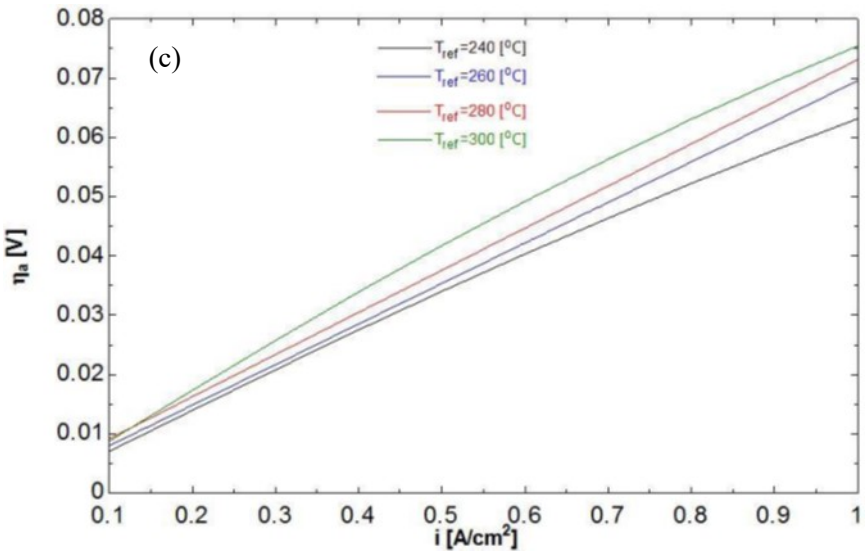

Figure S3 Voltage losses due to CO in the reformate gas with the variation of the reformer temperature and the current density. (a) Tcell=160 [°C], (b) Tcell=170 [°C], (c) Tcell=180 [°C], and SC=1.5, cathode stoichiometric ratio=2.

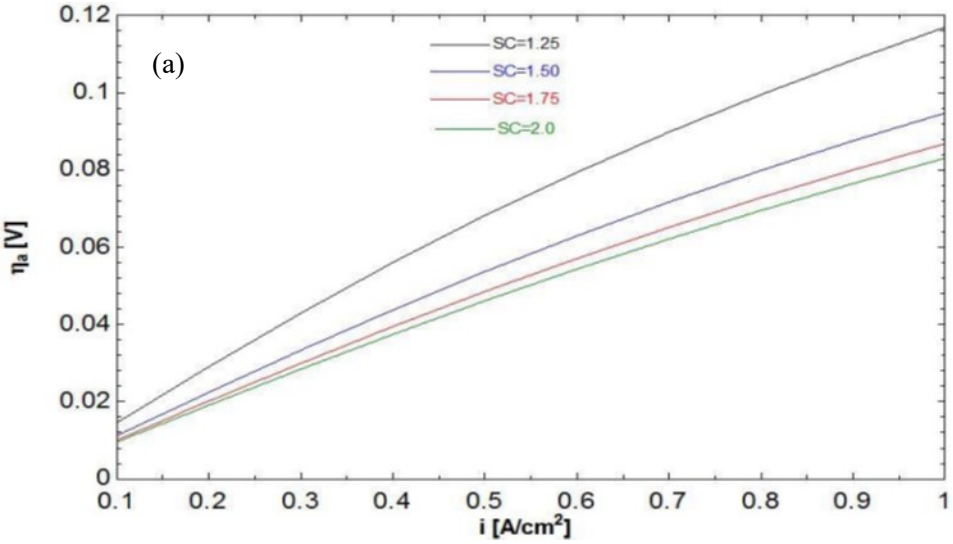

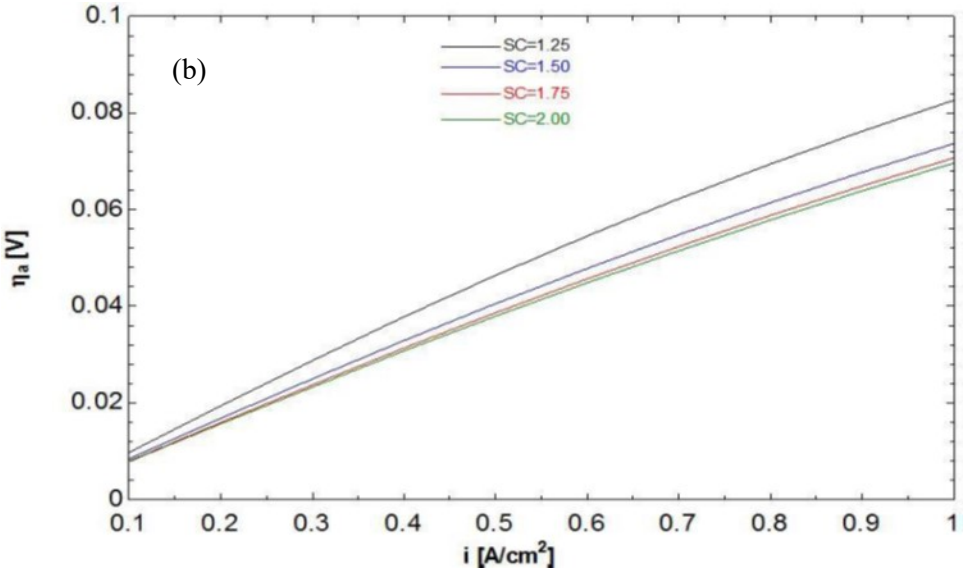

Figure S4 Voltage losses due to CO in the reformate gas with the variation of the steam-to-carbon ratio and the current density. (a) Tcell=160 [ºC], (b) Tcell=170 [ºC], and Tref=240 [ºC], cathode stoichiometric ratio=2.

The heat exchangers in the below figures are shown in Figure 3-1 in chapter-3. The results are added to show the effects of the different parameters on the heat duties of the heat exchangers.

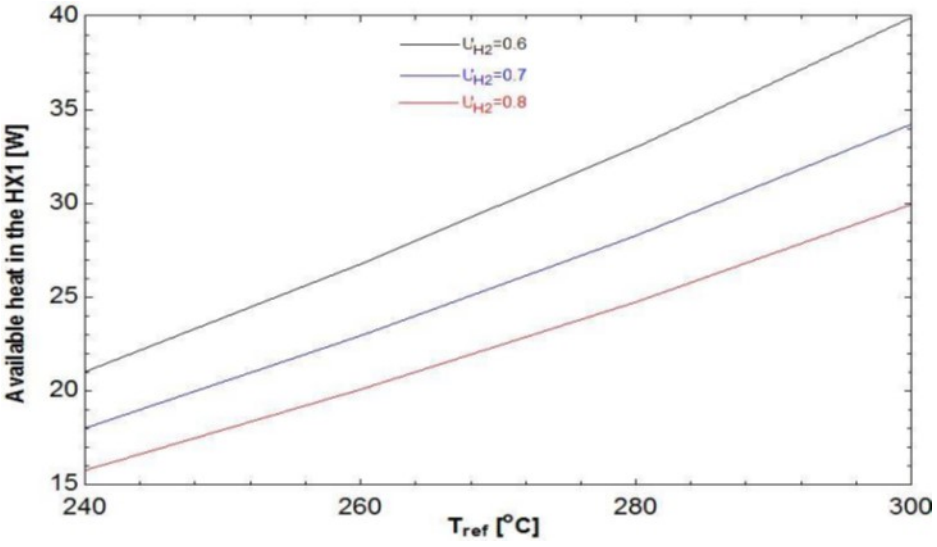

Figure S5 Change of the heat rate which is removed from the HX1 with the variation of the reformer temperature and the hydrogen utilization ratio for 350 W power production from the fuel cell stack. Tcell=160 [ºC], and cathode stoichiometric ratio=2.

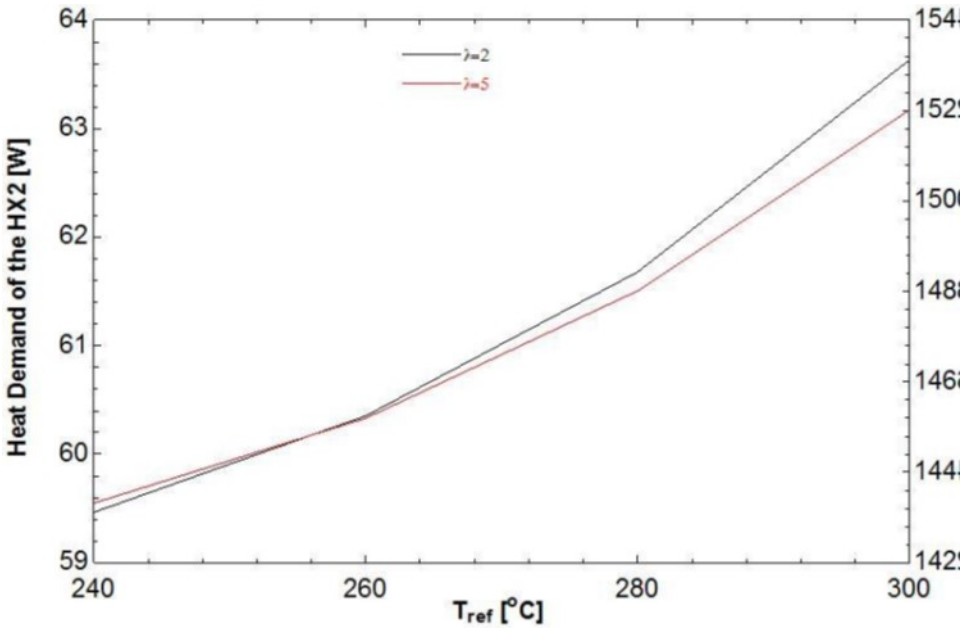

Figure S6 Change of the heat rate which is transferred to the HX2 with the variation of the reformer temperature and the cathode stoichiometric ratio for 350 W power production from the fuel cell stack.

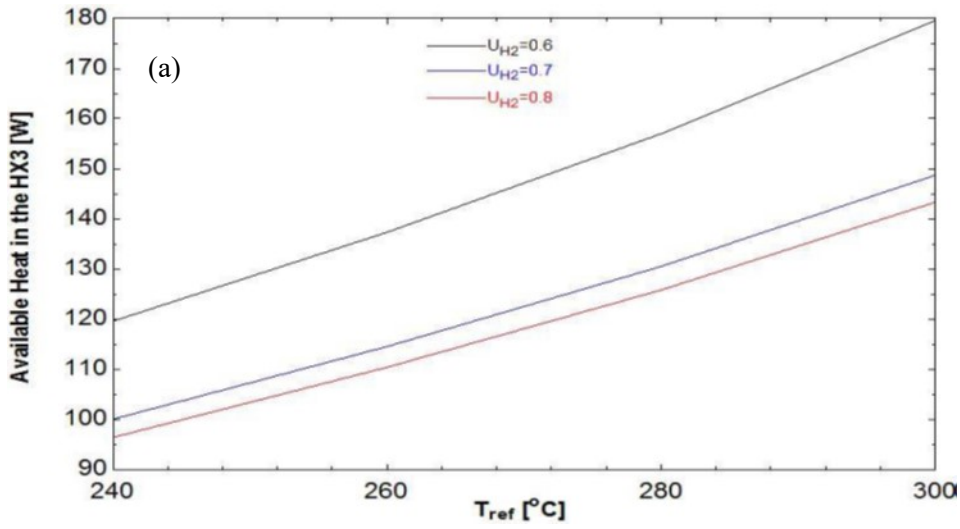

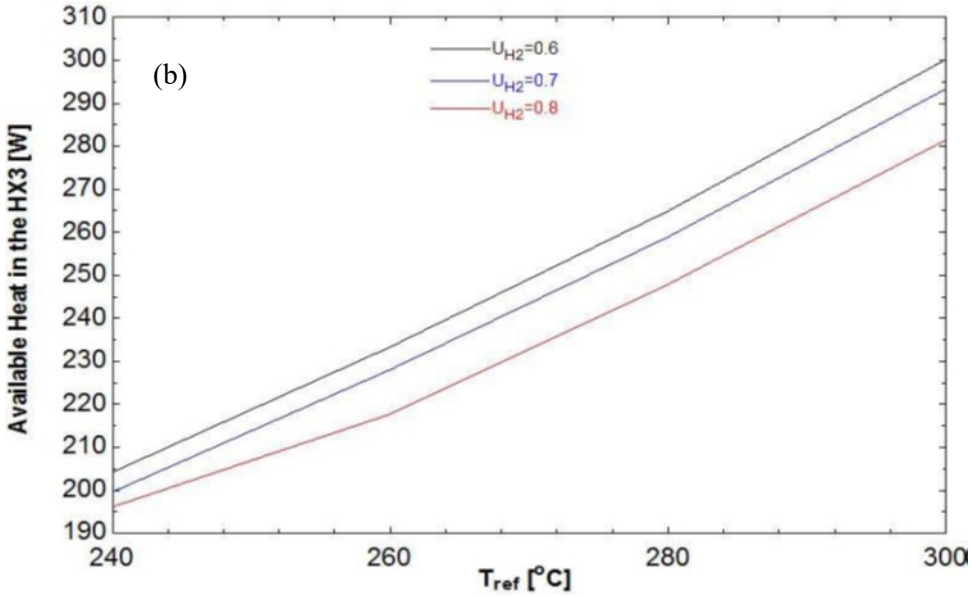

Figure S7 Change of the heat rate which is transferred from the HX3 with the variation of the reformer temperature and hydrogen utilization ratio for 350 W power generation from the fuel cell. (a) Cathode stoichiometric ratio=2, (b) Cathode stoichiometric ratio=5. Tcell=160 [^{o}C].

Table S2 The streams inlet and outlet temperature of the heat exchangers.

Heat Exchanger	Inlet Stream Temperature [^{o}C]	Outlet Stream Temperature [^{o}C]
HX1	Equals to reformer temperature	160
HX2	25	160
HX3	Equals to combustor temperature	160

Appendix B

Supporting Information of Chapter 5

Physical Properties

Table B.1 The parameters to calculate the binary diffusivity of the pairs [253].

$\Omega_D = \frac{A}{(T^*)^B} + \frac{C}{\exp(DT^*)} + \frac{E}{\exp(FT^*)} + \frac{G}{\exp(HT^*)}$ $T^* = \frac{kT}{\varepsilon_{ij}} \quad \varepsilon_{ij} = \left(\varepsilon_i \varepsilon_j\right)^{\frac{1}{2}} \; A = 1.06036 \; B = 0.1561$ $C = 0.19300 \; D = 0.47635 \; E = 1.03587 \; F = 1.52996$ $G = 1.76474 \; H = 3.89411$
$\sigma_{ij} = \frac{\sigma_i + \sigma_j}{2}$
$M_{ij} = \frac{2}{\frac{1}{M_i} + \frac{1}{M_j}}$
Explanations: Ω_D: Diffusion collision integral [dimensionless] σ_{ij}: The characteristic length [Å] M_i, M_j: Molecular weights of i and j [g/mol] k: Boltzmann`s constant- 1.3805x10^{-23} [J/K] ε: The characteristic Lennard-Jones energy [J]

Table B.2 The characteristic length and Lennard-Jones Potentials [253].

Substance	σ [Å]	$\varepsilon/k \; [K]$
CH_3OH	3.626	481.8
H_2O	2.641	809.1
H_2	2.827	59.7
CO_2	3.941	195.2
CO	3.69	91.7

Table B.3 Viscosity constants for components [256].

Component	a	b	c	d
CH_3OH	3.0663E-7	0.69655	205	0
H_2O	1.7096E-8	1.1146	0	0
H_2	1.797E-7	0.685	-0.59	140
CO_2	2.148E-6	0.46	290	0
CO	1.127E-6	0.5338	94.7	0

Table B.4 Thermal conductivity constants for components [256].

Component	c_1	c_2	c_3	c_4
CH_3OH	5.7992E-7	1.7862	0	0
H_2O	6.2041E-6	1.3973	0	0
H_2	0.002653	0.7452	12	140
CO_2	3.96	-0.3838	964	1860000
CO	5.9882E-4	0.6863	57.13	501.92

Table b.5 Specific heat capacity constants for components [205].

Component	$\propto$	$\propto_1$	$\propto_2$	$\propto_3$
CH_3OH	19.0	9.152E-2	-1.22E-5	-8.039E-9
H_2O	32.24	0.1923E-2	1.055E-5	-3.595E-9
H_2	29.11	-0.1916E-2	0.4003E-5	-0.8704E-9
CO_2	22.26	5.981E-2	-3.501E-5	7.469E-9
CO	28.16	0.1675E-2	0.5372E-5	-2.222E-9

Kinetic Parameters

a. Reaction kinetic model of Jiang *et al.*[246]

Rate expression [mol kg^{-1} s^{-1}]

$$r_{SR} = k_1 P_{CH_3OH}^{0.26} P_{H_2O}^{0.03} P_{H_2}^{-0.2}$$

Rate constant

$$k_1 = 5.307E12 \exp\left(\frac{-105000}{RT}\right) \; [mmol\ kPa^{-0.296}\ kg^{-1} s^{-1}]$$

b. Reaction kinetic model of Purnama *et al.* [120]

Rate expressions [mol g_{cat}^{-1} s^{-1}]

$r_{SR} = k_1 P_{CH_3OH}^{m} P_{H_2O}^{n}$

$r_{rWGS} = k_2 P_{CO_2} P_{H_2} - k_{-2} P_{H_2O} P_{CO}$

$m = 0.6; n = 0.4$

Rate constants

$k_1 = 8.8E8 \exp\left(\frac{-76000}{RT}\right)\ [mol\ bar^{-1} g_{cat}^{-1}\ s^{-1}]$

$k_2 = 6.5E9 \exp\left(\frac{-108000}{RT}\right)\ [mol\ bar^{-2}\ g_{cat}^{-1}\ s^{-1}]$

$k_{-2} = 4E7 \exp\left(\frac{-67000}{RT}\right)\ [mol\ bar^{-2}\ g_{cat}^{-1}\ s^{-1}]$

c. Reaction kinetic model of Sa *et al.*[143] (model-1)

Rate expression [mol kg_{cat}^{-1} s^{-1}]

$r_{SR} = k_1 P_{CH_3OH}^{a} (\propto + P_{H_2})^{b}$

$a = 0.47; b = -0.55; and\ \alpha = 0.30$

Rate constant

$k_1 = 3.9E9 \exp\left(\frac{-104000}{RT}\right)\ [mol\ bar^{0.08}\ kg_{cat}^{-1}\ s^{-1}]$

d. Reaction kinetic model of Peppley *et al.*[138]

Rate expressions [mol kg_{cat}^{-1} s^{-1}]

$$r_{SR} = \frac{k_R K^*_{CH_3O(1)} \left(\frac{P_{CH_3OH}}{P_{H_2}^{0.5}}\right)\left(1 - \frac{P_{H_2}^3 P_{CO_2}}{K_R P_{CH_3OH} P_{H_2O}}\right) C_{S_1}^T C_{S_{1a}}^T S_C}{\left(1 + K^*_{CH_3O(1)}\left(\frac{P_{CH_3OH}}{P_{H_2}^{0.5}}\right) + K^*_{HCOO(1)} P_{CO_2} P_{H_2}^{0.5} + K^*_{OH(1)}\left(\frac{P_{H_2O}}{P_{H_2}^{0.5}}\right)\right)\left(1 + K_{H(1a)}^{0.5} P_{H_2}^{0.5}\right)}$$

$$r_{MD} = \frac{k_D K^*_{CH_3O(2)} \left(\frac{P_{CH_3OH}}{P_{H_2}^{0.5}}\right)\left(1 - \frac{P_{H_2}^2 P_{CO}}{K_D P_{CH_3OH}}\right) C_{S_2}^T C_{S_{2a}}^T S_C}{\left(1 + K^*_{CH_3O(2)}\left(\frac{P_{CH_3OH}}{P_{H_2}^{0.5}}\right) + K^*_{OH(2)}\left(\frac{P_{H_2O}}{P_{H_2}^{0.5}}\right)\right)\left(1 + K_{H(1a)}^{0.5} P_{H_2}^{0.5}\right)}$$

$$r_{WGS} = \frac{k_W K^*_{OH(1)} \left(\frac{P_{CO} P_{H_2O}}{P^{0.5}_{H_2}}\right)\left(1 - \frac{P_{H_2} P_{CO_2}}{K_W P_{CO} P_{H_2O}}\right)(C^T_{S_1})^2 S_C}{\left(1 + K^*_{CH_3O(1)}\left(\frac{P_{CH_3OH}}{P^{0.5}_{H_2}}\right) + K^*_{HCOO(1)} P_{CO_2} P^{0.5}_{H_2} + K^*_{OH(1)}\left(\frac{P_{H_2O}}{P^{0.5}_{H_2}}\right)\right)^2}$$

Kinetic Parameters [138, 152, 309]

Kinetic Parameter	Value
k_R	$7.4E14 \exp\left(-\frac{10200}{RT}\right) [m^2\, mol^{-1}\, s^{-1}]$
k_D	$3.8E20 \exp\left(-\frac{170000}{RT}\right) [m^2\, mol^{-1}\, s^{-1}]$
k_W	$5.9E13 \exp\left(-\frac{87600}{RT}\right) [m^2\, mol^{-1}\, s^{-1}]$
K_R	$\exp\left(-\frac{50240 - 170.98T - 2.64E-02T^2}{RT}\right) [bar^2]$
K_W	$\exp\left(-\frac{-41735 + 46.66T - 7.55E-03T^2}{RT}\right)$
K_D	$\frac{K_R}{K_W} [bar^2]$
$K^*_{CH_3O(1)}$	$\exp\left(\frac{41.8}{R} - \left(-\frac{20000}{RT}\right)\right) [bar^{-0.5}]$
$K^*_{CH_3O(2)}$	$\exp\left(\frac{30}{R} - \left(-\frac{20000}{RT}\right)\right) [bar^{-1}]$
$K^*_{HCOO(1)}$	$\exp\left(\frac{179.2}{R} - \left(-\frac{100000}{RT}\right)\right) [bar^{-1.5}]$
$K^*_{OH(1)}$	$\exp\left(\frac{-44.5}{R} - \left(-\frac{20000}{RT}\right)\right) [bar^{-1.5}]$
$K^*_{OH(2)}$	$\exp\left(\frac{30}{R} - \left(-\frac{20000}{RT}\right)\right) [bar^{-1}]$
$K_{H(1a)}$	$\exp\left(\frac{-100.8}{R} - \left(-\frac{50000}{RT}\right)\right) [bar^{-1}]$

$K_{H(2a)}$	$\exp\left(\frac{-46.2}{R} - \left(-\frac{50000}{RT}\right)\right)[bar^{-1}]$
$C_{S_1}^T$	7.5E-06 $[mol\ m^{-2}]$
$C_{S_{1a}}^T$	1.5E-05 $[mol\ m^{-2}]$
$C_{S_2}^T$	7.5E-06 $[mol\ m^{-2}]$
$C_{S_{2a}}^T$	1.5E-05 $[mol\ m^{-2}]$
S_C	102,000 $[m^2\ kg^{-1}]$